Structural and Photo-physical Properties of Cyclic Aromatic Imides or Anthracene Tethered to Nitrogen-Containing Rings: Sensing of Nitrophenols

A Dissertation submitted to the Indian Institute of Technology Guwahati as partial fulfillment for the Degree

Doctor of Philosophy in Chemistry

Submitted by
Munendra Pal Singh

(Roll No. 156122020)

Thesis Supervisor: Prof. Jubaraj B. Baruah

Department of Chemistry

Indian Institute of Technology Guwahati

Guwahati-781039, Assam, India

August 2020

Dedicated to My Parents

Indian Institute of Technology Guwahati

Department of Chemistry

Declaration

I do hereby declare that this thesis entitled "***Structural and Photo-physical Properties of Cyclic Aromatic Imides or Anthracene Tethered to Nitrogen-Containing Rings: Sensing of Nitrophenols***" is the outcome of research work carried out by me under the supervision of **Prof. Jubaraj B. Baruah**, at the Department of Chemistry, Indian Institute of Technology Guwahati, India.

In keeping with the general practice of reporting scientific observations, due acknowledgement has been made whenever work described here has been based on the findings of other investigators.

IIT Guwahati
August, 2020

Munendra Pal Singh
Roll No. 156122020

Prof. Jubaraj B. Baruah
Department of Chemistry
Indian Institute of Technology Guwahati
Guwahati, 781039, Assam, India

Phone no. +91-361-258-2311(O)
Fax no. +91-361-269-0762
Email: juba@iitg.ac.in

CERTIFICATE

This is to certify that the research work presented in this thesis entitled "***Structural and Photo-physical Properties of Cyclic Aromatic Imides or Anthracene Tethered to Nitrogen-Containing Rings: Sensing of Nitrophenols***" is an authentic record of the results obtained from the research work carried out by **Mr. Munendra Pal Singh** (**Roll No. 156122020**) under my supervision in the Department of Chemistry, Indian Institute of Technology Guwahati, India. This work is original and has not been submitted elsewhere for a degree or award.

IIT Guwahati
August 2020

Prof. Jubaraj B. Baruah
(Thesis Supervisor)

Acknowledgements

I would like to acknowledge all the people who have contributed to this thesis in many ways.

First of all my deep sense of gratitude goes to my supervisor **Prof. Jubaraj B. Baruah** for his guidance during the course of my research. I have been enlightened by his wide knowledge and logical way of thinking. This thesis would not have been possible without his assistance. His encouragement has given me so much confidence. When I succeeded, he gave me great congratulation and encouragement. When I failed, he consoled, encouraged me. He is such a capable instructor and mentor that he can always help me to solve problems. His kindness, patience, positive direction lightened the way of my doctoral studies here. I especially thank him for spending numerous hours on my project, along with getting this thesis through its final stages.

I am highly indebted to "**Indian Institute of Technology Guwahati**" for the doctoral fellowship.

I would like to thank my doctoral committee members **Prof. Anil Kumar Saika** (IIT Guwahati), **Prof. T. Punniyamurthy** (IIT Guwahati) and **Prof. V. Manivannan** (IIT Guwahati) for their valuable suggestions during progress my research work.

I am grateful to all faculty members in the Department of Chemistry, IIT Guwahati for their help and encouragement and also the non-teaching staff of the Department for their technical support. I am thankful to the Central Instrument Facility (CIF), IIT Guwahati for various characterization facilities.

- Thanks to, Dr. Babulal Das, Mr. Aniruddha Gogoi, Mr. Basab Bhattacharjee, Mr. Imdadul Islam, Mr. Diganta Kumar Hira, Mr. John Sangma Dangou, Mrs. Abhilasha M. Baruah, and Dr. Kulakamal Senapati for their support at instrumental laboratory during the research work.
- I express my sincere thanks to my lab mates namely; Dr. Jayanta Kumar Nath, Dr. Prithiviraj Khakhlary, Dr. Nithi Phukan, Dr. Krapa Shankar, Dr. Arup Tarai, Rinki, Jitendra and Abhay for their advice, well wishes, encouragement and constant support during the research period at IIT Guwahati.
- I am thankful to my friends, seniors and juniors namely; Dr. Srikanth Turlapati, Dr. Sameer Hussain, Dr. Akhtar Hussain, Dr. Wajid Ali, Dr. Shad Ansari, Dr. Sahnawaz, Dr. Adil Afroz, Dr. Aniruddha Das, Dr. Adil Rather, Vinod, Arnav, Biswajit, Tushar, Laxmi, Subrata, tousif, Suhaib, Bishwanath, Shavez, Shagir, and Maimur for their timely help, support and for the wonderful time we shared during this period.

- I would like to acknowledge my teachers Mr. Manoj Yadav, Mr. Ajay Sharma and my all teachers of AMU for their excellent teaching, motivation, love and blessing.
- This Thesis wouldn't have seen the light of this day without the care, encouragement and help of some wonderful person like Shivam Dubey, Vimal Kumar, Jitendra Yadav, Arjun Bhai, Maya Prakash, Ajeet sahu, Avinish Tiwari, Ashwini Rawat, Maheswar Reddy, Dr. Asif Ansari, Saurabh Chaudhary and Anirudha Yadav. I would like to furnish my sincere gratitude to these wonderful people in my life for their constant motivation which made me reach this point.

Finally, my Ph. D. endeavor could not be completed without the endless love, unending support, tolerance and blessings from my family. I wish to express my sincere gratitude to my parents (Mr. Kunwar Pal Singh and Mrs. Suresha Devi), my elder brothers (Hariom Singh, Jagdish Singh, and Homendra Pal Singh), sisters-in-law (Sunita Devi and Himanshi Yadav), My sister Geeta and brother-in-law Ravindra yadav, nephews (Saurabh, Mohit and Jatin) and niece (Gunjan). They are the main soul and inspiration for each and every step that I achieve in my life.

Thesis Abstract

The thesis entitled "**Structural and Photo-physical Properties of Cyclic Aromatic Imides or Anthracene Tethered to Nitrogen-Containing Rings: Sensing of Nitro-phenols**" deals with structure and fluorescence emission properties of various non-covalently linked self-assemblies of salts and cocrystals of cyclic imide derivatives and an anthracene derivative with phenolic compounds. The content of the thesis is divided into five chapters. Details of structural description, synthetic procedure and spectroscopic characterization of each compounds are available in the experimental section which is included at the end of each chapter.

Chapter 1: Introduction

Necessary supramolecular features of cyclic imide derivatives to form non-covalently self-assemblies are discussed in this chapter. It contains discussions on pharmaceutical applications, molecular or ion recognition properties, coordination chemistry and biological activities of cyclic imide derivatives and their metal complexes. The fundamental aspects discussed in this chapter is based on interplay of weak interactions guide's geometrical aspects of non-covalently linked self-assemblies. Photo-luminescence of a substrate in cocrystal, salt and metal complexes changes from the original compound. Mechanistic paths of emissions are routinely modulated by changing weak interaction schemes which influence intensity and wave-length of emissions. Cyclic imide derivatives have scopes to modulate π-π interactions, along with other interplaying weak interactions. The dipolar nature and electron deficient properties of cyclic imides make them versatile in providing wide varieties of supramolecular assemblies. Imidazole and pyridine derivatives are chosen in this thesis as they have ability to act as ligands and have ability to form salts, cocrystals and metal complexes. Hence, interactions of imidazole and pyridine to a substrate influencing the photoluminescence properties at a remote site are taken up through a crystal engineering approach. A correlation of emission properties of the salts of those substrates and their properties in solution are correlated.

Chapter 2 (Part A): Imidazole-Tethered Phthalimide and Pyromellitic Diimide in sensing of picric acid and 2,4-dinitrophenol

In this chapter synthesis, characterisation and photoluminescence properties of 2-(3-(1H-imidazol-1-yl)propyl)isoindoline-1,3-dione (**2.1.1)** and N,N´-bis(3-imidazol-1-yl-propyl)-pyromelliticdiimide (**2.1.2)** and their nitrophenolate salts are presented. Crystal structures of the nitrophenol salts of **2.1.1** and **2.1.2** are determined to emphasize role of packing

influencing respective fluorescence emission property are discussed through a crystal engineering approach. Comparative fluorescence emission study in solution and solid state are discussed in this chapter.

Chapter 2 (Part B): Photo physical properties of Imidazole-Tethered Naphthalimide Derivative upon interactions with nitro-phenols and mineral acids

A similar approach is demonstrated as in the earlier section with N-(3-imidazol-1-yl-propyl)-1,8-naphthalimide (**2.2.1)** by preparing its salts with mineral acids (hydrobromic and nitric acid) and nitro-phenols (2,4-dinitrophenol and 2,4,6-trinitrophenol). Comparisons of emission properties in solutions and effect of water on the fluorescence emission are discussed.

In this chapter we established that: (a) in solid state water of crystallization makes a large difference packing pattern and influence the photoluminescence properties. (b) Naphthalimide derivative **2.2.1** recognizes nitro-phenols and mineral acids differently in solid and solution states. (c) In nitrophenolate salts, fluorescence quenching caused by π-interactions dominates over PET effect. (d) In the presence of water the flexible arm of **2.2.1** undergoes conformation adjustments influencing the emission spectra of the compound.

Chapter 3: Photo-physical Properties of Nitrophenolate and Carboxylate Salts of 9-N-(3-imidazolylpropylamino)methylanthracene

In this chapter a structural study and fluorescence emission of a di-topic compound 9-N-(3-imidazolylpropylamino) methylanthracene (**3.1**) and salts of **3.1** with three nitro-phenols, namely 4-nitrophenol (**3.2**), 2,4-dinitrophenol (**3.3**), 2,4,6-trinitrophenol (**3.4**) and two organic carboxylic acids namely 2-nitrobenzoic acid (**3.5**) and 2,3-dihydroxybenzoic acid (**3.6**) are presented. The molecule **3.1** has two or more protonation sites selective protonation of which provided scope to modulate emission properties. The effect of protonation and π-stacks on the photoluminescence properties are discussed.

This chapter has revealed following facts: (a) Protonation and π-stacks influence the photoluminescence properties. (b) In solution the protonation of secondary amine NH of **3.1** affect the PET and generate fluorescence ON-state at low concentrations and at high concentration of nitrophenols charge-transfer is predominant over the PET phenomenon resulting fluorescence OFF-state. (c) The fluorescence ON-state by 2,4,6-trinitrophenol in solution is a rare observation, suggesting that the adequate hold on hierarchical weak interactions make such a phenomenon possible.

Chapter 4: Detection of Hydroxyaromatics by (N,N'-bis(3-imidazolium-1-yl propyl)naphthalenediimide)di[bis-2,6-pyridinedicarboxylate ferrate] in Water

Many organic-cation containing metal-pyridinedicarboxylate complexes are known to forming inclusion complex with phenolic compounds. In this chapter, such a study is reported with (N,N'-bis(3-imidazolium-1-yl-propyl)naphthalenediimide)di[bis-2,6-pyridine dicarboxylate ferrate] (**4.1**) and the study is extended to develop a method for the removal of iron and hydroxy-aromatics from water. In this chapter utility of the iron complex to detect different hydroxyl-aromatic compounds in water is presented.

Conclusions from this chapter are (a) **4.1** detects hydroxyaromatics in a comparable manner as that of several other reported MOF and nanomaterials reported earlier. (b) The flexible arms of **4.1** occupying different orientations in the multicomponent systems while accommodating different phenolic guest. (c) This study provided a way to detect as well as crystalize out phenolic compounds from water in presence of iron ions.

Chapter 5: Photo-physical Properties of Ag, Zn, Cd Complexes Having N-(4 Pyridylmethyl)-1, 8-naphthalimide

The fifth chapter is on synthesis of dinuclear silver and mononuclear zinc and cadmium, complexes possessing N-(4-pyridylmethyl)-1,8-naphthalimide (**5.1**) and 4-formylcarboxylate as co-ligand are described. Three d^{10}-metal complexes $[Ag_2(\mathbf{5.1})_2(4\text{-formylcarboxylate})_2]$ **(5.2)**, $[Zn(\mathbf{5.1})_2(4\text{-formylcarboxylate})_2\cdot 2CH_3OH]$ **(5.3)** and $[Cd(\mathbf{5.1})_2(4\text{-formylcarboxylate})_2\cdot 2CH_3OH]$ **(5.4)** each having same sets of ligands, but having different metal ion differing also in structures were prepared and characterized. Photoluminescence properties of ligand **5.1** and its metal complexes in solid and solution are discussed. Aggregation-induced-emission enhancement (AIEE) of naphthalimide derivative **5.1** and its metal complexes are also discussed.

Following points were revealed in this chapter: (a) fluorescence emission of each solid sample of the complex differ as a result of packing effect; whereas they closely resemble in solution suggesting that the mechanism of emission solution and solid samples are different. (b) Fluorescence emission of powdered samples of ligand could be modulated by coordination to metal ions to show monomer or excimer like emissions.

A conclusion on the finding of the thesis is compiled at the end of the thesis. Certain spectra and crystallographic table for each compound is given at the end of the thesis. The crystallographic information files are also included.

CONTENTS

Table of content: **Page No.**

ABBREVIATIONS

CH_3CN: Acetonitrile

ACQ: Aggregation Caused Quenching

AIE: Aggregation induced emission

AIEE: Aggregation Induced Enhanced Emission

Å: Angstrom

DFT: Density functional theory

DHB: Dihydroxy benzene

DNP: Dinitrophenol

DMSO: Dimethyl sulfoxide

DMF: Dimethyl formamide

DNA: Deoxyribonucleic acid

DLS: Dynamic light scattering

EtOH: Ethanol

ESIPT: Excited state intramolecular proton transfer

FESEM: Field emission scanning electron microscope

FRET: Forster resonance energy transfer

HOMO: Highest occupied molecular orbital

IR: Infrared

ICT: Internal charge transfer

ICT: Isothermal calorimetric titration

LUMO: Lowest unoccupied molecular orbital

MS: Mass spectrometry

MeOH: Methanol

μ_M: Micromolar

nM: Nanomolar

NP: Nitrophenol

HNO_3: Nitric acid

NMR: Nuclear magnetic resonance

PET: Photo-induced electron transfer

KBr: Potassium bromide

PDC: Pyridinedicarboxylate

RET: Resonance energy transfer

RNA: Ribonucleic acid

RT: Room temperature (30 °C)

THF: Tetrahydrofuran

TGA: Thermo-gravimetric analysis

THB: Trihydroxy benzene

TNP: Trinitrophenol

UV-vis: Ultraviolet-visible

H_2O: Water

Chapter 1

Introduction

1.1: Introductory aspects on Supramolecular Chemistry

The term supramolecular chemistry was first described by J. M. Lehn, which means 'chemistry beyond the molecule' or 'the chemistry of the non-covalent bond'.[1] This branch is now established with large numbers of applications in different areas of chemistry and biology. Lehn got the Nobel Prize for his work in this area in 1987 sharing with Cram and Pedersen for their discoveries of molecular assemblies in the host-guest chemistry.[2] He describes the chemistry of molecular assemblies and intermolecular bond. This branch of chemistry deals with various non-covalently linked molecules interacting with one another. The supramolecular chemistry is maintained by non-covalent forces to develop functional complex architectures. Reversible intermolecular interactions enable one to control the formation of large non-covalently linked assemblies originally formed between two or more chemical species. Multicomponent systems held by non-covalent linkages increases complexities and challenges in constructions of new supramolecular assemblies with novel properties. Those non-covalently linked components may be organic or inorganic molecules or combination of both. The main objective of supramolecular chemistry is to design and develop new non-covalent assemblies of chemically and biologically important species that finds utilities in drug development,[3] molecular sensor,[4] catalysis,[5] nano-science,[6] protein-receptor binding,[7] DNA-drug binding,[8] molecular machine.[9] They also show varieties of optical[10] and magnetic[11] properties depending on the type of assemblies. It is an interdisciplinary subject, widely studied and practiced often by chemists, biologists, environmental scientists, material scientists, physicists, theoreticians, crystallographers and drug designers. "A supramolecular assembly can be guided by various non-covalent interactions including metal ligand coordination[12] are routinely envisaged by supramolecular chemists." "Hydrogen bonds[13] together with other weak interactions such as π-π interactions,[14] cation-π interactions,[15] anion-π interactions,[16] C-H-π interactions[17] and van der Waals forces[18] are often overcome in supramolecular systems." Many synthetic supramolecular architectures used as biological mimic are inspired by nature. Self-assemblies of nucleobases present in deoxyribonucleic acid (DNA) or ribonucleic acids (RNA)[19] and proteins[20] are such examples. Several sub-branches such as host-guest chemistry,[21] self-assemblies,[22] molecular recognitions,[23] supramolecular architectures,[24] molecular machines[25]

have spanned out from the core subject of supramolecular chemistry. Interlocked ring systems[26] such as rotaxane, catenane have contributed to the fundamental understanding of molecular machines, switches, and sensors.

Strength of non-covalent interactions leaving aside ionic interactions are always weak than a conventional covalent bond.[27] A comparison on energetics of some covalent bond and non-covalent interactions are listed in Table 1.1. As the energy value associated with non-covalent interactions are relatively small, the supramolecular assemblies are held by relatively weak interactions. Hence, supramolecular assemblies are easily disrupted and also can be reorganized with an ease. While covalently linked systems are tightly held, provides less scope for reorganization of structures through segregation and reassembling process.

Table 1.1 Strength of different supramolecular interactions and covalent bonds.

Non-covalent bonds (kJ/mol)		Covalent bonds (kJ/mol)	
Hydrogen bond	4-120	C-C bond	360
Electrostatic interaction	4.1-80	C-H bond	430
Van-der Waals interaction	0.4-4	C=C bond	600
π-π interaction	0-50	C=O bond	690
Cation-π interaction	5-80		
Ion-dipole	50-200		
Ion-ion	200-300		
Dipole-dipole	5-50		

1.2: Hydrogen bond in Supramolecular Chemistry

Hydrogen bond is defined as an interaction between a hydrogen atom and an electronegative atom from an intra or inter molecular fragment like X–H bond, where X is more electronegative atom than H. Hydrogen bond is represented as D-H···A, where D is the electronegative atom such as O or N to donate hydrogen to another electronegative atom bearing a lone pair as an acceptor (A) as shown in Figure 1.1a[28] where hydrogen bond and covalent bond are represented by dashed line and solid line respectively. There is also a literature where carbon-hydrogen bond acts as a hydrogen bond donor to link heteroatom.[29] Such very weak hydrogen bonds like C-H···X (X = halide, halogen), C-H···O, C-H···N etc, are very important in biological molecules. Furthermore, the C-H···π interactions have important contributions in different self-assemblies and responsible to be a part of it in

providing interplay of weak interactions parting in directional assemblies. Besides these halogen-halogen, anion···π, cation···π interactions are responsible for tuning the optical and catalytic properties.

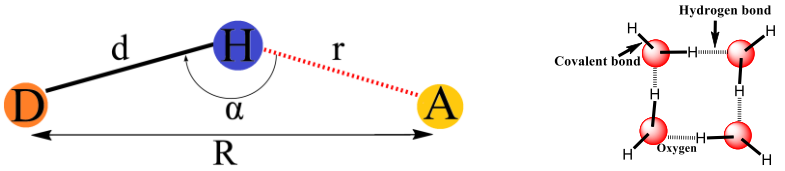

(a) (b)

Figure 1.1: (a) Representation of hydrogen bond and (b) Hydrogen bonds formed between four water molecules.

Depending on the distances and donor-acceptor angles, hydrogen bonds (H-bonds) offer broad range of bond lengths and angles to construct supramolecular assemblies. The hydrogen bonds are classified into three different categories namely strong, moderate and weak H-bonds.[30] Strong H-bond is formed between strong acid and good hydrogen bond acceptor and has similarity in character to a covalent bond. A moderate hydrogen-bond adopts slightly bent geometry and are generally formed by interaction between lone pairs of electron on a neutral atom with a neutral hydrogen bond acceptor. The bond-parameters of three different categories of hydrogen bonds, namely strong, moderate and weak hydrogen bonds are listed in Table 1.2. In general hydrogen bond energies range between about 60-120 kJmol^{-1} for a strong, 16-60 kJmol^{-1} for a moderate and 12 kJmol^{-1} for a weak bond (Table 1.2).

Table 1.2: Donor -acceptor distances and angles in different type of hydrogen bonds.

Parameters	Strong	Moderate	Weak
Bond energy (kJmol^{-1})	60-120	16-60	Less than12
H···A (r Å)	1.2-1.5	1.5-2.2	2.2-3.2
D···A (R Å)	2.2-2.5	2.5-3.2	3.2-4.0
∠D-H···A (α°)	175-180	130-180	90-150

H-bonds play an important role in supramolecular chemistry for the construction of non-covalent assemblies.[31] The roles played by hydrogen-bonds in controlling structures of DNA base pairs in self- or cross-associations of biological molecules such as adenine, thymine, guanine, uracil and cytosine provide multifaceted avenues to understand and mimic biological systems. (Figure 1.2).[32]

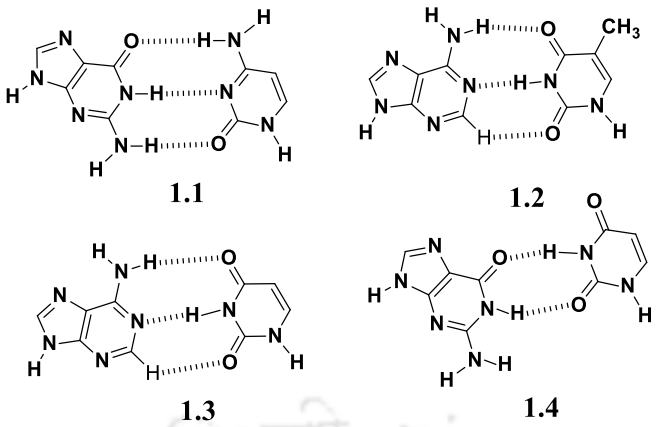

Figure 1.2: Hydrogen bonds among different nucleic acid base pairs, guanine-cytosine **1.1**, adenine-thymine **1.2**, adenine- uracil **1.3** and guanine-uracil **1.4**.

Depending on the multiple atoms connecting a pivot site to form hydrogen bonds, they are also classified into categories as linear, bifurcated and trifurcated hydrogen bonds. Examples based on such a classification from the donor or the acceptor site acting as the pivot to provide multiple hydrogen bonds across the particular pivot are shown in Figure 1.3. The geometries of bifurcated and trifurcated hydrogen bonds are bent (non-linear). Such bonds help in stabilizing bridged structures. The two centered linear hydrogen bond possessing one donor and one acceptor as shown in Figure 1.3a is a stronger bond than the bifurcated and trifurcated hydrogen-bonds. In bifurcated[33] hydrogen bond, one hydrogen atom interacts with two acceptor atoms or two hydrogen atoms interact with one acceptor atom, while in trifurcated,[34] one hydrogen atom interact with three acceptor atoms or three hydrogen atoms interact with one acceptor atom.

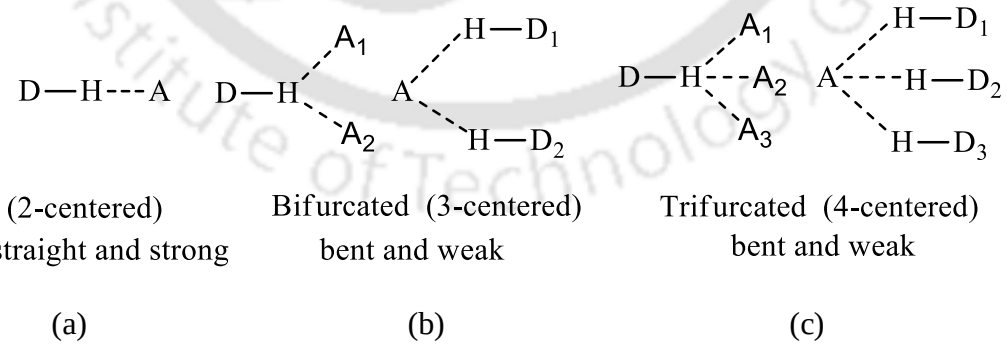

Figure 1.3: Three different types of hydrogen bonds with (a) one acceptor having linear, (b) one or two acceptors having bifurcated and (c) one or three acceptors having trifurcated interaction.

Etter, and coworkers have introduced graph set notations for describing different types of hydrogen bonds in supramolecular assemblies.[35] According to Etter rules of graph-set

notation, graph set designator 'G' is assigned into four different notations, R for ring, D for discrete, C for chain and S for self or intramolecular hydrogen bonded systems. The total number of atoms involved in hydrogen bonding is denoted in brackets and the number of donors and acceptors present in the assemblies are designated as subscript and superscript respectively as shown in Figure 1.4.

$$G_d^a(n)$$

Where G = Graph set designator C/R/D/S, d = Number of donor atoms, a = Number of acceptor atoms, n = Total number of atoms present in hydrogen-bonded motifs

Figure 1.4: A generic graph-set descriptor.

Desiraju introduced the concept of synthon[36] to describe non-covalent hydrogen bonded self-assemblies. Supramolecular 'synthon' is defined as the smallest intermolecular contact or non-covalent interaction between two molecules in supramolecular assemblies.[37] Supramolecular synthons are generally used to describe the hydrogen bonds formed between organic solids. Some of the commonly observed cyclic hydrogen bonded synthons with corresponding graph-set notation are represented in Figure 1.5. Energetics of synthons play important role in predesigned synthesis. Thus, identification of supramolecular synthons in homologous series becomes important.

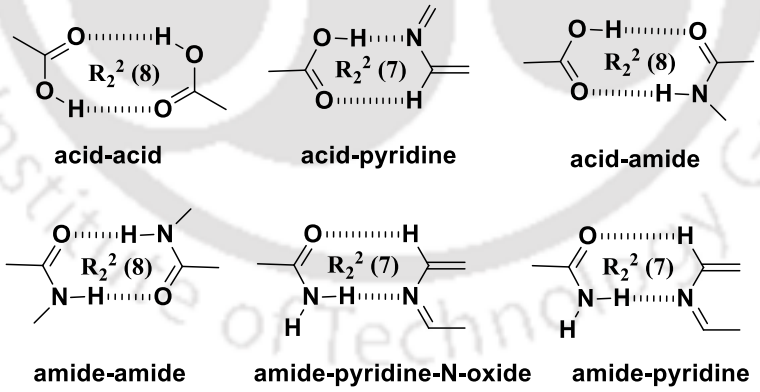

Figure 1.5: Homo and hetero supramolecular synthons with their corresponding graph-set notations.

1.3: Hydrogen Bonded Supramolecular Assemblies

Self-assemblies of organic and inorganic compounds have immense importance in biology[38] and material sciences.[39] Physical properties of a molecule changes upon change in packing pattern and the hydrogen bonds associated to them also changes. This is especially true with

polymorphs. Two different hydrogen bonded assemblies are formed by polymorph of 5, 5-diethylbarbituric acid **1.5** to adopt flat chain like structure or a cyclic square structure[40] as shown in Figure 1.6. These assemblies are formed by self-organization of N-H···O hydrogen bonds of **1.5**, in different orientations.

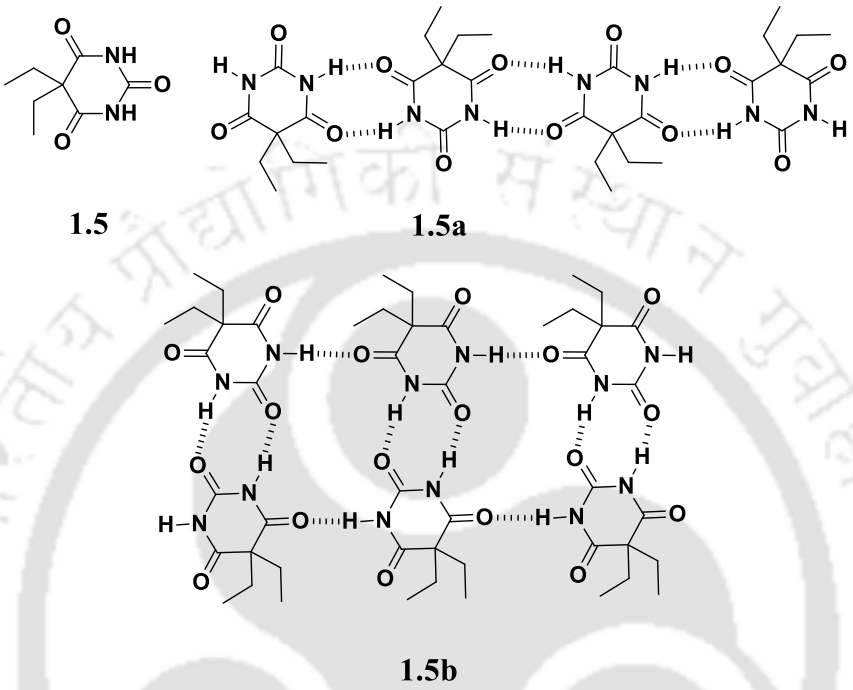

1.5 **1.5a**

1.5b

Figure 1.6: 5,5-diethylbarbituric acid **1.5** and two different hydrogen bonded self-assemblies formed by the polymorph of **1.5**.

The self-assemblies of inorganic complexes, or an inorganic complex interacting with organic molecules alters originally present intra or inter molecular interactions in discrete units. Self-assemblies between inorganic complexes with organic molecules leads to inclusion complexes or between inorganic complexes results in coordination polymers and metal-organic frameworks with different shape, sizes and dimensions.[41] Self-assemblies of inorganic complexes also provide host systems with different types of networks with pores of different kinds.[42]

Among biological molecules supramolecular assemblies of guanosine and its derivatives are extensively studied. Self-assembly of Guanosine formed in water in the presence of Na^+ or K^+ ions is made up of four molecules of guanosine forming a quartet by N-H···O and the N-H···N hydrogen bonds. Similarly isoguanosine also forms hydrogen-bonded quartet structure, around alkali metal cations[43] as shown in Figure 1.7.

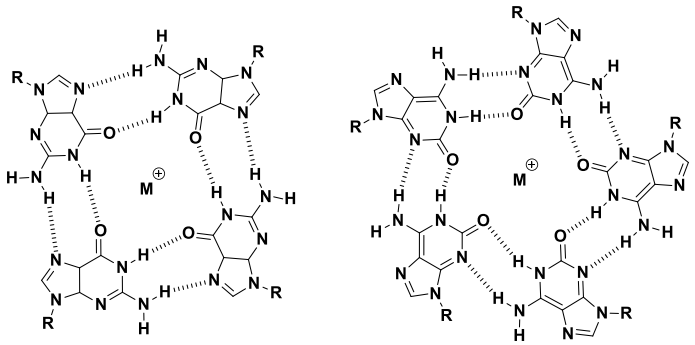

1.6 **1.7**

Figure 1.7: Hydrogen bonded self-assembly of guanosine **1.6** and isoguanosine **1.7** in the presence of metal ions (M^+).

Another interesting hydrogen-bonded assembly **1.8** formed between of guanidinium cation and arenesulfonate anion[44] is shown in Figure 1.8. In this case guanidinium cations use six hydrogen bond donor sites whereas three equivalent sites of oxygen atoms of sulfonate anions form hydrogen bonds forming a hexagonal structure.

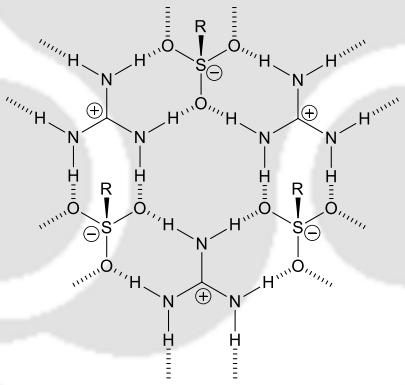

1.8

Figure 1.8: Hexagonal hydrogen bonded supramolecular assemblies of Guanidinium-sulfonate.

There are large numbers of supramolecular assemblies of inorganic complexes guided by hydrogen bonds to provide different geometrical arrangements. Examples of linear and zig-zag assemblies from similar set of ligands are observed[45] in square planar complexes. The cis platinum(II) complex **1.9** has a zig-zag chain like arrangement whereas square planar cis palladium(II) complex **1.10** has a linear chain like arrangement. Though both the networks are interconnected by amide-amide hydrogen bonds, still there is a large difference in the supramolecular properties.

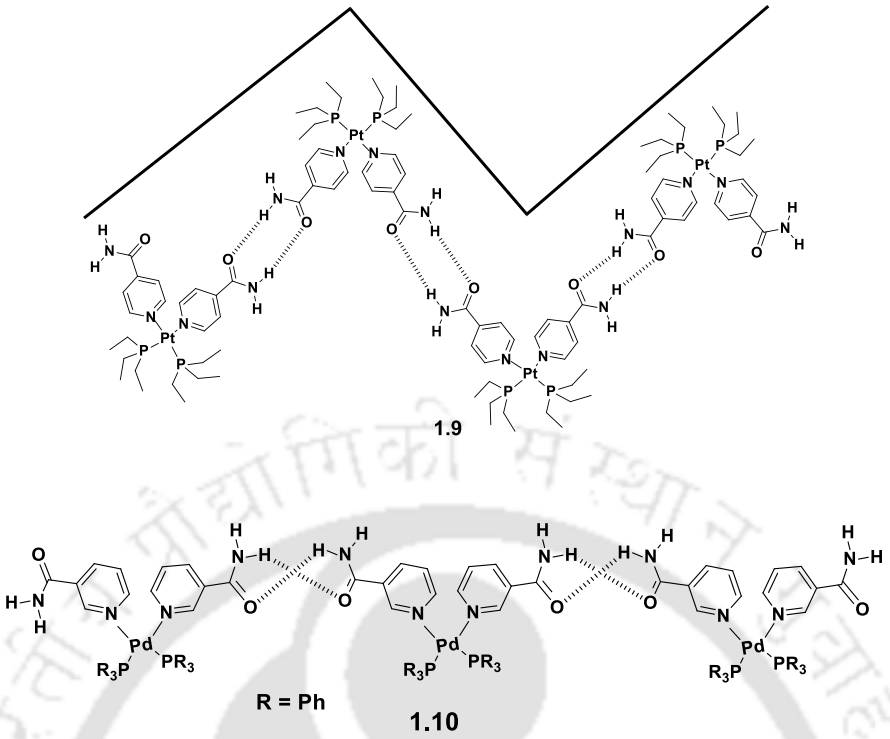

Figure 1.9: Zig-zag and linear hydrogen-bonded chains of **1.9** platinum (II), **1.10** palladium (II) complexes.

These two examples shows that the supramolecular assemblies are modified by changing the position of a functional group, participating ligand in self-assembies.

1.4: General Features of Cyclic Imides as a Supramolecular Host

Organic compounds containing two flanked acyl groups bound to a nitrogen atom are known as imides. The general structure of imide is thus -CO-N(R)-CO-. The cyclic imides are those where imide unit is constituent of a cyclic ring. Cyclic imide derivatives have versatile applications.[46] Some of the commonly known cyclic aromatic imides are shown in Figure 1.10. These backbones provide avenues for supramolecular assemblies due to the carbonyl groups participating as hydrogen bond donors. In the case of aromatic unit anchored to imide such as in phthalimide, napthalimides are dipolar. These amides have planar rings to form stacked structures in supramolecular assemblies.

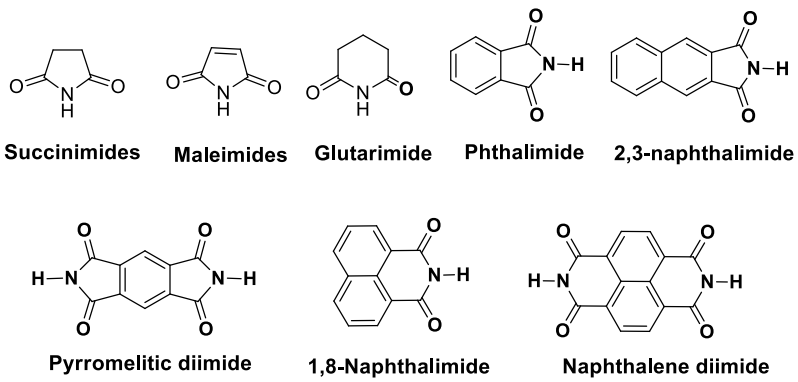

Figure 1.10: Some of the well-known cyclic imides.

Cyclic imide derivatives are generally prepared by condensation of an acid anhydride with ammonia or primary amine or aryl amine or urea. These reactions are carried out in solid state or as conventional reactions in solution. The conventionally used reaction to synthesize imides is given in Scheme **1.1**. There are several other procedures available for industrial synthesis of cyclic imides from commercially available substrates in solid or liquid state.[47]

$$(RCO)_2O + R'NH_2 \rightarrow (RCO)_2NR' + H_2O$$

Scheme 1.1

Cyclic imide derivatives are used as fluorescent sensors for different analytes,[48] fluorescent imaging agents,[49] and have applications in solar cell,[50] and organic light emitting diode.[51] Phthalimide derivatives are studied for photochemical reactions,[52] in which photo induced single electron transfer (SET) reactions are widely studied.[53] Due to strong intermolecular π-π stacking ability, 1, 8-naphthalimide and naphthalenediimide derivatives are widely used for colorimetric and fluorescent sensors for different anions[54] and cations.[55]

1.5: Cyclic Imides in Biological Systems

Cyclic imides are parts of many biologically active compounds showing anti-bacterial,[56] anti-fungal,[57] anti-inflammatory,[58] anti-tumor,[59] anxiolytic,[60] nerve conduction blocking[61] properties. Some of those are used as DNA targeting,[62] anticancer[63] and cellular imaging agents,[64] because of planar π-deficient aromatic systems.

Certain phthalimide derivatives have therapeutic applications.[65] For example, N-phenyl phthalimide shows anti-convulsant activity and neurotoxic properties.[66] 2-[4-[4-(1,2-benzisothiazol-3-yl)-1-piperazinyl]butyl]-1-phthalimide (**1.11**) is an anti-psychotic agent.[67]

Stiz *et al.* synthesized two different sub-families of phthalimide derivatives, viz. butylaminophthalimides (**1.12**) and 1-hydroxy butylaminophthalimidines (**1.13**) and, these compounds have been used as anesthetic activity.[68] Antimony(III) and zinc(II) complexes of 2-(2-methoxyphenyl)-1H-isoindole-1, 3 (2H)-dione **1.14** showed higher anti-bacterial activity in comparison to their parent ligand.[69]

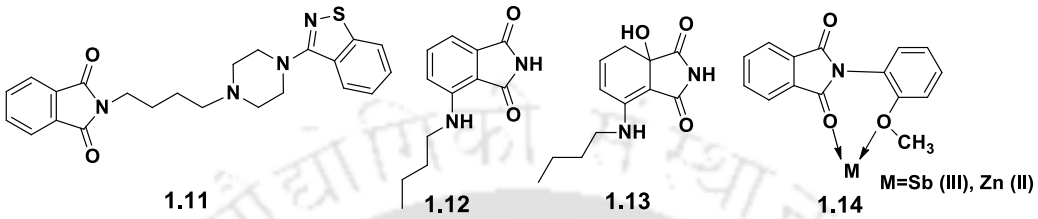

Pyromelliticdiimide derivatives **1.15-1.17** are also studied for the treatment of antimicrobial activities.[70] These compounds showed high to moderate anti-bacterial activity against different types of bacteria and fungi.

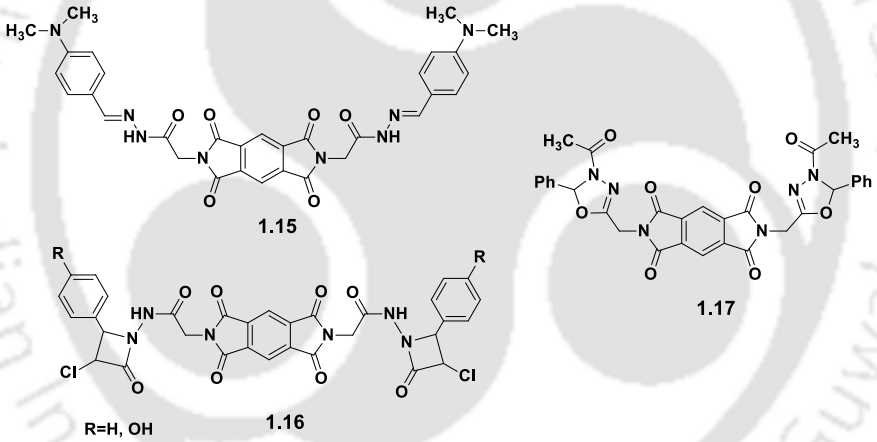

Planar π-conjugated chromophoric 1,8-naphthalimide derivatives possessing hydrophobicity, are good DNA binding agent.[71] DNA binding with 1,8-naphthalimide derivative was initiated by Brana in 1973.[72] Amonafide **1.18**, mitonafide **1.19**, azonafide **1.20** have shown potential drugs for treatment of tumors. The compound **1.18** stabilizes double stranded DNA against heat denaturation.[73] Elinafide **1.21**, is a bisnaphthimide compound have good DNA binding ability and anti-tumour activity.[74]

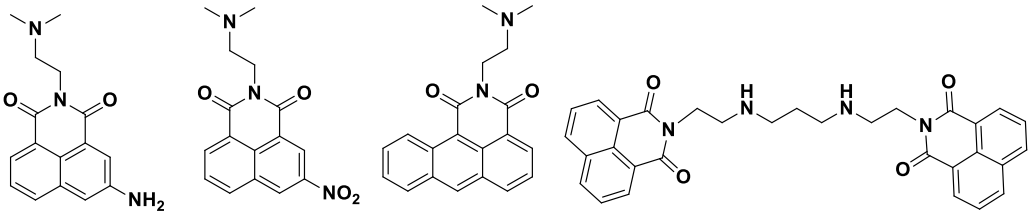

1.18 **1.19** **1.20** **1.21**

Imperiali *et al.* have reported 4-N,N-Dimethylamino-1,8-naphthalimide derivatives **1.22-1.25** for the fluorescence detection of biomolecular interactions.[75] They used calcium-sensing protein calmodulin as a model system for development of these highly effective sensors of dynamic biomolecular interactions. Chiral amino acid based compound **1.26** detect dynamic protein-protein interactions through FRET (fluorescence resonance energy transfer) process in water.[76]

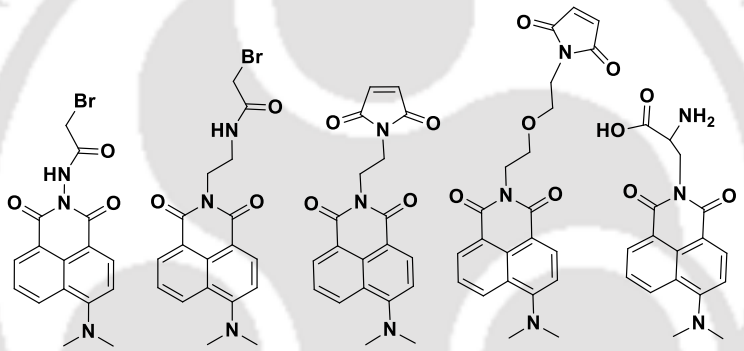

1.22 **1.23** **1.24** **1.25** **1.26**

Several 1,8-naphthalimide based prodrugs, **1.27-1.29**, possessing tertiary amine N-oxide moiety on the side chain were synthesized.[77] These derivatives show lower affinity to bind a double stranded DNA compared to the corresponding amine. This was attributed to lack of the protonated side chain in the ligand, which favoring electrostatic binding with DNA. Importantly, the N-oxide derivatives exhibit less cytotoxicity in oxic A375 cell lines compared to the corresponding amine, while they are found to be highly cytotoxic in hypoxic tumour cell lines.

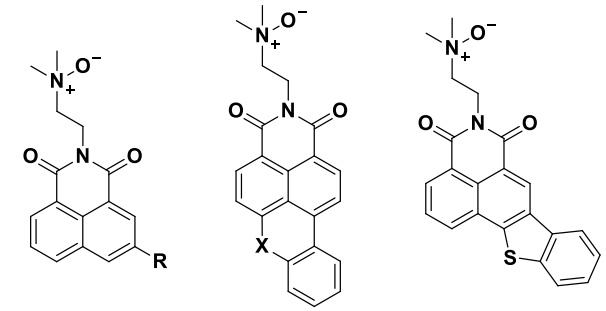

1.27 a R = NO_2
1.27 b R = NH_2

1.28 a X = O
1.28 b X = S

1.29

Several new naphthalimide derivatives have been synthesized by Kamal and co-workers and evaluated for their therapeutic activities in which the pyrrolobenzodiazepine-naphthalimide linked compound **1.30** and **1.31** showed good DNA-binding ability and anticancer activity in certain cancer cell lines. DNA-binding affinity in **1.30** was enhanced when the numbers of -CH_2- group in the carbon chain was increased from two to three.[78]

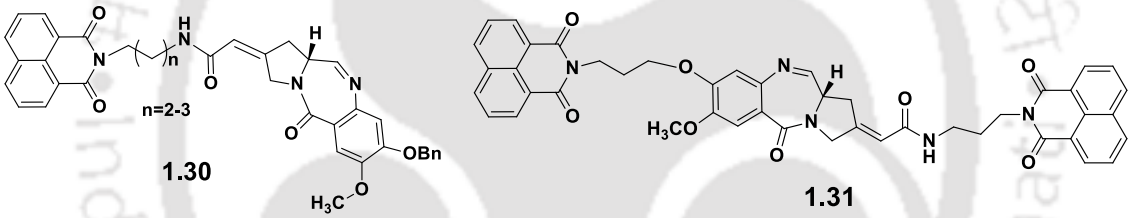

1.30

1.31

Imidazole based naphthalimides have also been developed which shows significant cytotoxic activity against human colon carcinoma cell lines. The increased affinity of these derivatives towards DNA were attributed to the presence of the additional heterocyclic ring that increased stacking interactions. Qian and co-workers developed a series of imidazonaphthalimides **1.32-1.33**, where the naphthalimide ring is fused onto an imidazole ring bearing an un-fused aryl or heteroaryl ring.[79] Viscosity of these derivatives established their binding to DNA via classical intercalation mode. The intercalated DNA showed extra stability against heat denaturation (ΔT_m 4-13.3 ºC). There were well-defined spectral changes to further confirm that they behave as DNA-intercalating agents.

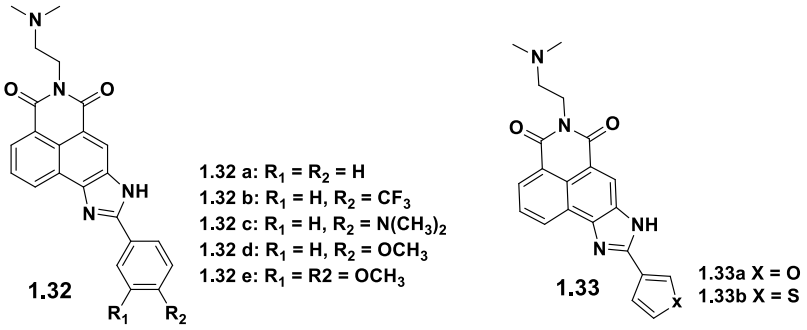

Naphthalimide based transition metal complexes have provided wide ranges of therapeutic activity such as imidazole based 3d-metal Scorpionates'' bearing pyridyl ligand with a 1,8-naphthalimide chromophores **1.34** exhibit DNA and bovine serum albumin (BSA) protein binding propensities.[80] Cobalt(II) and copper(II) complexes of this ligand have ability to photo-chemically cleave BSA. They also exhibit significantly high cytotoxicity against HeLa cervical cancer cells upon ultra-violet light irradiation.

Dyson and co-workers have synthesized ruthenium(II) arene complexes **1.35** and **1.36** having naphthalimide moieties linked by imidazole and arene unit. It was found that intercalating moiety of the 1,8-naphthalimide in both cases increased the cytotoxicity (2-49mM) of the ruthenium arene unit with cancer cells.[81] Study on intercalation mechanism of these naphthalimide unit within DNA and also from study on the binding of the ruthenium(II) arene unit with proteins were extrapolated to explain anticancer selectivity of **1.35a-d** over model healthy cells. Bichromophore containing ruthenium(II) complexes **1.37a-b** are good DNA binders and photocleaving agents[82]. These complexes show significant hypochromism shift in absorption peak in UV-visible spectra originating from metal to ligand charge transfer transition in the presence of DNA. The 4-aminonaphthalimide conjugate was found to be better photo-cleaving agent than the 4-nitro analogue.

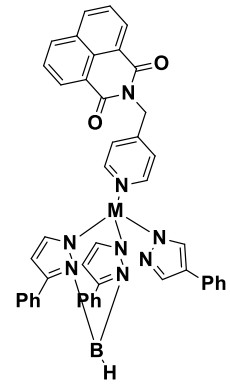

M = Co(II), Cu(II) and Zn(II)

1.34

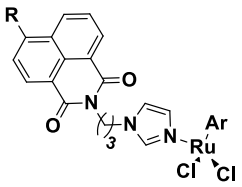

1.35a Ar = p-cymene, R = NMe_2
1.35b Ar = p-cymene, R = H
1.35c Ar = toluene, R = NMe
1.35d Ar = toluene, R = H

1.35

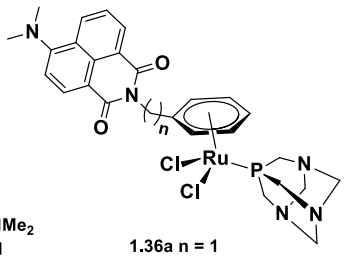

1.36a n = 1
1.36b n = 2
1.36c n = 3

1.36

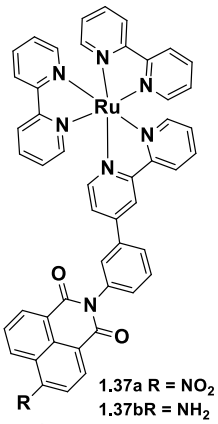

1.37a R = NO_2
1.37bR = NH_2

1.37

In vitro antitumor activities of a series of metal complexes of naphthalimide-cyclam conjugates **1.38** are reported in literature.[83] The compounds with long alkyl chains and their zinc(II), chromium(III) complexes showed effective antiproliferative effect. Among all the complexes, Zinc(II) complex (R = methyl), served as antiproliferative agent against fifteen numbers of cancer cell lines.

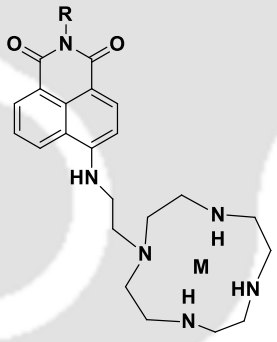

1.38

M = Zn^{2+}, Cu^{2+}, Ni^{2+}, Co^{2+}, Cr^{3+}

R = CH_3, C_4H_9, C_8H_{17}, $C_{12}H_{25}$

Among the heavy metals complexes, Platinum-bis-naphthalimide complexes **1.39-1.40,** have anti-neoplastic properties, to overcome the cellular resistance to cis-platin.[84] the high cytotoxicity exerted by these derivatives results from the intercalation of the bis-naphthalimide unit combined with the platination of DNA bases. Banerjee *et al.* also developed Platinum(II) based bifunctional DNA binder **1.41** which incorporates the terpyridyl and the 4-N,N'-dimethylamino-1,8-naphthalimide. The complex shows enhanced DNA binding affinity and cytotoxicity (IC5018mM) against MCF-7 cell lines.[85] Gold(I) phosphine complexes bearing a thio-naphthalimide ligand such as **1.42** also shows anti-proliferative activity.[86]

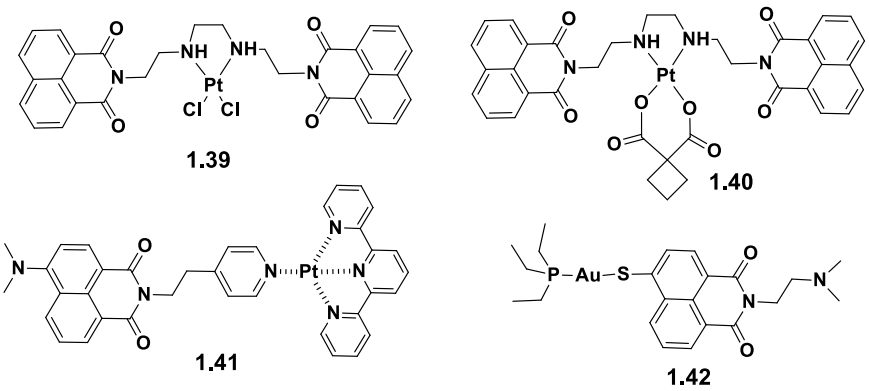

1.39 1.40 1.41 1.42

1.6: Cyclic Imides in Detection of Anions

Photoluminescent and colorimetric anion recognition and sensing is a developed field in supramolecular chemistry.[87] Nature also provides many examples of anion binding receptors based on hydrogen-bonding interactions of charged or neutral species.[88] In the last decade, many excellent examples of naphthalimide-based anion sensors have been published by different groups.[89] Due to its unique photophysical properties, the cyclic imide derivatives are important to detect different hazardous materials for environment causing concern to human life. Many cyclic imides chemosensors are designed out of which several ones are based on modulation of emission spectra of naphthalimide derivatives binding to anions.

Li and his co-workers have developed a thiourea based naphthalimide sensor **1.43** for selective and sensitive detection of fluoride and acetate anions.[90] The compounds forms 1:1 complexes with anions by forming hydrogen-bonds, involving the N-H naphthalimide as well as of thiourea. The recognition was monitored by changes in absorption and emission spectra by adding fluoride and acetate to the solution of **1.43**, while the other anions do not cause changes. A representative binding mode of fluoride ion with **1.43** is shown in Scheme 1.2.

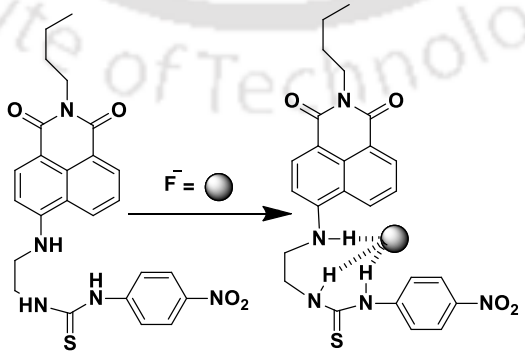

1.43

Scheme 1.2: Possible binding mode of **1.43** with fluoride ion.

Another thiourea based naphthalimide anion sensors **1.44a** and **1.44b** were synthesized by Gunnlaugsson and coworkers.[91] These compounds also forms 1:1 complexes with fluoride, acetate and dihydrogenphosphate anions. Compounds have a strong green fluorescent emission at 525 nm in DMSO, this emission is quenched upon addition of anions. The compounds also change color from light yellow to deep purple on addition of those anions. The quenching of fluorescence emission is due to photoelectron transfer, takes place from the receptor unit to the fluorophore. The quenching factors of fluoride is greater than other anions. Chloride and bromide did not show any changes upon addition to **1.44a** and **1.44b**, possibly due to their large size and low charge density. Receptor **1.45** also forms salt with dihydrogenphosphate anion in 1:1 stoichiometry. The assembly of the salt is formed through hydrogen bonds involving naphthalimide N-H and thiourea N-H groups with the oxygen atoms of the anion.[92] Receptor **1.45** was further modified to new prepare sensors **1.46a** and **1.46b**.[93] Anion binding capabilities of the compounds with dihydrogenphosphate and acetate anions were evaluated by monitoring the changes in ^{1}H-NMR and fluorescence spectra of the **1.46a** and **1.46b** in the presence of the anions.

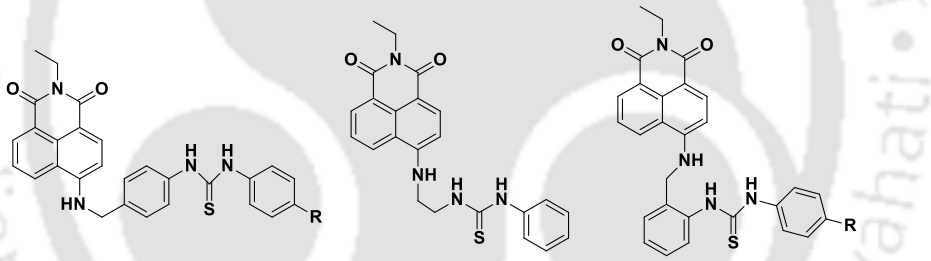

Symmetrical bis-naphthalimide-based sensor **1.47**, which contain two naphthalimide units are connected at the 4-position via a urea moiety were used for detection of fluoride and hydroxide anions.[94] In the presence of excess fluoride or hydroxide ion in dimethylsulphoxide, **1.47** undergoes stepwise deprotonation of both N-H protons of urea part. The step-wise deprotonation gave rise to two distinct types of changes in the visible spectra to show a large difference in color, the changes were clearly visible to the naked eye. Addition of excess dihydrogenphosphate and acetate anion could not deprotonate the second N-H proton making distinction from fluoride and hydroxide ions.

Naphthalimide-based compound **1.48** is a selective chemosensor to detect fluoride ion in solution by absorption and emission spectroscopy.[95] Colorless solution of the **1.48** turns to jade-green showed a new emission peak upon interaction with fluoride ion. The absorption

peak of **1.48** is at 365 nm decreases in the presence of fluoride ions and new absorption at 487 nm appears; whereas, the emission wavelength at 449 nm decreases and a new peak at 508 nm appears. These properties are ascribed to a fluoride-triggered Si-O bond cleavage.

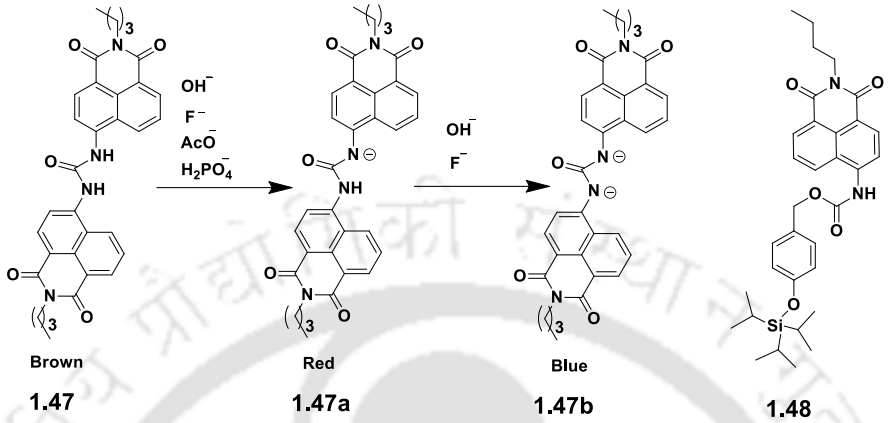

Colorimetric sensor **1.49** showed excellent sensing of F^-, OH^- and AcO^- anions.[96] The receptor recognized these three anions without an interference of other anion, such as ClO_4^-, PF_6^-, HSO_4^- and $H_2PO_4^-$. Initially hydrogen-bonds were formed between anion and receptor at lower concentration of fluoride, but at a higher concentration of fluoride deprotonation took place as a second process (Scheme 1.3). Similar hydrogen bonds were also observed in the case of hydroxide anion. In the case of acetate interactions, two molecules of receptors form hydrogen bonds with an acetate.

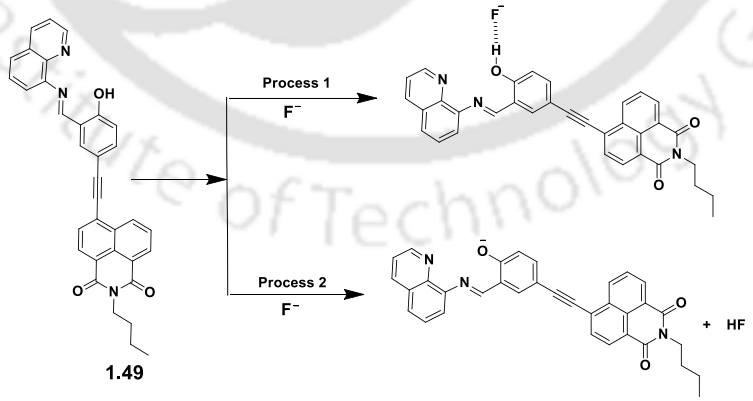

Scheme 1.3: Two different ways of binding of **1.49** with F^-.

Flood *et al.* have reported an aryl-triazole receptor containing naphthalimide unit **1.50** which showed effective binding with chloride anion. The binding occurred with both triazole and

phenylene units. The binding strength of Cl^- ion with **1.50** showed that the naphthalimide provides greater anion stabilization than phenylene ring.[97] The Hydrogen bonded interaction of **1.50** with chloride ion is shown in scheme 1.4.

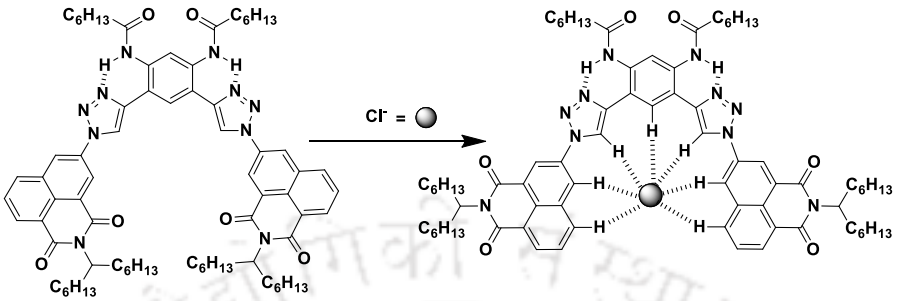

1.50

Scheme 1.4: Interaction of Cl^- with **1.50**.

Recently, a hydrazine based fluorescent organo-gelator **1.51** showing emission through photo-induced electron transfer (PET) and intramolecular charge transfer (ICT) paths have been designed.[98] The compound **1.51** could selectively recognize the fluoride and acetate, anions in both solution as well as in gel systems with different sensing behaviors. The **1.51** in benzene solution recognize fluoride immediately by change in fluorescence intensity and color changed from green to blue whereas the addition of acetate ion to the solution of **1.51**, the fluorescence intensity increased with time and the color changed from green to light blue. Interesting aspect of these result is that, in the fluoride recognition process the organogel undergoes a gel-sol phase transition, while in the case of acetate recognition process, the absorption and fluorescence changes were observed without a phase change.

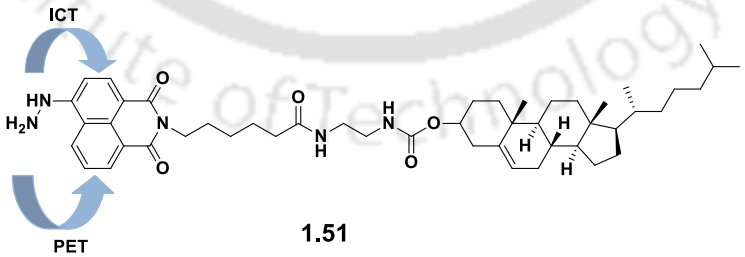

1.51

The squaramide-naphthalimide conjugates **1.52** and **1.53** showed a significant fluorescence enhancement upon addition of bromide ion in aqueous DMSO solution. The detection limits were found in micromolar level for both **1.52** and **1.53**, they were also capable to detect bromide ion in cellulo.[99]

Kubinyi *et al.* synthesized two naphthalimide-bipyridinium conjugates, **1.54** and **1.55** which form radical pairs with anions such as F^-, AcO^-, and BzO^- via intermolecular electron transfer from the anions to the bipyridinium units.[100] Initially these compounds show weak fluorescence due to the intramolecular photoinduced electron transfer (PET) from the naphthalimide to the bipyridinium moiety, but the fluorescence intensity got enhanced upon addition of some selective anions such as F^-, AcO^-, and BzO^- by 10, 15 and 20 times respectively in acetonitrile solutions. Intermolecular electron-transfer from the anion to bipyridinium unit to be a reason for changes in emission spectra. It was confirmed by the appearance of a characteristic absorption peak of the bipyridinium radicals. Color changes were also observed by naked eye, for example, a colorless solution of **1.54** turned to purple; whereas, a yellow solution of **1.55** turned green.

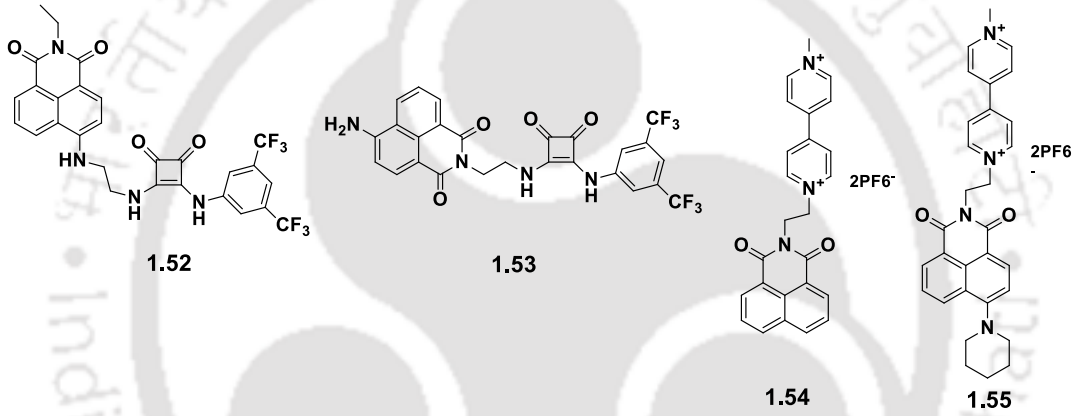

1.7: Cyclic Imides in Detection of Cations

Heavy and transition-metal ions have toxic impact on the environment. The 1,8-naphthalimide derivatives are commonly used for specific signal transduction due to those cation binding and are useful in their detections. Detection processes depend on different approaches, for example, 4-Aminonaphthalimide derivatives are widely used as fluorescent cation sensors for different metal ions because they are easily functionalized at 4-position or at imide side. The amine group of 4-amino-1,8-naphthalimide derivatives provide a 'push-pull' effect to internal charge transfer (ICT) at excited state. This happens due to electron withdrawing ability of imide unit whereas amine group has the ability to donate electron.[101] Use of 4-aminonaphthalimide derivative for sensing of cations in water is also well established.[102]

Gunnlaugsson *et al.* have extensively studied the 4-amino 1,8-naphthalimide derivatives as colorimetric cation sensors for various metal ions. They reported highly selective and

sensitive fluorescent water soluble photo induced electron transfer chemosensors **1.56a** and **1.56b** that display excellent selectivity with a large enhancement of emission upon zinc(II) recognition, at pH 7.4.[103] The change in the emission spectra were due to binding of the zinc(II) with the carboxylate groups. The complexation increases the oxidation potential of the receptor, prevents photo induced electron transfer quenching taking place from the receptor to the excited state of the fluorophore. This effect switches on the fluorescence of the naphthalimide.

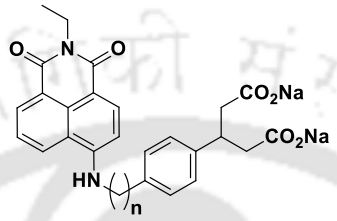

1.56a n=1,
1.56b n =2,

Quin *et al.* have reported an 4-amino naphthalimide based di(2-picolyl)amine containing fluorescent sensor **1.57** for recognition of transition metal ions utilizing characteristic binding modes.[104] The receptor **1.57** shows selectivity towards Zn^{2+} and Cd^{2+} over most other transition metal ions reflected in the increments of fluorescence intensity. A red-shift in emission from 483 nm to 514 nm by Zn^{2+} and blue-shift from 483 to 446 nm by Cd^{2+} ions were observed. The sensor **1.57** is cell permeable and can detect Zn^{2+} in living zebrafish embryos. In aqueous solution, **1.57** bound to Zn^{2+} in an imidic acid, which is a tautomeric form of the naphthalimide based di-2-picolylamine receptor. On the other hand, most of the transition metal ions were bound to the ligand in an amide tautomeric form (Scheme 1.5). The binding modes were confirmed by ^{1}H-NMR spectroscopic titrations of **1.57** with Zn^{2+} and Cd^{2+} in different solvents, and from the 2D NOESY, infrared-spectra, emission and absorption spectra.

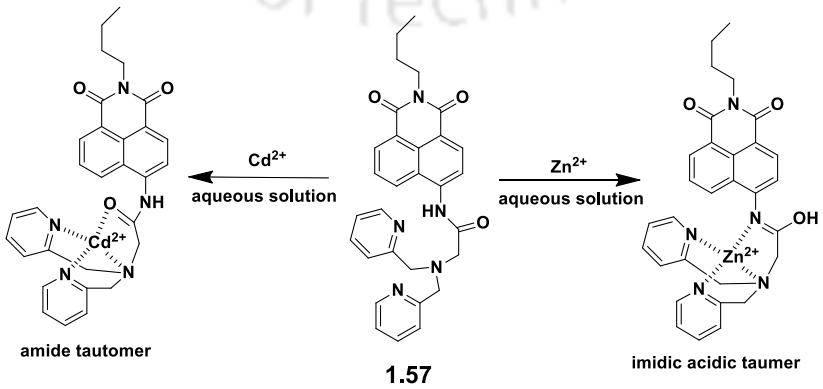

Scheme 1.5: Binding modes of **1.57** with Zn^{2+} and Cd^{2+} in aqueous solution.

Di(2-picolyl)amine based naphthalimide ligand **1.58** act as a ratiometric fluorescent sensor for Cd^{2+} ion in neutral medium. The compound **1.58** discriminate Cd^{2+} from Zn^{2+} by undergoing internal charge transfer (ICT) processes.[105]

Di(2-picolyl)amine containing compound **1.59** for recognition of copper(II) ion has been reported by Wang and co-workers. The compound **1.59** selectively binds with Cu^{2+} ion. This caused color change, and the color change occurred without interference by the presence of Zn^{2+}, Cd^{2+} and Ni^{2+} cations in solution together with Cu^{2+} ion. The binding through di(2-picolyl)amino moiety enabled efficient tridentate coordination for Cu^{2+} ion.[106]

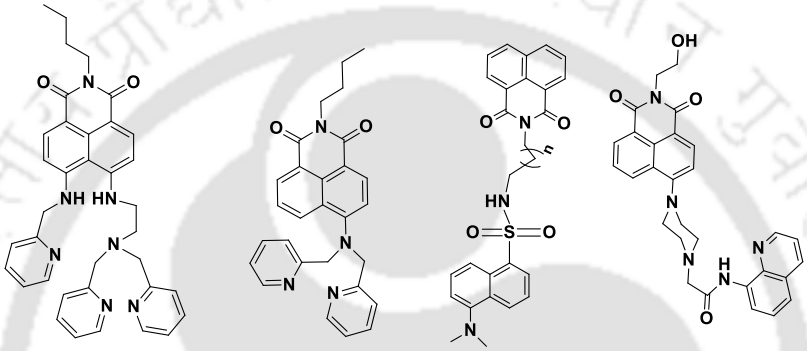

Naphthalimide derivatives linked through dansyl unit such as in **1.60a**, **1.60b**[107] and quinoline unit **1.61**[108] are fluorescence ratiometric probes for the specific detection of Cu^{2+} ions in aqueous medium. These sensors showed a specific Cu-induced deviation in the ratio of its two emission bands due to the different quenching effects of Cu^{2+} on its two constituent fluorophores.

Compound **1.62** is a "turn on" fluorescent chemosensor for trivalent Fe^{3+}, Al^{3+} and Cr^{3+} cations. Interactions of sensor **1.62** with trivalent metal cations inhibit the PET operating in the sensor leading to complexation in aqueous samples and live cells. The mode of binding is shown in Scheme 1.6.[109]

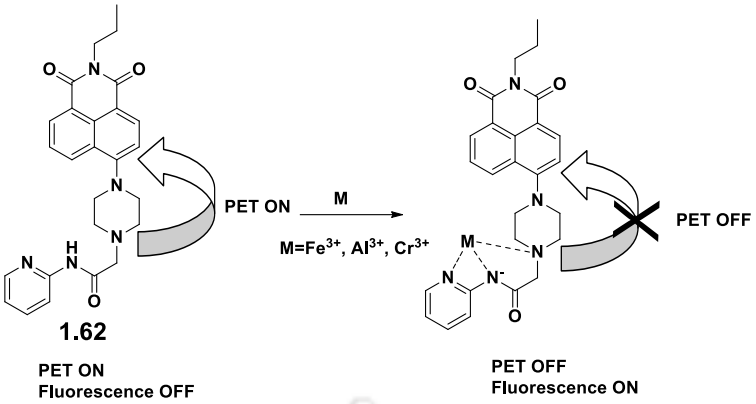

Scheme 1.6: Proposed mechanism for fluorescence changes of **1.62** on addition of Fe^{3+}, Al^{3+} and Cr^{3+}.

Quinoline linked naphthalimide probe **1.63** is also a selective, fluorescence ratiometric sensor for trivalent ions (Fe^{3+}, Al^{3+} and Cr^{3+}). It operates through internal charge transfer mechanism.[110] Emission spectra of **1.63** showed a large red-shift (390 to 484 nm) in presence of those metal ions. Whereas coumarin containing naphthalimide compound **1.64** showed a fluorescence "turn-on" state specific for Fe^{3+} ion.[111] Piperazine based 1, 8-naphthalimide compounds **1.65-1.67** are selective and sensitive fluorescent chemosensor for Fe^{3+} in aqueous solutions. The detection limit for Fe^{3+} ion are in the order **1.65** (7.40×10^{-6} M) > **1.66** (2.73×10^{-7} M) > **1.67** (4.27×10^{-8} M) trend.[112]

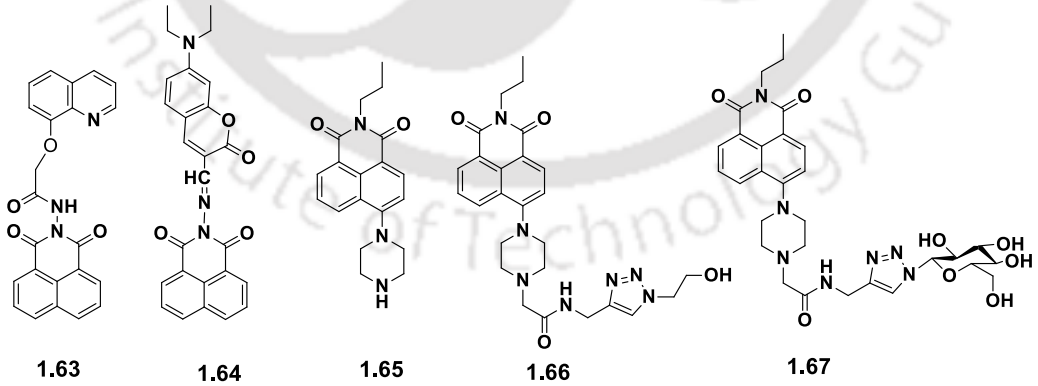

Mercury ions are environmental pollutants gets into human body through inhalation and bio-accumulating through food chain .[113] Due to these environmental health hazard issue, a large number of chemosensors based on naphthalimides for detection of mercury have been reported till date. A simple and water soluble compound **1.68**, is a highly selective and

sensitive "turn on" fluorescent PET chemosensor for Hg^{2+} ion.[114] Naphthalimide-porphyrin hybrid compound **1.69** is a selective ratiometric sensor for Hg^{2+} in aqueous solution and in living cell. The molecule containing two independent fluorophores, which shows reversible fluorescence responses for Hg^{2+} based on ICT mechanism.[115]

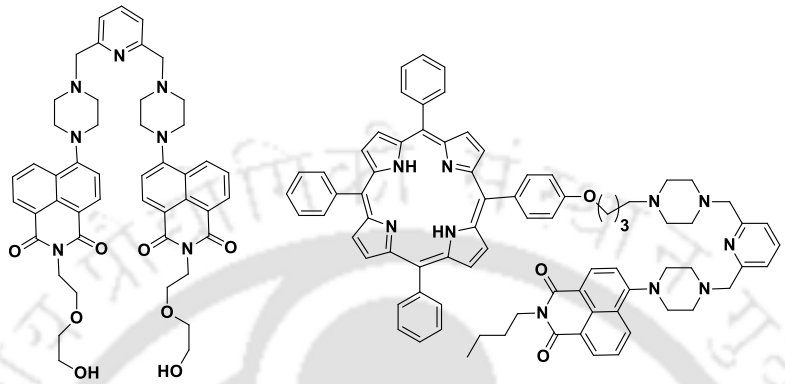

Thiourea based compounds **1.70a** and **1.70b** are selective fluorescent chemosensors for Hg^{2+} in aqueous media. These compounds show fluorescence quenching behavior due to PET occurring from the thiourea group to the naphthlamide group. Upon complexation with Hg^{2+} no PET occurred; hence, fluorescence enhancement was observed (Scheme 1.7).[116]

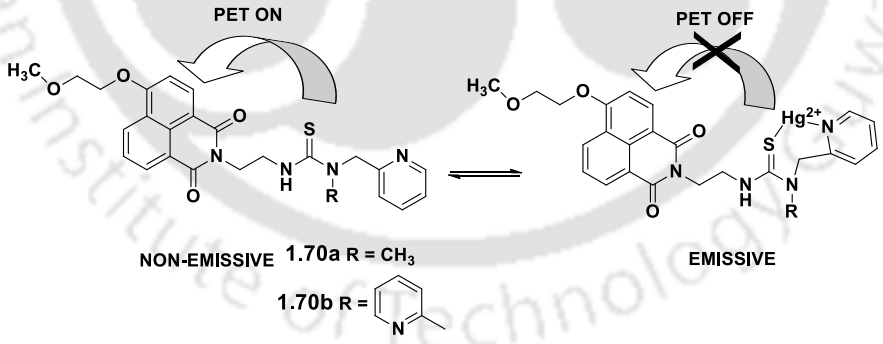

Scheme 1.7: Fluorescence behavior of **1.70a** and **1.70b** upon interacting with Hg^{2+}.

1.8: Cyclic Imides as Sensors for Nitroaromatics

Due to their interesting π-stacking ability, and ability to formed strong charge-transfer complexes influencing photoluminescence properties, cyclic imide derivatives are promising sensors for the recognition of nitro-aromatics. There are different types of interactions between cyclic imide ring and analytes, which lead to different fluorescence mechanisms

such as photo-induced electron transfer (PET), resonance energy transfer (RET), intramolecular charge transfer (ICT) etc. The fluorescence sensing of the nitro-phenols using cyclic imide derivatives leads to change their fluorescence. Nitroaromatic derivatives are in general known to be explosive and pollutant.[117]

Naphthalimide based compounds **1.71** with pyridine group, showed high sensitivity and selectivity towards 2,4,6-trinitrophenol (2,4,6-TNP). The fluorescence emission changes occurred through intramolecular charge transfer mechanism. The electron transfer take place from the electron-rich **1.71** molecule to the electron deficient 2,4,6-TNP resulting the formation of charge transfer complex between **1.71** and 2,4,6-TNP as shown in Scheme 1.8.[118] Another pyridine based naphthalimide compounds **1.72** and **1.73** also detects nitrophenols through ICT mechanism by forming supramolecular hydrogels.[119]

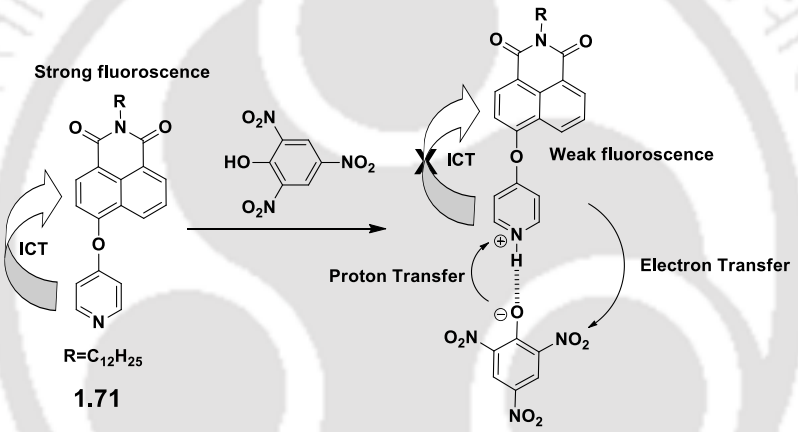

Scheme 1.8: Intramolecular charge transfer mechanism in compound **1.71**.

1,8-Naphthalimide derivatives conjugated with sulfonamide **1.74** and **1.75** with one and two naphthalimide units are also useful in detection of 2,4,6-TNP in water. Compound **1.75** showed aggregation-induced emission enhancement (AIEE) in DMSO/water solvent mixture, and this emission was completely quenched by two equivalents of 2,4,6-TNP.[120]

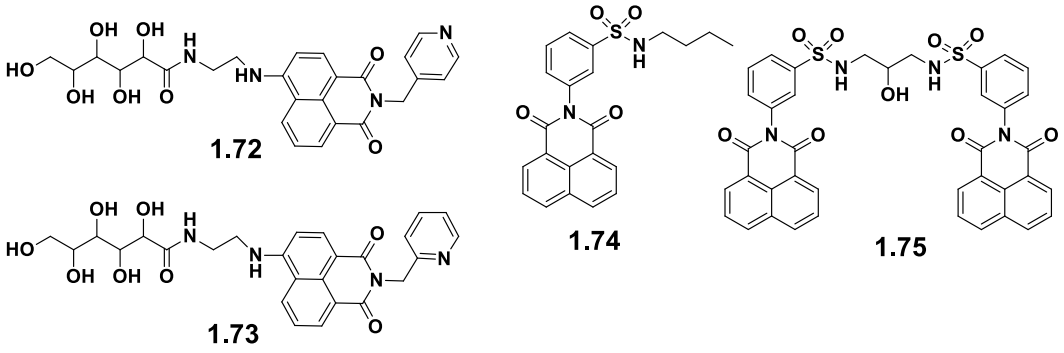

Chemosensor **1.76**[121] has been found to shows high selectivity to bind 2, 4-dinitrophenol (2,4-DNP) and 2,4,6-TNP over other nitroaromatics. The absorption spectra of **1.76** showed an absorption band at 429 nm got increased along with the appearance of new band at 378 nm in presence of 2,4,6-TNP in acetonitrile solution due to interaction between receptor **1.76** and 2,4,6-TNP, whereas absorption gradually increases in presence of 2,4-DNP. The fluorescence emission of the compound **1.76** was completely quenched by 2,4,6-TNP due to PET mechanism. The calculated limit of detection for 2,4,6-TNP and 2,4-DNP are found to be 1.61×10^{-10} M and 3.83×10^{-10} M, respectively. Fluorescence emission of the compound **1.77** is also sensitive to detect 2,4,6-TNP.[122]

4-Amino-1,8-naphthalimide Troger's base **1.78** has phenylterpyridine unit, it showed aggregation induced emission (AIE). The compound showed red shift in emission spectrum upon increasing polarity of solution which indicate the presence of internal charge transfer (ICT) state due to the push-pull nature of the donating amine and the withdrawing imide. This compound is an effective sensor for 2,4,6-TNP and 2,4-DNP.[123]

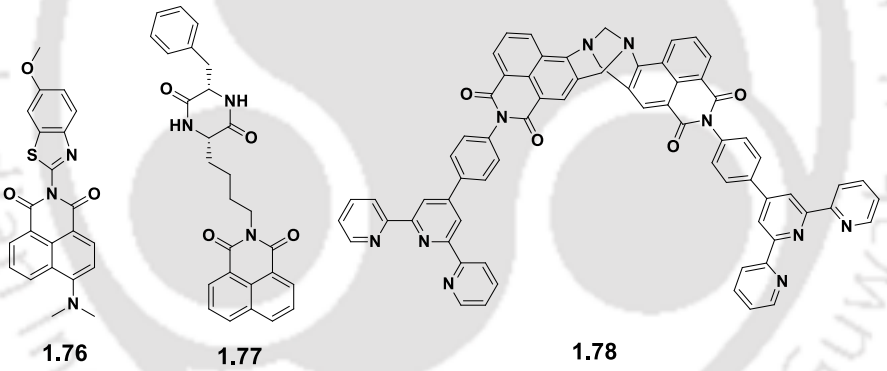

1.76 **1.77** **1.78**

Naphthalene diimide derivative are also used to detect nitrophenols such as compound **1.79** has been shown to be a selective fluorescent chemosensor for 2,4,6-TNP through fluorescence quenching in tetrahydrofuran/water (1:9) solvent mixture with 0.90 ppm detection limit.[124]

The works on detection of 2,4,6-TNP has been extended to metal-organic frameworks (MOF), for example zinc-MOF **1.80** bearing N,N′-di-(4-pyridyl)-1,4,5,8-naphthalene diimide and 2-aminoterephthalic acid displayed high detection limit of 0.3 ppm in such detection. Selectivity of **1.80** for 2,4,6-TNP over other nitro aromatics is observed because of strong hydrogen bond formed between -NH_2 group of **1.80** and hydroxyl group of 2,4,6-

TNP. Coordination environment around the zinc ion in the asymmetric unit of the MOF **1.80** of the structure determined by X-ray diffraction is shown in below. [125]

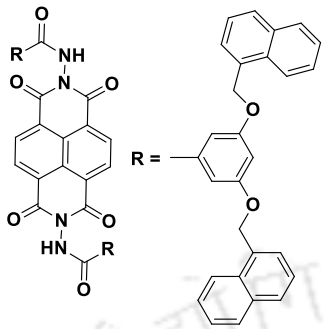

1.79

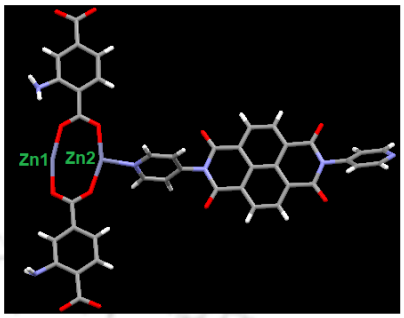

1.80

1.9: Self-assemblies of Cyclic Imide Derivatives

Cyclic imides derivatives are well known to show polymorphism, versatile self-assemblies by forming cocrystals to show interesting material properties. Furthermore self-assemblies of salts and metal complexes provide versatile supramolecular architectures. The supramolecular assemblies of cyclic imides having complementing aromatic stacking interactions and other weak interactions such as C-H···π, O-H···π, N-H···π interactions[126] make them suitable for tuning optical properties. Cyclic imide derivatives form host-guest complexes where stacking among π-systems occur in different ways.[127]

Polymorphism is the ability of a substance to crystallize in different crystal forms.[128] Many cyclic imides based molecules exhibiting potential drug activity shows polymorphism such as two polymorphic forms of 1,8-naphthalimide derivative Lumogen F Violet 570 **1.81** are fully characterized by single crystal X-ray diffraction.[129] The crystals of these polymorphs were obtained from the solution in tetrahydrofuran at room temperature with different evaporation rates 3.9 (slow) mg/min and 89.6 mg/min (fast) respectively. The slowly dried powder sample was blue showing emission peak at 453 nm and fast dried powders was green colour emitting at 508 nm upon emission under a 365 nm light-emitting lamp. Photoluminescence quantum yield (PLQY) of the green powder was 8.2%, whereas 43% for the blue powder. The differences in the PLQY and other spectroscopic properties are due to the stacking interactions adopted by the naphthalimide units in lattices, namely aromatic stacking was weaker in the blue crystal in comparison to the green crystal. The difference in packing arises as a consequence of the conformation

originating from the torsion angles of the alkyl group, as shown in the Scheme 1.9 causing significant packing differences.

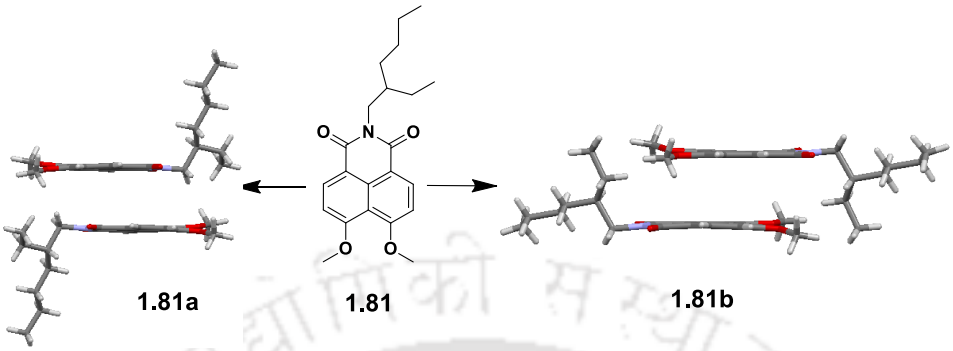

Scheme 1.9: Orientation of two repeating units in the polymorph of **1.81**.

Two cocrystals of 2-hydroxyethylphthalimide **1.82** with 1,3-dihydroxybenzene and 1,3,5-trihydroxybenzene show interesting supramolecular layered structures which are formed through hydrogen bonds and charge-transfer interactions between phthalimide and phenolic partner molecules.[130] These structures are extensively guided by aromatic charge-transfer interactions.

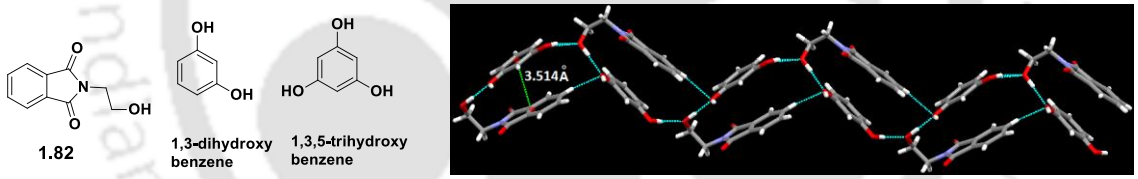

(a) (b)

Figure 1.11: (a) Structure of **1.82** and phenolic coformers and (b) two-dimensional networks of **1.82** with 1,3-dihydroxybenzene showing charge transfer interaction.

Earlier our group showed the formation of extended molecular assemblies through π-deficient and π-rich stacking interactions. N,N´-bis(glycinyl)pyromellitic diimide **1.83** forms molecular complexes with anthracene, phenanthrene, perylene and tetrathiafulvalene.[131] The guest molecule are stacked between pyromellitic rings and forms different types of arrangements such as 1D zig-zag chains and step like arrangements derived from the hydrogen bonds between the carboxylic acid groups of **1.83** and stacking interactions.

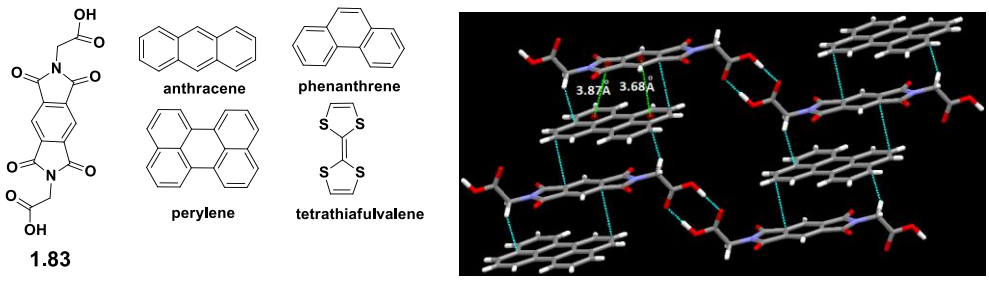

(a) (b)

Figure 1.12: (a) Structure of **1.83** and aromatic guest molecules and (b) 2-D step-like structure of **1.83** with perylene.

Our research group also reported a series of cyclic imide viz. phthalimide and naphthalimide tethered carboxylic acids **1.84a-f** which can form inclusion compounds with pyridine and quinoline. Crystal structures of these complexes revealed that the solvent molecules formed host-guest complexes with the host molecules via different hydrogen bond motif in the solid state. The host molecules have the ability to accommodate the guest molecules in different ratios.[132]

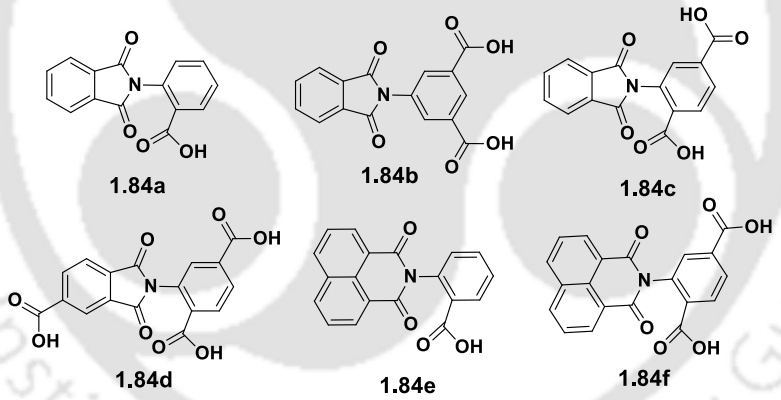

Hydroxybenzoic acid tethered cyclic imide hosts **1.85-1.87** also forms inclusion compounds with pyridine and quinolone. π···π Stacking of aromatic imide rings and hydrogen bonding of carboxylic acid as well as hydroxyl groups lead to the formation higher dimensional supramolecular assemblies. Guest molecules fill the channels and cavities that are formed by interacting of carboxylic acid and hydroxyl groups.[133]

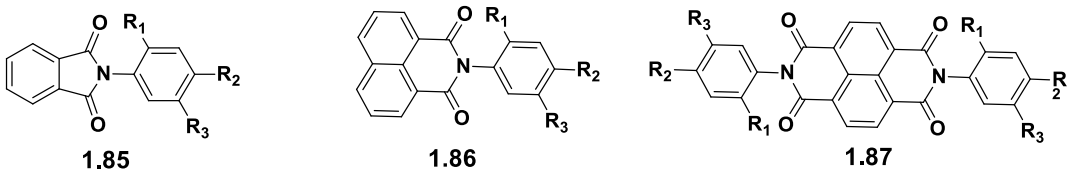

1.85

1.85 a: R_1 = COOH, R_2 = OH, R_3 = H
1.85 b: R_1 = OH, R_2 = COOH, R_3 = H

1.86

1.86 a: R_1 = COOH, R_2 = OH, R_3 = H
1.86 b: R_1 = OH, R_2 = COOH, R_3 = H
1.86 c: R_1 = OH, R_2 = H, R_3 = COOH

1.87

1.87 a: R_1 = COOH, R_2 = OH, R_3 = H
1.87 b: R_1 = OH, R_2 = COOH, R_3 = H
1.87 c: R_1 = OH, R_2 = H, R_3 = COOH

Bis-(N,N´-n-butyl) pyrromelliticdiimide **1.88** and tris-(N,N´,N"-n-butyl) mellitictriimide **1.89** formed H-bonded assemblies with di-N-alkyl thiourea by interacting carbonyl group of cyclic imide and amide N-H group of thiourea derivatives, which decreases the redox potentials of the parent imide compounds. [134]

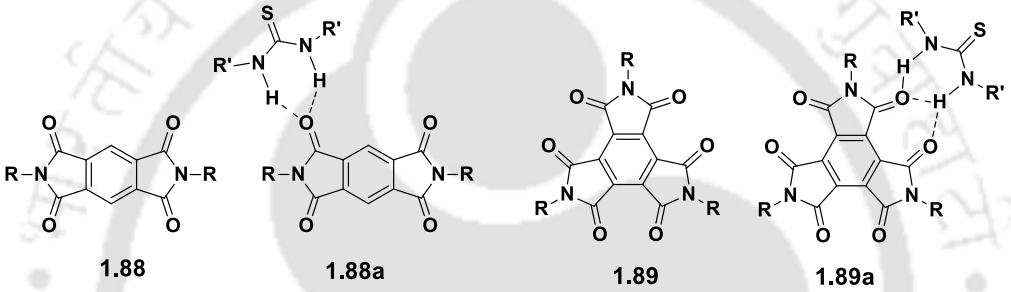

1.88 **1.88a** **1.89** **1.89a**

R= $-CH_2CH_2CH_2CH_3$
R'=$-CH_2CH_3$

A bis-pyridyl based receptor **1.90** was synthesized by Shimizu *et al.* bearing pyromellitic diimide chromophoric unit. It formed charge transfer (CT) complexes with phenols and naphthols (Scheme 1.10). These complexes had varying color with different intensities.[135] The difference in the colorimetric responses are due to electronic structure and combination of the abilities of the guests to form stable hydrogen-bonded complexes.

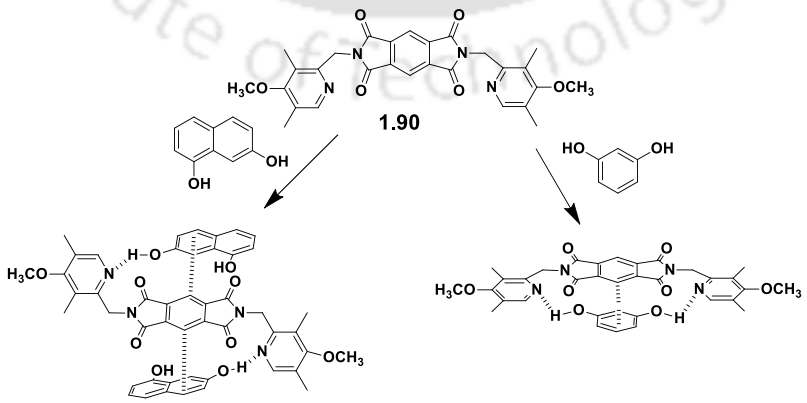

1.90

Scheme 1.10

Scheme 1.10: Inclusion complexes of naphthalene diol and resorcinol.

Our group has reported a series of solvates and salts derived from a Chiral Zwitter ionic host N-(2-Imidazol-5-yl-1-carboxyethyl)-1,8-naphthalimide **1.91** that contain imide and imidazole functionalities.[136] The packing patterns of the solvates and salts is governed by hydrogen bonds, and π-stacking. Chain-like structures and channels of different dimensionalities in the self-assemblies were identified. Guest molecules filled the pores of the channel-like structures that were formed by interactions of carboxylate and imidazole units.

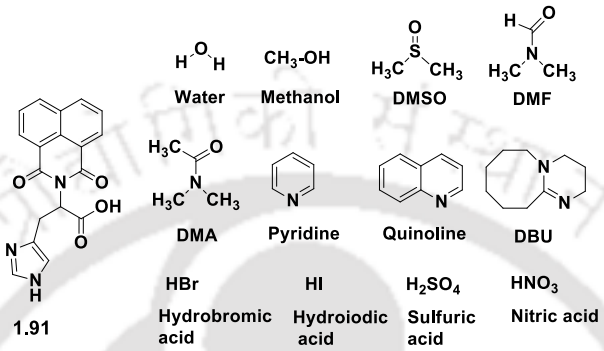

Figure 1.13: Structure of **1.91** and partner solvents and mineral acids.

The luminescent properties of an imide derivative get modulated through supramolecular cocrystal formation. Hisaeda *et al.* showed such example in multicomponent crystals of naphthalenediimide derivative **1.92**, tris-(pentafluorophenyl)borane with aromatic guest molecules listed in Figure 1.14a.[137] Depending on the ionization potential of the aromatic guest molecule each showed multicolour photoluminescence ranging between deep blue to orange (450-600 nm). Electron-deficient naphthalenediimide **1.92** linked to tris(pentafluorophenyl)borane by boron-nitrogen dative bonds accommodate electron-rich aromatic guest molecules through charge-transfer interactions.

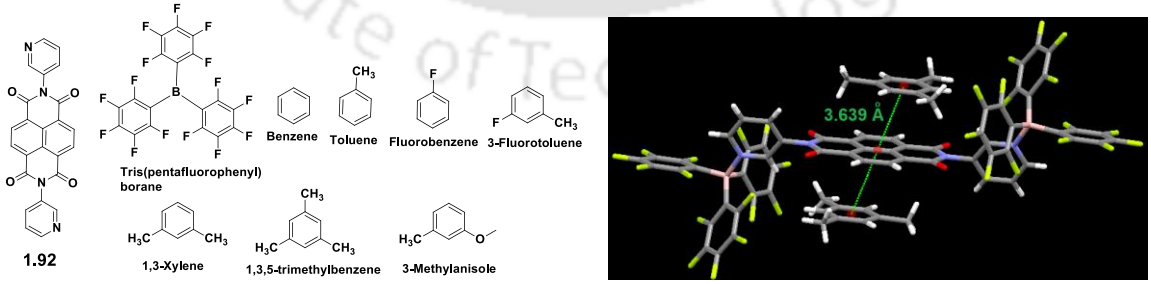

(a) (b)

Figure 1.14: **(a)** Compound **1.92** and the cocrystal partners; (b) crystal structure of **1.92** with 1,3,5-trimethylbenzene.

Cocrystals of N,N′-di-(4-pyridyl)-1,4,5,8-naphthalene diimide **1.93** with naphthalene derivatives (Figure 1.15a) showed excited state charge transfer interactions between electron-deficient **1.93** and electron-rich naphthalene derivatives.[138] The cocrystals showed guest-dependent colour-tunable emissions. A two-dimensional supramolecular network of **1.93** with naphthalene is shown in Figure 1.15b. The nitrogen atoms of the pyridine rings contribute as hydrogen bond acceptor of the C-H···N bonds involved in formation of assembly of host molecules into 1D chains. A second set of π…π stacking interactions between the aromatic π-donor guest molecules and electron deficient π-acceptor part of the host molecules link those chains to form sheets.

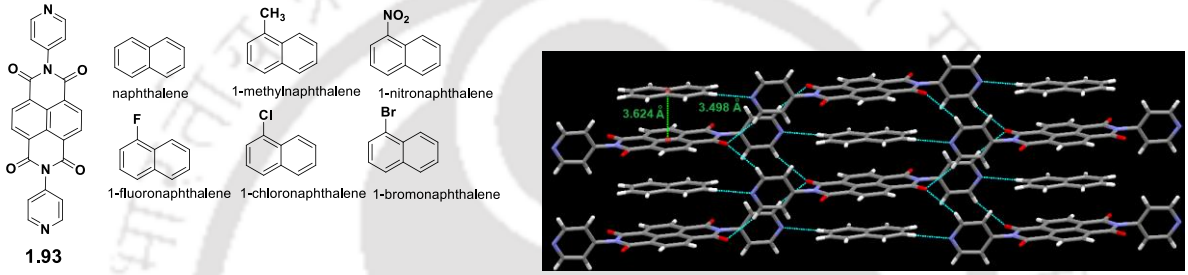

(a) (b)

Figure 1.15: (a) Compound **1.93** and guest molecules and (b) two-dimensional networks in cocrystal of **1.93**.

Due to existence of multiple ways of possibility to form hydrogen bonds, different supramolecular synthons arises from the same functional groups. Such cases lead to polymorphs or solvates. For example, crystallization of silver complex of compounds **1.94a** and **1.94b** containing bis(pyrazolyl)methane and 1,8-naphthalimide groups resulted in the formation of two solvates in each case.[139] π…π Stacking and other noncovalent interactions, such as, C-H…π and weak C-H…O bonds led to the formation of higher dimensionality supramolecular architectures.

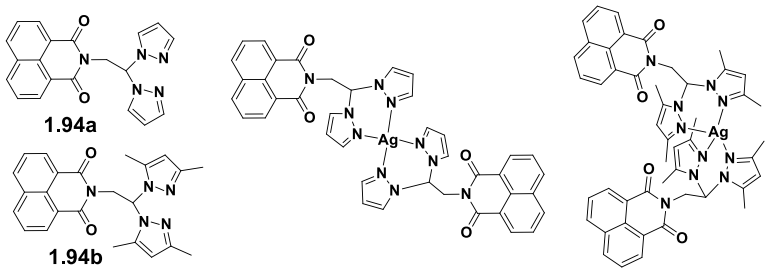

(a) (b)

Figure 1.16: (a) two ligands **1.94a-b**, and (b) Cationic part of the Ag(I) complex of **1.94a** and **1.94b**.

Tris(pyrazolyl)methane based 1,8-naphthalimide compound **1.95** in which the ligand form syn **1.95a** and anti **1.95b** conformation (Scheme 1.11) with divalent copper, iron and cadmium ions. Strong π···π stacking among the 1,8-naphthalimide rings dominate packing patterns of these supramolecular structures.[140]

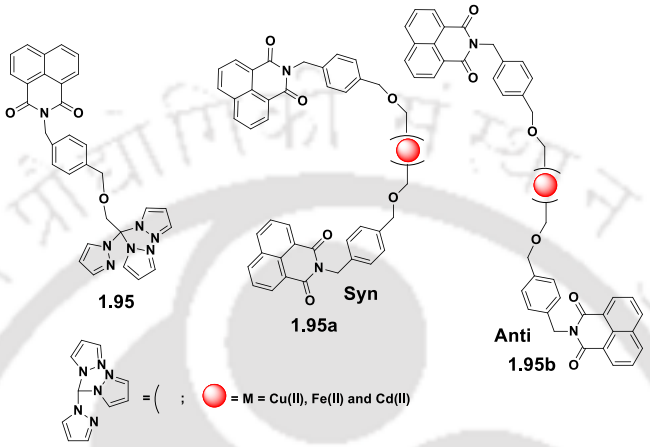

Scheme 1.11

Gunnlaugsson *et al.* reported different mononuclear and dinuclear copper complexes of pyridyl 4-nitro-1,8-naphthalimide based ligands **1.96a** and **1.96b** (Scheme 1.12). In these metal complexes, naphthalimide units provide different π-interactions such as π···π, anion···π, nitro···π, solvent···π and C=O···π interactions controlling the overall supramolecular assemblies.[141]

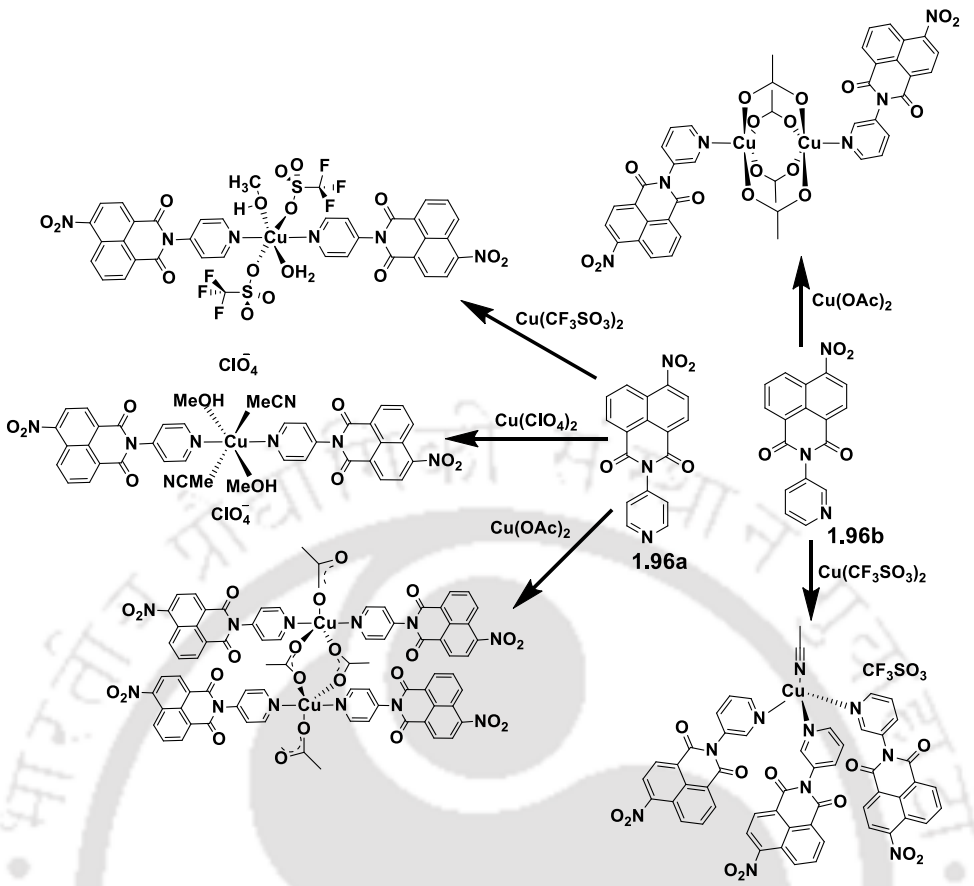

Scheme 1.12: Formation of variety of Cu(II) complexes from **1.96a** and **1.96b**.

The complexes of ligand, **1.92** with divalent cobalt, zinc, cadmium and mercury have versatility in dimensions. These structures are stabilized by hydrogen bonds and π···π interactions in their respective crystal lattice. Counter anions of these complexes also play important roles. Different assemblies, such as 1D chain, metallacycle, grid network and herringbone network formed by different metal salts are shown in the Scheme 1.13.[142]

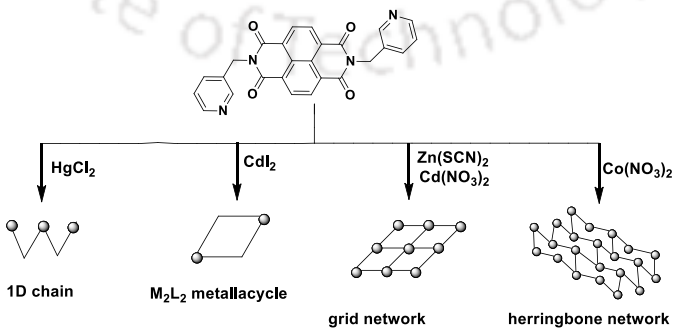

Scheme 1.13: Different types of self-assemblies of coordination polymer of **1.92**.

Gunnlaugsson *et al.* designed two pyridine based ligands namely **1.97** and **1.98** and also a series of coordination polymers of **1.97** with d-block metal ions. Complexes such as poly-[Zn(**1.97**)Cl_2].3(C_3H_6O) **1.97a**, poly-[$ZnCl_2$(**1.97**)].CH_3CN **1.97b**, [H_2**1.97**][$ZnCl_4$].2H_2O **1.97c** and [Ag**1.97**]SbF_6 **1.97d** were formed from the different salts on reaction with **1.97** in different conditions.[143] Due to the flexibility and π…π stacking interactions of the **1.97**, the complexes adopt different conformations in polymeric structures. The reaction **1.97** with divalent copper ions formed dihydrochloride salt, whereas the compound **1.98** did not form isolable metal complex.

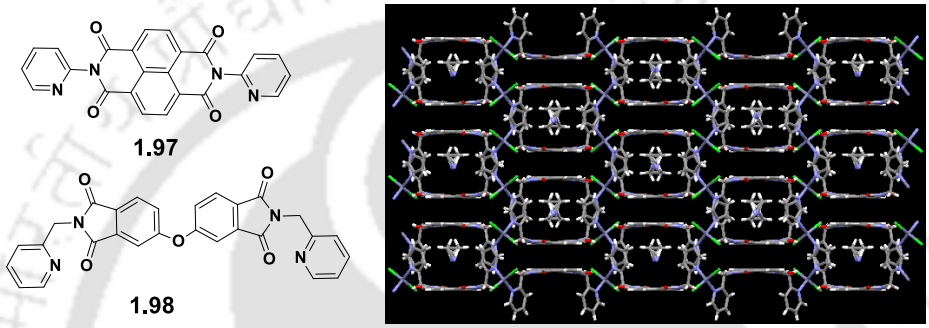

Figure 1.17: (a) Structures of the **1.97** and **1.98** and (b) Solvent assisted channels in complex **1.97b**.

1.10: Scope of the Present Work

From the above literature survey, it is clear that cyclic imide derivatives and its analogues containing heterocyclic ring are suitable building blocks for crystal engineering. Among the different cyclic imides, the naphthalimide derivatives show interesting optical properties[144] and they have great potential in medicinal chemistry. Some of those show high antibacterial,[145] antitumor activity[146] and high index as DNA binders.[147] The discussions also made it evident that the self-assemblies of cyclic imide molecules leading to supramolecular architectures serve as host and have vast possibility for guest binding. Some of them were used for the selective separation of small organic molecules. Cyclic imide derivatives have scopes to modulate π-π interactions, along with other interplaying weak interactions.The dipolar nature and electron deficient properties of cyclic imides make them versatile in providing wide varieties of supramolecular assemblies. some of the stacking interaction between naphthalimide rings are shown in Figure 1.18.

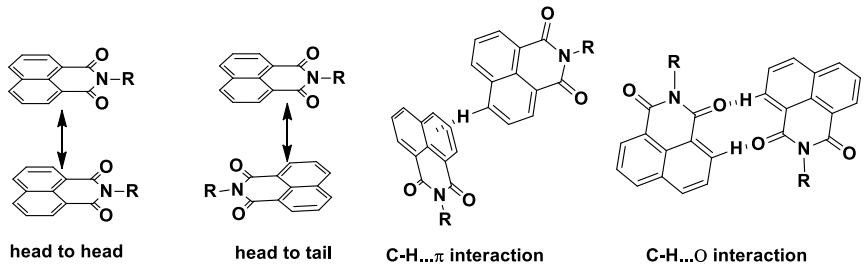

Figure 1.18: Different stacking interactions and hydrogen bonds between naphthalimide rings.

Moreover, anchoring a unit having one or more electronegative heteroatom such as nitrogen to the cyclic imide would provide sites for additional interactions for new supramolecular assemblies. Furthermore, those additional heteroatoms upon protonation would interact with different anions to give rise to new charge-assisted assemblies of cyclic imides derivatives.

Imidazole ring containing fluorogenic small molecules are well known for colorimetric and fluorescent sensing of different analytes and they generate interest for enzyme activities[148] and are used as ionic liquids.[149] Many imidazole derivatives are studied for their therapeutic activities such as antibacterial,[150] antifungal[151] and antitumor activity.[152] The imidazole ring tethered to fluorophores play important roles to modulate emission property upon changing environment and conformers.[153] Phenol-imidazole interactions control activities of many biological enzymes and influence photoluminescence properties of many biological systems.[154] Several imidazole based cyclic imide derivatives and their supramolecular assemblies were studied by our groups such as 2-(3-(1H-imidazol-1-yl)propyl)isoindoline-1,3-dione **1.99** forms anion dependent copper (II) complexes. It forms mononuclear complexes **1.99a** and **1.99b** either in case of copper (II) chloride or nitrate whereas a three dimensional coordination polymer **1.99c** was formed with the reaction of copper(II) acetate through ring opening reactions as shown in scheme 1.14.[155]

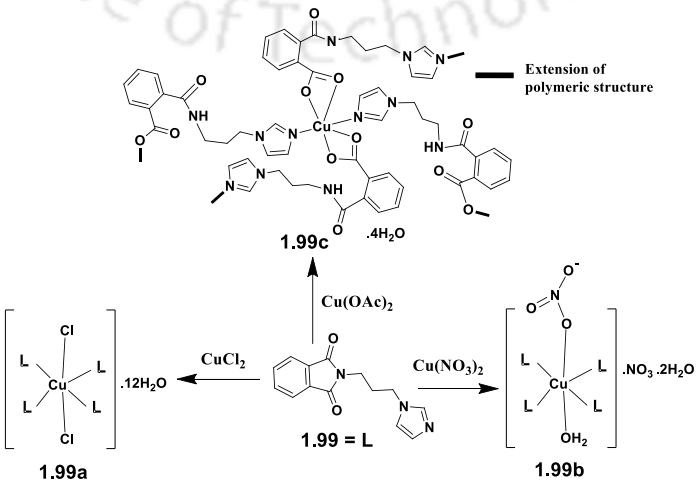

Scheme 1.14: Different copper complexes of an imidazole tethered cyclic imide ligand.

N-(3-imidazol-1-yl-propyl)-1,8-naphthalimide **1.100** forms divalent transition metal complexes of manganese, cobalt, zinc, cadmium and mercury by occupying different geometries. The compound **1.100** having bend orientation in the isomorphous complexes such as [M**1.100**$_2$Cl$_2$] (M = Zn, Cd, Hg) with distorted tetrahedral geometry of each complexes. When thiocyanate as counter anion the ratio of the ligand to the metal ions varied; such as, 1:2 complex was formed with zinc thiocyanate and 1:3 with cadmium thiocyanate. [Zn**1.100**$_2$(SCN)$_2$] has a distorted tetrahedral and [Cd**1.100**$_3$(SCN)$_2$DMF]·DMF has distorted octahedron geometry. The thiocyanate complexes of (M = Mn, Co) [M**1.100**$_4$(SCN)$_2$]·2CH$_3$CN also have distorted octahedral geometry in which the ligands are at axial positions.[156]

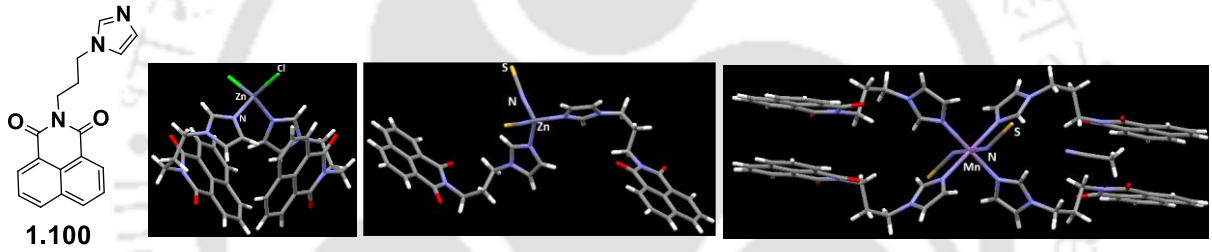

Figure 1.19: (a) Compound **1.100**, structure of the complexes (b) [Zn**1.100**$_2$Cl$_2$], (c) [Zn**1.100**$_2$(SCN)$_2$] and (d) [Mn**1.100**$_4$(SCN)$_2$]·2CH$_3$CN showing different orientations of ligand **1.100**.

The reaction of N,N´-bis(3-imidazol-1-yl-propyl)-pyromelliticdiimide **1.101** with AgSbF$_6$ and AgNO$_3$ formed 1D polymeric chain structures such as [Ag**1.101**.SbF$_6$.CH$_2$Cl$_2$] **1.101a** and [Ag**1.101**.NO$_3$.MeOH] **1.101b** respectively.[157] The complex **1.101a** has catenation-like arrangement in 1D chains whereas complex **1.101b** has a triple-stranded helical structure formed by hydrogen bonds and other weak interactions.

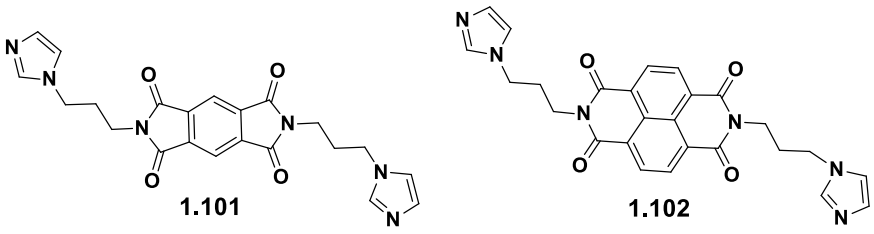

Our group has reported a series of inorganic salts by treating **1.102** with different mineral acids. It is found that the structure of these salts are influenced by type of anions and mainly dependent on the shape and charge on the anions. The compound **1.102** shows anion dependent fluorescence emission, the emission was quenched by hydrochloric and hydrobromic acid because of anion-π interactions of the chloride and bromide with **1.102** whereas it shows fluorescence enhancement with perchloric, sulphuric, phosphoric and nitric acid by protonation of **1.102**.[158]

Thus, imidazole containing cyclic imide derivatives provide new scopes in formation of new self-assemblies. They are useful materials for anion and cation binding as well as for molecular recognition. 2,4,6-TNP is explosive and environmental pollutant.[159] So the detection of 2,4,6-TNP and other pollutant phenols are very important for public safety and security. We proposed here to utilize aggregation induced emission of imidazole based cyclic imides for detection of 2,4,6-TNP and other phenolic compounds in water. Another problem proposed here is to avoid the interference of iron ion that is found abundant in water and generally interferes in detection of nitrophenolic compounds by fluorescence technique. Furthermore, due to ability of the cyclic imide derivatives to form cocrystals an integrated process in detection as well as crystallization of nitrophenolic compound along with iron ions would provide a remedy to the issue on separation and detection.

Functionalization of fluorogenic small molecules with imidazole and pyridine tethers are used in molecular recognition. They provides site for coordination to metal ion and hence to modulate emission properties at a remote site to which it is anchored. Thus, imidazole and pyridine based imides are explored in the work presented in this thesis to understand their self-assemblies and optical properties. In anticipation of new avenues on utilities of cyclic imide derivatives in the form of salts, cocrystals and metal complexes, structural aspects, fluorescence emission and other spectroscopic studies were undertaken in the works presented in this thesis.

1.11: References:

1. (a) J. M. Lehn, *Proc. Nat. Acad. Sci*., USA, 2002, **99**, 4763-4768; (b) J. M. Lehn, Supramolecular Chemistry: Concepts and Perspectives, VCH, Weinheim, 1995.

2. J. M. Lehn, *Angew. Chem., Int. Ed*., 1988, **27**, 89-112.

3. (a) M. J. Webber, R. Langer, *Chem. Soc. Rev.*, 2017, **46**, 6600-6620; (b) K. Kawakami, M. Ebara, H. Izawa, N. M. Sanchez-Ballester, J. P. Hill, K. Ariga, *Current Medicinal Chemistry*.,

2012, **19**, 2388-2398; (c) J. Sunamoto, *Advanced Biomaterials in Biomedical Engineering and Drug Delivery Systems*., Springer, Tokyo, 1996, 76-80.

4. E. A. Meyer, R. K. Castellano, F. Diederich, *Angew. Chem. Int. Ed. Eng*., 2003, **42**, 1210-1250.

5. Z. Feng, T. Zhang, H. Wang, B. Xu, *Chem. Soc. Rev.*, 2017, **46**, 6470-6479.

6. X. Y. Ling, D. N. Reinhoudt, J. Huskens, *Pure Appl. Chem.*, 2009, **81**, 2225-2233.

7. S. v. Dun, C. Ottmann, L. G. Milroy, L. Brunsveld, *J. Am. Chem. Soc*., 2017 **139**, 13960-13968.

8. X. Ma, Y. Zhao, *Chem. Rev*., 2015, 115, **15**, 7794-7839.

9. S. Erbas-Cakmak, D. A. Leigh, C. T. McTernan, A. L. Nussbaumer, *Chem. Rev*., 2015, **115**, 10081-10206.

10. Q. Yan, K. Cai, D. Zhao, *Phys. Chem. Chem. Phys*., 2016, **18**, 1905-1910.

11. G. Beobide, O. Castillo, A. Luque, U. G-. Couceiro, J. P. Garcıa-Teran, P. Roman, *Inorg. Chem*., 2006, **45**, 5367-5382.

12. J. A. Whiteford, C. V. Lu, P. J. Stang, *J. Am. Chem. Soc*., 1997, **119**, 2524-2533.

13. (a) J. M. Lehn, *Pure Appl. Chem.*, 1978, **50**, 871-892; (b) J. M. Lehn, *Acc. Chem. Res*., 1978, **11**, 49-57.

14. S. K. Burley, G. A. Petsko, *Science*, 1985, **229**, 23-28.

15. (a) J. C. Ma, D. A. Dougherty, *Chem. Rev*., 1997, **97**, 1303-1324: (b) P. B. Crowley, A. Golovin, *Proteins Struct. Funct. Bioinf*., 2005, **59**, 231-239.

16. (a) D. Quinonero, C. Garau, C. Rotger, A. Frontera, P. Ballester, A. Costa, P. M. Deya, *Angew. Chem., Int. Ed. Eng*., 2002, **41**, 3389-3392; (b) C. Garau, A. Frontera, D. Quinonero, P. Ballester, A. Costa, P. M. Deya, *ChemPhysChem*., 2003, **4**, 1344-1348; (c) D. Quinonero, A. Frontera, C. Garau, P. Ballester, A. Costa, P. M. Deya, *ChemPhysChem*., 2006, **7**, 2487-2491.

17. A. Gil, V. Branchadell, M. J. Calhorda, *RSC Adv*., 2016, **6**, 85891-85902.

18. (a) J. P. Sauvage, *Acc. Chem. Res*., 1998, **31**, 611-619; (b) M. Fujita, *Acc. Chem. Res*., 1999, **32**, 53-61; (c) D. L. Caulder, K. N. Raymond, *Acc. Chem. Res*., 1999, **32**, 975-982; (d) S. Leininger, B. Olenyuk, P. J. Stang, *Chem. Rev*., 2000, **100**, 853-908.

19. S. Sivakova, S. J. Rowan, *Chem. Soc. Rev*., 2005, **34**, 9-21.

20. F. Zeng, S. C. Zimmerman, *Chem. Rev*., 1997, **97**, 1681-1712.

21. S. Roche, C. Haslam, H. Adams, S. L. Heath, J. A. Thomas, *Chem. Commun*., 1998, 1681-1682.

22. M. Chiper, M. A. R. Meier, D. Wouters, S. Hoeppener, C. A. Fustin, J. F. Gohy, U. S. Schubert, *Macromolecules*., 2008, **41**, 2771-2777; (b) S. J. Rowan, J. B. Beck, *Faraday Discuss*., 2005, **128**, 43-53.

23. A. Harada, K. Kobyashi, Y. Takashima, A. Hashidzume, H. Yamaguchi, *Nature Chem.*, 2011, **3**, 34-37.

24. F. Diederich, Symposium on Molecular Architecture Volume **67** Number 10 October 1990. 813.

25. B. H. Northrop, F. Africo, N. Tangchiavang, J. D. Badjic, J. F. Stoddart, *Org. Lett.*, 2006, **8**, 3899-3902.

26. V. Balzani, A. Credi, F. M. Raymo, J. F Stoddart, *Angew. Chem. Int. Ed*., 2000, **39**, 3348-3391.

27. G. R. Desiraju, *Acc. Chem. Res*., 1991, **24**, 290-296.

28. G. R. Desiraju, *Acc. Chem. Res*., 1996, **29**, 441-449.

29. (a) G. R. Desiraju, *Acc. Chem. Res.*, 1991, **24**, 290-296; (b) G. R. Desiraju, *Acc. Chem. Res.*, 1996, **29**, 441-449; (c) J. A. R. P. Sarma, G. R. Desiraju, *Acc. Chem. Res.*, 1986, **19**, 222-228.

30. T. Steiner, *Angew. Chem. Int. Ed*., 2002, **41**, 48-76.

31. (a) G. R. Desiraju, *Acc. Chem. Res*., 2002, **35**, 565-573; (b) G. R. Desiraju, *Angew. Chem. Int. Ed. Eng*., 2011, **50**, 52-59; (c) G. R. Desiraju, *Angew.Chem., Int. Ed. Engl*., 1995, **34**, 2311-2327; (d) G. A. Jeffrey, *An Introduction to Hydrogen bonding*, Oxfod University Press, London, **1997**.

32. J. D. Watson, F. H. Crick, *Nature*., 1953, **171**, 737-738.

33. I. Rozas, I. Alkorta, J. Elguero, *J. Phys. Chem. A*., 1998, **102**, 9925-9932.

34. G. R. Desiraju, T. Steiner, The weak hydrogen bond in structural chemistry and biology. 1999, Oxford: Oxford University Press.

35. M. C. Etter, J. C. MacDonald, J. Bernstein, *Acta. Crystallogr*., 1990, **B46**, 256-262.

36. (a) G. R. Desiraju, *Angew. Chem. Int. Ed. Eng*., 1995, **34**, 2311-2327; (b) G. R. Desiraju, *Chem. Commun*., 1997, 1475-1482.

37. E. Peresypkina, A. Virovets, M. Scheer, *Cryst.Growth Des*., 2016, **16**, 2335-2341.

38. J. D. Hartgerink, E. Beniash, S. I. Stupp, *Science*., 2001, **294**, 1684-1688.

39. (a) K. Ariga, M. Nishikawa, T. Mori, J. Takeya, L. K. Shrestha, J. P. Hill, *Sci Technol Adv Mater*., 2019, **20**, 51-95; (b) S. I. Stupp, L. C. Palmer, *Chem. Mater*., 2014, **26**, 507-518.

40. B. M. Craven, E. A. Vizzini, M. M. Rodrigues, *Acta Cryst*., 1969, **B25**, 1978-1993.

41. H. E. Bakkali, A. Castineiras, I. G. Santos, J. M. G. Perez, J. N. Gutierrez, *Cryst. Growth Des.*, 2014, **14**, 249-260.

42. J. Teyssandier, S. D. Feyter, K. S. Mali, *Chem. Commun*., 2016, **52**, 11465-11487.

43. (a) J. R. Williamson, M. K. Raghuraman, T. R. Cech, *Cell*., 1989, **59**, 871-880; (b) V. Abet, R. Rodriguez, *New J. Chem*., 2014, **38**, 5122-5128.

44. K. T. Holman, A. M. Pivovar, J. A. Swift, M. D. Ward, *Acc. Chem. Res*., 2001, **34**, 107-118.

45. A. M. Beatty, *Coordination Chemistry Reviews*., 2003, **246**, 131-143.

46. (a) J. Iwanejko, E. Wojaczynska, *Org. Biomol. Chem.*, 2018, **16**, 7296-7314; (b) A. Kumar, T. Janes, N. A. E. Jalapa, D. Milstein, *J. Am. Chem. Soc*., 2018, **140**, 7453-7457; (c) J. L. Segura, H. Herrera, P. Bauerle, *J. Mater. Chem.*, 2012, **22**, 8717-8733.

47. (a) P. Y. Reddy, S. Kondo, Y. U. T. Toru, *J. Org. Chem*., 1997, **62**, 2652-2654; (b) S. Chandrasekhar, M. Takhi, G. Uma, *Tetrahedron Lett.*, 1997, **38**, 8089-8092; (c) M. L. Cheney, G. J. McManus, , J. A. Perman, Z. Wang, M. J. Zaworotko, *Cryst. Growth Des*., 2007, **7**, 616-617; (d) Z. G. Le, Z. C. Chen, Y. Hu, Q. G. Zheng, *Synthesis*., 2004, 208-212; (e) S. E. Sen, S. L. Roach, *Synthesis*, 1995, 756-758; (f) S. Rouhani, K. Gharanjig, M. H. Nezhad, *Green Chemistry Letters and Reviews*., 2014, **7**, 174-178.

48. (a) H. T. Li, Z. Q. Jiang, J. Zheng, X. Wang, Y. Pan, F. Wang, S. Q. Yu, Res, *Chem. Intermed*., 2006, **32**, 43-57; (b) A. S. Oshchepkov, R. R. Mittapalli, O. A. Fedorova, E. A. Kataev, *Chem. Eur. J*., 2017, **23**, 9657-9665.

49. (a) V. Bojinov, T. Konstantinova, *Dyes and Pigments*., 2002, **54**, 239-245; (b) M. Li, H. B. Ge, V. Mirabello, R. L. Arrowsmith, G. KociokKohn, S. W. Botchway, W. H. Zhu, S. I. Pascu, T. D. James, *Chem. Commun*., 2017, **53**, 11161-11164; (c) K. Yang, K. G. Leslie, S. Y. Kim, B. Kalionis, W. Chrzanowski, K. A. Jolliffe, E. J. New, *Org. Biomol. Chem*., 2018, **16**, 619-624.

50. (a) D. V. Pogozhev, M. T. Bezdek, P. A. Schauer, C. P. Berlinguette, *Inorg. Chem*., 2013, **52**, 3001-3006; (b) X. Qian, K. Zhu, K. Chen. *Dyes Pigm*., 1989, **11**, 13-20.

51. (a) D. Kolosov, V. Adamovich, P. Djurovich, M. E. Thompson, C. Adachi, *J. Am. Chem. Soc*., 2002, **124**, 9945-9954; (b) R. F. Jin, S. S Tang, W. D. Sun, *Tetrahedron*., 2014, **70**, 47-53.

52. (a) K. Maruyama, Y. *J.* Kubo., *Org. Chem*., 1985, **50**, 1426-1435; (b) M. Freccero, E. Fasani, A. Albini, *J. Org. Chem*., 1993, **58**, 1740-1745.

53. J. Gawronsky, F. Kazmierczak, K. Gawronska, U. Rychlewska, B. Norden, A. Holmen, *J. Am. Chem. Soc*., 1998, **120**, 12083-12091.

54. (a) H. D. P. Ali, P. E. Kruger, T. Gunnlaugsson, *New J. Chem*., 2008, **32**, 1153-1161; (b) S.V. Bhosale, S.V. Bhosale, M. B. Kalyankar. S. J. Langford, *Org. Lett*., 2009, **11**, 23, 5418-5421; (c) F. M. Pfeffer, M. Seter, N. Lewcenko, N. W. Barnett, *Tetrahedron Lett*., 2006, **47**, 5241-5245.

55. (a) M. Bahta, N. Ahmed, *Journal of Photochemistry & Photobiology A: Chemistry*., 2019 **373**, 154-161; (b) L. Zong, C. Wang, Y. Song, J. Hu, Q. Li, Z. Li, *RSC Adv*., 2019, **9,** 12675-12680; (c) R. K. Jackson, Y. Shi, X. Yao, S. C. Burdette, *Dalton Trans*. 2010, **39**, 4155-4161; (d) H. Wang, L. Yang. W. Zhang. Y. Zhou. B. Zhao, X. Li,. *Inorganica Chimica Acta*., 2012, **381**, 111-116.

56. D. Staneva, E. V. Tonkova, I. Grabchev, *journal of Photochemistry & Photobiology A: Chemistry*., 2019, **382**, 1119242; (b) A. E. Khalil, M. A. Berghot, M. Gouda. *Chem. Paper*., 2010, **64**, 637-644.

57. (a) M. M. Patil, S. S. Rajput, *Int J Pharm Sci*., 2014 **6**, 8-14; (b) Y. Y. Zhang, C. H. Zhou, *Bioorg. Med. Chem. Lett*., 2011, **21**, 4349-4352.

58. F. d. Campos, R. Correa, M. M. D. Souza, R. A. Yunes, R. J. Nunes, V. C. Filho, *Arzneim.-Forsch./Drug Res*., 2002, **52**, 455-461.

59. (a) A. Kamal, B. S. N. Reddy, G. S. K Reddy, G. Ramesh, *Bioorg. Med. Chem. Lett*., 2002, **12**, 1933-1935; (b) Z. Li, Qi. Yang, X. Qian, *Bioorg. Med. Chem*., 2005, **13**, 4864-4870.

60. F. Hassanzadeh, M. Rabbani, G. A Khodarahmi, A. Fasihi, G.H. Hakimelahi, M. Mohajeri, *Res Pharm Sci*., 2007, **2**, 35-41.

61. G. J. Kaczorowski, O. B. McManus, B. T. Priest, M. L. Garcia, *J. Gen. Physiol*., 2008, **131**, 399-405.

62. (a) M. F. Brana, M. Cacho, A. Gradillas, B. Pascual-Teresa, A. Ramos, *Curr. Pharm. Des*., 2001, **7**, 1745-1780; (b) R. K. Y. Zee-Cheng, C. C Cheng. *J. Med. Chem*., 1985, **28**, 1216-1222.

63. (a) Y. Wang, J. Zhang, M. Li, M. Li, S. Xie, C. Wang, *Chem. Biol. Drug. Des*., 2017, **89**, 670-680; (b) M. D. Tomczyk, K.Z. Walczak, *Eur. J. Med. Chem*., 2018, **159**, 393-422.

64. E. E. L. Jones, N. O. Symonds, S. E. Yates, A. J. Hayes, D. Lloyd, R. Williams, S. J. Coles, P. N. Horton, S. J. A. Pope, *Inorg. Chem*., 2014, **53**, 3788-3797.

65. J. M. C. Jr, G. H. Cocolas, I. H. Hall, *J. Med. Chem*., 1979, **22**, 1399-1401.

66. J. Vamecq, P. Bac, C. Herrenknecht, P. Maurois, P. Delcourt,| J. P. Stables, *J. Med. Chem*., 2000, **43**, 1311-1319.

67. M. H. Norman, D. J. Minick, G. C. Rigdon, *J. Med. Chem*., 1996, **39**, 149-157.

68. A. D. Settimo, G. Primofiore, P. L. Ferrarini, M. Ferrettf, P. L. Barili, N. Tellini, P. Bianchini, *Eur. J. Med. Chem*., 1989, **24**, 263-270.

69. K. Sultana, N. H. Khan, K. Shahid. *Int. J. Pharm. Sci. Rev. Res*., 2014, **28**, 1-5.

70. A. M. A. Azzawi, K. K. H. Al-Obiadi, *Int. J. Res. Pharm. Chem.*, 2016, **6**, 1-8.

71. S. Banerjee, E. B. Veale, C. M. Phelan, S. A. Murphy, G. M. Tocci, L. J. Gillespie, D. O. Frimannsson, J. M. Kelly, T. Gunnlaugsson, *Chem. Soc. Rev.*, 2013, **42**, 1601-1618.

72. (a) M. F. Brana, J. M. C. Berlanga, C. M. Roldan, *DE patent*., 2, 318, 136 (**1973**), C.A. 86; 106, 236 (**1977**); (b) P. F Bousquet, M. F. Brana, D. Conlon, K. M. Fitzgerald, D. Perron, C. Cocchiaro, R. Miller, M. Moran, J. George, X. D. Qian, *Cancer Res*., 1995, **55**, 1176-1180.

73. M. F. Brana, A. M. Sanz, J. M. Castellano, C. M. Roldan, C. Roldan., *Eur. J. Med. Chem*., 1981, **16**, 207-212.

74. (a) M. F. Brana, J. M. Castellano, M. Moran, *Anti-CancerDrug Des*., 1993, **8**, 257-268; (b) M. F. Brana, J. M. Castellano, D. Perron, C. Maher, D. Conlon, P. F. Bousquet, J. George, X. D. Qian, S. P. Robinson, *J. Med. Chem*., 1997, **40**, 449-454.

75. G. Loving, B. Imperiali, *Bioconjugate Chem*., 2009, **20**, 2133-2141.

76. (a) G. Loving, B. Imperiali, *J. Am. Chem. Soc*., 2008, **130**, 13630-13638; (b) E. Socher, B. Imperiali, *ChemBioChem*., 2013, **14**, 53-57.

77. H. Yin, Y. Xu, X. Qian, Y. Li, J. Liu, *Bioorg. Med. Chem. Lett*., 2007, **17**, 2166-2170.

78. A. Kamal, O. Srinivas, P. Ramulu, G. Ramesh, P. P Kumar, *Bioorg. Med. Chem. Lett.*, 2003, **13**, 3577-3581.

79. F. Li, J. Cui, L. Guo, X. Qian, W. Ren, K. Wang, F. Liu, *Bioorg. Med. Chem*., 2007, **15**, 5114-5121.

80. S. Roy, S. Saha, R. Majumdar, R. R. Dighe, A. R. Chakravarty, *Inorg. Chem*., 2009, **48**, 9501-9509.

81. K. J. Kilpin, C. M. Clavel, F. Edafe, P. J. Dyson, *Organometallics*., 2012, **31**, 7031-7039.

82. G. J. Ryan, S. Quinn, T. Gunnlaugsson, *Inorg. Chem*., 2008, **47**, 401-403.

83. S. Tan, K. Han, Q. Li, L. Tong, Y. Yang, Z. Chen, H. Xie, J. Ding, X. Qian, Y. Xu, *Eur. J. Med. Chem*., 2014, **85**, 207-214.

84. J. M. Perez, I. Lopez-Solera, E. I. Montero, M. F. Bran, C. Alonso, S. P. Robinson, C. Navarro-Ranninger, *J. Med. Chem*., 1999, **42**, 5482-5486.

85. S. Banerjee, J. A. Kitchen, S. A. Bright, D. C. Williams, J. M. Kelly, T. Gunnlaugsson, *Chem. Com*mun., 2013, **49**, 8522-8524.

86. C. P. Bagowski, Y. You, H. Scheffler, D. H. Vlecken, D. J. Schmitz, I. Ott, *Dalton Trans*., 2009, 10799-10805.

87. (a) R. Martınez-Manez, F. Sancenon, *Chem. Rev*., 2003, **103**, 4419-4476; (b) P. D. Beer, P. A. Gale, *Angew. Chem., Int. Ed*., 2001, **40**, 486-516.

88. E. Bianchi, K. BowmanJames, E. Gracıa-Espana, *Supramolecular Chemistry of Anions*., Eds.; Wiley-VCH: New York, 1997.

89. (a) M. Kluciar, R. Ferreira, B. D. Castro, U. Pischel, *J. Org. Chem*., 2008, **73**, 6079-6085; (b) U. Pischel, P. Remon, R. Ferreira, *J. Phys. Chem. C*., 2009, **113**, 5805-5811; (c) A. Bamesberger, C. Schwartz, Q. Song, W. Han, Z. Wang, H. Cao, *New J. Chem*., 2014, **38**, 884-888.

90. X. P. Bao, L. Wang, L. Wu, Z. Y. Li, *Supramol. Chem*., 2008, **20**, 467-472.

91. T. Gunnlaugsson, P. E. Kruger, T. C. Lee, R. Parkesh, F. M. Pfeffer, G. M. Hussey, *Tetrahedron Lett*., 2003, **44**, 6575-6578.

92. F. M. Pfeffer, A. M. Buschgens, N. W. Barnett, T. Gunnlaugsson, P. E. Kruger, *Tetrahedron Lett*., 2005, **46**, 6579-6584.

93. F. M. Pfeffer, M. Seter, N. Lewcenko, N. W. Barnett, *Tetrahedron Lett*., 2006, **47**, 5241-5245.

94. D. E. Gomez, L. Fabbrizzi, M. Liechelli, *J. Org. Chem*., 2005, **70**, 5717-5720.

95. J. F Zhang, C. S. Lim, S. Bhuniya, B. R. Cho, J. S. Kim, *Org. Lett*., 2011, **13**, 1190-1193.

96. L. Y. Zhao, G. K. Wanga, J. H. Chen, L. M. Zhang, B. Liu, J. F. Zhang, Q. H. Zhao, Y. Zhou, *Journal Of Fluorine Chemistry*., 2014, **158**, 53-59.

97. K. P. McDonald, R. O. Ramabhadran, S. Lee, K. Raghavachari, A. H. Flood, *Org. Lett*., 2011, **13**, 6260-6263.

98. X. Pang, J. Ge, X. Yu, Y. Li, F. Shen, Y. Wang, J. Ren, *New J. Chem*., 2019, **43**, 10554-10559.

99. L. K. Kumawat, A. A. Abogunrin1, M. Kickham, J. Pardeshi, O. Fenelon, M. Schroeder, R. B. P. Elmes, *Front. Chem*., 2019, **7**, 354.

100. Z. Szakacs, M. Bojtar, D. Hessz, S. Rousseva, I. Bitter, L. Drahos, M. Hilbers, H. Zhang, M. Kallay, M. Kubinyi, *New J. Chem.*, 2019, **43**, 6666-6674.

101. E. B. Veale, G. M. Tocci, F. M. Pfeffer, P. E. Kruger, T. Gunnlaugsson, *Org. Biomol. Chem.*, 2009, **7**, 3447-3454.

102. D. Liu, H. Zhu, J. Shi, X. Deng, T. Zhang, Y. Zhao, P. Qi, G. Yang, H, He, *Anal. Methods*., 2019, **11**, 3150-3154.

103. R. Parkesh, T. C. Lee, T. Gunnlaugsson, *Org. Biomol. Chem*., 2007, **5**, 310-317.

104. Z. Xu, K. H. Baek, H. N. Kim, J. Cui, X. Qian, D. R. Spring, I. Shin, J. Yoon, *J. Am. Chem. Soc*., 2010, **132**, 601-610.

105. C. Lu, Z. Xu, J. Cui, R. Zhang, X. Qian, *J. Org. Chem*. 2007, **72**, 3554-3557.

106. H. Wang, L. Yang, W. Zhang, Y. Zhou, B. Zhao, X. Li, *Inorg. Chim. Acta*., 2012, **381**, 111-116.

107. V. S. Jisha, A. J. Thomas, D. Ramaiah, *J. Org. Chem*., 2009, **74**, 6667-6673.

108. Z. Liu, C. Zhang, X. Wang, W. He, Z. Guo, *Org. Lett*., 2012, **17,** 4378-4381.

109. S. Janakipriya, N. R. Chereddy, P. Korrapati, S. Thennarasu, A. B. Mandal, *Spectrochimica Acta Part A: Molecular and Biomolecular Spectroscopy*., 2016, **153**, 465-470.

110. S. Goswami, K. Aich, A. K. Das, A. Manna, S. Das, *RSC Adv*., 2013, **3**, 2412-2416.

111. Z. Li, Y. Zhou, K. Yin, Z. Yu, Y. Li, J. Ren, *Dyes and Pigments*., 2014, **105**, 7-11.

112. F. Liu, P. Tang, R. Ding, L. Liao, L. Wang, M. Wang, J. Wang, *Dalton Trans.*, 2017, **46**, 7515-7522.

113. J. M. Benoit, W. F. Fitzgerald, A. W. Damman, *Environ. Res*., 1998, **78**, 118-133.

114. X. Guo, X. Qian, L. Jia, *J. Am. Chem. Soc*., 2004, **126**, 2272-2273.

115. C. Y. Li, X. B. Zhang, L. Qiao, Y. Zhao, C. M. He, S. Y. Huan, L. M. Lu, L. X. Jian, G. L. Shen, R. Q. Yu, *Anal. Chem*., 2009, **81**, 9993-10001.

116. M. Vonlanthen, C. M. Connelly, A. Deiters, A. Linden, N. S. Finney, *J. Org. Chem*., 2014, **79**, 6054-6060.

117. (a) S. Singh, *J. Hazard. Mater*., 2007, **144**, 15-28; (b) G. Xue, M. Gao, Z. Gu, Z. Luo, Z. Hu, *Chem. Eng. J*., 2013, **218**, 223-231.

118. X. Cao, N. Zhao, H. Lv, Q. Ding, A. Gao, Q. Jing, T. Yi, *Langmuir*., 2017, **33**, 7788-7798.

119. X. Yu, J. Guo, P. Peng, F. Shen, Y. Li, L. Geng, T. Wang, *Applied Surface Science*., 2019, **487**, 473-479.

120. A. Kumar, P. S. Chae, *Sensors and Actuators*., 2017, **240**, 1-9.

121. P. D. J. Patil, R. D. Ingle, S. M. Wagalgave, R. S. Bhosale, S. V. Bhosale, R. P. Pawar, S.V. Bhosale. *Chemosensors*., 2019, **7**, 38.

122. C. Balachandra, T. Govindaraju, *J. Org. Chem*., 2020, **85**, 1525-1536.

123. J. M. Delente, D. Umadevi, S. Shanmugaraju, O. Kotova, G. W. Watson, T. Gunnlaugsson, *Chem. Commun*., 2020, **56**, 2562-2565.

124. P. Lasitha, E. Prasad, *RSC Adv.*, 2015, **5**, 41420-41427.

125. S. S. Dhankhar, N. Sharma, S. Kumar, T. J. D. Kumar, C. M. Nagaraja, *Chemistry - A European Journal*., 2017, **23**, 16204-16212.

126. (a) T. K. Park, J. Schroeder, J. R. Jr. *J. Am. Chem. Soc*., 1991, **113**, 5125-5127; (b) J. K. Nath, J. B. Baruah, *CrystEngComm*, 2015,**17**, 8575-8595.

127. (a) M. A. Kobaisi, S. V. Bhosale, K. Latham, A. M. Raynor, S. V. Bhosale, *Chem. Rev*., 2016, **116**, 19, 11685-11796; (b) D. L. Reger, J. D. Elgin, P. J. Pellechia, M. D. Smith, B. K. Simpson, *Polyhedron*., 2009, **28**, 1469-1474; (c) D. Singh, J. B. Baruah, *Cryst. Growth Des*., 2012, **12**, 2109-2121; (d) C. P. Carvalho, R. Ferreira, J. P. D. Silva, U. Pischela, *Supramolecular Chemistry*., **2013**, 25, 92-100.

128. W. C. McCrone, *Polymorphism.* In *Physics and Chemistry of the Organic Solid State*; D. Fox, M. M. Labes, A. Weissberger Eds.; Wiley-Interscience: New York, 1965, **2**, 725.

129. K. Jo, S. Lee, A. Yi, T. Jeon, H. H. Lee, D. Moon, D. M. Lee, J. Bae, S. T. Hong, J. Gene, S.G. Lee, H. J. Kim, *ACS Omega*., 2019, **4**, 19705-19709.

130. N. Barooah, R. J. Sarma, J. B. Baruah, *Cryst. Growth Des.*, 2003, **3**, 639-641.

131. N. Barooah, R. J. Sarma, J. B. Baruah, *CrystEngComm*, 2006, **8**, 608-615.

132. D. Singh, P. K. Bhattacharyya, J. B. Baruah, *Cryst. Growth Des*., 2010, **10**, 348-356.

133. D. Singh, J. B. Baruah, *Cryst. Growth Des*., 2012, **12**, 3169-3180.

134. J. B. Carroll, M. Gray, K. A. McMenimen, D. G. Hamilton, V. M. Rotello, *Org. Lett*., 2003, **5**, 3177-3180.

135. R. D. Rasberry, M. D. Smith, K. D. Shimizu, *Org. Lett*., 2008, **10**, 2889-2892.

136. J. K. Nath, A. M. Kirillov, J. B. Baruah, *Cryst. Growth Des*., 2015, **15**, 737-751.

137. T. Ono, M. Sugimoto, Y. Hisaeda, *J. Am. Chem. Soc*., 2015, **30**, 9519-9522.

138. J. J. Liu, L. Teng, S. B. Xia, C. X. He, F. X. Cheng, M. J. Lin, C. C. Huang, *Dyes and pigments.*, 2018, **149**, 59-64.

139. D. L. Reger, R. F. Semeniuc, J. D. Elgin, V. Rassolov, M. D. Smith, *Cryst. Growth Des*., 2006, **6**, 2758-2768.

140. D. L. Reger, E. Sirianni, J. J. Horger, M. D. Smith, *Cryst. Growth Des*., 2010, **10**, 386-393.

141. J. A. Kitchen, P. N. Martinho, G. G. Morgan, T. Gunnlaugsson. *Dalton Trans.*, 2014, **43**, 6468-6479.

142. H. Y. Deng, J. R. He, M. Pan, L. Li, C. Y. Su, *Cryst.EngComm*., 2009, **11**, 909-917.

143. J. I. Lovitt, C. S. Hawes, T. Gunnlaugsson, *CrystEngComm*., 2019, **21**, 207-217.

144. S. Seraj, S. Rouhani, F. Faridbod, *RSC Adv*., 2019, **9**, 17933-17940.

145. Y. Y. Chen, L. Gopala, R. R. Y. Bheemanaboina, H. B. Liu, Y. Cheng, R. X. Geng, C. H. Zhou, *ACS Med. Chem. Lett*., 2017, **8**, 1331-1335.

146. Z. Chen, X. Liang, H. Zhang, H. Xie, J. Liu, Y. Xu, W. Zhu, Y. Wang, X. Wang, S. Tan, D. Kuang, X. Qian, *J. Med. Chem.*, 2010, 53, **6**, 2589-2600.

147. S. Murphy, S. A. Bright, F. E. Poynton, T. McCabe, J. A. Kitchen, E. B. Veale, D. C. Williams, T. Gunnlaugsson, *Org. Biomol. Chem*., 2014, **12**, 6610-6623.

148. R. Breslow, *Acc. Chem. Res*. 1995, **28**, 146-153.

149. (a) X. Mu, N. Jiang, C. Liu, D. Zhang, *J. Phys. Chem*., 2017, **121**, 1133-1139; (b) K. Dong, S. Zhang, D. Wang, X. Yao, *J. Phys. Chem. A*., 2006, **110**, 9775-9782.

150. (a) S. Khabnadideh, Z. Rezaei, A. K. Nezhad, R. Bahrinajafi, R. Mohamadi, A. A. Farrokhroz, *Bioorganic & Medicinal Chemistry Letters*., 2003 **13**, 2863-2865; (b) R. V. Shingalapur, K. M. Hosamani, R.S. Keri, *European Journal of Medicinal Chemistry*., 2009, **44**, 4244-4248.

151. (a) K. D. Cremer, K. D. Brucker, I. Staes, A. Peeters, F. V. d. Driessche, T. Coenye, B. P. A. Cammue, K. Thevissen, *Sci. Rep*., 2016, **6**, 27463; (b) X. M. Peng, G. X. Cai, C. H. Zhou, *Curr. Top. Med. Chem*., 2013, **13**, 1963-2010; (c) G. P. Ellis, C. Epstein, C. Fitzmaurice, L. Golberg, G. H. Lord, *J. Pharm. Pharmacol*., 1964, **16**, 400-407.

152. M. A. Iradyan, N. S. Iradyan, G. M. Stepanyan, F. G. Arsenyan, B. T. Garibdzhanyan, *Pharmaceutical Chemistry Journal*., 2010, **44**, 11-18.

153. (a) Y. Zhang, F. Liu, K. A. Li, *Anal. Chem*., 2004, **76**, 7336-7345; (b) A. Tarai, J. B. Baruah, *New J. Chem.*, 2017, **41**, 10750-10760.

154. (a) Y. D. Cao, Q. Y. Zheng, C. F. Chen, Z. T. Huang, *Tetrahedron Lett*., 2003, **44**, 4751-4755; (b) A. Kundu, S. Karthikeyan, D. Moon, S. P. Anthony, *Journal of Fluorescence*., 2019, **29**, 1359-1369.

155. J. K. Nath, J. B. Baruah, *Inorganic Chemistry Communications*., 2013, **30** 128-132.

156. J. K. Nath, J. B. Baruah, *Inorg. Chem. Front*., 2014, **1**, 342-351.

157. X. Q. Lu, Y. Q. Qiao, J. R. He, M. Pan, B. S. Kang, C. Y. Su, *Crystal Growth & Design*., 2006 **6**, 1910-1914.

158. J. K. Nath, J. B. Baruah, *New J. Chem*., 2013, **37**, 1509-1519.

159. Y. Salinas, R. M. Manez, M. D. Marcos, F. Sancenon, A. M. Castero, M. Parra, S. Gil, *Chem. Soc. Rev*., 2012, **41**, 1261-1296.

Chapter 2: (Part A)

Imidazole-Tethered Phthalimide and Pyromellitic Diimide in Sensing of Picric acid and 2,4-dinitrophenol

2.1.1: Introduction

Crystal engineering has scope to understand optical properties of different self-assemblies.[1] Single crystal X-ray diffraction technique has been extensively used in study to understand the role of weak interactions in assessing those properties. In the recent years, such studies have provided insight on designed-assemblies for sensing various energetic nitro-aromatic compounds.[1e] Some physical properties of organic compounds observed in solution may differ from the one measured with solid sample.[2] It is a well-known fact that weak interactions influence the photo-luminescence properties of many aromatic systems.[3] Photo-luminescence of a component in cocrystal, salt or ligand of a metal complex changes from the original component.[4] Among the weak interactions, π-stacking interactions of a molecule or a component of a molecule plays a key role in influence photophysical and chemical properties.[5]

Cyclic imides occupy a special status among various photoluminscent compounds and shows interesting photophysical properties.[6] Phthalimide and pyromellitic diimide derivatives attract much attention as modulation of their emission properties by various factors, such as solvents, functional groups etc.[7] Most of the photophysical properties of these compounds are studied in solution.[8] The flexible environments in solution where inter-molecular interactions are minimized makes those properties highly dependent on solute-solvent interactions. In solid state, molecules are tightly held together, so inter-molecular interactions become a prominent factor in influencing spectroscopic properties. Thus, a property observed from a solid sample may not be identical as the one observed from the same sample in a confined media.[9] Correlation of a property observed in solid-state with the same property determined through a solution study may lead to incoherence. Thus, it is necessary to take up integrated study on properties in solid as well as in solution to reach conclusions.

Nitro-phenolic compounds are generally explosive and hazardous.[10] The most common example is 2,4,6-trinitrophenol (picric acid), which is highly explosive and used in battle fields.[11] Spectroscopic techniques are generally utilized for detection of particular analytes. Fluorescence spectroscopic technique is one of the most sensitive techniques for recognition

of different analytes. Recognition of different nitroaromatic guests by fluorescence-based organic small molecules,[12] conjugated polymers,[13] metal-organic frameworks,[14] organic-inorganic hybrid materials,[15] luminescent gels,[16] dendrimers,[17] nano-particales[18] have received attention in the recent years due to their toxic nature. In such studies, different aspects of fluorescence emission processes such as turn-on or turn-off or shift in the emission wavelength by changing the fluorescence emission paths are well demonstrated. Among the reported examples of different sensors used for recognition of nitro-aromatic explosive compounds, majority of studies are based on relative sensitivity of the fluorescence emission quenching. There are only few examples that show fluorescence "turn on" while sensing.[19] Due to relatively higher acidity among the organic compounds, the nitrophenols interact with various nitrogen based heterocycles to form salts or cocrystals, among which imidazole derivatives generate additional interest for their role in enzyme activities and supramolecular catalysis.[20] A few of such heterocyclic derivatives also generate interest as ionic liquids.[21] The imidazole compound tethered to fluorophores play an important role to modulate emission upon changing environment and conformers.[22]

Thus, understanding the effect of proton transfer from nitrophenol to an imidazole tethered cyclic imide derivatives would throw light on the possible modulation of the imide fluorophore. Furthermore, such studies would allow insight into structural features of self-assemblies to understand any difference observed from a property in solution than the same property observed in the solid-state study. Hence, we took up structural study of nitrophenolate salts of imidazole tethered phthalimide and pyromellitic diimide derivatives (**Figure 2.1.1)**. The corresponding salts listed in **Fig. 2.1.2** were prepared as a basis to understand the interplay of weak interactions in respective self-assemblies in solid salt.

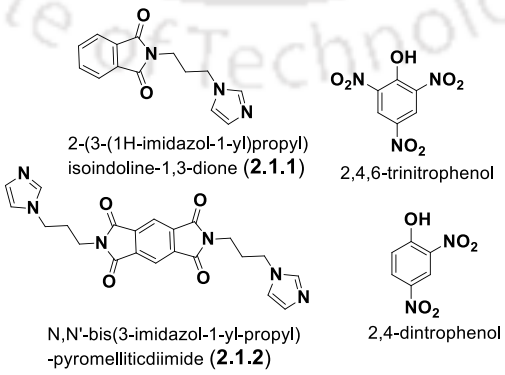

Figure 2.1.1: The imidazole derivatives and nitrophenols.

2.1.2: Synthesis of Nitrophenolate salts 2.1.3-2.1.5

Three different nitrophenolate salts **2.1.3-2.1.5** of imidazole linked cyclic imide derivatives were synthesized and characterized by various spectroscopic and X-ray diffraction techniques. 2,4,6-trinitrophenol (2,4,6-TNP) forms 1:1 and 1:2 anhydrous salts, viz. **2.1.3** and **2.1.4** with 2-(3-(1H-imidazol-1-yl)propyl)isoindoline-1,3-dione (**2.1.1**) and N,N´-bis(3-imidazol-1-yl-propyl)-pyromellitic diimide (**2.1.2**) respectively; whereas, the similar 1:2 salt of 2,4-dinitrophenol **2.1.5** with **2.1.2** was obtained as dihydrate. Crystals from the solution of the **2.1.1** with 2,4-dintrophenol (2,4-DNP) could not be obtained. We attempted the crystallization of the salt from the solution of the **2.1.1** with 2,4-DNP in various solvents such as methanol, dimethylsulphoxide, acetone, tetrahydrofuran, chloroform, dimethylformamide and acetonitrile, but without a success.

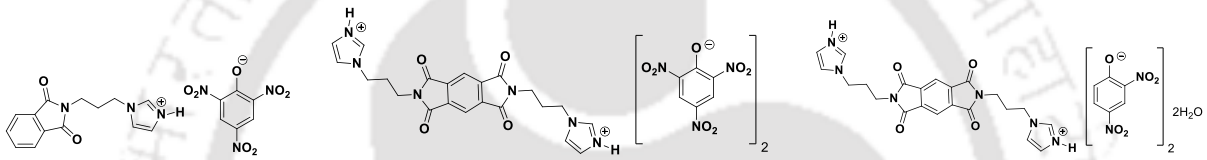

2.1.3 **2.1.4** **2.1.5**

Figure 2.1.2: The nitrophenolate salts.

2.1.3: Structural Descriptions of Nitrophenolate Salts 2.1.3-2.1.5

The crystal structures of the salts have revealed that protonation of the imidazole/s form mono-cation (H**2.1.1**)$^{+}$ or di-cation (H_2**2.1.2**)$^{2+}$ respectively in the respective salt. The self-assembly of the salt **2.1.3** has bifurcated hydrogen bonds involving N1-H···O5 and N1-H···O6 hydrogen bonds. Among these two hydrogen bonds, the former is a charge-assisted hydrogen bond: it has a D···A distance 2.653 Å and ∠D-H···A 161.57. The other N-H···O bond is a moderate hydrogen bond with bond parameters D···A distance 2.897 Å and <D-H…A 119.48. The non-covalently linked sub-assembly of the salt is formed by C11-H···O3 interactions (D···A distance 3.425 Å and <D-H···A 149.89) between neighboring molecules (Figure 2.1.3). These dimeric sub-assemblies further assemble together by O-π interactions between O6 atom of one nitro-group of the 2,4,6-trinitrophenolates and the C18=C19 bond of another ring of the 2,4,6-trinitrophenolate ion. The distance of separation between the centroid of C18=C19 to the O6 atom is 3.187 Å. This provides parallel arrangements among

the rings which are ordered in a sequence as….A-D-D-A…. where D and A represent phthalimide and 2,4,6-trinitrophenolate ring respectively.

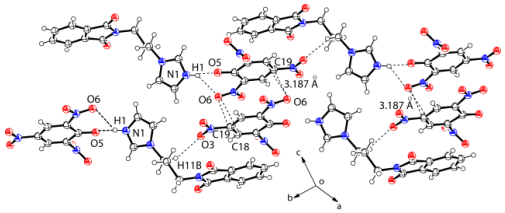

Figure 2.1.3: Hydrogen bonded self-assemblies of the salt **2.1.3**.

The crystal structure of the H_2**2.1.2**.(2,4,6-TNP)$_2$ shows that the cations are organized in step-like arrangements (Figure 2.1.4). The 2,4,6-TNP anions are positioned at slightly oblique orientations above the pyromellitic diimide rings of neighboring salt molecules. The distances of separation between the centroids of parallel pyromelleticdiimide and 2,4,6-trinitro phenolate ring is 4.30 Å. In general, a distance of ~3.5 Å is suitable for the two parallel π-rings to have π-π interaction.[23] The absence of π-interactions in this salt is an interesting point, as the π-π interactions of the aromatic imide derivatives are very commonly observed.[24] The nearest neighbour cations are linked to each other through C=O···H interactions. Such interactions arise from interaction of C=O of the imide-group interacting with C-H of an imidazole ring. The $^+$N-H bond of imidazolium cation is involved in bifurcated N-H···O hydrogen bond (N1-H···O5 and N1-H···O6 respectively) utilizing the O-atom of oxy-anion and O atom of a nitro-group located at *ortho*-position. The nitro group at *para*-position is not involved in such a bifurcated hydrogen bond but gets involved in inter-molecular C-H···O interactions. This C-H···O interaction involving one oxygen atom of this nitro group with C-H bond of the central carbon atom of the propylene unit and another oxygen atom of the same nitro group with a C-H of imidazolium cation (C8-H8B···O9 and C9-H9···O8 Figure 2.1.4) locks the particular orientation of the flexible propylene arms. The intriguing feature in the salt is the presence of O···π interactions. This interaction occurs through one oxygen atom of an *ortho*-nitro group with π-cloud of a C-N bond having an sp^2 carbon center. The π-bond involving the C5=N3 bond of the pyromellitic dimide ring interacts with the O4 atom of one of the nitro-group. The distance of separation from the centroid of C5=N3 to O4 is 2.898 Å, suggesting it to be a relatively strong interaction of such a kind. The C=O of imide is involved in C-H···O interaction, contributing to form a robust $R^2_2(18)$ motif in the self-assembly.

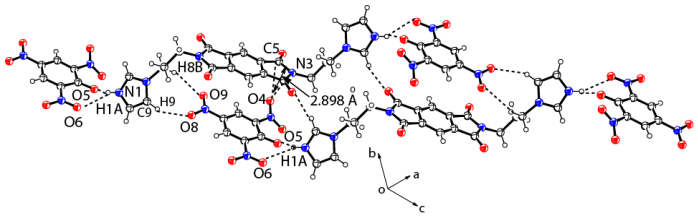

Figure 2.1.4: Hydrogen bonded self-assemblies of the salt **2.1.4**.

The hydrated salt H_2**2.1.2**.(2,4-DNP)$_2$.2H_2O has distinguishable hydrogen bonds from the anhydrous salts due to the additional contribution of water molecules towards hydrogen bonding. The 2,4-dinitrophenol has less number of hydrogen bonding sites than 2,4,6-trinitrophenol. Hence, the 2,4-dinitrophenolate salt is hydrated to gain higher stability to obtain a tight-packed structure. The water molecules present in the 2,4-dinitrophenolate salt are used as fillers using more number of hydrogen bonds. The 2,4-dinitrophenolate anions are connected to $(H_2$**2.1.2**$)^{2+}$ through intervening hydrogen bonded water molecules (Figure 2.1.5). In this salt, the N^+-H bond of the imidazolium cations of $(H_2$**2.1.2**$)^{2+}$ is hydrogen bonded to water and the 2,4-dinitrophenolate is connected to water molecules.

In this hydrated salt, one of the O-H bonds of water molecule does a similar role as that of the N^+-H bond in the anhydrous salt of 2,4,6-trinitrophnolate salt of **2.1.2**. Namely, one of the O-H bond of water molecule acts as the pivot hydrogen bond donor to form the bifurcated hydrogen bonds with an oxygen atom of the phenoxy-group and an oxygen atom of the nitro group at 2-position of the ring. The bifurcated hydrogen bonds are O8-H···O5 and O8-H···O6 hydrogen bonds shown in figure 2.1.5. The water molecule acts as a bridge by linking N^+-H by hydrogen bond, where O8 atom acts as a hydrogen bond acceptor. Hence, the role of water is to act as a bridge by offering hydrogen bond donor as well as acceptor sites. The rings of 2,4-dinitrophenolate and pyromellitic diimide are located on top of each other at locations separated by centroid to centroid distance of 3.707 Å. These rings are slightly oblique; hence there is a very weak charge-transfer interaction. On the other hand, the nitrogen atom (N5) of one of the nitro group is positioned over exactly opposite to a carbon atom (C2) of the pyromellitic diimide ring with a separation distance of 3.222 Å. The prominent hydrogen bond parameters of the salts are listed in the Table 2.1.4.

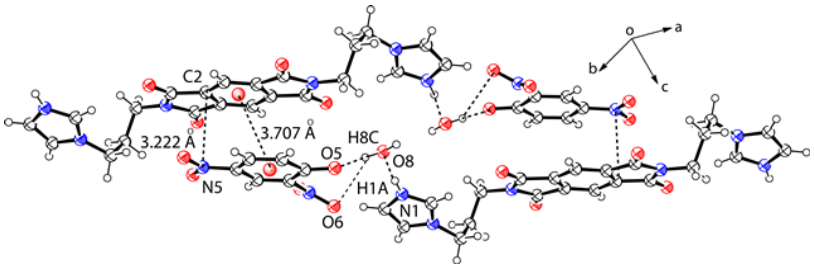

Figure 2.1.5: Hydrogen bonded self-assemblies of the salt **2.1.5**.

The orientations of the two flexible arms bearing imidazolium cations of $(\mathbf{2.1.2})^{2+}$ are *trans* across the pyromellitic diimide ring in the salts **2.1.4** and **2.1.5**. Both the salts have interesting bifurcated hydrogen bonds. The bifurcated hydrogen bond in the salt of **2.1.2** with 2,4,6-TNP involves imidazole ring (A of Table 2.1.1), whereas, a water molecule is involved in hydrate salt of **2.1.2** with 2,4-DNP (B of Table 2.1.1), making different synthons.[25] The oxygen atom of phenoxy, N-oxide, carbonyl groups are some functional groups that routinely form bifurcated hydrogen bonds.[26] These bifurcated hydrogen bonds involve oxygen atom as a pivotal hydrogen bond acceptor site to interact with two hydrogen bond donor sites. There are examples of bifurcated hydrogen bonds formed by participation of water molecules.[27] The present examples are the bifurcated hydrogen bonds having N^+-H or O-H bonds bridging nitro-group and phenoxy-oxygen. These examples of bifurcated hydrogen bonds are representative of graph-set notation $R^2_1(6)$.[28] The anhydrous salts **2.1.3** and **2.1.4** have bifurcated hydrogen bonds involving N^+-$H_{(imidazolium)}$ bond/s with the 2,4,6-trinitrophenolate ion/s. Both these salts have bifurcated hydrogen bonds involving two oxygen atoms, one each from phenoxy and a nitro group at 2-position of the respective anion. To suggest the geometrical aspects of bifurcated motifs, the various bond angles between hydrogen bonds are labeled and listed in Table 2.1.1. The differences among the observed bifurcated hydrogen bonds of the salts **2.1.3-2.1.5** are reflected in the angles θ_1 and θ_2 ($\Delta\theta$) as illustrated in the structural motif in Table 2.1.1. The $\Delta\theta$ refers to the dis-symmetry arising from the differences of the two hydrogen bonds of bifurcated hydrogen bonds in each case. The observed $\Delta\theta$ values for the salts **2.1.3-2.1.5** are 13.18º, 6.88º and 26.23º respectively. Ideally, a zero difference of $\Delta\theta$ would give a symmetrically disposed bifurcated hydrogen bonded motif. Geometrically, the **2.1.4** has the most symmetric bifurcated hydrogen bonds among the three salts.

Table 2.1.1: Different bond-angles in the hydrated and anhydrous ion-pairs

Bifurcated hydrogen bonded sub-assemblies	**2.1.3** (º)	**2.1.4**(º)	**2.1.5** (º)
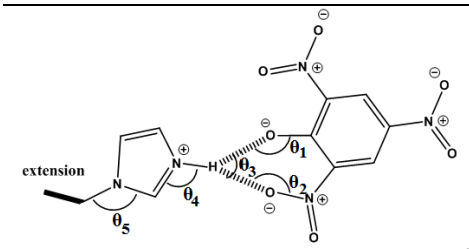 **A**	θ_1 =133.10 θ_2 =119.82 θ_3 =78.28 θ_4 =119.70 θ_5 =124.04	θ_1 =132.03 θ_2 =125.15 θ_3 =75.36 θ_4 =122.28 θ_5 =125.98	---- ---- ---- ---- ----
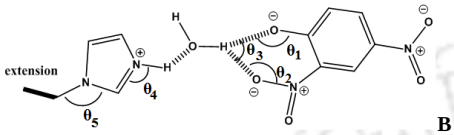 **B**	---- ---- ---- ---- ----	---- ---- ---- ---- ----	θ_1= 122.99 θ_2 = 96.76 θ_3 = 71.98 θ_4 = 126.02 θ_5 = 126.28

2.1.4: Hirshfeld Studies of Nitrophenolates Salts 2.1.3-2.1.5.

The Hirshfeld surface analyses have revealed quantitatively the major interactions in these self-assemblies as O-H interactions,[29] quantitatively the salts **2.1.3**, **2.1.4**, and **2.15** have O-H interactions, 45.6 %, 45.3 % and 41.5 % respectively (Figure 2.1.6). The surface analysis showed the interactions corresponding charge assisted hydrogen bond, formed due to the proton-transfer in each case, thereby suggesting the formation of ion-pair/s in respective self-assemblies. The analyses suggest the predominant contributions from the nitro groups, carbonyls, and the oxy-anion to the weak interaction schemes. The hydrophobic nature of the salts was reflected in the H…H interactions in each case. Among the various interactions, the contributions from the H···H interactions were of second hierarchical order and varied from 23.2 % to 29.7 %. The surface analyses also suggested the percentages of interactions involving N-H bond in these salts were between 2 % to 4 %. The relative contributions of various interactions from the Hirshfeld surface analysis are listed in Table 2.1.3.

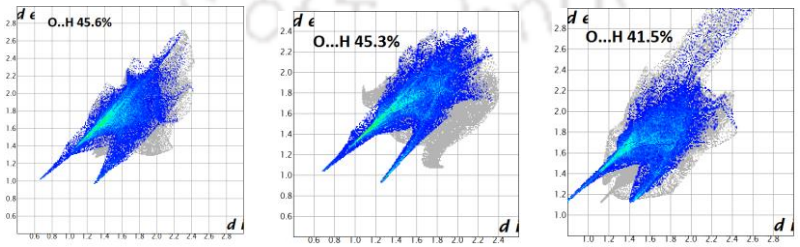

(a) (b) (c)

Figure 2.1.6: Fingerprint plots for (a) **2.1.3**, (b) **2.1.4** and (c) **2.1.5** (with O···H interactions highlighted in color).

2.1.5: Aggregation Caused Quenching (ACQ) of 2.1.1 and 2.1.2

Some conformational flexible fluorescent compounds show aggregation induced emission,[30] which result in new fluorescence emission at a longer wavelength upon addition of water. Certain fluorescent compounds also lose fluorescence upon interaction with water.[31] Fluorescence emissions of certain aromatic amines such as aniline derivatives are quenched by water.[32] Upon addition of water to the solution of **2.1.1** or **2.1.2** in acetonitrile, none showed a new emission peak. But such additions caused quenching of original emissions shown by the compounds in their respective solutions. The compound **2.1.1** emits at 377 nm (upon excitation at 270 nm) in acetonitrile; this emission was quenched upon addition of water (Figure 2.1.7a). Same was the case with **2.1.2**; this compound has fluorescence emissions at 431 nm and 450 nm. Those emissions were quenched upon addition of water (Figure 2.1.7b).

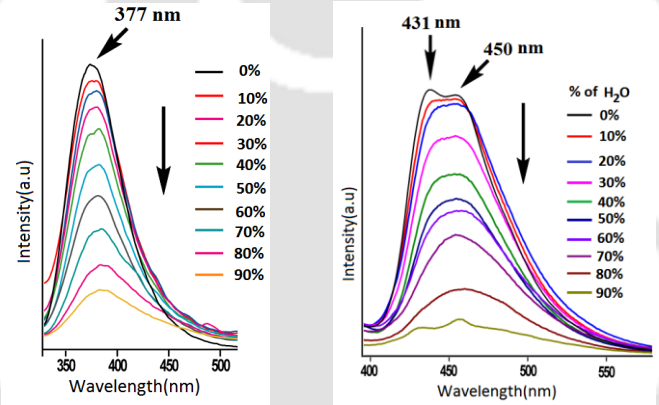

(a) (b)

Figure 2.1.7: Fluorescence spectra (10^{-4} M in ACN) upon addition of Water in different ratio of (a**) 2.1.1** (λ_{ex}= 270 nm) and (b) **2.1.2** (λ_{ex}= 364 nm).

But the nitrophenolate salts showed weak fluorescence emission upon addition of water. These emissions occurred at slightly different wavelength from the emission shown by the parent imide compound. This is an important observation, as the quenched state of the nitrophenolate salts could be recovered to ON-state by the addition of water (Figure 2.1.22 and 2.1.23). The water molecules compete to set apart the ion pairs present in the salt to have a hydrolytic equilibrium, hence the recovery of emission from the salt upon addition of water was possible. ^{1}H-NMR study on the two compounds (**2.1.1** and **2.1.2**) in acetonitrile-d_3 by adding D_2O had shown that on the addition of D_2O the signals of the -CH_2-CH_2-CH_2- groups were affected (Figure 2.1.8 and Figure 2.1.21). As D_2O concentration was increased, the

residual water peak of the solvent moved downfield, suggesting that there is an interaction of it with the exchangeable proton and suggest hydrolytic equilibrium, to form salt and free forms of the acid-base counterparts.

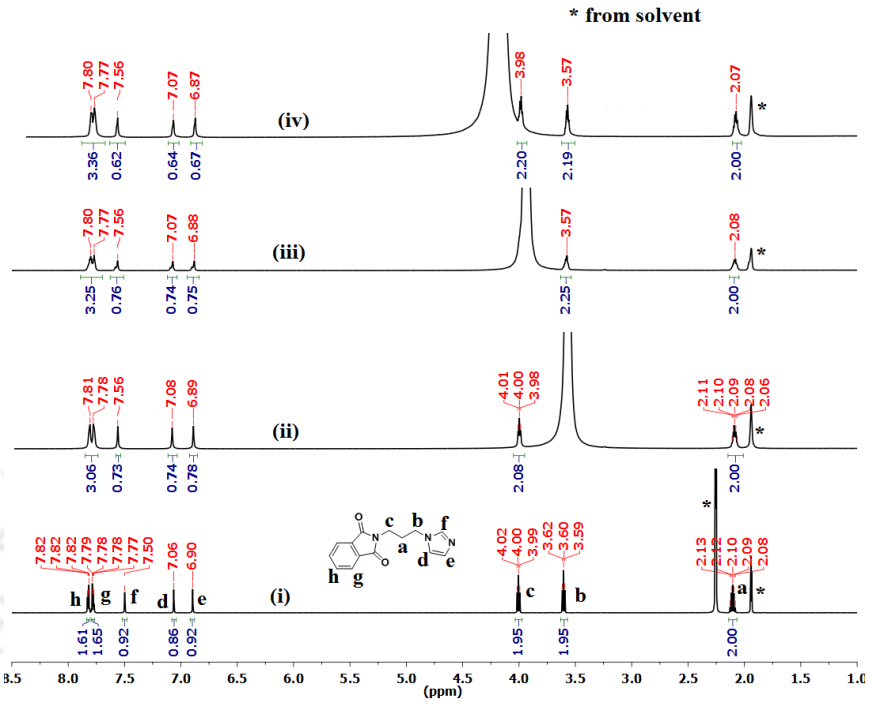

Figure 2.1.8: ^{1}H-NMR (600 MHz) spectra of **2.1.1** in (i) CD_3CN-d_3, (ii) 20% D_2O in CD_3CN-d_3, (iii) 40% D_2O in CD_3CN-d_3 and (iv) 50% D_2O in CD_3CN-d_3.

This indicated conformational changes involving the flexible arms. Moreover, dynamic light scattering studies revealed the aggregation of the salts under different conditions. For example, in acetonitrile the average size of the self-assembled aggregates of compounds **2.1.1** and **2.1.2** were 1810 nm and 2212 nm respectively. The average sizes of these aggregates increased to 2315 nm and 2748 nm respectively on addition of water to each solution (Figure 2.1.9). Since the self-assemblies have charge-transfer interactions among the rings and such interactions are responsible for Dexter quenching of fluorescence emission observed in the salts. The increase in size of aggregates with dilution showed that the aggregations of the molecules were affected by addition of water and ^{1}H-NMR study supported the fact that the dilution caused changes in the orientation of the propylene unit to influence the charge-transfer process. Hence, the combined spectroscopic study suggests that the Dexter quenching is facilitated by water molecules, due to conformational changes and flexibility provided to bifurcated hydrogen bonds favoring π-interactions among the rings.

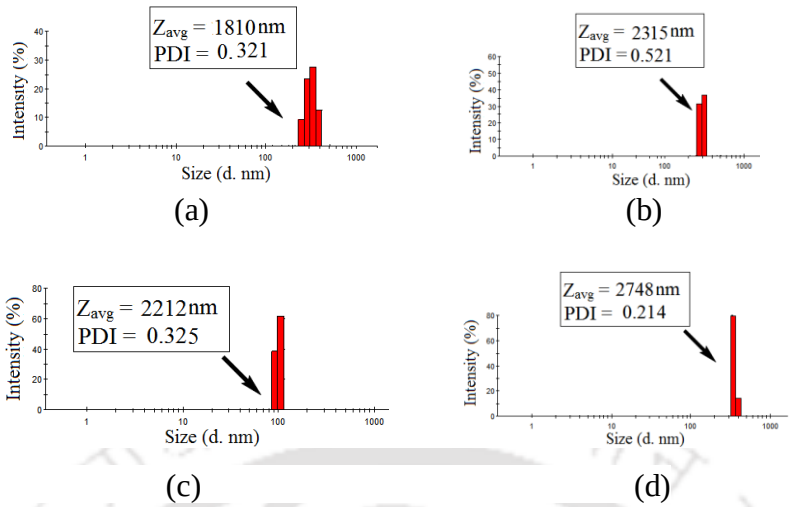

Figure 2.1.9: DLS-based particle size analysis of **2.1.1** from (a) acetonitrile, (b) 1:1 acetonitrile-H_2O solvents mixture and **2.1.2** from (c) acetonitrile, (d) 1:1 acetonitrile -H_2O solvents mixture.

2.1.6: Solid state UV-visible, Fluorescence studies

The absorptions and emissions of the solid samples (Figure 2.1.10) of parent compounds and salts are listed in Table 2.1.2. The solid sample of **2.1.1** is weakly fluorescent at 466 nm whereas **2.1.2** emits strongly at 481 nm upon excitation at 350 nm. Quantum yield of emission of the individual salt suggested that they are very weakly fluorescent with respect to the parent imide derivative. The life-time of fluorescence decay profile of each salt was determined (Figure 2.1.24-2.1.28). Each has good fit for three exponential decay paths. Another point revealed from the life-time data was that the dominant path of emission decay in the solid state emission of the **2.1.2** was drastically reduced in the respective salt. The preferred path shown in decay profile of the salts had very short life-time. Namely~87% of the molecule of the **2.1.2** followed a decay path with life-time 25.34 ns, whereas for **2.1.5**, the~51% of molecules followed very short life-time of 1.03 ns and rest of the molecules followed short-lived paths with life-times 0.35 ns and 6.85 ns. Similarly, the preferred paths in the salt **2.1.3** and **2.1.4** had lifetime 1.42 ns and 1.36 ns respectively.

Table 2.1.2: Characteristic UV-visible absorbance, fluorescence emission and fluorescence life-time of **2.1.1**, **2.1.2** and their salts in the solid state.

Compound/Salts	λ_{ab} (nm)	λ_{ex}(nm)	λ_{em}(nm)	(Quantum yields)Φ_F	lifetime and fraction (ns, %)	Goodness to fit (χ^2)
2.1.1	316	350	466	0.021	0.54 (31.36), 1.99 (24.15), 18.14 (44.48)	1.097
2.1.2	407	350	481	0.478	0.97 (1.05), 10.73 (11.46), 25.34 (87.47)	1.009
2.1.3	376-447(broad)	400	516	0.004	0.46 (19.85), 1.42 (58.87), 15.54 (21.27)	0.999
2.1.4	402-475(broad)	350	454	0.001	0.45 (36.97), 1.36 (41.23), 9.28 (21.78	1.006
2.1.5	386-472(broad)	350	462	0.012	0.35 (29.86), 1.03 (51.11), 6.85 (19.02)	1.001

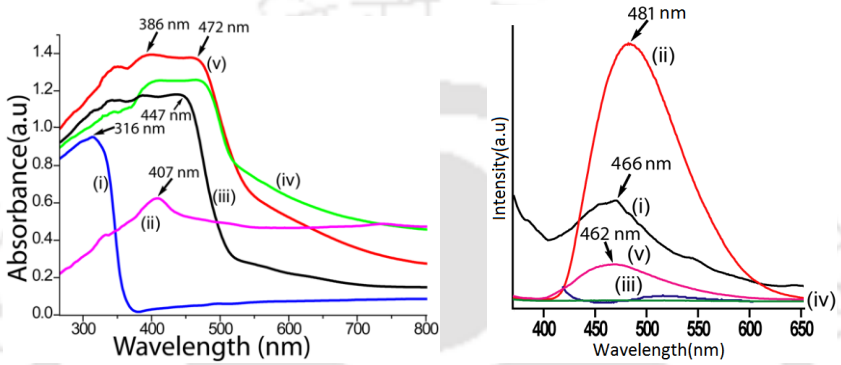

(a) (b)

Figure 2.1.10: (a) Solid-state UV-visible and (b) Fluorescence emission spectra of (i) **2.1.1**, (ii) **2.1.2**, (iii) **2.1.3**, (iv) **2.1.4** and (v) **2.1.5**.

The emission of different fluorophore containing compounds are quenched by nitrophenolic compounds and these are projected as quencher with different quenching ability depending on the substrate.[1e,33] Such studies on changes of emission whose sensing operates through a similar mechanistic path would allow to distinguish among nitrophenols. So we took up a comparative quenching study of the fluorescence emission of compound **2.1.1** or **2.1.2** in solution by 2,4-DNP and 2,4,6-TNP. The titration plots of decrease in the intensity of the fluorescence emissions of **2.1.1** and **2.1.2** upon addition of 2,4-DNP and 2,4,6-TNP are shown in Figure 2.1.11. The changes in emission intensity of the receptor molecules caused by the two nitrophenol derivatives were similar. But there are large differences in the slopes on the plots of changes that were caused by 2,4-DNP and 2,4,6-TNP. Hence, distinctions of these two nitrophenols were possible by the phthalimide and pyromellitic diimide based receptors.

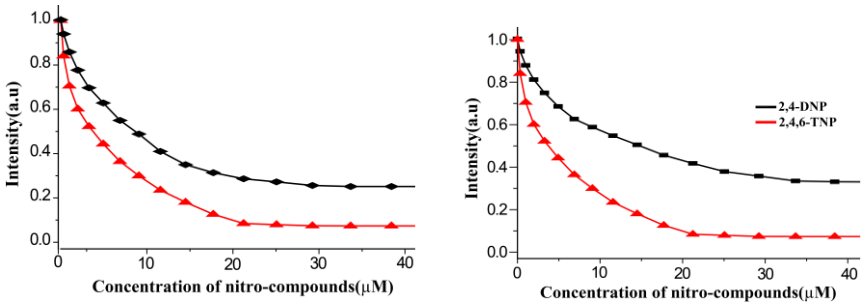

(a) (b)

Figure 2.1.11: Changes in the fluorescence intensity (a) at 377 nm of **2.1.1** and (b) at 431 nm of **2.1.2** at different concentrations of 2,4-DNP and 2,4,6-TNP. (10^{-4} M in ACN), (10 μL in each aliquot.

Hence, less significant host dependent emission quenching shown by a particular nitrophenolic compound with different imidazole tethered imide hosts suggested an intermolecular quenching mechanism. Upon acidification of the imidazole by mineral acid in analogous naphthalimide derivative[34] increased the intensity of emissions due to photo-electron transfer (PET). The nitrophenols are acidic, hence an increase in emission intensity would have taken place if the PET mechanism was the solely operative mechanism. The quenching of fluorescence in the present cases showed that the PET was insignificant relative to the quenching caused by charge-transfer interactions. The observed quenching in these cases are Dexter-quenching.

2.1.7: Gas phase DFT calculation

The gas-phase DFT calculations based on B3LYP functional and 6-31+G (d,p) basis set have shown that the HOMO of **2.1.1** and **2.1.2** are localized on the imidazole ring whereas LUMO are localized on the phthalimide or pyromellitic diimide of the respective compounds (Figure 2.1.19). The HOMO-LUMO gap of **2.1.1** and **2.1.2** are comparable (2.886 eV and 2.501 eV respectively). The selective portions of calculated electronic energy levels of the different salts are shown in the Figure 2.1.12. The HOMO-LUMO energy-gap in each salt is comparable. Upon salt formation the magnitude of energy gaps between the HOMO and LUMO as compared to that of the **2.1.1** and **2.1.2** are not changed but the corresponding molecular orbitals altogether changes. In these salts, the HOMOs are localized on the nitrophenolate ring and the LUMOs are on the respective phthalimide or pyromellitic diimide ring. Thus, in the case of the salts inter-molecular charge transfer is required which is not favorable and leads to quenching.

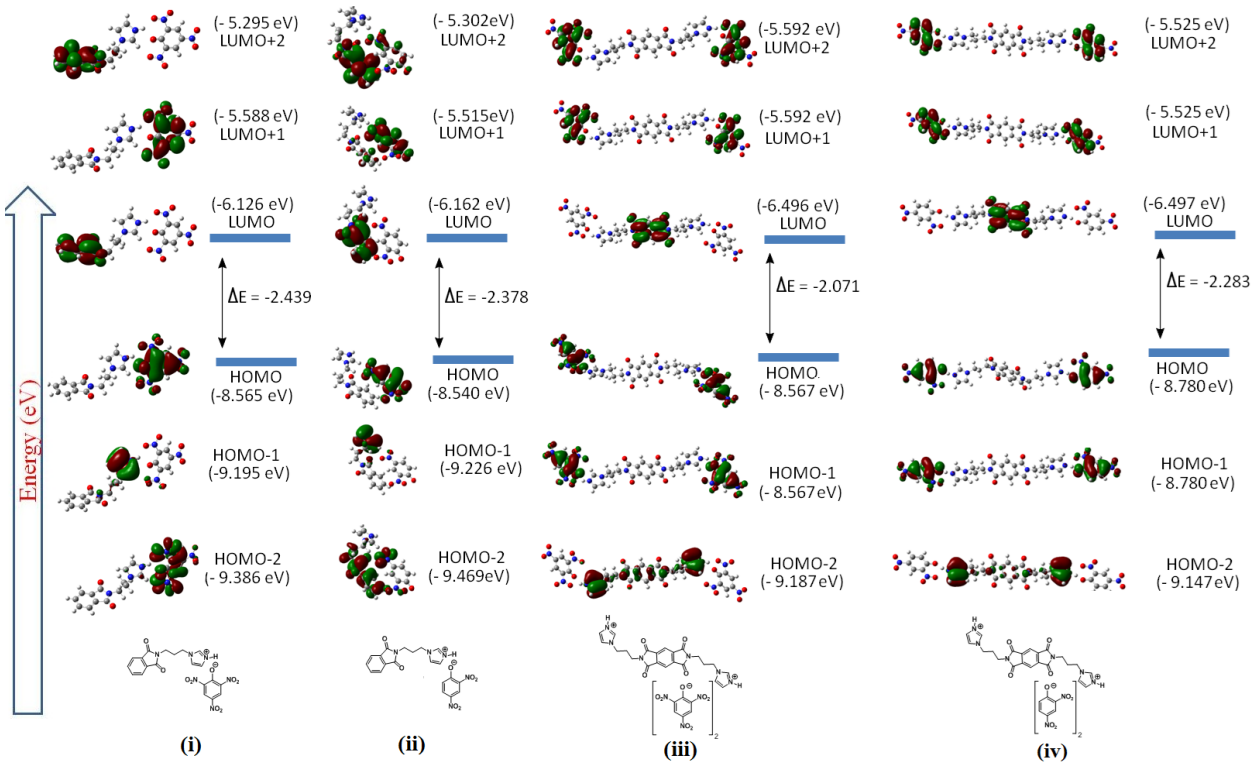

Figure 2.1.12: HOMO-LUMO of (i) **2.1.3**, (ii) **H2.1.1.(2,4-DNP)**, (iii) **2.1.4** and (iv) **2.1.5** calculated by gas-phase DFT using B3LYP functional and 6-31+G (d,p) basis set.

2.1.8: Conclusions

In conclusion, the combined solid state and solution study established that the relative fluorescence emission quenching caused by 2,4-DNP and 2,4,6-TNP of the imidazole tethered phthalimide and pyromellitic dianhydride derivatives were widely distinguishable in solution as well as in solid. Such interactions of 2,4-DNP and 2,4,6-TNP did not distinguish individually the two receptors with different fluorphores. The anhydrous salts of the receptors considered here had direct hydrogen bonds between the anion and cation but in the case of hydrated salt the oppositely charged ions are separated by water molecule by the intervening $N^{+}_{(imidazole)}$-H···$O_{(water)}$ hydrogen bond. The effect of water in self-assembly was also reflected in the fluorescence emission studies in different solutions of the parent imides, where the emissions were quenched by water. The quenched fluorescence emissions of the nitrophenolate salts of **2.1.1** and **2.1.2** were partially recovered upon addition of water to the solutions due to hydrolytic equilibrium. In solid state, the oxygen-π interactions predominated in the 2,4,6-trinitrophenolate salt of **2.1.2**, leading to complete quenching of

emission. The photo-electron transfer emission that generally occurs due to the protonation of nitrogen atom of imidazole became insignificant in such a situation.

2.1.9: Experimental section

Synthesis and characterization of cyclic imide derivatives and their salts 2.1.1-2.1.5:

2-(3-(1H-imidazol-1-yl)propyl)isoindoline-1,3-dione (**2.1.1**)[35] and N,N'-bis(3-imidazol-1-yl-propyl)-pyromelliticdiimide(**2.1.2**)[36] were synthesized and characterized by reported procedure. Slow evaporation of respective solution of **2.1.1** or **2.1.2** (1 mmol each) with 2,4,6-trinitrophenol or 2,4-dinitrophenol in appropriate molar ratio (1 : 1 for **2.1.1** and 1 : 2 for **2.1.2**) in methanol (10 ml) yielded the crystals of the corresponding salt. The solid salts were characterized by recording the IR, NMR and finally by comparing the experimentally determined powder XRD pattern of the respective sample with the PXRD pattern generated from the crystallographic information file (Figure 2.1.16-2.1.18).

Spectral data of the salts:

2.1.1: Isolated yield: 67 %. ^{1}H-NMR (600 MHz, $CDCl_3$): 8.93 (s, 1H), 8.62 (s, 1H), 7.89-7.88 (m, 2H), 7.78-7.77 (m, 2H), 7.52 (s, 1H), 7.36 (s, 1H), 4.23 (t, J = 12 Hz, 2H), 3.77 (t, J = 6 Hz, 2H), 2.31-2.29 (m, 2H). Elemental anal calcd for $C_{20}H_{16}N_6O_9$, C, 49.59; H, 3.33; N, 17.35; found, C, 49.67; H, 3.36; N, 17.71. IR (KBr, cm^{-1}): 3591 (br), 3464 (s), 3155 (s), 3069 (s), 2954 (s), 2819 (m), 1771 (s), 1712 (s), 1612 (s), 1568 (s), 1526 (s), 1544 (s), 1463 (s), 1435 (s), 1398 (s), 1363 (s), 1337 (s), 1314 (s), 1271(s), 1185 (s), 1162 (s), 1130 (m), 1104 (s), 1019 (s), 938 (s), 917 (s), 898 (s), 836 (s), 817 (s), 784 (s), 751 (s), 719 (s), 630 (s), 530 (s), 426 (m).

2.1.2: Isolated yield: 60 %.^{1}H-NMR (400 MHz, DMSO-d_6): 9.08 (s, 1H), 8.59 (s, 4H), 8.18 (s, 1H), 7.81 (d, J = 8 Hz, 1H), 7.73 (d, J = 12 Hz, 1H), 4.29 (t, J = 4 Hz, 2H), 3.21 (t, J = 6 Hz, 2H), 2.05 (m, 2H). Elemental anal calcd for $C_{34}H_{26}N_{12}O_{18}$; C, 45.85; H, 2.94; N, 18.87; found, C, 45.79; H, 2.94; N, 19.01. IR (KBr, cm^{-1}): 3141 (br), 1773 (m), 1725(s), 1632 (s), 1580 (s), 1557 (s), 1515 (w), 1434 (s), 1392 (s), 1362 (s), 1338 (s), 1309 (s), 1266 (s), 1159 (m), 1075 (m), 1037 (m), 728 (m), 728 (s).

2.1.3: Isolated yield: 62 %. ^{1}H-NMR (600 MHz, $CDCl_3$): 9.04 (s, 1H), 8.34 (d, J = 6 Hz, 1H), 8.25 (s, 2H), 7.52(s, 1H), 7.12 (d, J = 6 Hz, 1H), 6.96 (d, J = 18 Hz, 2H), 4.05 (t, J = 6 Hz, 2H), 3.81 (t, J = 6 Hz, 2H), 2.25 (m, J = 6 Hz, 2H). Elemental anal calcd for $C_{34}H_{32}N_{10}O_{16}$, C, 48.81; H, 3.86; N, 16.74; found, C, 48.78; H, 3.89; N, 16.79. IR (KBr, cm^{-1}): 3409 (br,), 1770

(m), 1713 (s), 1598 (s), 1554 (m), 1528 (m), 1468 (m), 1395 (s), 1371 (s), 1264 (s), 1131 (s), 1046 (s), 923 (m), 837 (s), 751 (s), 726 (s), 631 (s).

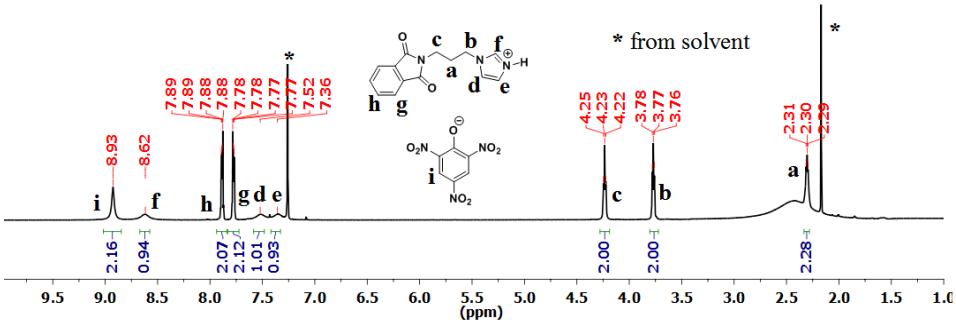

Figure 2.1.13: ^{1}H-NMR (600 MHz, $CDCl_3$) spectra of **2.1.1**.

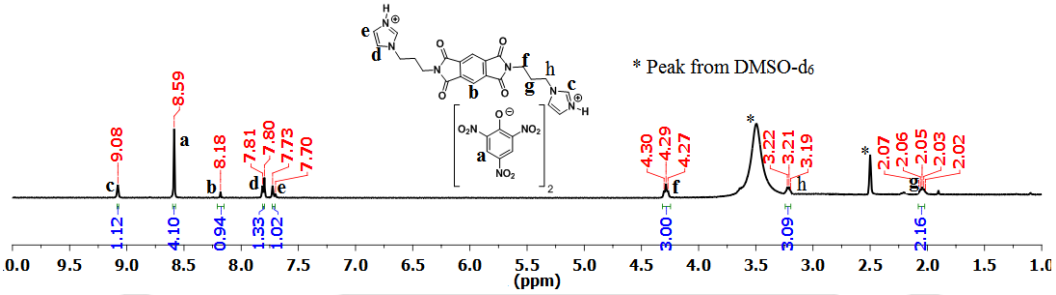

Figure 2.1.14: ^{1}H-NMR (400 MHz, DMSO-d_6) spectra of **2.1.2**.

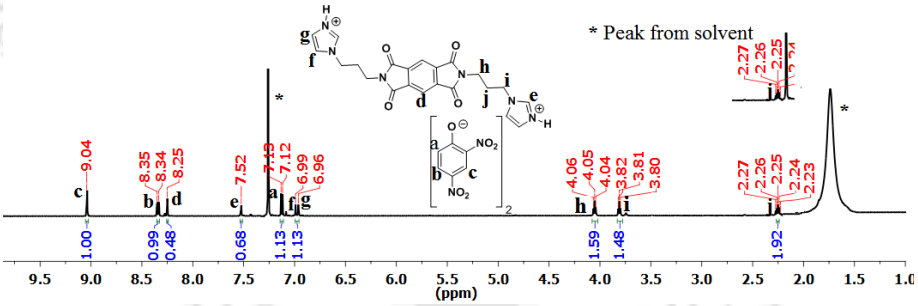

Figure 2.1.15: ^{1}H-NMR (600 MHz, $CDCl_3$) spectra of **2.1.3**.

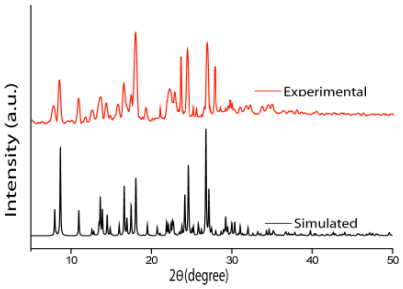

Figure 2.1.16: PXRD patterns of salt **2.1.3** (Red = Experimental, Black = Simulated), Simulated pattern generated from crystallographic information file.

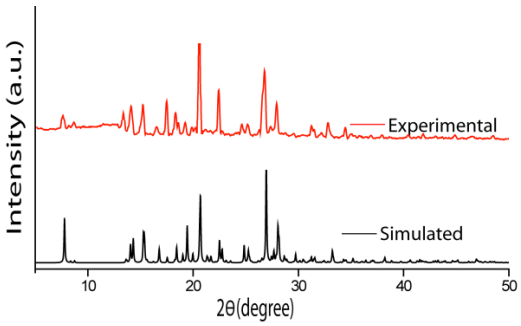

Figure 2.1.17: PXRD patterns of salt **2.1.4** (Red = Experimental, Black = Simulated), Simulated pattern generated from crystallographic information file.

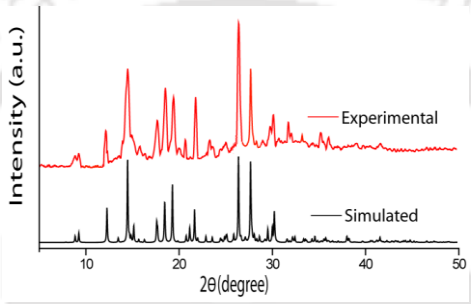

Figure 2.1.18: PXRD patterns of salt **2.1.5** (Red = Experimental, Black = Simulated), Simulated pattern generated from crystallographic information file.

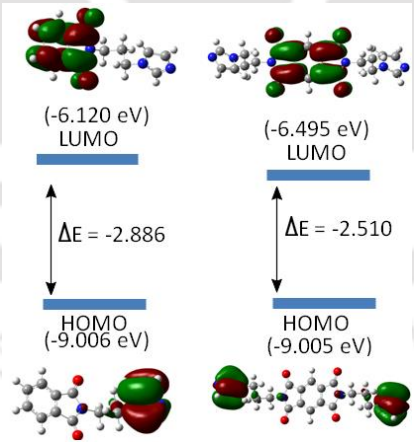

(a) (b)

Figure 2.1.19: HOMO-LUMO of (a) **2.1.1**, (b) **2.1.2** calculated by DFT using B3LYP/6-31+G (d,p) functional.

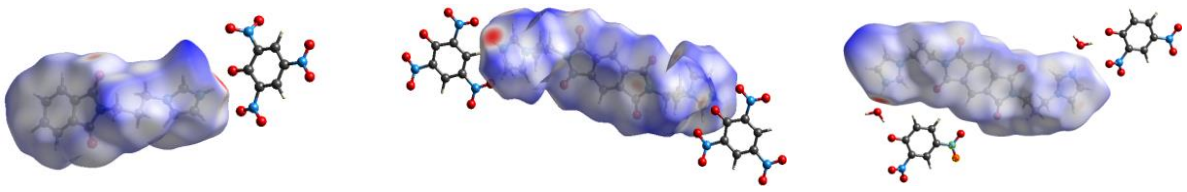

(a) (b) (c)

Figure 2.1.20: Hirshfeld surface of (a) **2.1.3**, (b) **2.1.4** and (c) **2.1.5**.

Table 2.1.3: Relative contributions of various interactions in percentages from Hirshfeld surface analysis.

Intercation	2.1.3	2.14	2.15
O···O	0.7	5.3	2.4
N···O	2.4	2.2	1.9
C···O	4.3	6.6	5.7
H···O	45.6	45.3	41.5
C···N	1.1	1.2	2.1
N···H	2.0	4.3	2.5
C···H	6.0	9.7	6.9
C···C	8.0	2.3	5.9
H···H	29.7	23.2	28.8

Table 2.1.4: Prominent hydrogen bond parameters of salts **2.1.3-2.1.5**.

Salts	D-H…A	d_{D-H} (Å)	$d_{H\cdots A}$ (Å)	$d_{D\cdots A}$ (Å)	∠D-H…A (°)
2.1.3	N(1)-H(1)…O(5) [-1+x,1+y,z]	0.87(5)	1.82(4)	2.653(6)	162(5)
	N(1)-H(1)…O(6) [-1+x,1+y,z]	0.87(5)	2.37(5)	2.897(6)	120(4)
	C(11)-H(11B)…O(3) [x,y,z]	0.97(4)	2.55(4)	3.425(8)	150(5)
	C(13)-H(13)…O(2) [-x,1-y,1-z]	0.93(4)	2.47(5)	3.144(6)	130(3)
	C(18)-H(18)…O(1) [-x,1-y,-z]	0.93(4)	2.38(3)	3.171(6)	143(5)
2.1.4	N(1)-H(1A)…O(5) [2-x,1-y,1-z]	0.88(4)	1.83(3)	2.641(4)	151(4)
	N(1)-H(1A)…O(6) [2-x,1-y,1-z]	0.88(3)	2.41(5)	3.069(5)	132(3)
	C(7)-H(7B)…O(5) [1-x,1-y,1-z]	0.97(3)	2.47(3)	3.408(4)	162(2)
	C(9)-H(9)…O(8) [1-x,1-y,-z]	0.93(2)	2.49(3)	3.360(2)	156(2)
	C(11)-H(11)…O(2) [1-x,-y,1-z]	0.93(2)	2.32(4)	3.133(2)	146(3)
2.1.5	N(1)-H(1A)…O(8) [1+x,y,z]	0.89(4)	1.76(3)	2.650(4)	176(4)
	O(8)-H(8C)…O(5) [x,y,z]	0.87(2)	2.05(4)	2.866(5)	156(3)
	O(8)-H(8C)…O(6) [x,y,z]	0.87(2)	2.51(3)	3.091(4)	125(4)
	O(8)-H(8D)…O(5) [1-x,1-y,1-z]	0.88(2)	1.78(3)	2.649(2)	171(2)
	C(9)-H(9)…O(7) [1-x,1-y,1-z]	0.93(2)	2.30(2)	3.122(2)	147(3)

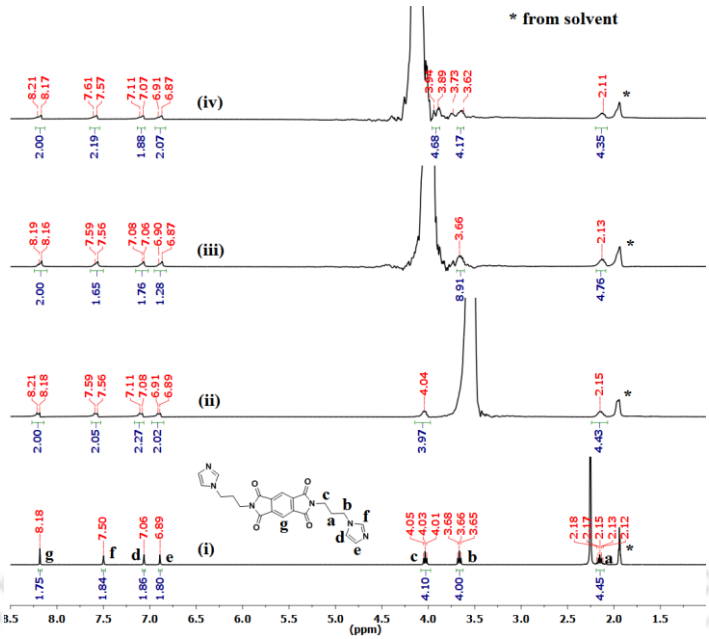

Figure 2.1.21: ^{1}H-NMR (600 MHz) spectra of **2.1.2** in (i) CD_3CN-d_3, (ii) 20% D_2O in CD_3CN-d_3, (iii) 40% D_2O in CD_3CN-d_3 and (iv) 50% D_2O in CD_3CN-d_3.

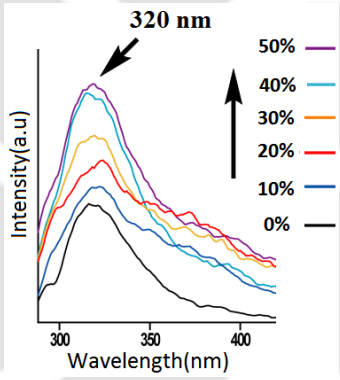

Figure 2.1.22: Fluorescence spectra (λ_{ex}= 270 nm) of **2.1.3** (10^{-4} M in acetonitrile) upon addition of different fraction of water.

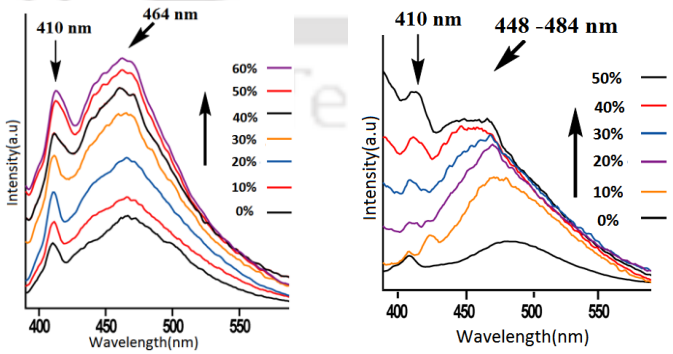

Figure 2.1.23: Fluorescence spectra of (a) **2.1.4**, (b) **2.1.5** (10^{-4} M in acetonitrile) upon addition of different fraction of water (λ_{ex}= 364 nm).

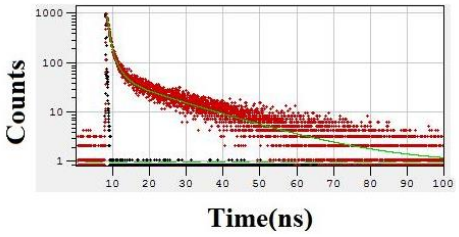

χ^2 : 1.097

	B_i	ΔB_i	f_i (%)	Δf_i (%)	τ_i (ns)	$\Delta\tau_i$ (ns)
1	0.1636	0.0074	31.362	5.348	0.546	0.068
2	0.0345	0.0025	24.154	2.033	1.996	0.022
3	0.0070	0.0001	44.484	0.827	18.146	0.001

Figure 2.1.24: Time resolved fluorescence emission of solid sample of **2.1.1** (λ_{ex} = 375 nm, λ_{em} = 466 nm).

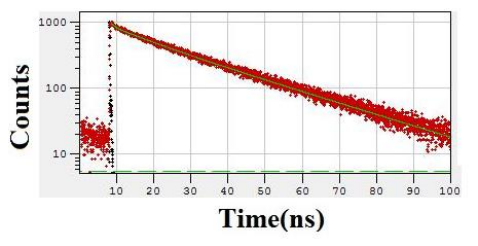

χ^2 : 1.009

	B_i	ΔB_i	f_i (%)	Δf_i (%)	τ_i (ns)	$\Delta\tau_i$ (ns)
1	0.0307	0.0102	1.057	0.595	0.976	0.227
2	0.0303	0.0080	11.469	3.053	10.730	0.017
3	0.0978	0.0086	87.475	7.704	25.344	0.002

Figure 2.1.25: Time resolved fluorescence emission of solid sample of **2.1.2** (λ_{ex} = 375 nm, λ_{em} = 481 nm).

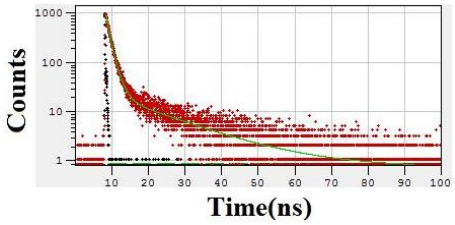

χ^2 : 0.999

	B_i	ΔB_i	f_i (%)	Δf_i (%)	τ_i (ns)	$\Delta\tau_i$ (ns)
1	0.1017	0.0042	19.852	6.974	0.463	0.143
2	0.0983	0.0043	58.871	3.099	1.421	0.013
3	0.0032	8.7e-5	21.277	0.575	15.546	0.002

Figure 2.1.26: Time resolved fluorescence emission of solid sample of **2.1.3** (λ_{ex} = 375 nm, λ_{em} = 516 nm).

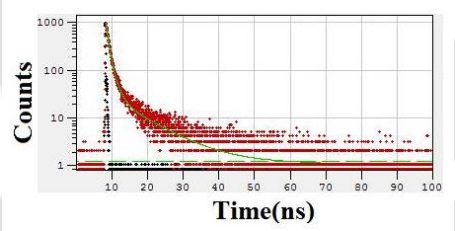

χ^2 : 1.006

	B_i	ΔB_i	f_i (%)	Δf_i (%)	τ_i (ns)	$\Delta\tau_i$ (ns)
1	0.1515	0.0066	36.977	9.379	0.454	0.095
2	0.0562	0.0042	41.239	3.938	1.365	0.028
3	0.0044	0.0002	21.784	1.042	9.280	0.004

Figure 2.1.27: Time resolved fluorescence emission of solid sample of **2.1.4** (λ_{ex} = 375 nm, λ_{em} = 454 nm).

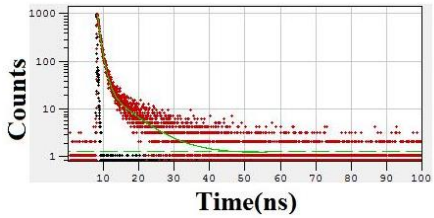

χ^2: 1.001

	B_i	ΔB_i	f_i (%)	Δf_i (%)	τ_i (ns)	$\Delta\tau_i$ (ns)
1	0.1357	0.0075	29.860	15.372	0.351	0.161
2	0.0790	0.0066	51.113	5.976	1.031	0.034
3	0.0044	0.0003	19.026	1.120	6.859	0.006

Figure 2.1.28: Time resolved fluorescence emission of solid sample of **2.1.5** (λ_{ex} = 375 nm, λ_{em} = 462 nm).

2.1.10: References:

1. (a) S. V. Eliseeva, J. C. G. Bunzli, *Chem. Soc. Rev*., 2010, **39**, 189-227; (b) K. Binnemans, *Chem. Rev*., 2009, **109**, 4283-4374; (c) D. Yan, D. G. Evans, *Mater. Horizons*., 2014, **1**, 46-57; (d) L. D. Carlos, R. A. S. Ferreira, V. d. Z. Bermudez, B. Julian-Lopez, P. Escribano, *Chem. Soc. Rev*., 2011, **40**, 536-549; (e) X. Sun, Y. Wang, Y. Lei, *Chem. Soc. Rev*., 2015, **44**, 8019-8061; (f) S. Varghese, S. Das, *J. Phys. Chem. Lett*., 2011, **2**, 863-873; (g) G. W. Coates, A. R. Dunn, L. M. Henling, D. A. Dougherty, R. H Grubbs, *Angew. Chem. Int. Ed*., 1997, **36**, 248-251.

2. (a) J. -M. Lehn, *Proc. Nat. Acad. Sci. USA* 2002, **99**, 4763-4768; (b) L. R. Nassimbeni, *Acc. Chem. Res*., 2003, **36**, 631-637; (c) G. M. Whitesides, J. P. Mathias, C. T. Seto, *Science*., 1991, **254,** 1312-1319.

3. (a) E. A. Mikhalyova, A. V. Yakovenko, M. Zeller, M. A. Kiskin, Y. V. Kolomzarov, I. L. Eremenko, A.W. Addison, V. V. Pavlishchuk, *Inorg. Chem*., 2015, **54**, 7, 3125-3133; (b) A. J. Calahorro, E. S. Sebastian, A. S. Castillo, J. M. Seco, C. M. Fierro, B. Fernandez, A. R. Dieguez, *CrystEngComm*, 2015, **17,** 3659-3666; (c) Y. Shao, G. Z. Yin, X. Ren, X. Zhang, J. Wang, K. Guo, X. Li, C. Wesdemiotis, W. B. Zhang, S. Yang, M. Zhu, B. Sun, *RSC Adv.*, 2017, **7**, 6530-6537.

4. (a) Y. Yano, T. Ono, S. Hatanaka, D. T. Grykoc, Y. Hisaeda. *J. Mater. Chem. C*., 2019, **7**, 8847-8854; (b) C. Lochenie, K. G. Wagner, M. Karg, B. Weber, *J. Mater. Chem. C*., 2015, **3**,

7925-7935; (c) G. Fan, X. Yang, R. Liang, J. Zhao, S. Lib, D. Yan, *CrystEngComm*, 2016, **18**, 240-249.

5. (a) M. A. Kobaisi, S. V. Bhosale, K. Latham, A. M. Raynor, S. V. Bhosale, *Chem. Rev*., 2016, **116**, 11685-11796; (b) F. Grepioni, S. D. Agostino, D. Braga, A. Bertocco, L. Catalano, B. Ventura, *J. Mater. Chem. C*., 2015, **3**, 9425-9434; (c) R. J. Sarma, C. Tamuly, N. Barooah, J. B. Baruah, *J. Mol. Struct*., 2007, **829**, 29-36; (d) J. K. Nath, J. B. Baruah, *CrystEngComm*, 2015, **17**, 8575-8595.

6. (a) J. Nath, J. B. Baruah, *CrystEngComm*, 2015, **17**, 8575-8595; (b) M. A. Kobaisi, S. V. Bhosale, K. Latham, A. M. Raynor, S. V. Bhosale, *Chem. Rev*., 2016, **116**, 11685-11796.

7. (a) H. Yan, X. Meng, B. Li, S. Ge, Y. Lu, *J. Mater. Chem. C*., 2017, **5**, 10589-10599; (b) L. Dehmel, F. Berndt, M. Weinberger, M. Sajadi, I. Ioffe, H. A. Wagenknecht, N. P. Ernsting, *Phys. Chem. Chem. Phys*., 2016, **18**, 6813-6820; (c) C. Reichardt, *Chem. Rev*., 1994, **94**, 2319-2358; (d) A. Mitrovic, N. Todorovic, A. Zekic, D. Stankovic, D. Milic, V. Maslak, *Eur. J. Org. Chem*., 2013, 2188-2193; (e) X. M. Huang, G. B. Li, R. K. Pan, S. G. Liu, *Transition Metal Chemistry*., 2020, **45**, 187-193; (f) G. B. Li, X. M. Huang, R. K. Pan, S. G. Liu, *Spectrochimica Acta Part A: Molecular and Biomolecular Spectroscopy*., 2020, **229**, 117941.

8. (a) A. G. Griesbeck, B. Ongel, M. Atar, *J. Phys. Org. Chem*., 2017, **30**, e3741; (b) A. G. Griesbeck, S. Schieffer, *Photochem. Photobiol. Sci*., 2003, **2**, 113-117; (c) H. Okamoto, H. Konishi, K. Satake, *Chem. Commun.*, 2012, **48**, 2346-2348; (d) G. Saroja, B. Ramachandram, S. Saha, A. Samanta, *J. Phys. Chem. B.*, 1999, **103**, 2906-2911; (e) X. Liu, L. Gao, L. Yang, L. Zou, W. Chen, X. Song, *RSC Adv*., 2015, **5**, 18177-18182; (f) A. J. Greenlee, C. K. Ofosu, Q. Xiao, M. M. Modan, D. E. Janzen, D. D. Cao, *ACS Omega*., 2018, **3**, 240-245; (g) A. G. Dal-Bo, R. d. C. Duarte, R. Cercena, M. Peterson, J. Rafique, S. Saba, E. Zapp, E. S. Gil, P. F. B. Gonçalves, F. S. Rodembusch, T. E. A. Frizonf, *Dyes and Pigments*., 2018, **157**, 143-150.

9. (a) G. Y. Zheng, D. P. Rillema, *Inorg. Chem*., 1998, **37**, 1392-1397; (b) D. Kolosov, V. Adamovich, P. Djurovich, M. E. Thompson, C. Adachi, *J. Am. Chem. Soc*., 2002, **124**, 9945-9954; (c) A. Tarai, J. B. Baruah, *Cryst. Growth Des*., 2018, **18**, 456-465; (d) A. Tarai, J. B. Baruah, *Cryst. Growth Des*., 2016, **16**, 126-135.

10. (a) S. Singh, *J. Hazard. Mater*., 2007, **144**, 15-28; (b) G. Xue, M. Gao, Z. Gu, Z. Luo, Z. Hu, *Chem. Eng. J*., 2013, **218**, 223-231.

11. K. Zhang, H. B. Zhou, Q. S. Mei, *J. Am. Chem. Soc*., 2011, **133**, 8424-8427.

12. (a) S. Shanmugaraju, P. S. Mukherjee, *Chem. Eur. J*., 2015, **21**, 6656-6666; (b) M. Alfonso, A. Espinosa, A. Tarraga, P. Molina, *Chemistry Open*., 2014, **3**, 242-249; (c) D. S. Kim, V. M. Lynch, K. A. Nielsen, C. Johnsen, J. O. Jeppesen, J. L. Sessler, *Anal. Bioanal. Chem*., 2009, **395**, 393-400; (d) J. Pan, F. Tang, A. Ding, L. Kong, L. Yang, X. Tao, Y. Tiana, J. Yang, *RSC Adv*., 2015, **5**, 191-195.

13. B. Xu, X. Wu, H. Li, H. Tong, L. Wang, *Macromolecules.*, 2011, **44**, 5089-5092.

14. S. S. Nagarkar, A. V. Desai, P. Samanta, S. K. Ghosh, *Dalton Trans*., 2015, **44**, 15175-15180.

15. J. Liu, S. Yang, F. Li, L. Dong, J. Liu, X. Wang, Q. Pu, *J. Mater. Chem. A*., 2015, **3** 10069-10076.

16. K. K. Kartha, A. Sandeep, V. K. Praveen, A. Ajayaghosh, *Chem. Rec*., 2015, **15**, 252-265.

17. J. Geng, P. Liu, B. Liu, G. Guan, Z. Zhang, M. Y. Han, *Chem. Eur. J*., 2010, **16**, 3720-3727.

18. S. Xu, H. Lu, *Chem. Commun*., 2015, **51**, 3200-3203.

19. (a) B. Gogoi, N. S. Sarma, *ACS Appl. Mater. Interfaces*., 2015, **7**, 11195-11202; (b) Y. Erande, S. Chemate, A. More, N. Sekar, *RSC Adv*., 2015, **5**, 89482-89487; (c) R. Mitra, A. Saha, *ACS Sustainable Chem. Eng*., 2017, **5**, 604-615; (d) G. Sivaraman, B. Vidya, D. Chellappa, *RSC Adv*., 2014, **4**, 30828-30831.

20. R. Breslow, *Acc. Chem. Res*., 1995, **28**, 146-153.

21. (a) X. Mu, N. Jiang, C. Liu, D. Zhang, *J. Phys. Chem*., 2017, **121**, 1133-1139; (b) K. Dong, S. Zhang, D. Wang, X. Yao, *J. Phys. Chem. A*., 2006, **110**, 9775-9782.

22. (a) J. Jayabharathi, V. Thanikachalam, N. Srinivasan, M. V. Perumal, *Spectrochim. Acta A: Mol. Biomol. Spec*., 2012, **90**, 125-130; (b) Y. Zhang, F. Liu, K. A. Li, *Anal. Chem*., 2004, **76**, 7336-7345; (c) Y. -D. Cao, Q. -Y. Zheng, C. -F. Chen, Z. -T. Huang, *Tetrahedron Lett*., 2003, **44**, 4751-4755.

23. C. A. Hunter, J. K. M. Sanders, *J. Am. Chem. Soc*., 1990, **112**, 5525-5534.

24. A. M. Kobaisi, S. V. Bhosale, K. Latham, A. M. Raynor, S. V. Bhosale, *Chem. Rev*., 2016, **116**, 11685-11796.

25. G. R. Desiraju, *Angew. Chem. Int. Ed. Engl*., 1995, **34**, 2311-2327.

26. (a) I. Rozas, I. Alkorta, J. Elguero, *J. Phys. Chem. A*., 1998, **102**, 9925-9932; (b) E. S. Feldblum, I. T. Arkin, *Proc. Nat. Acad. Sci. USA*., 2014, **111**, 4085-4090.

27. S. Bawa, M. L. Cote, P. Dubois, R. A. Lalancette, H. W. Thompson, *Acta. Crystallogr*., 2004, **60B**, 438-446.

28. M. C. Etter, *Acc. Chem. Res*., 1990, **23**, 120-126.

29. M. C. Etter, J. C. MacDonald, J. Bernstein, *Acta Crystallogr*., 1990, **46B**, 256-262.

30. Y. Hong, J. W. Y. Lam, B. Z. Tan, *Chem. Soc. Rev*., 2011, **40**, 5361-5388.

31. G. E. Dobretsov, T. I. Syrejschikova, N. V. Smolina, *Biophysics*., 2014, **59**, 183-188.

32. S. Tobita, K. Ida, S. Shiobara, *Res. Chem. Intermed*., 2001, **27**, 205-218.

33. (a) A. Tarai, J. B. Baruah, *New J. Chem*., 2017, **41**, 10750-10760; (b) A. Tarai, J. B. Baruah, *New J. Chem*., 2018, **42**, 4757-4765.

34. M. P. Singh, A. Tarai, J. B. Baruah, *ChemistrySelect*., 2018, **3,** 6364-6373.

35. J. K. Nath, J. B. Baruah, *Inorg. Chem. Commun*., 2013, **30**, 128-132.

36. X. -Q. Lu, Y. -Q, Qiao, J. -R. He, M. Pan, B. -S. Kang, C. -Y. Su, *Cryst. Growth Des*., 2006, **6**, 1910-1914.

Chapter 2: (Part B)

Photo physical properties of Imidazole-Tethered Naphthalimide Derivative upon interactions with nitro-phenols and mineral acids

2.2.1: Introduction

As a continuation of earlier part of this chapter, in this part we present results from a structural and photo physical properties of receptors possessing naphthalimide units. These compounds belong to a class called Rylenes[1], where the π-stacking charge transfer interactions causes quenching of fluorescence emissions[2] and colour changes.[3] On the other hand, many of such fluorophores upon ion binding or change in hydrogen bonding affects fluorescence emissions.[4] A large numbers of receptor molecules in which photo-induced electron transfer due to the lone pair of electrons present on nitrogen atom of heterocyclic compound at remote site can be modulated by protonation.[5] Naphthalimides are such fluorophores where modulation of emission can be caused by different ways and particularly emission changes caused at remote sites are utilized for ion recognition and molecular recognition.[6] The naphthalimides are dipolar π-systems which stack among themselves or can stacks with π-systems either electron rich or electron deficient aromatic molecules.[7] We have been studying molecular recognitions, ion recognitions and conformational aspects of imide containing compounds that have nitrogen based heterocyclic units attached through flexible tether.[8] Those studies have been carried out with a expectation that a flexible tether either keeps away or brings close to a fluorophore from an interacting group located at a remote site. Such effects influence fluorescence emissions through non-covalent interactions between the fluorophore and the interacting counterpart.

While forming self-assembly a molecule may involve one or more π-interactions such as C-H···π, O-H···π, N-H···π or π–π interactions.[9] Each of these interactions has own directional requirements. These requirements decide the overall architecture of a supramolecular assembly. Among these interactions, the π-interactions between two aromatic rings may occur in different ways. Weak nature of these interactions changes the contributions from each counterpart in solid and solution, as a result of which the emission properties of a compound in solid and solution may differ.[10]

We have chosen to study the naphthalimide derivative N-(3-imidazol-1-yl-propyl)-1,8-naphthalimide (**2.2.1**), which has a naphthalimide ring attached through propylene tether

connected to imidazole. The imidazole part is chosen to attach to naphthalimide through flexible tether as it can be protonated easily by mineral acid or organic acids. Such assemblies will be formed in different ways by arranging the cationic and anionic parts, some such arrangements are shown in Figure 2.2.1. Such arrangements of the naphthalimide units are possible by either self-interacting or by interacting naphthalimide unit with an anionic unit through charge-transfer or anion π-interactions.[11]

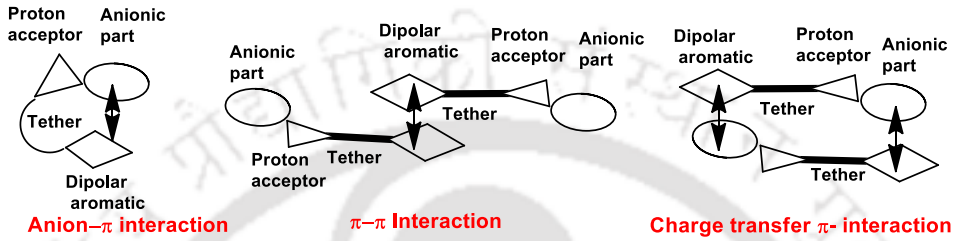

Figure 2.2.1: Schematic ways of representation of intra and inter-molecular π-interactions in a salt of a compound having cationic part comprised of dipolar aromatic unit tethered to a proton acceptor and anionic part having π-character.

The rings may also adopt arrangements such that the two or more aromatic rings are eclipsed to each other or occupying slightly parallel but at translated positions or in arrangement where two rings are in slightly oblique positions on top of each other or slightly displaced from each other. In order to delineate the fluorescence emission properties of the naphthalimide due to such arrangements of fluorophores and also to understand interactions among the cationic and anionic parts, four salts of **2.2.1** with different nitro-phenols or mineral acids listed in Figure 2.2.2 were prepared and their structural aspects and photophysical properties were investigated.

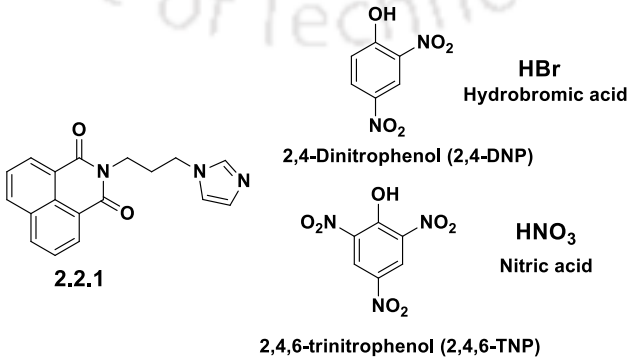

Figure 2.2.2: Naphthalimide derivative (**2.2.1**), nitrophenols and mineral acids used as coformer for **2.2.1**.

2.2.2: Synthesis and Structural descriptions of salts of N-(3-imidazol-1-yl-propyl)-1,8-naphthalimide(2.2.1)

The reactions of **2.2.1** with mineral acids such as hydrobromic acid and nitric acid, or nitrophenols such as 2,4-dinitrophenol (2,4-DNP) and 2,4,6-trinitrophenol (2,4,6-TNP) resulted in formation of the corresponding imidazolium salt. Each salt is structurally characterized by determining structure using single crystal X-ray diffraction technique (Figure 2.2.3 and 2.2.4). The bromide salt (**2.2.2**) has a conventional structure, where the two bromide ions forms hydrogen bond with N^+-H of the imidazolium cation for which D···A distance is 3.198(8) Å and 3.232(8) Å. The unit cell has two symmetry independent molecules. On the other hand, in the nitrate salt (**2.2.3**), two oxygen atoms of the anion form bifurcated hydrogen bonds as shown in Figure 2.2.3b. Each nitrate anion provides two different oxygen atoms as anchoring pivots to interact with hydrogen atom of N1-H or C16-H bond of imidazole. The hydrogen atom of N^+-H hydrogen bonded to O4 and O5 atoms; whereas, H atom of C16-H bond, acts as hydrogen bond donor to O3 and O5 atoms. The N1-H…O4 and N1-H…O5 bond parameters are 3.035 Å and 2.768 Å respectively. Similarly the C16-H…O3 and C16-H…O5 bond parameters are 3.369 Å and 3.096 Å respectively. Two molecules of this salt are held together by nitrate ion bridging two cationic units through N-H···O and C-H···O interactions.

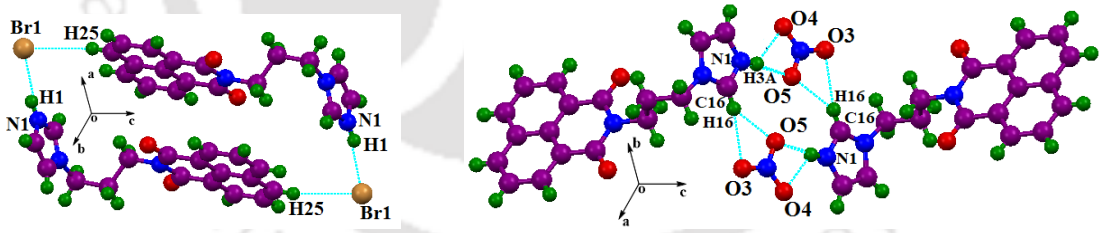

(a) (b)

Figure 2.2.3: Hydrogen bonded self-assemblies of salts (a) **2.2.2** and (b) **2.2.3**.

However, analysis of the packing patterns of the salts of **2.2.1** with 2,4-DNP and with 2,4,6-TNP have shown certain striking differences in π-stacking patterns from the packing patterns of the salts of the **2.2.1** with mineral acids. The packing patterns observed in the structures of these two nitrophenolate salts are shown in Figure 2.2.4. The 2,4-DNP salt (**2.2.4**) has stacking interactions among the naphthalimide rings of two independent neighboring molecules. This occurs through parallel arrangements of the dipolar naphthalimide rings. The

stacking arrangements have partially negative side of one naphthalimide ring lying over the partially positive portion of another naphthalimide ring. The centroid to centroid distance between the rings is 3.492 Å. Hence, there is a clear indication of strong π-π interactions.[12]

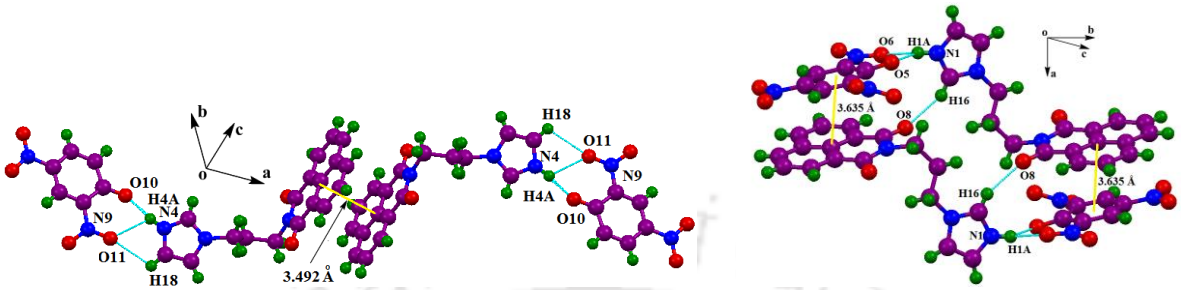

(a) (b)

Figure 2.2.4: Hydrogen bonded self-assemblies of salts (a) **2.2.4** showing Parallel arrangements of the dipolar napthalimide rings through π-interactions and (b) **2.2.5** showing Charge-transfer interactions between cation and anion.

Since, naphthalimide ring is dipolar, considering the imide portion of the ring as the head part and the naphthalene ring part as the tail, the packing pattern may be described to have naphthalimide units organized in head to tail arrangements. It may be noted that depending on the tethers naphthalimide compounds form stacks among their aromatic rings either in head to tail or head to head arrangements.[1e] Such arrangements were observed in different positional isomers of naphthalimide tethered to pyridine unit through methylene tether. Those could be modulated by changing hydrogen bond patterns through formation of salts.[13] On the other hand, naphthalimide rings arrange among themselves in different ways in lattices due to the factors like coordination, solvent and crystallization process.[7] The packing pattern of the 2,4,6-trinitrophenolate salt (**2.2.5**) of **2.2.1** has no π-stacking interactions among the naphthalimide rings. But two hydrogen bonded molecules of the salt form dimeric assembly in which the naphthalimide ring of one molecule is located parallel over the ring of 2,4,6-trinitrophenolate anion of another molecule. The distance between two such parallel rings is 3.653 Å. This distance is good enough for a weak π-interaction between the rings.[12] It indicates a charge-transfer interaction between the electron deficient nitrophenolate ring and electron rich naphthalene part of naphthalimide unit. We could not crystallize the parent compound **2.2.1** to determine the crystal structure, so the stacking pattern in the parent compound is not clear. The prominent hydrogen bond parameters of the salts are listed in the Table 2.1.3. The bulk purity of each salt was determined by recording the individual powder

X-ray diffraction patterns of each sample and comparing independently such diffraction patterns with the powder X-ray diffraction patterns generated from the respective crystallographic information files (Figure 2.2.18). The powder patterns in each case has tally among the peaks of respective Miller indices showing that each salt in solid form is in single phase.

Table 2.2.1: Different torsion angles in structures of the salts of **2.2.1**.

Imidanap	Torsion angle (°)	**2.2.2**	**2.2.3**	**2.2.4**	**2.2.5**
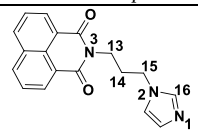	N3-C13-C14-C15	-178.23/-175.98	178.15	-174.27/62.29	-64.62
	C13-C14-C15-N2	-69.59/-67.12	66.12	56.06/168.47	178.09
	C14-C15-N2-C16	104.52/112.63	-108.38	100.01/86.18	18.67
	C15-N2-C16-N1	-179.30/179.13	-179.95	-171.55/178.64	177.55

Conformation adjustments in different organic crystals of flexible organic compounds occur due to weak solute-solvent interactions encountered during crystallization to adopt a tight packed structure. This is possible as weak non-covalent interactions have comparable energies to cause conformation changes such that it is neither the conformer of lowest energy state nor the highest energy but an intermediate one.[14] In the present study the cationic part in the structure of the salts show different conformational adjustments. Different torsion angles reflect the spatial orientations of the imidazole unit in each salt. The relevant torsion angles helpful to explain orientations of the observed conformational adjustments are listed in Table 2.2.1. It is clear that the orientation in the two mineral acids are similar, whereas large deviation in the orientation is observed in the salt of 2,4,6-TNP. The origin of this large difference is attributed to strong charge-transfer interactions between the cationic and anionic parts.

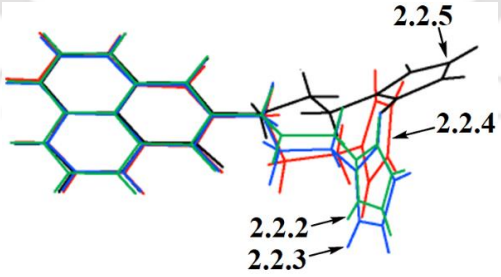

Figure 2.2.5: Overlaid structural diagram of the cationic part in the salts **2.2.4**-**2.2.5**.

2.2.3: Thermal study and Hirshfeld surface analysis

Thermal properties of the salts **2.2.2**-**2.2.5** and **2.2.1** were studied by differential scanning calorimetry (DSC) studies. DSC plots for **2.2.1** and corresponding salts are shown in Figure 2.2.6. The bromide and nitrate salt shows sharp melting at 280 ºC and 218 ºC respectively.

Due to ionic nature of the salts, the melting points of the salts are obviously higher than the melting point of the parent compound. The parent compound melts at 164 ºC. The exception is that the 2,4-dinitrophenolate salt melts slightly lower temperature than the melting point of **2.2.1** and it does not show significant exothermic process at higher temperature, which is commonly observed in nitro-phenols. Whereas, 2,4,6-trinitrphenolate salt has melting point at 173 ºC, which is slightly higher than the melting point of the parent compound. This salt shows highly exothermic decomposition process around 290-320 ºC, suggesting it to be a material of high energy.

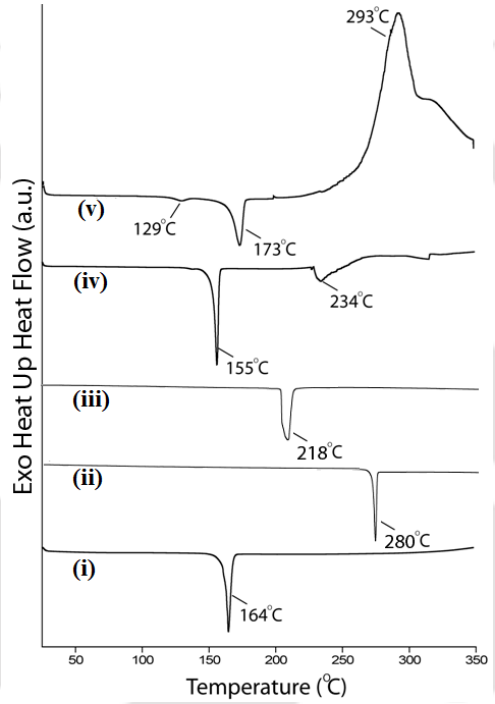

Figure 2.2.6: DSC plots of (i) **2.2.1**, (ii) **2.2.2**, (iii) **2.2.3**, (iv) **2.2.4**, and (v) **2.2.5**.

Hirshfeld surface analysis revealed that the nitrophenolate salts and nitrate salt have substantial amount of contributions ranging from 29.8% to 38.8% of hydrogen bonds involving O-H bonds, whereas such a contribution is lower in the case of the bromide salt, which is 14.5% (Figure 2.2.7). On the other hand, the packing pattern of bromide salt and nitrate salt has comparable hydrogen bonds involving C-H bonds, which are 18.9% and 20.7% respectively. The 2,4-nitrophenolate salt has such interactions 12% as compared to the 6.4% similar interactions observed in the 2,4,6-trinitrophenolate salt. Thus, there are clear differences in hydrophobicity of the salts of mineral acids from the nitro-phenols.

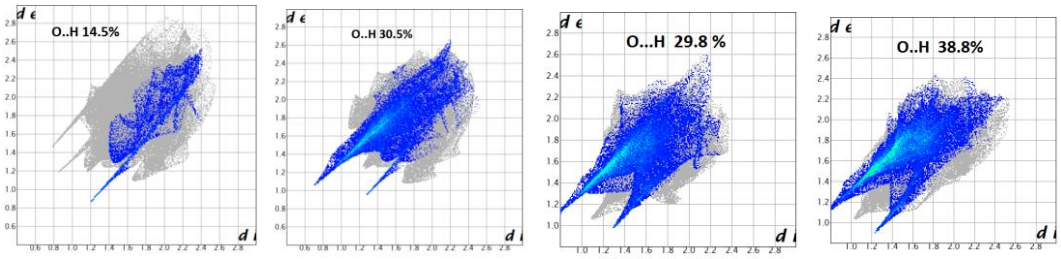

(a) (b) (c) (d)

Figure 2.2.7: Fingerprint plots for salts (a) **2.2.2**, (b) **2.2.3**, (c) **2.2.4** and (e) **2.2.5** with O···H interactions highlighted in colour.

2.2.4: Fluorescence emission study and Aggregation behaviour of 2.2.1

The salts of the **2.2.1** show color differences under ordinary light as well as on exposure to UV-light. The powdered samples of **2.2.1**, bromide and nitrate salts are fluorescent, whereas the powdered samples of two nitrophenolate salts are non-fluorescent (Figure 2.2.8). The fluorescence emission spectra of the powdered samples of the compound and the salts show that the nitrate and bromide salt of **2.2.1** has similar fluorescence emission at 488 nm, whereas the **2.2.1** has emission at 474 nm. Visually there is difference in colors of the salts where the cationic part is common, the observed differences in colors (Figure 2.2.8a and b) are attributed to combined effects of the anions and cations.

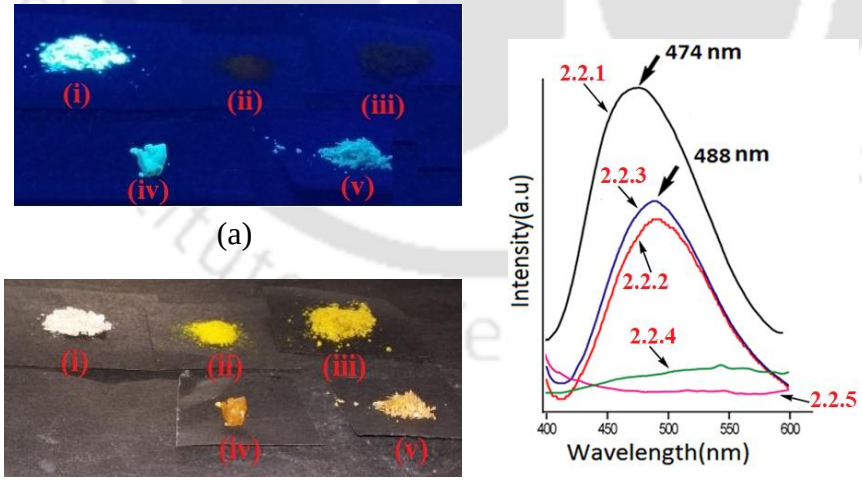

(a) (b) (c)

Figure 2.2.8: Fluorescence images of solid samples of (i) **2.2.1**, (ii) **2.2.4**, (iii) **2.2.5**, (iv) **2.2.3** and (v) **2.2.2** on exposure of (a) 365 nm UV-light and (b) normal light. (c) Fluorescence emission of solid sample of **2.2.1**-**2.2.5**. (λ_{ex}= 320 nm).

It is also clear from the structural study that the nitro-phenolate salts either have π-interactions between pair of naphthalimide rings or between naphthalimide and nitrophenolate rings. Hence, the π-stacking interactions rather than the protonation of imidazole caused the observed quenching of fluorescence emission of powdered samples. Similar quenching of emission caused by π-stacking is also found in common π-aromatic fluorophores.[2] The emission positions and quantum yields of the parent compound and the respective salts are listed in Table 2.2.2. The results show that fluorescence emission maximum of each solid sample of nitrophenolate salt occurs with large shifts from the excitation wavelength. On the other hand, the emission peak of the **2.2.1** and its nitrate and bromide salts are at comparable wavelength to that of the parent compound.

Table 2.2.2: Absorbance, fluorescence excitation and emission of solid samples the compound **2.2.1-2.2.5.**

Compound/Salts	λ_{ab} (nm)	λ_{ex} (nm)	λ_{em} (nm)	Φ_F (Quantum yield)
2.2.1	365	320	474	0.48
2.2.2	387	375	488	0.30
2.2.3	398	370	488	0.34
2.2.4	400-472 (broad)	320	545	0.011
2.2.5	410-460 (broad)	320	540	0.010

As a consequence of the salt formation the quantum yield in the case of the nitrate and bromide salts are relatively less than the **2.2.1** and nitrophenolate salts show fluorescence quenching. To get insight to this issue, we have theoretically calculated by DFT using B3LYP functional with 6-31+G (d,p) as basis set the energy and obtained the orbital pictures of HOMO and LUMO of the **2.2.1** to compare with that of the corresponding nitrophenolate salts. We observe an interesting picture on the localized HOMO and LUMO of the salts (Figure 2.2.9). In the case of the **2.2.1** the HOMO-1 and LUMO are localized at respective naphthalimide fluorophore, whereas the HOMO in this case is localized at the imidazole ring. Thus, an emission involving LUMO to HOMO-1 requires extra energy to overcome the effect of the HOMO namely the effect of electrons in the imidazole ring; hence it is a partially quenched state than an ordinary naphthalimide. The nitrophenolates salts are formed by protonation on imidazole by the nitrophenols; in all cases the LUMO are localized at naphthalimide ring.

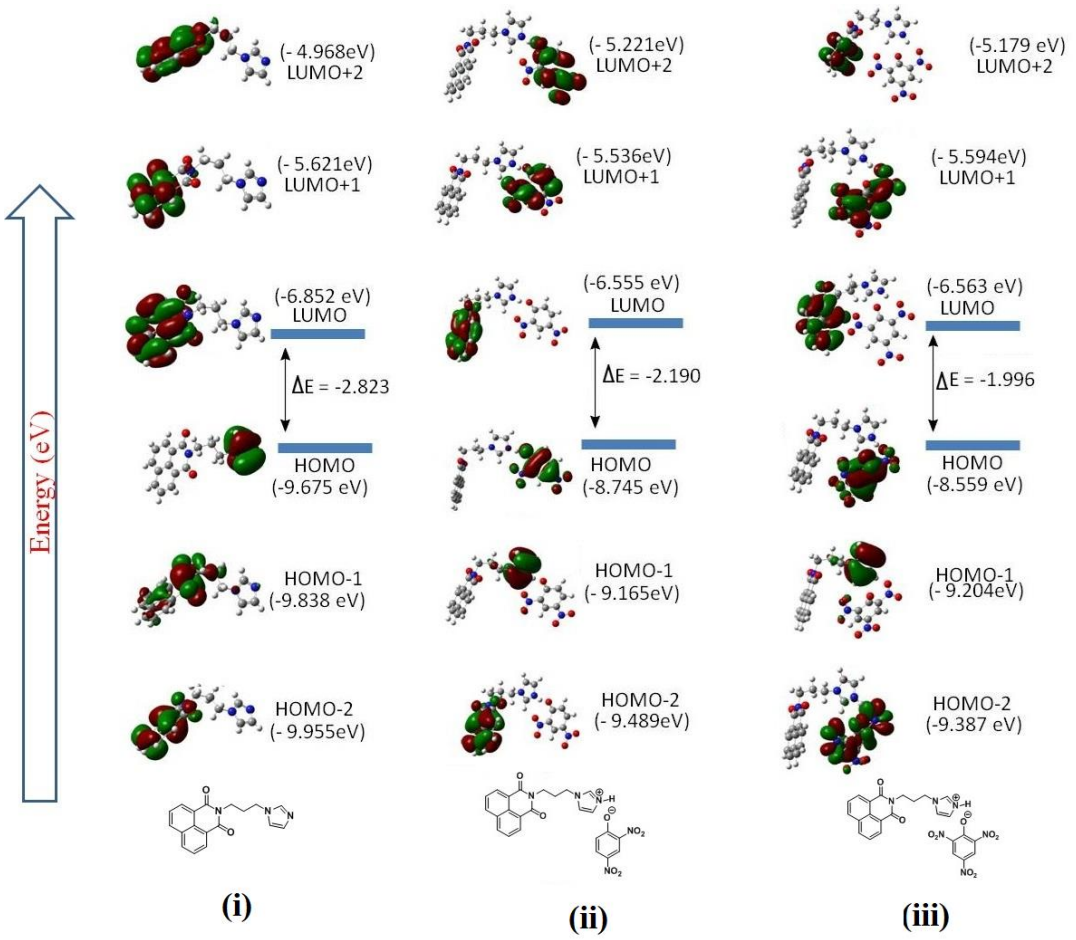

Figure 2.2.9: HOMO-LUMO of (i) **2.2.1**, (ii) **2.2.4**, and (iii) **2.2.5** calculated by DFT using B3LYP functional with 6-31+G (d,p) as basis set.

In the case of the salt of 2,4-dinitrophenol with **2.2.1** the HOMO is localized at the nitrophenolate ring, and HOMO-1 has orbitals localized at imidazole ring whereas the HOMO-2 is localized at naphthalimide ring. Similarly the salt of 2,4,6-trinitrophenol with **2.2.1** has the modified energy levels, having wide differences in energies and in sequence from the parent compound. Thus, the emission gets quenched in these cases due to the modification of the energy levels by putting the level having orbitals localized on naphthalimide rings at lower hierarchy in energy than the HOMO.

In solution, the salts of the **2.2.1** have much different fluorescence emission features from those ones observed from the respective powdered samples (Figure 2.2.10). Conventional fluorescence emission shown by naphthalimide derivatives is observed in **2.2.1**, it shows an emission at 377 nm in acetonitrile upon excitation at 320 nm. This emission is photo-induced electron transfer (PET) OFF state due to the intervention of emission path by the lone-pair of electrons on the nitrogen atom of imidazole. Once an acid is added to a solution of **2.2.1**, the

nitrogen atom gets protonated and a PET-ON state is generated, due to which the fluorescence emission intensity at 377 nm increases from a solution of **2.2.1**. This observation is evident from the fact that, upon addition of mineral acids, namely nitric acid or hydrobromic acid **(**Figure 2.2.9a and b) there is increase in emission intensity without a significant shift in wavelength of emission. The conformational effect[15] as well as protonation of the nitrogen atom located at remote site/s or on a fluorophore[16] causing PET is an established fact, but in the present case there is conformational change as well as protonation of the imidazole while interacting with an acid. On the other hand, similar effect of PET to cause fluorescence enhancement was not observed on addition of a solution of 2,4-DNP or 2,4,6-TNP to an acetonitrile solution of **2.2.1**. In these two cases, emission intensities were decreased and such decreases were also not accompanied any significant shift in the position of the emission maximum **(**Figure 2.2.9c and d). In addition to the electrostatically guided hydrogen bonds in these two nitrophenolate salts there are charge-transfer interactions occurring through π-interactions among the rings. The latter contributes to the fluorescence quenching. Our group previously showed that fluorescence emission intensity of naphthalenediimide change in dissimilar manner by different anions depending on the extent of anion-π interactions. Such changes were observed due to protonation at remote site of a tether affecting a partially PET-OFF state of the parent compound.[8d] In those examples, the interplay of weak interactions provided anion-π interactions to influence emission spectra of the parent compound. There are also examples in which the fluorescence emissions of poly-aromatics are quenched by π-stacking with pyromelleticdiimide derivatives.[17]

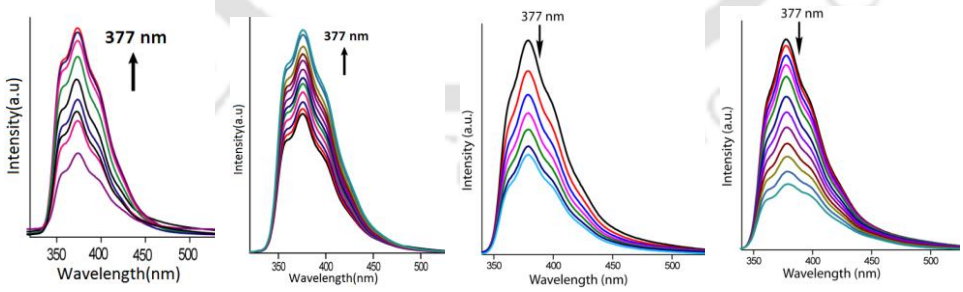

(a) (b) (c) (d)

Figure 2.2.10: Fluorescence emission of **2.2.1** (10^{-4} M in acetonitrile), was enhanced upon addition of (a) HBr, (b) HNO_3. Decrease in emission of **2.2.1** upon addition of solution of (c) 2,4,-DNP, (d) 2,4,6-TNP (excitation at 320 nm, 10^{-4} M in acetonitrile, 20 µl in each aliquot).

We also had another interesting observation at this stage; we found that addition of water to a solution of **2.2.1** in acetonitrile enhanced the intensity of the emission maxima at 377 nm (Figure 2.2.11a). This increase in intensity reached a maximum at a particular concentration when there is 50% water in acetonitrile. Beyond this concentration of water, the emission intensity started to decrease; and this decrease occurred with a shift of 20 nm towards longer wavelength. Since the solubility of the **2.2.1** in water is low, hence we had an apprehension that the decrease in intensity of the fluorescence emission could be due to precipitation of the compound from solution upon addition of water. But such apprehension was nullified, as we observed quenching of emission at 377 nm from a solution of **2.2.1** in mixed solvent comprising of acetonitrile and water in those ratios in a similar manner without any visible precipitation from the solution. The initial increase in emission intensity upon addition of water is attributed to weakening of π-interactions that is present in less-polar aprotic solvent upon addition of water, but as the concentration of water was increased the effect of water as independently act in hydrogen bonded scheme was enhanced. Thus at higher concentration of water the reorganization of molecules took place to once again permit π-interaction to cause quenching of fluorescence emission. It was also found that when 2,4,6-TNP solution in acetonitrile was added to a solution of **2.2.1** the intensity of emission at 397 nm decreases and finally emission at this wavelength gets quenched with increase in concentrations of 2,4,6-TNP (Figure 2.2.11b). This result suggested that the aggregates formed by assistance of water molecules transform or degrade to form the corresponding salts by interacting with 2,4,6-trinitrophenol.

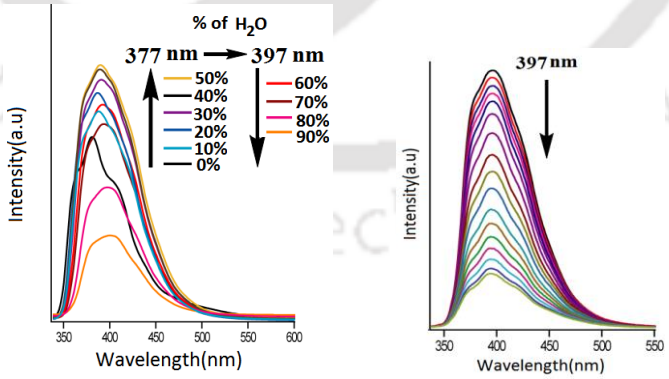

(a) (b)

Figure 2.2.11: (a) Fluorescence emission spectra (λ_{ex} = 320 nm) of **2.2.1** (10^{-4} M in acetonitrile) upon addition of different amounts of water and (b) quenching of fluorescence emission of **2.2.1** in 50% water in acetonitrile (10^{-4} M) upon addition of 2,4,6-TNP (20 µL in each aliquot).

To ascertain the formation of aggregates in solution upon addition of water and also to understand the consequences of addition of 2,4,6-TNP solution to such aggregates, dynamic light scattering study was performed under different conditions. The parent compound has average particle size 1546 nm in acetonitrile solution, whereas in acetonitrile-water solvent mixture the average particle size is 1733 nm. The average particle size is further higher, namely 3490 nm in the solution of **2.2.1** having 2,4,6-TNP (Figure 2.2.12). These results suggest that different kinds of self-assemblies (aggregates) are present in the respective solution. Images of dropcasted samples from the precipitate obtained from the respective solution also have revealed that each precipitate had different morphology. The precipitate obtained from acetonitrile solution of **2.2.1** had fibrous appearance, whereas the precipitate obtained from mixed solvent comprising of water and acetonitrile the precipitate had particles with globular appearance and the precipitate obtained from **2.2.1** and 2,4,6-trinitrophenol from a solution in water acetonitrile mixture was fluffy (Figure 2.2.19). The fluorescence emission of each salt was measured independently by dissolving the respective salt in acetonitrile. The emission spectra of the salts in solution follow more or less similar emission trend as those were observed from the respective solid sample. The solid sample of 2,4-dinitrophenolate salt was non-fluorescent but in solution it was very weakly fluorescent. This difference is attributed to partial loss of π-interactions between the naphthalimide rings in solution due to solute-solvent interactions.

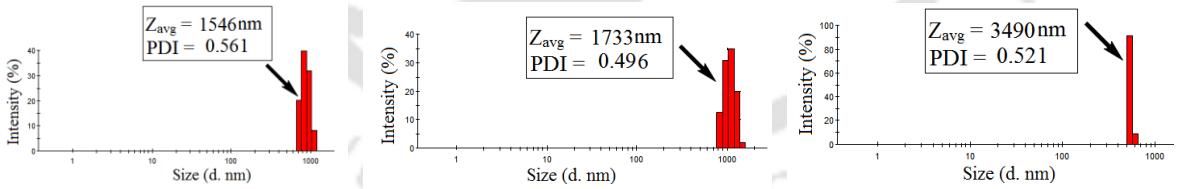

(a) (b) (c)

Figure 2.2.12: Particle size analysis from dynamic light scattering of solution of **2.2.1** in (a) acetonitrile (b) acetonitrile-water (1:1 v/v) mixed solvent; (c) acetonitrile-water (1:1 v/v) having equivalent amount of 2,4,6-TNP with respect to **2.2.1**.

The ^{1}H-NMR spectra of nitrate and bromide salts showed that protonation at imidazole ring, affect the chemical shift of this ring protons, alone differs from the chemical shifts of the similar protons in the parent compound (Figure 2.2.14). The chemical shift positions of the

protons on the nitrophenolate salts are wide-apart from the observed chemical shifts for the protons of the parent components; this is due to significant charge transfer interactions in solution among the aromatic rings of the salt (Figure 2.2.15 and 2.2.16.)

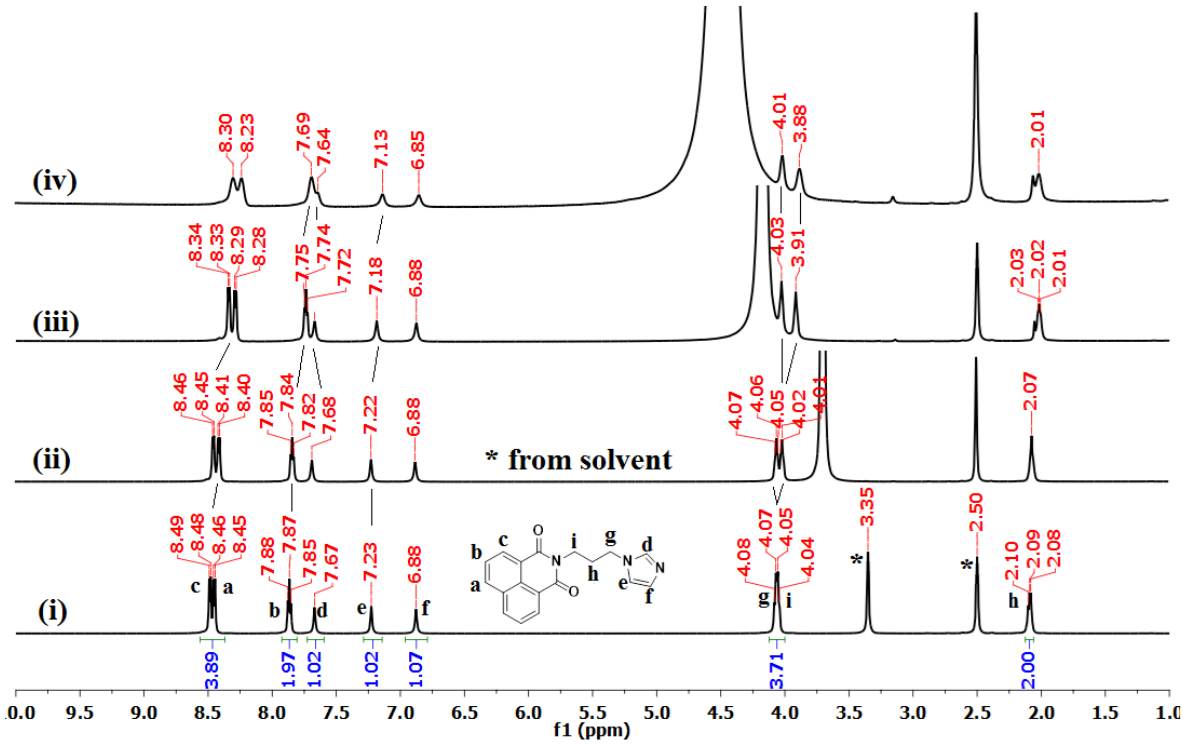

Figure 2.2.13: ^{1}H NMR (600 MHz) spectra of **2.2.1** in (i) DMSO-d_6, (ii) DMSO-d_6 with 20% D_2O, (iii) DMSO-d_6 with 40 % D_2O and (iv) DMSO-d_6 with 50 % D_2O.

Since the changes in fluorescence emission of a solution of **2.2.1** in DMSO upon addition of water was similar to the observed emission spectral changes of solution of **2.2.1** in acetonitrile upon addition of water **(**Figure 2.2.23). Hence, to see the effect of water addition on the changes in assembly of **2.2.1** in solution, we carried out ^{1}H-NMR titration of a solution of **2.2.1** in DMSO-d_6 by adding deuterated water (D_2O) **(**Figure 2.2.13**)**. The signal for proton on imidazole labeled as 'e' appears at 7.23 ppm. This signal was slightly shielded upon addition of D_2O and it appears at 7.13 ppm. This shift in the chemical shift position was due to the formation of hydrogen bond between imidazole and D_2O. Significant change in position of the chemical shift of the proton on the naphthalimide ring marked as 'b' was also observed. This signal of **2.2.1** appeared at 7.87 ppm, upon increase in D_2O concentration it shifted to 7.69 ppm. The signals from the protons 'b' merged with the signal from the proton 'd' of the imidazole ring. The protons 'a' and 'c' were shielded on addition of D_2O. The

chemical shifts of the signal for -CH_2- protons located next to the nitrogen atoms marked as 'i' and 'g' significantly changed. These two sets of protons appeared as multiplet at 4.04-4.08 ppm; the peaks splited up and separate into two sets of signals as the concentration of D_2O was increased. On the other hand, the chemical shift position of the protons of the -CH_2- group flanked by two methylene groups marked as 'h' were also split up. This suggested that there was conformation adjustments of the flexible arm to change the orientation of the imidazole unit. As the concentration of D_2O is increased the D_2O molecules form hydrogen bonds with **2.2.1**, this caused conformation adjustment to reorganize the orientation of imidazole ring across the imide unit. Hence, this change influenced the transition probability of emission; thereby enhanced the fluorescence intensity of the fluorescence emission peak. As the water content was increased to a particular concentration, the molecule adopted a conformation that is less suitable for PET-ON state and after that concentration it retraces the path to reorient the imidazole ring so as to disfavor PET-ON state. From this concentration, the increase in amount of water in solution changes the conformation to provide PET-OFF state. Subsequently the fluorescence quenching takes place beyond this critical concentration. Conformational flexible π-aromatic fluorophores show emission at longer wavelengths upon addition of water to a solution of such compound due to aggregation induced emission.[18] But in the present example, no such emission is observed.[18]

Hence, the present example is an example for fluorescence intensity modulation where nominal shift in wavelength but with large change in emission intensity upon interaction with acids were observed. The given examples on comparison of emission properties with analogous fluorophore[10c] establishes that same fluorophore upon change of tethers and substituent at remote site provide avenues for wavelength modulation or intensity modulation.

2.2.5: Conclusions

In solution the **2.2.1** shows a partially quenched fluorescence emission due to the photo-induced emission affected by the lone-pair of electrons on the nitrogen atom of the imidazole ring. Upon protonation of this proton by mineral acid, the PET-ON state is observed. The 2,4-dinitrophenolate salt of **2.2.1** has π-stacking between naphthalimide rings; whereas the 2,4,6-trinitrophenolate salt of **2.2.1** has stacks between the aromatic rings of nitrophenolate with naphthalimide ring. Though independent type of π-interactions in the nitro-phenolate salts of **2.2.1** with 2,4-DNP and 2,4,6-TNP are observed, each causes quenching of fluorescence. Due

to hydrogen bonds the flexible arm of **2.2.1** undergoes conformation adjustments in the presence of water; this effect causes fluorescence enhancement. Such enhanced emission state can be easily quenched by adding excess of water or by adding a strong π-acceptor such as 2,4,6-trinitrophenol. In summary, a naphthalimide derivative that showed PET emissions in solution, showed emissions in much different fashion in solid state. In solid state the stacking effect predominates to quench fluorescence. The emission properties in solid and solution state are highly case sensitive. It also has established that with prior knowledge on emission paths, a fluorophore decorated by using different tethers and substituents to cause predictable modulation of emission wavelength or intensity.

2.2.6: Experimental section

Synthesis and characterization of compound 2.2.1 and salts 2.2.2-2.1.5:

N-(3-imidazol-1-yl-propyl)-1,8-naphthalimide(**2.2.1**) was synthesized by a reported procedure.[5d] The crystals of salts were obtained by slow evaporation of respective solution of **2.2.1** (1mmol) with the corresponding acid (equimolar) namely nitric acid, hydrobromic acid, 2,4-dinitrophenol, 2,4,6-trinitrophenol in methanol (25 mL).

2.2.2: Isolated yield: 57%. ^{1}H-NMR (600 MHz, DMSO-d_6): 9.13 (d, J = 6 Hz, 1H), 8.50 (m, J = 6Hz, 4H), 7.90 (t, J =12Hz, 2H), 7.83 (t, J = 6Hz, 1H), 7.70 (t, J = 6Hz, 1H), 4.30 (t, J = 6Hz, 2H), 4.10 (t, J = 6 Hz, 2H), 2.24(m, J = 12 Hz, 2H). IR (KBr, cm^{-1}): 3447 (br,), 3136 (s), 3095 (w), 3013 (w), 2996 (m), 2923 (w), 2796 (s), 2750 (w), 2615 (s), 1700(s), 1662 (s), 1589 (s), 1546 (m), 1512 (w), 1453 (w), 1439 (s), 1393 (s), 1373 (m), 1269(m), 1237 (s), 1166 (m), 1144 (w), 1057 (w), 1030 (w), 974 (m), 906 (w), 880 (w), 850 (s), 787 (s), 766 (m), 741 (w), 630 (s), 579 (m), 541 (w), 419 (w).

2.2.3: Isolated yield: 57%. ^{1}H-NMR (600 MHz, DMSO-d_6): 9.11 (d, J = 6 Hz, 1H), 8.50 (m, J = 6 Hz, 4H), 7.90 (t, J = 6Hz, 2H), 7.82 (s, 1H), 7.69 (s, 1H), 4.30 (t, J = 6 Hz, 2H), 4.10 (t, J = 6 Hz, 2H), 2.24 (m, J = 6 Hz, 2H). IR (KBr, cm^{-1}): 3433 (br,), 3136 (s), 3108 (w), 3059 (w), 1699 (s), 1663 (s), 1625 (m), 1589 (s), 1453 (w), 1438 (m), 1384 (s), 1348 (m), 1286 (w), 1269 (m), 1236 (s), 1171 (m), 1111 (m), 1089 (w), 1073 (m), 1031 (s), 973 (w), 849 (s), 741 (w), 719 (s), 664 (m), 655 (w), 540 (s), 513(w).

2.2.4: Isolated yield: 65%. ^{1}H-NMR (600 MHz, $CDCl_3$): 9.06 (d, J = 6 Hz, 1H), 8.61 (d, J = 6Hz, 2H), 8.43 (s, 1H), 8.24 (d, J = 6Hz, 2H), 7.78 (t, J = 6Hz, 2H), 7.64 (s, 1H), 7.31 (d, J = 12Hz, 1H), 7.04 (d, J = 18 Hz, 1H), 4.26 (t, J = 6 Hz, 2H), 4.10 (t, J = 6 Hz, 2H), 2.29 (m, J = 6Hz, 2H). IR (KBr, cm-1): 3438 (br, w), 1699 (s), 1654(s) 1597 (s), 1556 (s), 1526 (s)

1483 (s), 1439 (s), 1372 (w), 1326 (w), 1313 (w), 1256 (w), 1235 (w), 1174 (s), 1130 (w), 1053 (s), 924 (s), 885 (w), 842 (w), 829 (w), 786 (w), 773 (s), 750 (s), 750 (w), 707 (s), 668 (w), 637 (w), 540 (w).

2.2.5: Isolated yield: 71 %. ^{1}H-NMR (600 MHz, $CDCl_3$): 8.92 (s, 1H), 8.77 (s, 1H), 8.63 (d, J = 6 Hz, 2H), 8.27 (d, J = 6Hz, 2H), 7.80 (t, J = 6Hz, 2H), 7.53 (s, 1H), 7.38 (s, 1H), 4.30 (m, 4H), 2.53 (m, 2H). IR (KBr, cm^{-1}): 3442 (br), 1697 (s), 1653 (s), 1609 (m), 1584(w), 1544 (s), 1387 (s), 1363 (s) 1337 (s), 1313 (s), 1267 (s), 1234 (w), 1158 (w), 1077 (w), 907 (w), 781 (s), 781 (w), 714 (w), 465 (s).

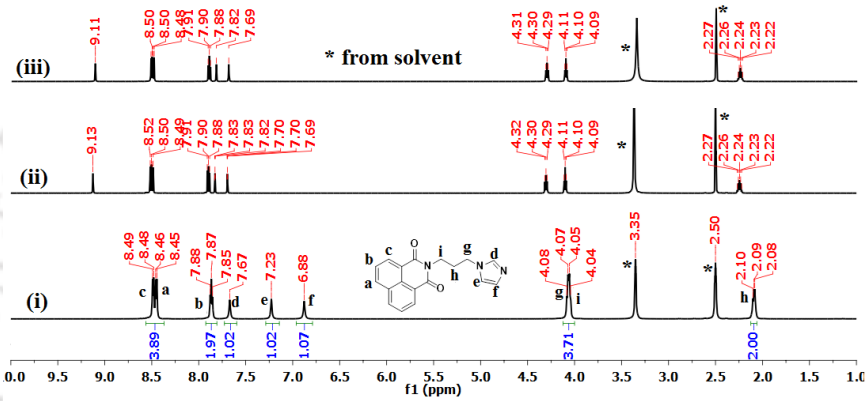

Figure 2.2.14: ^{1}H-NMR (600 MHz, DMSO-d_6) spectra of (i) **2.2.1**, (ii) **2.2.2** and (iii) **2.2.3**.

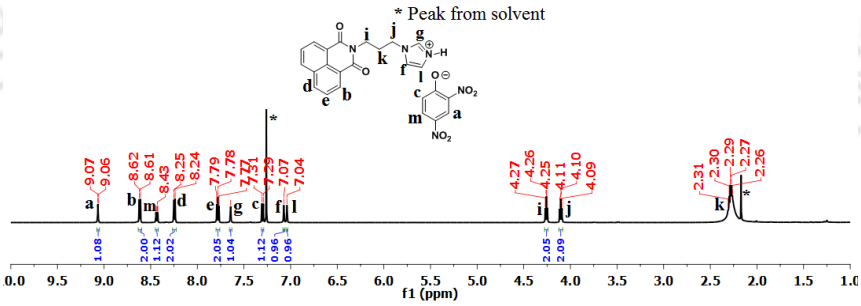

Figure 2.2.15: ^{1}H NMR (600 MHz, $CDCl_3$) spectra of **2.2.4**.

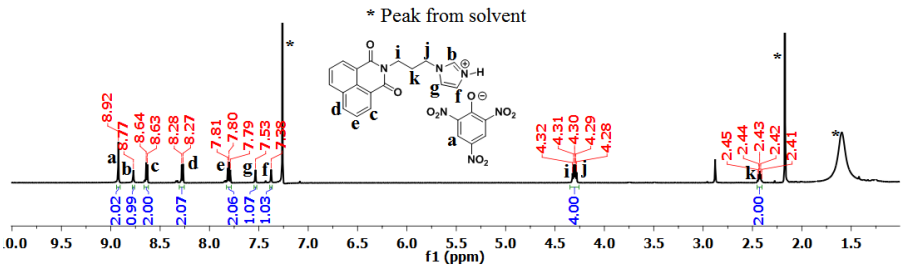

Figure 2.2.16: ^{1}H NMR (600 MHz, $CDCl_3$) spectra of **2.2.5**.

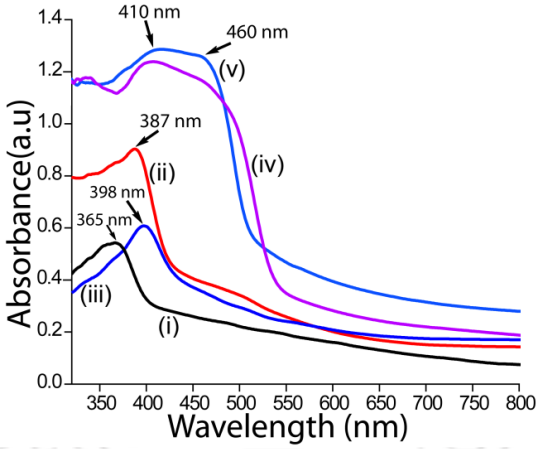

Figure 2.2.17: (a) Solid-state UV-visible spectra of (i) **2.2.1**, (ii) **2.2.2**, (iii) **2.2.3**, (iv) **2.2.4** (v) **2.2.5**.

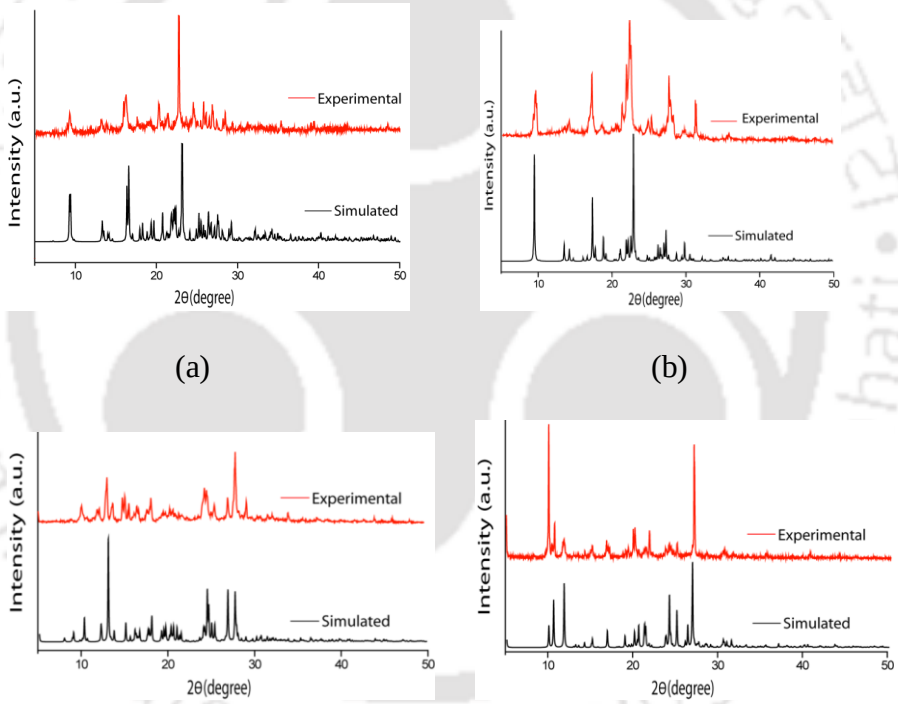

Figure 2.2.18: PXRD patterns of salt (a) **2.2.2**, (b) **2.2.3**, (c) **2.2.4**, and (d) **2.2.5** (Red= Experimental, Black= Simulated). Simulated PXRD pattern generated from cif file.

Table 2.2.3: Prominent hydrogen bond parameters of the salts of **2.2.1**

Salts	D-H…A	d_{D-H} (Å)	$d_{H...A}$ (Å)	$d_{D...A}$ (Å)	∠D-H…A (°)
2.2.2	N(1)-H(1)…Br(1) [1-x,1-y,1-z]	0.86(3)	2.39(3)	3.232(8)	167(3)
	N(4)-H(5A)...Br(2) [1-x,1-y,-z]	0.86(4)	2.35(5)	3.198(8)	170(6)
2.2.3	N(1)-H(3A)...O(4) [1/2-x,1/2+y,-z]	0.90(4)	2.34(4)	3.035(5)	134(3)
	N(1)-H(3A)...O(5) [1/2-x,1/2+y,-z]	0.90(4)	1.88(4)	2.768(4)	168(4)
	C(3)-H(3)...O(4 [-x,1+y,1/2-z]	0.93(4)	2.59(6)	3.231(6)	126(4)
	C(7)-H(7)...O(5) [-x,y,1/2-z]	0.93(5)	2.58(5)	3.379(6)	144(3)
	C(18)-H(18)…O(3)[1/2-x,1/2-y,1/2-z]	0.93(4)	2.48(3)	3.233(4)	138(5)
2.2.4	N(1)-H(1A)…O(5) [x,y,z]	0.88(2)	1.77(3)	2.627(4)	166(4)
	N(1)-H(1A)…O(6) [x,y,z]	0.88(3)	2.43(4)	2.904(4)	115(5)
	N(4)-H(4A)…O(10) [1-x,-y,1-z]	0.87(3)	1.77(3)	2.638(3)	171(2)
	N(4)-H(4A)…O (11) [1-x,-y,1-z]	0.87(5)	2.50(5)	2.938(4)	112(2)
2.2.5	N(1)-H(1A)…O(5) [1-x,1-y,-z]	0.94(4)	1.85(2)	2.700(3)	149(4)
	N(1)-H(1A)…O(6) [1-x,1-y,-z]	0.94(5)	2.13(9)	2.759(6)	123(7)
	C(7)-H(6)…O(7) [1-x,1-y,-z]	0.93(5)	2.46(7)	3.295(6)	150(6)
	C(16)-H(16)…O(8) [1-x,1-y,-z]	0.93(5)	2.28(4)	3.150(4)	155(2)
	C(18)-H(18)…O(8) [-x,1-y,-z]	0.93(5)	2.50(2)	3.295(3)	144(5)

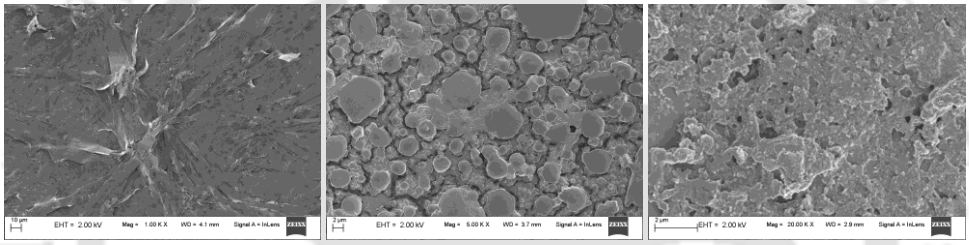

(a) (b) (c)

Figure 2.2.19: FESEM images of drop casted precipitates from solution of **2.2.1** in (a) acetonitrile; (b) acetonitrile-water (1:1 v/v) mixed solvent and (c) acetonitrile-water (1:1 v/v) with equivalent amount of 2,4,6-TNP and **2.2.1**.

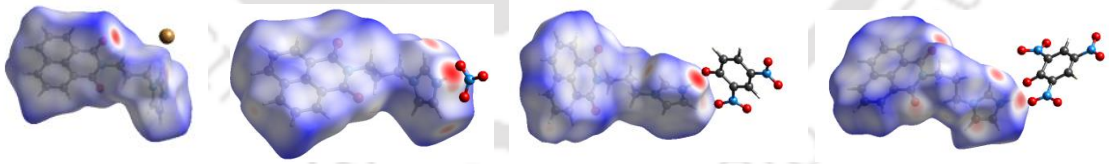

(a) (b) (c) (d)

Figure 2.2.20: Hirshfeld surface of (a) **2.2.2**, (b) **2.2.3**, (c) **2.2.4** and (d) **2.2.5**.

Table 2.2.4: Relative in percentages of various interactions from Hirshfeld surface analysis.

Bond	**2.2.2**	**2.2.3**	**2.2.4**	**2.2.5**
O···O	0.0	0.6	0.7	1.5
N···O	0.6	0.7	1.2	1.7
C···O	2.4	2.2	1.6	5.8
H···O	14.5	30.5	29.8	38.8
C···N	1.0	0.7	1.7	3.0
N···H	2.9	4.3	2.0	2.1
C···H	18.9	20.7	12.0	6.4
C···C	7.5	6.8	14.3	8.4
H···H	43.3	33.4	35.9	31.6

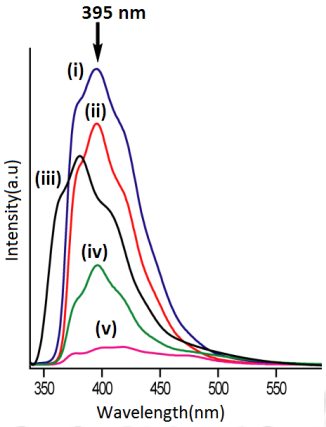

Figure 2.2.21: Fluorescence emission (10^{-4} M in acetonitrile, λ_{ex}= 320 nm) of (i) **2.2.3**, (ii) **2.2.2**, (iii) **2.2.1 (**iv) **2.2.4**, and (v) **2.2.5**.

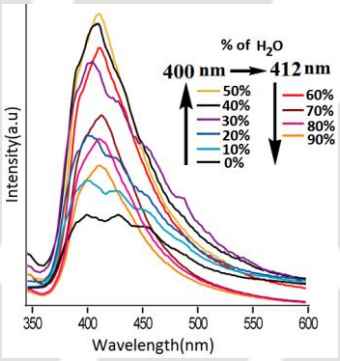

Figure 2.2.22: Fluorescence spectra (λ_{ex}= 320 nm) of **2.2.1**. (10^{-4} M in DMSO) with water in different ratio.

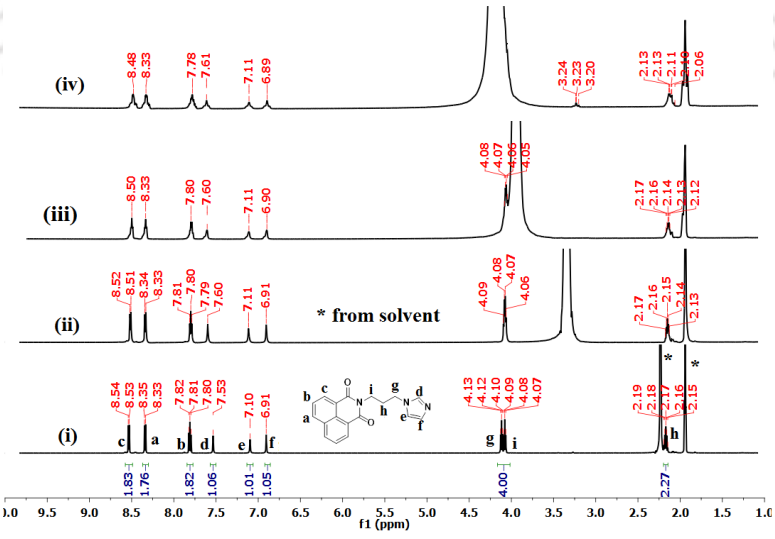

Figure 2.2.23: ^{1}H-NMR (600 MHz) spectra of **2.2.1** in (i) CD_3CN-d_3, (ii) 20% D_2O in CD_3CN-d_3, (iii) 40% D_2O in CD_3CN-d_3 and (iv) 50% D_2O CD_3CN-d_3.

2.2.7: References:

1. (a) M. A. Kobaisi, S. V. Bhosale, K. Latham, A. M. Raynor, S. V. Bhosale, *Chem. Rev*., 2016, **116**, 11685-11796; (b) B. Kupcewicz, M. Małecka, *Cryst. Growth Des*., 2015, **15**, 3893-3904; (c) G. K. Kole, R. Medishetty, L. L. Koh, J. J. Vittal, *Chem. Commun*., 2013, **49**, 6298-6300; (d) F. Grepioni, S. d. Agostino, D. Braga, A. Bertocco, L. Catalano, B. Ventura, *J. Mater. Chem. C*., 2015, **3**, 9425-9434; (e) J. K. Nath, J. B. Baruah, *CrystEngComm*., 2015, **17**, 8575-8595; (f) Y. Shao, G. -Z. Yin, X. R, X. Zhang, J. Wang, K. Guo, X. Li, C. Wesdemiotis, W. B. Zhang, S. Yang, M. Zhu, B. Sun, *RSC Adv*., 2017, **7**, 6530-6537.

2. (a) X. Zhao, M. R. Pinto, L. M. Hardison, J. Mwaura, J. Muller, H. Jiang, D. Witker, V. D. Kleiman, J. R. Reynolds, K. S. Schanze, *Macromolecules*., 2006, **39**, 6355-6366; (b) S. A. Jenekhe, J. A. Osaheni, *Science*., 1994, **265**, 765-768.

3. J. J. Reczek, K. R. Villazor, V. Lynch, T. M. Swager, B. L. Iverson, *J. Am. Chem. Soc*., 2006, **128**, 7995-8002.

4. (a) J. R. Askim, M. Mahmoudia, K. S. Suslick, *Chem. Soc. Rev*., 2013, **42**, 8649-8682; (b) P. Khakhlary, J. B. Baruah, *Inorg. Chim. Acta*., 2016, **440**, 53-61; (c) G. Farruggia, S. Iotti, L. Prodi, M. Montalti, N. Zaccheroni, P. B. Savage, V. Trapani, P. Sale, F. I. Wolf, *J. Am. Chem. Soc*., 2006, **128**, 344-350; (d) Y. K. Yang, K. J. Yook, J. Tae, *J. Am. Chem. Soc*., 2005, **127**, 16760-16761; (e) A. Coskun, E. U. Akkaya, *J. Am. Chem. Soc*., 2005, **127**, 10464-10465.

5. (a) A. P. de Silva, R. A. D. D. Rupasinghe, *J. Chem. Soc., Chem. Commun*., 1985, 1669-1670; (b) A. P. de Silva, S. A. de Silva, *J. Chem. Soc., Chem. Commun*., 1986, 1709-1710; (c) E. B. Veale, J. A. Kitchen, T. Gunnlaugsson, *Supramol. Chem*., 2013, **25**, 101-108; (d) J. K. Nath, J. B. Baruah, *Inorg. Chem. Front*. 2014, **1**, 342-351.

6. (a) K. Hanaoka, Y. Muramatsu, Y. Urano, T. Terai, T. Nagano, *Chem. Eur. J*., 2010, **16** 568-572; (b) Z. Xu, S. J. Han, C. Lee, J. Yoon, D. R. Spring, *Chem. Commun*., 2010, **46**, 1679-1681; (c) Z. Xu, K. H. Baek, H. N. Kim, J. Cui, X. Qian, D. R. Spring, I. Shin, J. Yoon, *J. Am. Chem. Soc*., 2010, **132**, 601-610; (d) R. Parkesh, T. C. Lee, T. Gunnlaugsson, *Org. Biomol. Chem*., 2007, **5**, 310-317; (e) T. Gunnlaugsson, T. C. Lee, R. Parkesh, *Org. Biomol. Chem*., 2003, **1**, 3265-3267; (f) P. Nadhinkonda, M. P. Begaye, Z, Chao, M. D. Heagy, *Org Biomol Chem*., 2010, **8**, 3195-3201; (g) J. Nath, A. Mondal, A. Powell, J. B. Baruah, *Cryst. Growth Des*., 2014, **14**, 4735-4748.

7. (a) D. L Reger, E. Sirianni. J. J. Horger, M. D. Smith, R. F. Semeniuc, *Cryst. Growth Des*., 2010, **10**, 386-393; (b) D. L. Reger, A. P. Leitner, M. D. Smith, *Cryst. Growth Des*., 2016,

16, 527-536; (c) Q. Feng, M. Wang, B. Dong, J. He, C. Xu, *Cryst. Growth Des*., 2013, **13**, 4418-4427; (d) D. Singh, J. B. Baruah, *Cryst. Growth Des*., 2012, **12**, 2109-2121.

8. (a) M. P. Singh, J. B. Baruah, *ChemistrySelect*., 2019, **4**, 10-16; (b) A. Tarai, J. B. Baruah, *ChemistrySelect*., 2017, **2**, 10101-10106; (c) A. Tarai, J. B. Baruah, *Cryst. Growth Des*., 2018, **18**, 456-465; (d) J. K. Nath, J. B. Baruah, *New J. Chem*., 2013, **37**, 1509-1519.

9. (a) The Importance of π-Interactions in Crystal Engineering: Frontiers in Crystal Engineering. E. R. T. Tiekink and J. Zukerman-Schpector (eds), 2012 John Wiley & Sons, Ltd; (b) F. J. Mizuguchi, G. Rihs, H. R. Karfunkel, *J. Phys. Chem*., 1995, **99**, 16217-16227; (c) K. Shirai, M. Matsuoka, K. Fukunishia, *Dyes and Pig*., **42**, 1999, 95-101; (d) C. A Janiak, *J. Chem. Soc., Dalton Trans*., 2000, 3885-3896; (e) M. Rubes, O. Bludsky, *Phys. Chem. Chem. Phys*., 2008, **10**, 2611-2615.

10. (a) M. P. Singh, N. Phukan, J. B. Baruah, *ChemistrySelect*., 2018, **3**, 963 -967; (b) K. Shankar, J. B. Baruah, *ChemistrySelect*., 2016, **1**, 3038-3044; (c) A. Tarai, J. B. Baruah, *Cryst. Growth Des*., 2016, **16**, 126-135.

11. (a) H. T. Chifotides, K. R. Dubar, Acc. *Chem. Res*., 2013, **46**, 894-906; (b) A. Frontera, P. Gamez, M. Mascal, T. J. Mooibroek, J. J. Reedijk, *Angew. Chem., Int. Ed*., 2011, **50**, 9564-9583; (c) B. L. Schottel, H. T. Chifotides, K. R. Dunbar, *Chem. Soc. Rev*., 2008, **37**, 68-83; (d) P. Molina, F. Zapata, A. Caballero, *Chem. Rev*., 2017, **117**, 9907-9972.

12. C. A. Hunter, J. K. M. Sanders, *J. Am. Chem. Soc*., 1990, **112**, 5525-5534.

13. R. J. Sarma, C. Tamuly, N. Barooah, J. B. Baruah, *J. Mol. Struct*., 2007, **829**, 29-36.

14. (a) A. J. Cruz-Cabeza, J. Bernstein, *Chem. Rev*., 2014, **114**, 2170-2191; (b) N. Phukan, J. B. Baruah, *CrystEngComm*, 2016, **18**, 7753-7763.

15. S. Doose, H. Neuweiler, M. Sauer, *ChemPhysChem*., 2009, **10**, 1389-1398.

16. (a) A. Karmakar, J. B. Baruah, *Supramolecular Chem*., 2008, **20**, 667-674; (b) R. Duke, T. Gunnlaugsson, *Tetrahedron Lett*., 2007, **48**, 8043-8047; (c) C. Tamuly, N. Barooah, M. Laskar, R. J. Sarma, J. B. Baruah, *Supramolecular Chem*., 2006, **18**, 605-613.

17. N. Barooah, R. J. Sarma, J. B. Baruah, *CrystEngComm*, 2006, **8**, 608-615.

18. Y. Hong, J. W. Y. Lam, B. Z. Tang, *Chem*. Soc. Rev., 2011, **40**, 5361-5388.

Chapter 3

Photo-physical Properties of Nitrophenolate and carboxylate Salts of 9-N-(3-imidazolylpropylamino)methylanthracene

3.1: Introduction

Di-topic compounds possessing two nitrogen atoms at two independent sites for non-covalent interactions are useful in designing molecular switches.[1] Such fluorophoric molecules, serve as probes for molecular and ion sensing.[2] Differentiable reactivity and geometrical constraints of such di-topic systems help them to be useful in molecular sorting.[3] These molecules are used as axles in rotaxanes; where motion of rings over an axel is controlled through external stimuli such as change of polarity of a solvent.[4] The self-assemblies of these compounds are essential to understanding differential behavior towards interacting substrates. Protonation or structural changes at remote site of a fluorophore influence photo-electron transfer (abbreviated as PET) mechanism that changes intensity of emission.[5] On the other hand, different conformers of a non-covalently linked assembly made up of several molecules of a structurally flexible compound may make impact on the fluorescence emission properties. There are also possibilities of unusual protonated/deprotonated states stabilizing unusual geometry in solid state.[6] Hence study of fluorescence emission that depends on these effects have advantages to get unusual behaviors. There are different mechanistic paths of emission such as photo-electron transfer,[7] excited state intramolecular proton transfer,[8] twisted intramolecular charge transfer,[9] excimer formation,[10] ion-pair formation[11] and charge-transfer interactions[12] operative in aromatic hydrocarbons.

The photoluminescence properties of anthracene derivatives depend on the nature of the self-assemblies.[13] The fluorescence emissions of anthracene derivatives changes depending on the nature of water assisted assemblies.[14] Based on those valuable information, we have chosen to study structural aspects and the photoluminescence of 9-N-(3-imidazolylpropylamino)methylanthracene (**3.1**) to divulge the role of protonation as well as π-stacking of the ditopic fluorescent molecule. The di-topic compound **3.1** has two different protonation sites as shown in Figure 3.1. It has a fluorophoric anthracene ring which has the ability to π-stack among themselves or with rings of a partner molecule. Thus, the molecule is expected to show fluorescence emission signals depending on the factors such as, self-assembly, extent of protonation and site-specific protonation. Presence of a flexible arm in

the structural scaffold increases opportunities to reorganize its geometries upon interaction with a substrate.

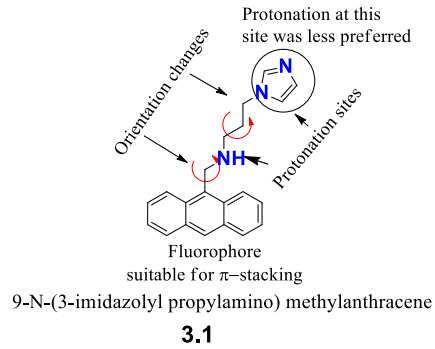

Figure 3.1: Structures of receptor **3.1** to modulate fluorescence.

Such studies also generate interest as anthracene derivatives are used as stoppers in non-covalently linked interlocked systems.[15] There are several ways for interactions among anthracene rings in solid state and in solution.[16] The salts of **3.1** with three nitrophenols (mono, di and tri-nitro derivative) and two organic carboxylic acids as shown in Figure 3.2 were prepared. These examples were chosen because each will independently contribute to the charge-transfer or hydrogen bond interactions in the respective assemblies. The predominance of any of those effects in solid or solution state is expected to influence the fluorescence emission, enforcing the ON or OFF states or shifting the emission wavelength.

3.2: Synthesis of ionic cocrystal and salts of 3.1

The compound 9-N-(3-imidazolylpropylamino)methylanthracene (**3.1**) was synthesized by the reported procedure.[17] Salts of the compound **3.1** with 2,4-dinitrophenol (2,4-DNP), 2,4,6-trinitrophenol (2,4,6-TNP), 2-nitrobenzoic acid (2-NBA) and 2,3-dihydroxybenzoic acid (2,3-DHBA), were obtained by the slow evaporation of respective solution of **3.1** with the respective organic acidic compound in a 1:1 molar ratio in methanol (20 mL). The crystallisation of the salts took place within two to three days and the crystals could be hand-picked after supernatant liquid was discarded to obtain the crystals. Exception was observed from the reaction of **3.1** with 4-nitrophenol (4-NP), which led to ionic cocrystal having 1:2 molar ratio irrespective of the molar ratio of the two components crystallised in an identical manner as those of the other salts.

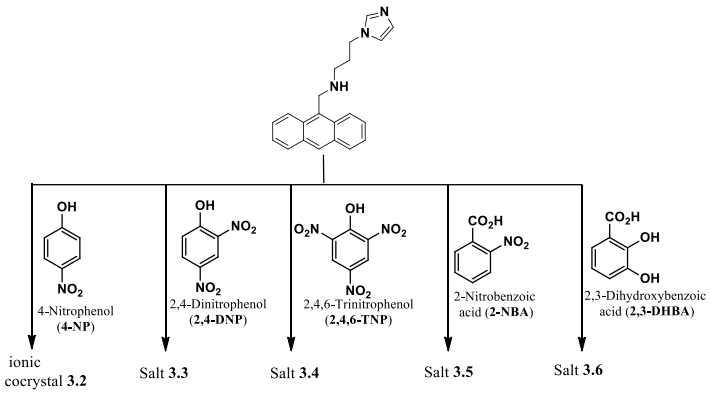

Figure 3.2: Synthesis of ionic cocrystal and salts of **3.1**.

3.3: Structural features of the salts

We identified five salts of 9-N-(3imidazolylpropylamino)methylanthracene with three nitrophenols and two carboxylic acid containing the nitro group (electron withdrawing) and hydroxyl-group (electron donating) that provided us with good quality crystals in sufficient amount, each comprising of a single phase. The salts of 4-NP, 2,4-DNP, and 2,4,6-TNP belong to a series of compounds with increasing numbers of nitro-groups on the backbone of phenol for a systematic comparison. Each salt has a 1:1 composition; except the salt of 4-nitrophenol, which is an ionic cocrystal with a 1:2 ratio. The powder-XRD patterns of the salts are listed in the Figure 3.15. These are compared with the powder-XRD patterns generated from the corresponding crystallographic information file and are presented to show their similar diffraction patterns. The salts are of single phase and are therefore suitable for the determination of photoluminescence properties to correlate with the structural features obtained from the single crystal X-ray study. The compounds were further characterized by recording IR spectroscopy, and ^{1}H-NMR spectroscopy. The ^{1}H-NMR spectra also provided confirmations on the compositions of the salts from the respective integration of signals (Figure 3.10-3.14).

The crystal structure confirmed that 4-Nitrophenol formed an ionic cocrystal with **3.1**, where two 4-nitrophenol molecules are associated with one molecule of **3.1** (Figure 3.3a). In this example, one 4-nitrophenol protonates the secondary N-H of the **3.1**, forming a salt and another 4-nitrophenol is attached to the imidazole part by O3-H···N1 hydrogen bonds. The phenolate oxygen atom forms intermolecular charge-assisted bifurcated hydrogen bonds by bridging the N^{+}-H bonds. The non-covalent assemblies having charge-assisted hydrogen bonds are of interest in recent days to construct flexible assemblies with relatively higher stability.[18] This salt is an exception; it has two 4-nitrophenols linked differently at two

locations of **3.1**, one of which is by charge-assisted hydrogen bonding and the other by conventional hydrogen bonding. In this salt, the anion and cation form a heteromeric assembly that comprises a hydrogen-bonded cyclic unit with the $R_2^2(8)$ graph-set notation.[19] Since these assemblies have charge-assisted hydrogen bonds, the weak C-H···O hydrogen bonds are subsidiary and are not discussed in detail, but additional packing diagrams are provided in the (Figure 3.16 and 3.17). The hydrogen bond parameters of each salt are listed in Table 3.2. In general, the angles of the intermolecular bifurcated hydrogen bonds of molecules such as urea are relatively small and there is the need for large intermolecular bifurcated bond-angles as bifurcated hydrogen-bonded units influence catalytic reactions.[18,20] In the present case, the bifurcated hydrogen bond-angle with the oxy-anion as the pivot is 101.89°.

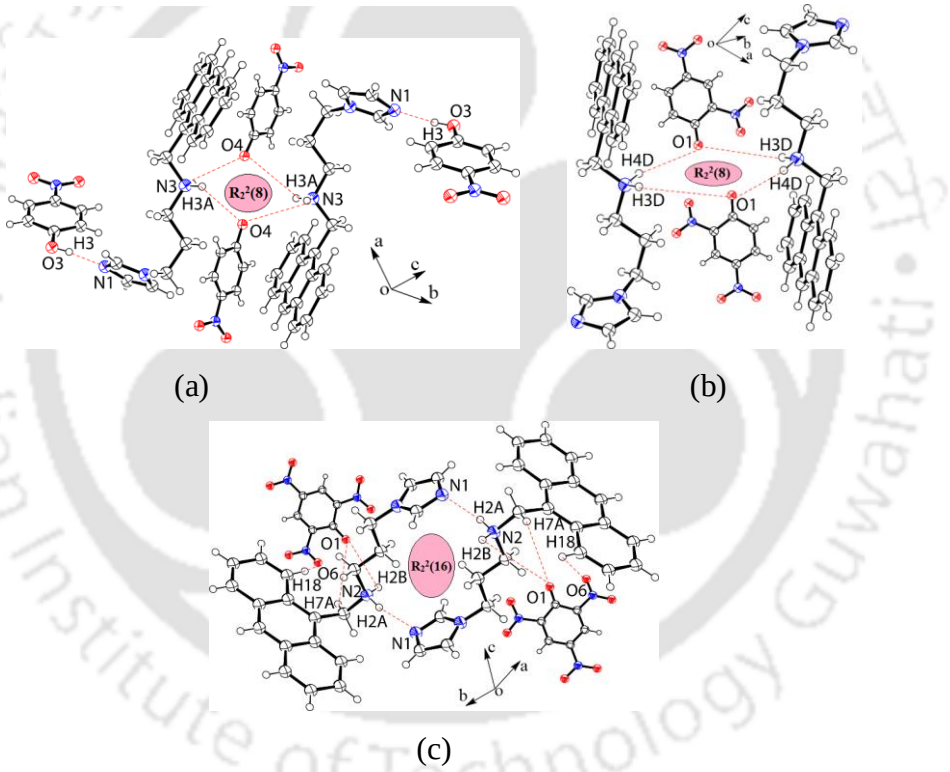

Figure 3.3: Prominent hydrogen bonds in the self-assembly of ionic cocrystals (a) **3.2**: O3-H3···N1 ($d_{D\cdots A}$ = 2.678 Å) and N3-H3A···O4 ($d_{D\cdots A}$ = 2.694 Å) and salts (b) **3.3**: N3-H3D···O1 ($d_{D\cdots A}$ = 2.778 Å) and N3-H4D···O1 ($d_{D\cdots A}$ = 2.768 Å) and (c) **3.4**: N2-H2A···N1 ($d_{D\cdots A}$ = 2.859 Å), N2-H2B···O1 ($d_{D\cdots A}$ = 2.692 Å), C7-H7A···O1 ($d_{D\cdots A}$ = 3.046 Å) and C18-H18···O6 ($d_{D\cdots A}$ = 3.282 Å).

The salts of **3.1** with 2,4-DNP and 2,4,6-TNP are 1:1 salts having a monoprotonated cation and a nitro-phenolate ion (Figure 3.3b and 3.3c). The self-assemblies of these two salts are

quite different. Without considering the hydrogen bonded 4-nitrophenol to the imidazole part in the 4-nitrophenolate ionic cocrystal, the 2,4-dintrophenolate salt has similar features as that of the former case in the self-assembly. The 2,4-dinitrophenolate acts as a bridge to hold two **3.1**$^+$, providing cyclic assemblies similar to the one found in the 4-nitrophenolate salt. In this case, the bifurcated hydrogen bond bearing the phenoxy-anion as the pivot has an angle of 102.82°. Though there are similarities between the heteromeric hydrogen-bonded cyclic assemblies of the two salts, in these cases, differences in the molar ratios of the phenolic components contributed as a factor to change the respective packing pattern. In contrast to these two structures, the assembly of the salt of 2,4,6-TNP has homo-dimers formed between a pair of **3.1**$^+$. Each anthracene ring has strong charge-transfer interactions with 2,4,6-trinitrophenolate ions, reflected in the parallel arrangements of the rings. The charge transfer interactions being strong, the hierarchical effect of charge-transfer interactions does not allow the phenolic oxy-anion to participate in bifurcated hydrogen bonds, as observed in the other two examples where there were no parallel eclipsing orderly arrangements among the rings to have adequate charge transfer interactions.

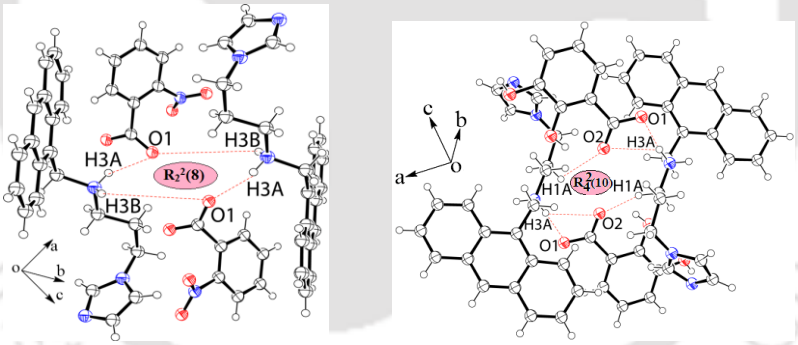

(a) (b)

Figure 3.4: Hydrogen bonded self-assemblies of the salts (a) **3.5**, N3-H3A···O1 ($d_{D\cdots A}$ = 2.740 Å) and N3-H3B···O1 ($d_{D\cdots A}$ = 2.745 Å) and (b) **3.6**, N3-H3A···O1 ($d_{D\cdots A}$ = 2.726 Å) and N3-H3A···O2 ($d_{D\cdots A}$ = 3.151 Å) and C1-H1A···O2 ($d_{D\cdots A}$ = 3.580 Å).

The dimeric self-assemblies of the 1:1 salts of the 2-nitrobenzoic acid as well as the 2,3-dihydroxybenzoic acid are dissimilar. The dimeric assemblies of the 2-nitrophenolate salt is similar to the one observed in the nitrophenol salts. In this case, the bifurcated hydrogen-bond angle of the $R_2^2(8)$ synthon is 110.77° (Figure 3.4a), having the oxy-anion as the central hydrogen-bond acceptor bonded to two N-H bonds. The oxyanion of the carboxylic acid group acts as the pivot in each case to bridge two cations, as illustrated in Figure 3.4a. In the

case of the salt of 2,3-dihydroxybenzoic acid, the self-assembly is guided by the $R_2^2(8)$ synthon formed by N3-H···O2 and C1-H···O2 hydrogen bonds as shown in Figure 3.4b. The bifurcated hydrogen bonds in the synthon are comprised of the oxyanion of the carboxylate with the C-H and N-H bonds, having an angle of 122.88°. The self-assembled salt has two molecules, in which the anthracene rings are parallel but in the opposite direction. The distance between the parallel anthracene rings is 4.107 Å (Figure 3.17b). The oxy-anions in all these salts, other than the salt of 2,4,6-TNP, are involved in bifurcated intermolecular hydrogen bonds, in which the angles are in the following order: 4-NP ~ 2,4-DNP < 2-NBA < 2,3-DHBA salts.

The $(-CH_2)_3$- containing arm is flexible enough to provide different conformers; we chose to study energy profiles by MM2 calculation relating three torsion angles, namely, C(8)-C(7)-N(3)-C(1), N(3)-C(1)-C(2)-C(3) and C(1)-C(2)-C(3)-N(2) (Figure 3.5a and b) by using ChemDraw Ultra. The experimental torsion angles observed in the structure of all the salts were sorted using the Mercury program and are listed in Table 3.1. The conformational energy profile for C(8)-C(7)-N(3)-C(1) shown in Figure 3.1a has the most stable conformer with a torsion angle of 180° and has two other conformers with torsion angles of + or -75°. Among the salts, the C(8)-C(7)-N(3)-C(1) torsion angle of the 2,4-DNP salt is 176.2(3)°, which is very close to the minimum energy conformer. The salt of 4-NP has a torsion angle of -166.5(2)°, whereas the torsion angles for the 2-NBA, 2,3-DHBA salts are 165.9(2)° and 169.4(2)°, respectively. These three observed values of C(8)-C(7)-N(3)-C(1) torsional angles in the corresponding salt are different from the theoretically observed energy minima at ±75° shown in the Figure 3.5a. Thus, there is the stabilization of an orientation, which does not correspond to an energetically favorable conformer. The C(8)-C(7)-N(3)-C(1) torsion angle of the 2,4,6-TNP salt is -34.7(4)°, which is exceptionally different from the other salts; this value is not close to any of the energies of a conformer. The value is on the higher energy side of the profile shown in Figure 3.5a.

The N(3)-C(1)-C(2)-C(3) and C(1)-C(2)-C(3)-N(2) torsion angles have similar energy profiles (Figure 3.5b); each has dissimilar conformers at 65° besides the one with 180°. The observed N(3)-C(1)-C(2)-C(3) torsion angle in each case falls between 175-179°. There is, therefore, no significant change in this torsion angle in the respective salt. On the other hand, the experimentally observed C(1)-C(2)-C(3)-N(2) torsion angle of the salt has its own characteristics. The salt of 4-NP, 2-NBA, and 2,3-DHBA have C(1)C(2)-C(3)-N(2) torsion angles of -69.9(2)°, -64.0(2)° and -63.0(2)°, respectively. These are comparable to the torsion

angle of the highest energy conformer having a torsion angle of -65°. However, the salt of 2,4-DNP has a torsion angle of 63.1(4)°, which is comparable to another possible conformer with a torsion angle of 65°. Finally, the C(1)-C(2)-C(3)-N(2) torsion angle of the 2,4,6-TNP salt is -179.2(3)°, which is the lowest energy from the profile shown in Figure 3.5b. These analyses have shown that the orientations of the flexible -$(CH_2)_3$- part anchoring the imidazole in the respective cation of the salts are different; this is also seen in the overlay diagram of the cationic part of the salts shown in Figure 3.5c.

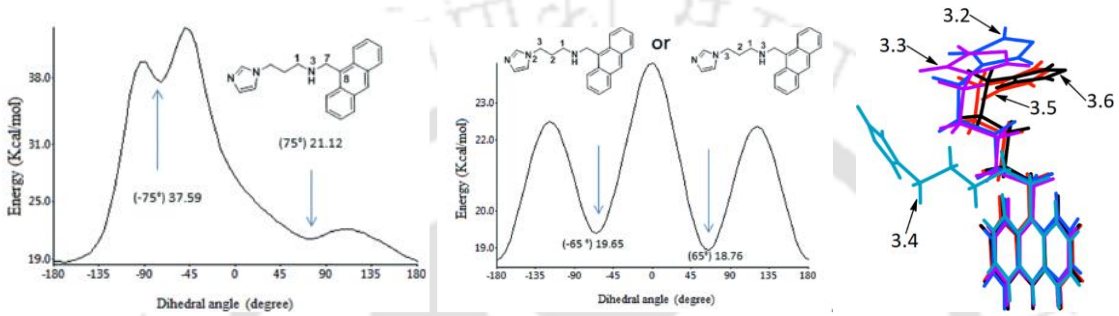

(a) (b) (c)

Figure 3.5: The plots of torsion angles (a) C8-C7-N3-C1, (b) N3-C1-C2-C3 or C1-C2-C3-N2 versus energy for the compound **3.1**. (c) Overlay diagram showing the orientation of the imidazole ring relative to the anthracene ring in the **3.1**$^+$ ions in different salts.

The observed conformations in the salts were adjusted near the torsion of the lowest energy or the other conformers or away from any of the conformers. These results show that the partner molecules have an impact on the adjustment of the torsion angles. This is like providing bends to different parts of a flexible geometry or like making imprints on a soft material. In the structures of conformation polymorphs, the lowest energy conformers are not necessarily observed and the torsion angle in such conformers are higher than the lowest maxima of a conformer; this effect is called as conformational adjustment.[21] As a consequence of different supramolecular interactions of the cation with the respective anions, the torsional angles associated with the flexible arm varies in each case, thus different geometries are observed in the cationic parts of respective salts.

Table 3.1: Torsion angles of **3.1**$^+$ in different salts.

Numbering of atoms of **3.1**	Torsion angle (°)	**3.2**	**3.3**	**3.4**	**3.5**	**3.6**
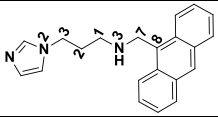	C8-C7-N3-C1	-166.5(2)	176.2(3)	-34.7(4)	165.9(2)	169.4(2)
	N3-C1-C2-C3	177.5(2)	176.8(3)	179.4(3)	176.1(2)	175.2(2)
	C1-C2-C3-N2	-69.9(2)	63.1(4)	-179.2(3)	-64.0(2)	-63.0(2)

3.4: Fluorescence studies in solution

The compound **3.1** in ethanol solution has three distinguishable fluorescence emission peaks at 395 nm, 417 nm and 443 nm upon excitation at 365 nm. These fluorescence emission peaks are the partially quenched states of the three components of the $S_1 \rightarrow S_0$ transition involving $v_0 \rightarrow v_0$, $v_0 \rightarrow v_1$, $v_0 \rightarrow v_2$ vibrational transitions. The assignments are based on the similar emission spectra of anthracene.[12e] Addition of halo-phenols are known to influence the photo-electron transfer (PET) process of **3.1**.[17] It is also an established fact that charge-transfer among donor and acceptor molecules causes fluorescence quenching of anthracene and related organic compounds. [12e],[22] We find that the acidic organic compounds, namely the nitrophenols or carboxylic acids enhance the intensities of emissions of **3.1** up to a limiting concentration. In the case of 2-NBA or 2,3-DHBA, a maximum intensity value is reached in such titrations but no further increase takes place. A nitrophenol acts differently; there is an initial increase in the intensities up to a certain concentration, beyond which it decreases. A representative titration plot on the fluorescence emission of **3.1** upon addition of 2-NBA is shown in Figure 3.6a, whereas, the addition of 2,4,6-TNP is shown in Figure 3.6b. In the latter case, the thick line shows the increase in intensity, followed by the dotted lines showing the decrease. The addition of excess amounts of 2,4,6-TNP causes complete quenching of the emission of **3.1**. The initial increase in the intensity followed by a decrease in emission upon the addition of 2,4,6-TNP to **3.1** draws general interest, as there have been only limited occasions[23] where the 2,4,6-TNP caused the emission enhancement of a receptor.

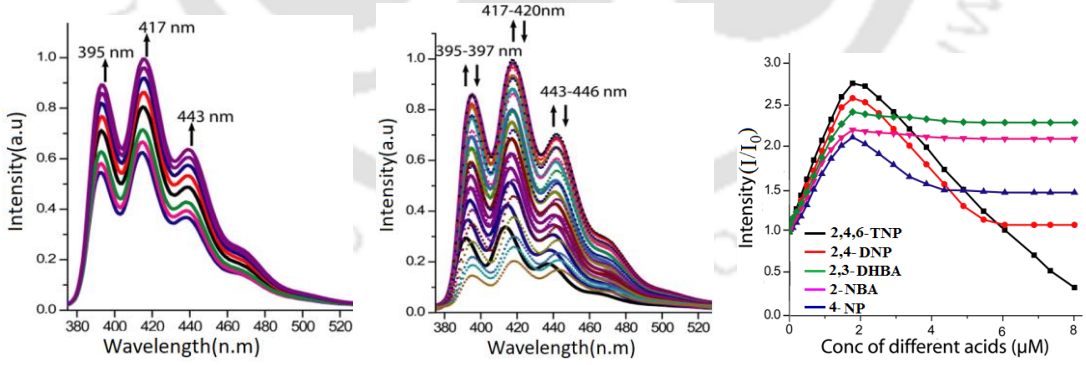

(a) (b) (c)

Figure 3.6: Fluorescence spectroscopic titration (λ_{ex} = 365 nm) of **3.1** (10^{-5} M in ethanol) by adding (a) 2-NBA, showing enhancement of emission, and upon addition of (b) 2,4,6-TNP (10^{-5} M in 10μL aliquots) showing enhancement (thick line) followed by quenching of emission (dashed line) and (c) The changes in the fluorescence intensities at 417 nm of **3.1** (10^{-5} M) at different concentrations of carboxylic acids and nitrophenols.

The 2,4-DNP does not completely quench the fluorescence of **3.1**. The plot for intensity versus concentration of the acidic component obtained from different emission titrations of **3.1** with organic-acids is given in Figure 3.6c. The non-linear plots in the case of **3.1** interacting with nitrophenols show an initial increase followed by a decrease in intensity values. The emission changes in these cases occur through two-paths; one is the dynamic Dexter quenching due to stacking among the donor and acceptor rings, and other is protonation (a ground state effect contributing to static quenching). As the concentration of nitrophenols are increased, the charge-transfer equilibrium is pushed forward; subsequently, there is quenching of emissions. The **3.1** is protonated by the two carboxylic acids and no π-stacking occurs in those cases in very dilute solutions. As a consequence, PET is affected,[24] leading to intensity enhancement to show the fluorescence ON-state. There was no significant difference upon changing the solvents from ethanol to acetonitrile (Figure 3.19).

3.5: Solid state UV-visible and Fluorescence studies

Anions are well known to reorganize the structures of receptors.[25] Hence, the availability of X-ray crystallographic structures prompted us to study the photoluminescence of solid samples of the salts to correlate with the packing behavior. The solid sample of the **3.1** and the salts absorb at 397 nm due to the π-π* transition. The charge-transfer transitions were also observed for salts of 4-NP and 2,4-DNP at 438 nm, whereas such peak was observed at 460 nm for the 2,4,6-TNP salt (Figure 3.7a). The salts with charge-transfer absorptions are brownish black (inset of Figure 3.7a). Anthracene-based compounds have interesting emission properties. Solvated anthracene derivatives, upon removal of the solvent, shift the emission wavelength.[25b] Quantum efficiencies of the anthracene derivatives depend on π-stacking.[13b] In general, the nitrophenols are well known to quench the fluorescence emission of aromatic fluorophores.[26] In the present case, we have a low efficiency of emission in the salts or in two cases complete quenching was observed. The solid samples of the salts studied here have characteristic photoluminescence, as illustrated in Figure 3.7b.

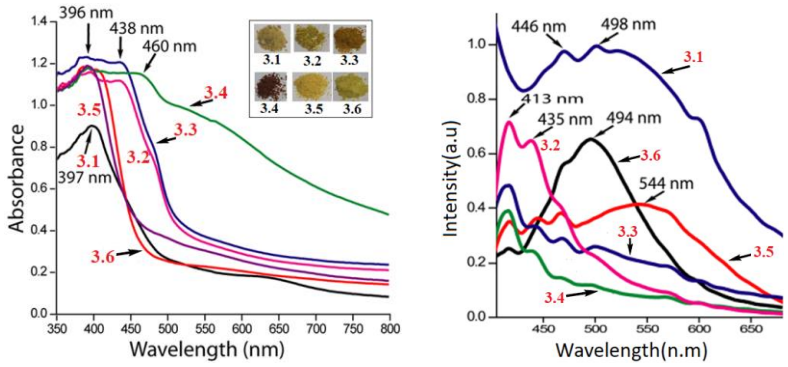

(a) (b)

Figure 3.7: (a) UV-visible spectra and (b) fluorescence emission spectra (excitation at 365 nm) of the solid samples of **3.1** and salts. The inset of the visible spectra shows the colours of **3.1** and salts.

A broad emission peak at 498 nm (Φ_F = 0.0804) was observed from compound **3.1**; this emission peak was partly quenched in the 2,3-DHBA salt without a shift in the original position with quantum yield 0.017. The emissions of the salt of 4-NP occur at 413 nm and 435 nm (Φ_F = 0.0141); these peak positions are blue-shifted from those of the parent compound by 85 nm and 63 nm, respectively. The changes are due to the packing of the salts. In the 4-nitrophenolate salt, the N^+-H of the secondary ammonium part of $\mathbf{3.1}^+$ as well as the nitrogen atoms of the imidazole ring are hydrogen bonded to 4-nitrophenol. The absence of π-stacking among the rings in the self-assembly and the segregation caused by the intervening 4-nitrophenol molecules allow it to show monomer-like emission, originating from the anthracene unit. The assignment on the monomer-like emission is also based on earlier precedence in the packing of anthracene-1,5-disulfonic acid with n-pentylamine; due to large separation among the anthracene units in its crystal packing, it showed monomer like emission.[27] In that example, the monomer emission was also confirmed by measuring emission from a dilute solution. The emissions of fluorescent molecules change with π-stacking patterns.[28] There are several possibilities for the aromatic rings to align parallelly to contribute to the emission. One of the ways is through the stacking among the anthracene rings in the lattice. In the salts of 4-NP, 2,4-DNP, and 2-NBA, the cations are aligned in a head to tail manner (considering the imidazole end as the head and the anthracene end as the tail). This arrangement is not suitable for stacking between anthracene-anthracene rings (Figure 3.8) in close proximity. The salt of 2,4,6-TNP has anthracene rings in parallel but placed off-set with a distance of 3.367 Å between the parallel planes; as the rings do not

eclipse each other, there are no effective stacking interactions. The salt of 2,3-DHBA is the lone example among the salts in which anthracene-anthracene stacking is found. In this case, the oppositely facing but near parallel anthracene rings incompletely eclipse each other with a distance of 3.446 Å between the two planes. The centroid to centroid distance between the rings is 4.107 Å, suggesting a very weak π-interaction.

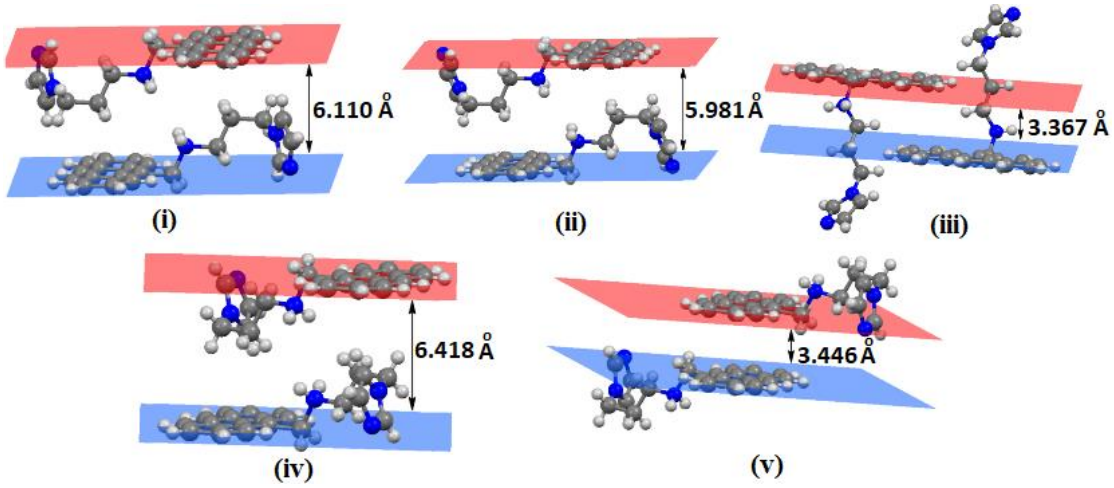

Figure 3.8: The arrangements of anthracene rings in salts (i) **3.2**, (ii) **3.3**, (iii) **3.4**, (iv) **3.5**, and (v) **3.6**.

Resonance energy-transfer emission at higher wavelengths is possible when donor and acceptor units have overlapping emissions and they are arranged non-parallelly but located within a limiting distance.[29] In the present case, the acceptor molecules are non-fluorescent and so resonance energy transfer is not feasible. Due to the stabilization of the protonated form in the excited state, 2-aminoanthracene shows an emission at a longer wavelength in a confined environment, but in the absence of a host, it shows an emission at a shorter wavelength.[30] The blue-shifted emission of salts of anthracene-1,5-disulfonic acid with tertiary-butylamine was earlier assigned to the face-to-face translated geometry among the anthracene rings.[27] Discrete dimeric anthracene molecules in solid state show enhanced emission.[10b]

Besides the possible anthracene-anthracene stacking in certain cases, there are different orientations among the donor (anthracene ring) and acceptor rings (of anions). The alignments of the planes of the anthracene and ring of the organic anions are illustrated in Figure 3.9.

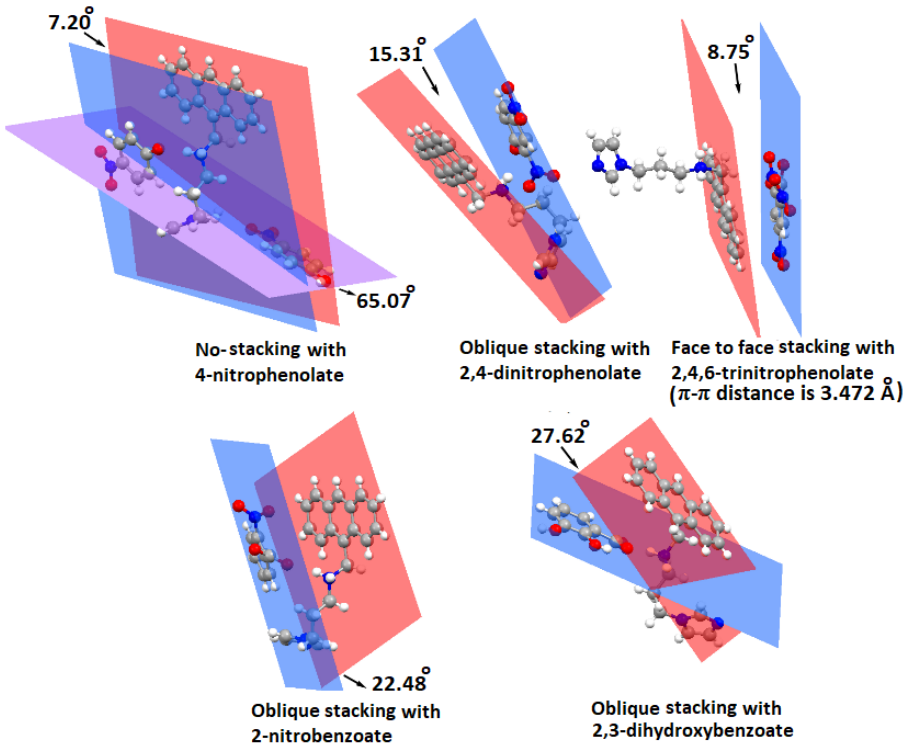

Figure 3.9: The arrangements of the aromatic rings of the salts.

In the case of 4-nitrophenolate salts, the plane of the donor and the plane of one acceptor are almost parallel, but they are located at translated positions. The 2,4-dinitrophenol ring is 15.31° oblique to the anthracene ring and they are located at translated positions. In such a situation, it is less likely to have effective Dexter-quenching; accordingly, incomplete quenching is observed. In the 2,4,6-trinitrophenolate salt, the nitro-aromatic ring of the anions are parallel and they are located above the anthracene ring to facilitate π-stacking. This interaction is reflected in the centroid to centroid distance of the parallel π-clouds of donor and acceptor (3.472 Å). These stacks cause Dexter electron-transfer to quench the emission. The aromatic planes of donors and acceptors in the 2-nitrobenzoate and 2,4-dihydroxybenzoate salt have the angles of 22.48° and 27.62° between such planes, respectively. This causes less effective π-interactions among the rings, and accordingly, Dexter quenching is partial in these cases and emission occurs at a slightly different position than the parent compound due to static quenching resulting from the modification of the ground state. Furthermore, the presence of stacking among the anthracene rings in the salt of 2,3-DHBA makes the distinction in the emission from the 2-nitrobenzoate salt. Hence, the π-interactions among the anthracene rings as well as between the anthracene ring and the ring of the anion are also the prime causes of changes in the emission intensity in solid samples.

However, in the case of the non-availability of such interactions, the protonation effect contributing to the change in the ground state energy contributes to the change in the position of emission. A similar explanation was provided for the different monomer, dimer, excimer emissions of anthracene derivatives, depending on the procedure used in sample preparation.[31] Based on these, the emission processes in the solution and solid states are schematically shown in Scheme 3.1.

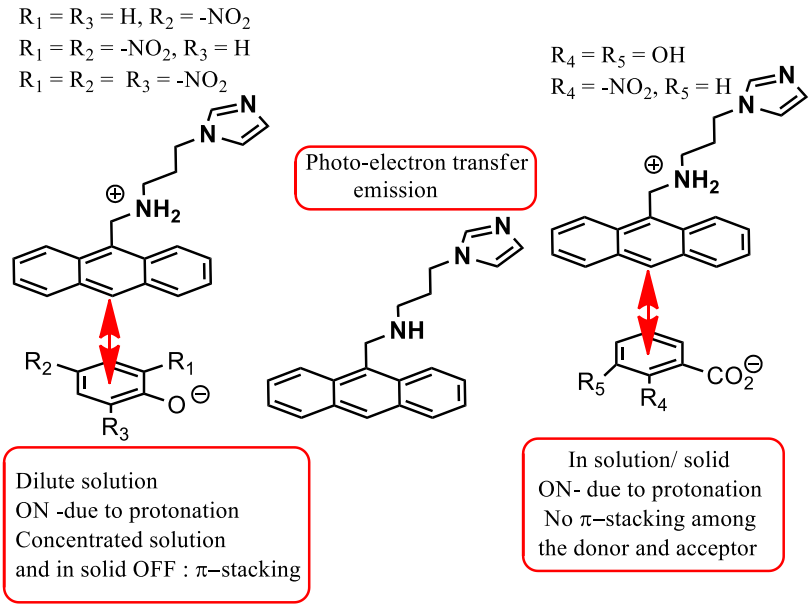

Scheme 3.1: The observed emissions of **3.1** on interactions with nitrophenols and carboxylic acids.

The fluorescence life-time of the solid samples of parent compound and the salts are found to be tri-exponential (Figure 3.20-3.25). In the parent compound, 36% of the population has a life-time of 6.5 ns, 49% has 1.1 ns and 14% has 0.29 ns. These three paths are present in each weakly emitting salt but the quantities differ. The variations in the life-times and fractions of molecules following a particular path are counter ion dependent. It was earlier suggested that in the solid state, the π-stacked dimers of anthracene moieties have longer lifetimes than the monomer emissions.[27] The magnitudes of the observed life-times are small as compared to the reported dimer emissions of anthracene moieties, but they have comparable values to monomer emission, and the salts show monomer-like emission.

3.6: Conclusions

It is established that the orientation of anthracene unit of the protonated **3.1** in crystal lattices differ depending on the organic anions. Those difference in orientations in the respective self-assembly provides different types of π-stacks among the rings to make distinctions in the observed fluorescence emission quenching. The salt of 4-NP does not have stacking among the rings. In this case, as a result of the compartmentalization of the cations by anions leads to monomer-like emission. The solid samples of the salt of 2,4-DNP, as well as of 2,3-DHBA, do not have suitable π-stacking required to show Dexter quenching, hence partial quenching in these cases were observed. The salt of 4-nitrobenzoic acid lacks anthracene-anthracene stacking, which is present in the salt of 2,3-DHBA, making a difference in the fluorescence emissions of the two salts. Fluorescence ON-states are observed for solutions of the **3.1** with nitrophenolic compounds at lower concentrations. The fluorescence ON-state by 2,4,6-trinitrophenol in solution is a rare observation, suggesting that the adequate hold on hierarchical weak interactions make such a phenomenon possible.

3.7: Spectroscopic details of the salts:

3.2: Isolated Yield: 67 %. Melting 127 °C. ^{1}H-NMR (600 MHz, DMSO-d_6): 8.56 (s, 1H), 8.42 (d, J = 12 Hz, 2H), 8.12 (m, 6H), 7.59 (d, J = 6 Hz, 2H), 7.54 (m, 3H), 7.09 (s, 3H), 6.91 (d, J = 12 Hz, 4H), 6.85 (s, 1H), 4.65 (s, 2H), 4.02 (t, J = 6 Hz, 2H), 2.75 (m, 2H), 1.94 (m, 2H). IR (KBr, cm^{-1}): 3436 (br, w), 3116 (w), 3053 (w), 2873 (w), 1629 (w), 1576 (s), 1511 (w), 1488 (m), 1471 (m), 1396 (m), 1329 (s), 1292 (m), 1251 (m), 1161 (s), 1106 (s), 1080 (w), 1051 (w), 988 (m), 927 (m), 891 (m), 848 (s), 790 (w), 729 (s), 664 (m), 639 (s).

3.3: Isolated Yield: 63 %. Melting 144°C. ^{1}H-NMR (600 MHz, DMSO-d_6): 8.78 (s, 1H), 8.59 (d, J = 6 Hz, 1H), 8.49 (d, J = 12 Hz, 2H), 8.20 (d, J = 6 Hz, 2H), 7.79 (d, J = 6 Hz, 1H), 7.72 (m, 3H), 7.63 (t, J = 6 Hz, 2H), 7.22 (s, 1H), 6.98 (s, 1H), 6.32 (m, 1H), 5.20 (s, 2H), 4.12 (t, J = 6 Hz, 2H), 3.24 (m, 2H), 2.15 (m, 2H). IR (KBr, cm^{-1}): 3431 (br, w), 3051 (w), 2960 (w), 2779 (w), 1624 (w), 1590 (s), 1558 (m), 1519 (s), 1467 (s), 1305 (m), 1283 (m), 1233 (m), 1130 (s), 1074 (w), 1060 (w), 985 (w), 920 (w), 887 (m), 828 (s), 789 (w), 730 (s), 684 (m), 636 (m).

3.4: Isolated Yield: 65 %. Melting 157 °C. ^{1}H-NMR (400 MHz, DMSO-d_6): 8.79 (s, 1H), 8.58 (s, 2H), 8.47 (d, J = 8 Hz, 2H), 8.20 (d, J = 8 Hz, 2H), 7.81 (s, 1H), 7.72 (t, J = 8 Hz, 2H), 7.64 (d, J = 8 Hz, 2H), 7.25 (s, 1H), 7.02 (s, 1H), 5.21 (s, 2H), 4.12 (t, J = 8 Hz, 2H),

3.27 (t, J = 8 Hz, 2H), 2.20 (p, J = 8 Hz, 2H). IR (KBr, cm^{-1}): 3459 (br, w), 3154 (w), 3053 (w), 2964 (w), 1631 (w), 1610 (m), 1557 (s), 1490 (w), 1364 (m), 1317 (s), 1266 (s), 1161 (m), 1080 (m), 1023 (w), 912 (w), 787 (m), 730 (m), 709 (m), 636 (m).

3.5: Isolated Yield: 65 %. Melting 171°C. ^{1}H-NMR (600 MHz, DMSO-d_6): 8.69 (s, 1H), 8.48 (d, J = 6 Hz, 2H), 8.15 (d, J = 6 Hz, 2H), 7.74 (d, J = 6 Hz, 1H), 7.68 (t, J = 6 Hz, 1H), 7.64-7.61 (m, 4H), 7.58-7.52 (m, 3H), 7.15 (s, 1H), 6.90 (s, 1H), 5.00 (s, 2H), 4.08 (t, J = 6 Hz, 2H), 3.03 (m, 2H), 2.08 (m, 2H). IR (KBr, cm^{-1}): 3417 (br, w), 3137 (w), 2943 (w), 2831 (w), 1626 (s), 1590 (m), 1570 (m), 1520 (s), 1471 (w), 1442 (w), 1375 (s), 1355 (s), 1279 (m), 1225 (m), 1189 (w), 1159 (w), 1076 (s), 1049 (w), 1030 (w), 963 (w), 892 (m), 831 (s), 785 (s), 733 (s), 663 (m), 644 (m).

3.6: Isolated Yield: 69 %. Melting 201°C. ^{1}H-NMR (600 MHz, DMSO-d_6): 8.76 (s, 1H), 8.50 (d, J = 12 Hz, 2H), 8.28 (s, 1H), 8.18 (d, J = 6 Hz, 2H), 7.68 (m, 3H), 7.61 (t, J = 6 Hz, 2H), 7.19 (s, 1H), 7.11 (d, J = 6 Hz, 1H), 6.95 (s, 1H), 6.69 (d, J = 6 Hz, 1H), 6.41 (t, J = 6 Hz, 1H), 5.15 (s, 2H), 4.11 (t, J = 6 Hz, 2H), 3.18 (m, 2H), 2.15 (m, 2H). IR (KBr, cm^{-1}): 3434 (br, w), 3132 (w), 3036 (w), 2838 (w), 1634 (s), 1560 (s), 1505 (s), 1468 (w), 1450 (w), 1392 (s), 1341 (w), 1274 (s), 1266 (s), 1232 (w), 1193 (w), 1152 (w), 1082 (s), 1067 (w), 996 (m), 920 (s), 890 (w), 826 (m), 783 (s), 735 (s), 661 (m), 632 (m).

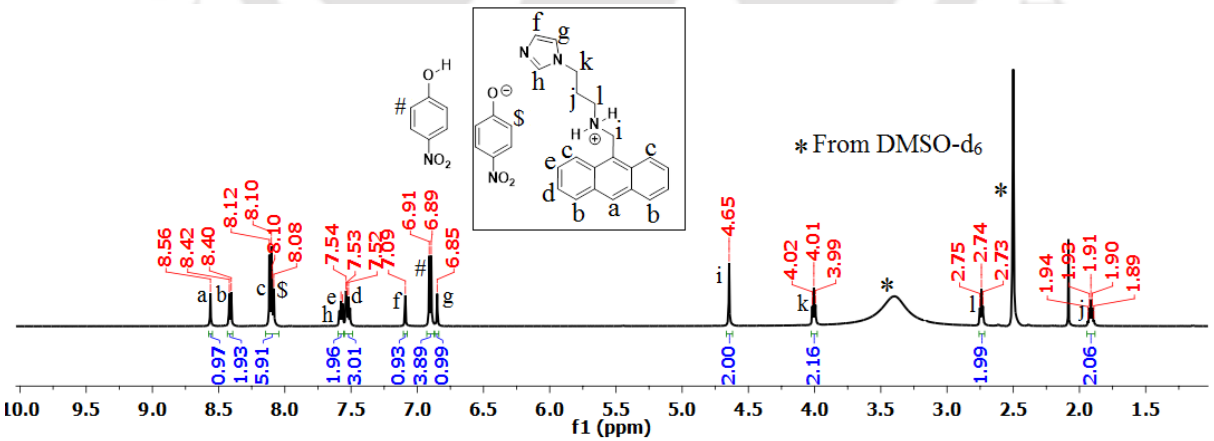

Figure 3.10: ^{1}H-NMR (600 MHz, DMSO-d_6) spectra of ionic cocrystal **3.2**.

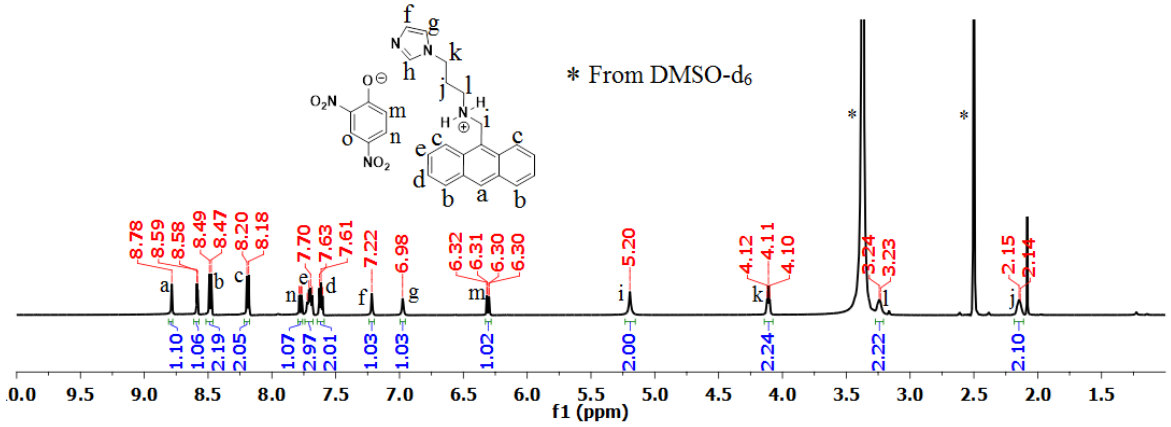

Figure 3.11: ^{1}H-NMR (600 MHz, DMSO-d_6) spectra of salt **3.3**.

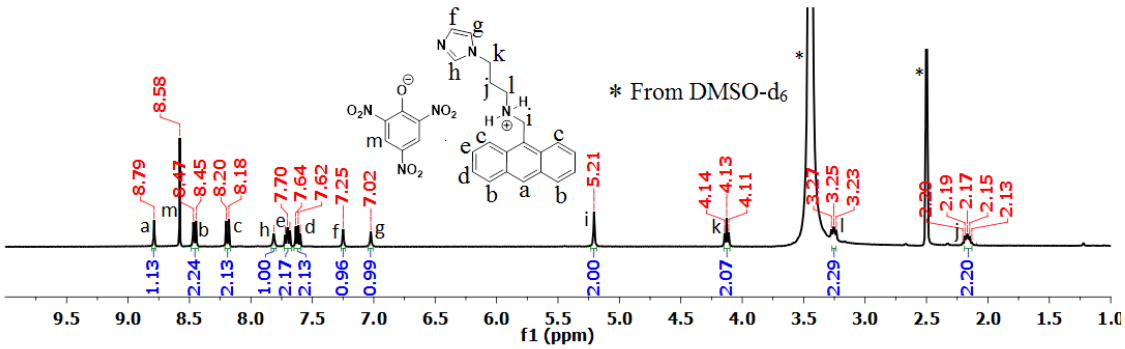

Figure 3.12: ^{1}H-NMR (400 MHz, DMSO-d_6) spectra of salt **3.4**

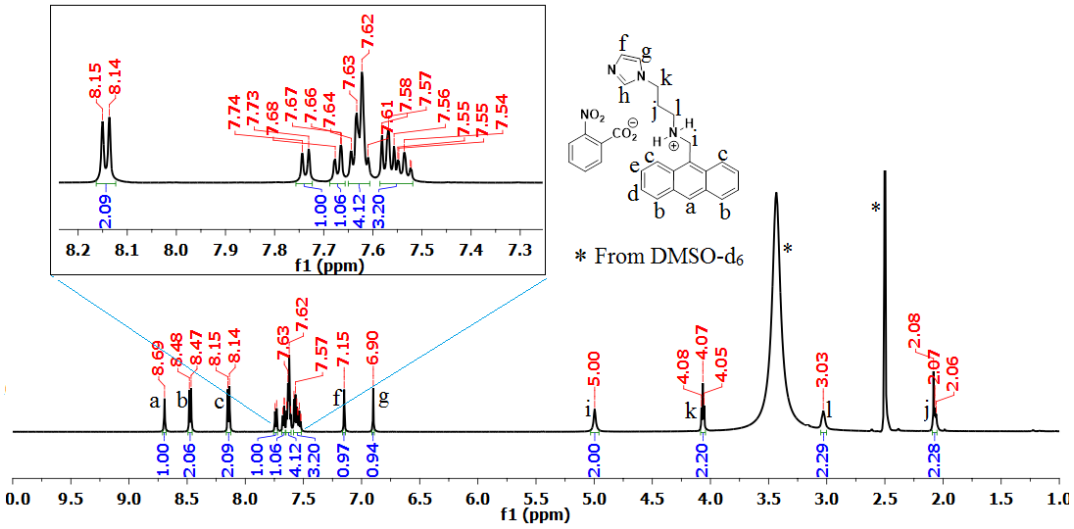

Figure 3.13: ^{1}H-NMR (600 MHz, DMSO-d_6) spectra of salt **3.5**.

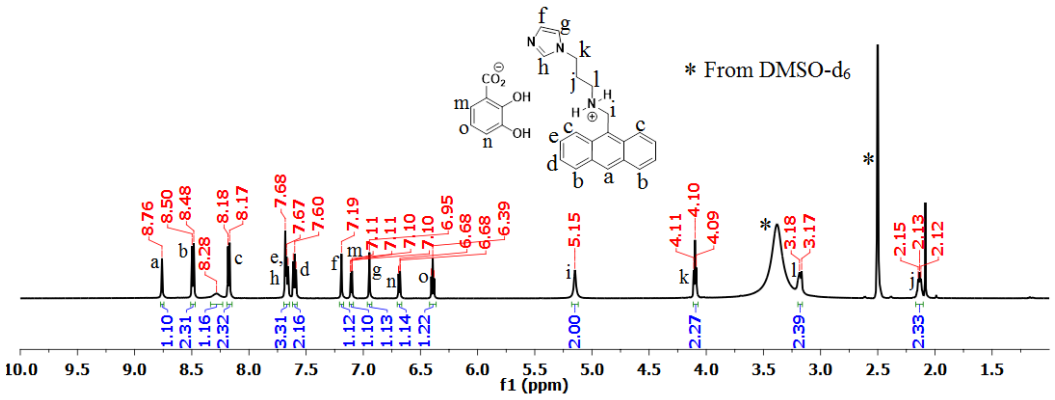

Figure 3.14: ^{1}H-NMR (600 MHz, DMSO-d_6) spectra of salt **3.6**.

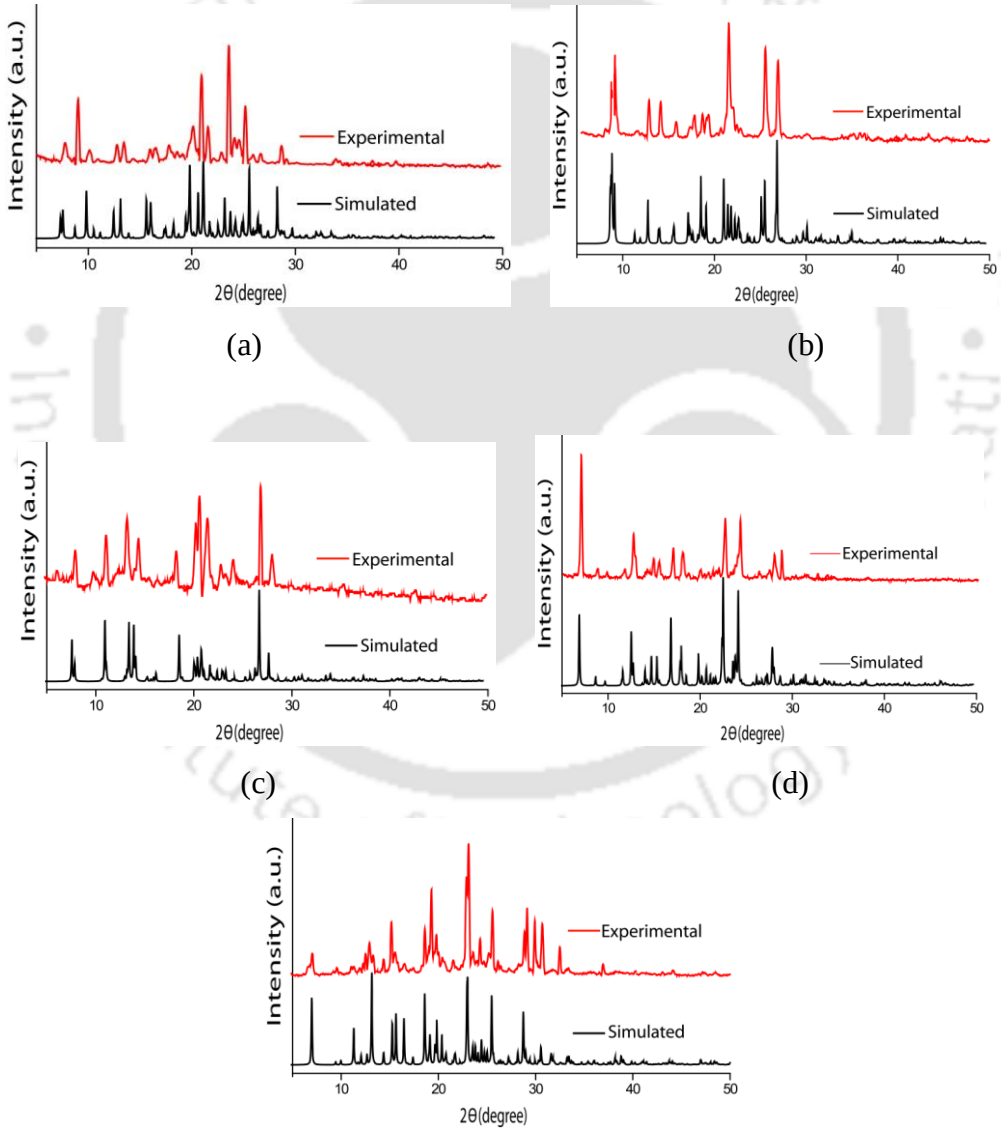

Figure 3.15: PXRD pattern of (a) **3 .2**, (b) **3.3**, (c) **3.4**, (d) **3.5** and (e) **3.6** (Red = Experimental, Black = Simulated). Simulated pattern generated from CIF file.

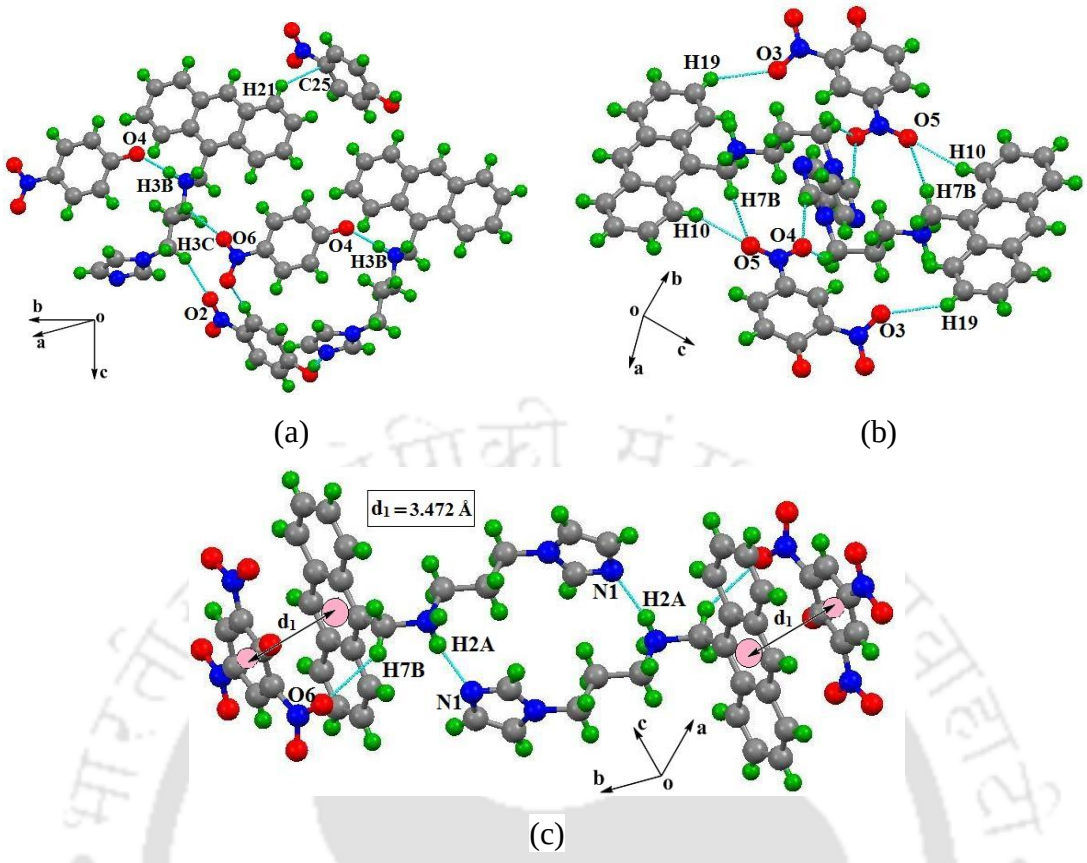

Figure 3.16: Different types of hydrogen bonds present in (a) ionic cocrystal **3.2**, (b) salt **3.3** and (c) **3.4**.

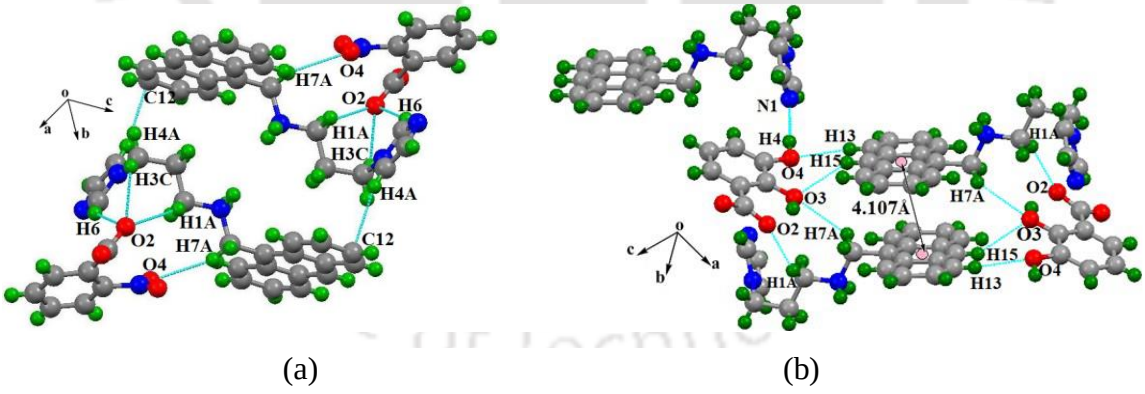

Figure 3.17: Different types of hydrogen bonds present in salt (a) **3.5** and (b) **3.6**.

Table 3.2: Prominent hydrogen bond parameters of different salts and ionic cocrystal of **3.1**.

Salts	D-H···A	d_{D-H} (Å)	$d_{H\cdots A}$ (Å)	$d_{D\cdots A}$ (Å)	∠D-H···A (º)
3.2	O(3)-H(3)···N(1) [x, y, -1+z]	0.82(2)	1.87(2)	2.678(3)	171(2)
	N(3)-H(3A)···O(4) [x, y, -1+z]	0.89(3)	1.88(3)	2.694(2)	151(3)
	N(3)-H(3B)···O(4) [1-x, 1-y, 1-z]	0.89(3)	1.79(3)	2.670(2)	168(2)
	C(2)-H(2B)···O(6) [1-x, -y, 1-z]	0.97(6)	2.58(4)	3.226(3)	124(2)
	C(3)-H(3C)···O(2) [x, y, z]	0.97(3)	2.51(3)	3.402(4	153(3)

3.3	N(3)-H(3D)···O(1) [1-x, 1-y, 1-z]	0.94(3)	1.85(3)	2.778(3)	170(3)
	N(3)-H(4D)···O(1) [x, y, z]	1.02(3)	1.80(3)	2.768(3)	156(3)
	N(3)-H(4D)···O(1) [x, y, z]	1.02(3)	2.33(4)	2.977(4)	120(2)
	C(1)-H(1B)···O(2) [x, y, z]	0.97(2)	2.53(5)	2.951(4)	106(3)
	C(2)-H(2A)···O(2) [x, y, z]	0.97(3)	2.51(4)	3.128(4)	121(3)
3.4	N(2)-H(2A)···N(1) [x, y, z]	0.89(3)	1.99(4)	2.859(3)	165(3)
	N(2)-H(2B)···O(1) [x, y, z]	0.89(3)	2.02(5)	2.692(3)	131(4)
	N(2)-H(2B)···O(2) [x, y, z]	0.89(3)	2.17(3)	2.907(4)	139(4)
3.5	N(3)-H(3A)···O(1) [1-x, -y, 1-z]	0.89(3)	1.86(2)	2.740(2)	171(2)
	N(3)-H(3A)···O(2) [1-x, -y, 1-z]	0.89(3)	2.55(5)	3.187(2)	129(2)
	N(3)-H(3B)···O(1) [x, y, z]	0.89(3)	1.95(3)	2.745(2)	147(4)
	C(1)-H(1A)···O(2) [1+x, y, z]	0.97(2)	2.53(5)	3.313(2)	138(2)
	C(10)-H(10)···O(2) [1-x, -y, 1-z]	0.93(3)	2.49(3)	3.336(3)	151(4)
3.6	N(3)-H(3A)···O(1) [x, y, z]	0.89(4)	1.84(6)	2.726(2)	173(5)
	N(3)-H(3A)···O(2) [x, y, z]	0.89(3)	2.52(4)	3.151(2)	128(2)
	N(3)-H(3B)···O(1) [1-x, 1-y, 1-z]	0.89(5)	1.94(3)	2.749(2)	151(4)
	O(4)-H(4)···N(1) [x, 1+y, -1+z]	0.82(2)	1.94(3)	2.744(3)	168(3)

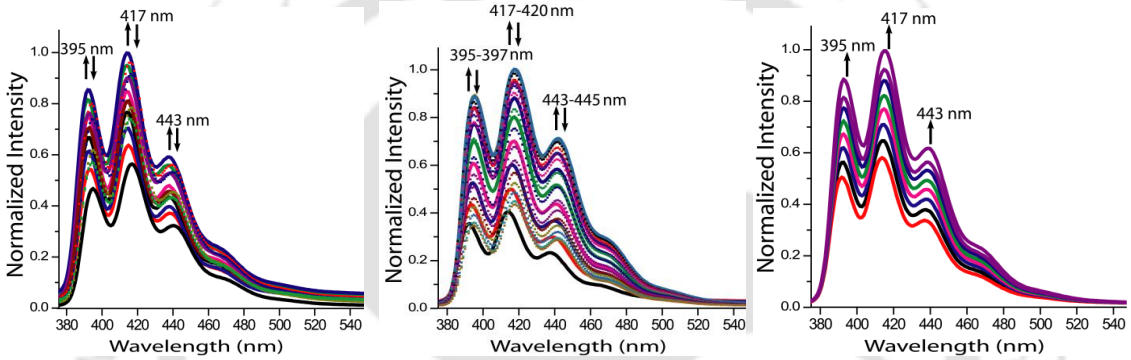

(a) (b) (c)

Figure 3.18: Fluorescence titration (excitation at 365 nm) of **3.1** (10^{-5} M in Ethanol) with (a) **4-NP**, (b) **2,4-DNP** and (c) **2,3-DHBA** (10 µl aliquot of 10^{-5} M in Ethanol). showing enhancement (thick line) followed by quenching of emission (dashed line).

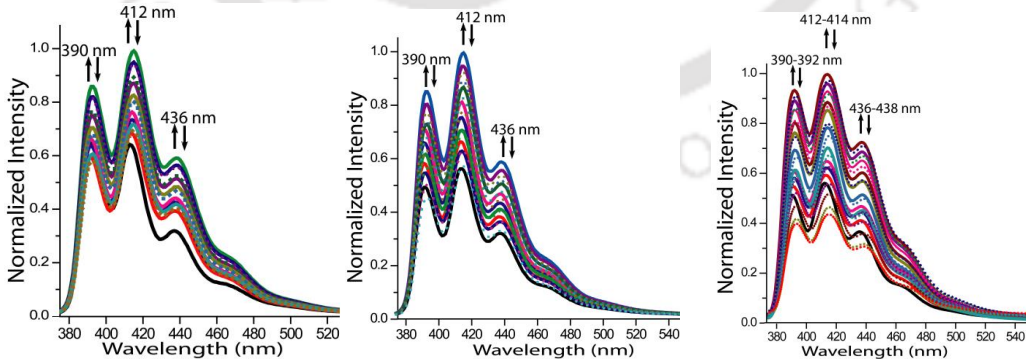

(a) (b) (c)

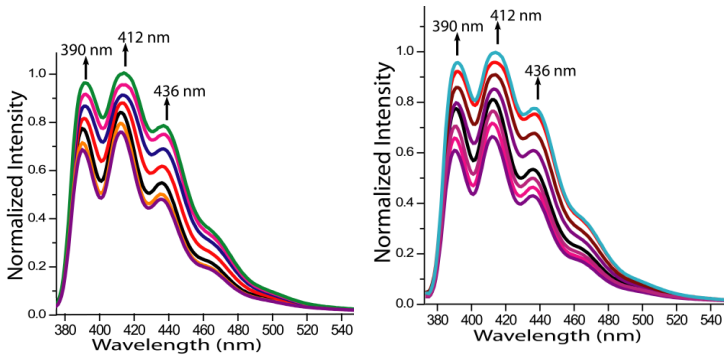

(d) (e)

Figure 3.19: Fluorescence titration (excitation at 365 nm) of **3.1** (10^{-5} M in Acetonitrile) with, (a) **4-NP**, (b) **2,4-DNP**, (c) **2,4,6-TNP**, (d) **2-NBA** and (e) **2,3-DHBA** (10 µL aliquot of 10^{-5} M in Acetonitrile). showing enhancement (thick line) followed by quenching of emission (dashed line).

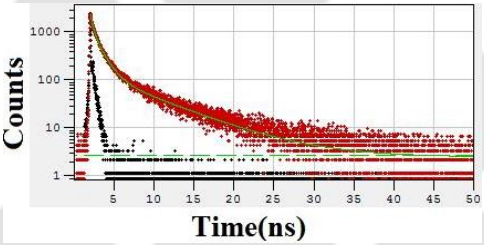

Fitting range : [148; 4096] channels

χ^2 : 1.318

	B_i	ΔB_i	f_i (%)	Δf_i (%)	τ_i (ns)	$\Delta\tau_i$ (ns)
1	1250.0144	23.7158	14.263	5.142	0.293	0.100
2	1115.1504	23.8301	49.495	1.616	1.141	0.013
3	142.8581	2.6750	36.242	0.689	6.520	0.002

Shift : 0 ns (± 0 ns)

Decay Background : 2.467 (± 0.077)

Figure 3.20: Time resolved fluorescence emission of solid sample of **3.1** (λ_{ex} = 365 nm, λ_{em} = 446 nm).

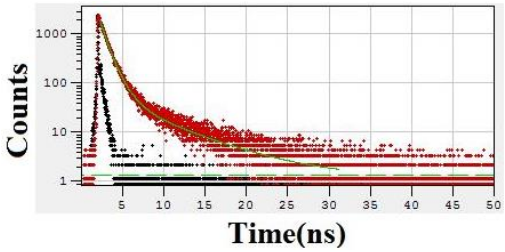

Fitting range : [168; 2550] channels

χ^2 : 1.175

	B_i	ΔB_i	f_i (%)	Δf_i (%)	τ_i (ns)	$\Delta\tau_i$ (ns)
1	1423.2976	150.3875	51.203	9.810	0.717	0.062
2	474.2506	149.8146	32.542	12.132	1.368	0.078
3	50.8017	5.6178	16.254	1.825	6.381	0.011

Shift : 0 ns (± 0 ns)

Decay Background : 1.228 (± 0.224)

Figure 3.21: Time resolved fluorescence emission of solid sample of **3.2** (λ_{ex} = 365 nm, λ_{em} = 413 nm).

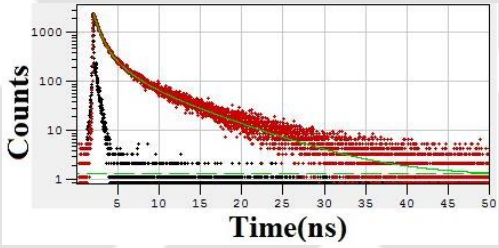

Fitting range : [150; 4096] channels

χ^2 : 1.086

	B_i	ΔB_i	f_i (%)	Δf_i (%)	τ_i (ns)	$\Delta\tau_i$ (ns)
1	1773.9342	29.1697	32.356	1.920	0.634	0.027
2	575.8865	27.1244	32.885	1.865	1.984	0.019
3	174.8727	7.2059	34.759	1.446	6.905	0.003

Shift : 0 ns (± 0 ns)

Decay Background : 1.203 (± 0.088)

Figure 3.22: Time resolved fluorescence emission of solid sample of **3.3** (λ_{ex} = 365 nm, λ_{em} = 413 nm).

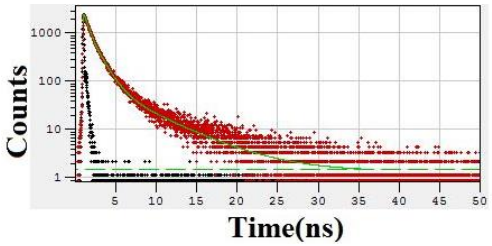

Fitting range : [62; 3000] channels

χ^2 : 1.106

	B_i	ΔB_i	f_i (%)	Δf_i (%)	τ_i (ns)	$\Delta\tau_i$ (ns)
1	0.0589	0.0009	20.893	5.141	0.340	0.079
2	0.0484	0.0009	61.685	1.722	1.221	0.011
3	0.0031	0.0001	17.422	0.771	5.324	0.004

Shift : -0.003 ns (± 0.080 ns)

Decay Background : 1.357 (± 0.094)

Figure 3.23: Time resolved fluorescence emission of solid sample of **3.4** (λ_{ex} = 365 nm, λ_{em} = 413 nm).

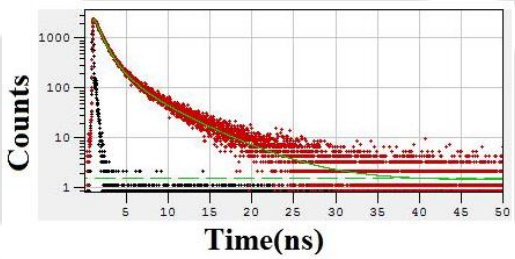

Fitting range : [66; 4096] channels

χ^2 : 1.079

	B_i	ΔB_i	f_i (%)	Δf_i (%)	τ_i (ns)	$\Delta\tau_i$ (ns)
1	0.0680	0.0025	40.328	3.286	0.752	0.034
2	0.0236	0.0024	33.354	3.910	1.789	0.031
3	0.0062	0.0004	26.318	1.668	5.347	0.004

Shift : -0.010 ns (± 0.179 ns)

Decay Background : 1.436 (± 0.062)

Figure 3.24: Time resolved fluorescence emission of solid sample of **3.5** (λ_{ex} = 365 nm, λ_{em} = 544 nm).

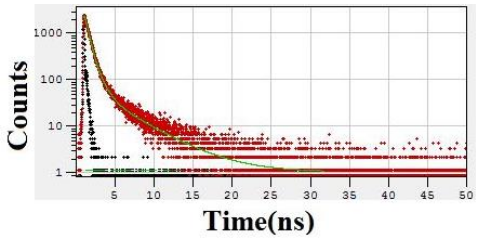

Fitting range : [64; 2600] channels

χ^2 : 1.013

	B_i	ΔB_i	f_i (%)	Δf_i (%)	τ_i (ns)	$\Delta\tau_i$ (ns)
1	0.0828	0.0029	52.223	10.543	0.405	0.067
2	0.0240	0.0031	33.984	6.491	0.907	0.055
3	0.0020	0.0001	13.793	0.844	4.344	0.007

Shift : -0.027 ns (± 0.178 ns)

Decay Background : 1.044 (± 0.082)

Figure 3.25: Time resolved fluorescence emission of solid sample of **3.6** (λ_{ex} = 365 nm, λ_{em} = 494 nm).

3.9: References:

1. W. Yang, Y. Li, H. Liu, L. Chi, Y. Li, *Small.*, 2012, **8**, 504-516.

2. (a) S. Erbas-Cakmak, D. A. Leigh, C. T. McTernan, A. L. Nussbaumer, *Chem. Rev*., 2015, **115**, 10081-10206; (b) D.-H. Qu, Q.-C. Wang, Q.-W. Zhang, X. Ma, H. Tian, *Chem. Rev*., 2015, **115**, 7543-7588; (c) H. Zhang, J. Hu, D.-H. Qu, *Org. Lett*., 2012, **14**, 2334-2337.

3. (a) W. Jiang, C. A. Schalley, *Proc. Nat. Acad. Sci. U. S. A*., 2009, **106**, 10425-10429; (b) W. Jiang, A. Schafer, P. C. Mohr, C. A. Schalley, *J. Am. Chem. Soc*., 2010, **132**, 2309-2320.

4. (a) J. B. Baruah, Concepts for Molecular Machines, World Scientific, Singapore, 2018; (b) T. B. Gasa, C. Valente, J. F. Stoddart, *Chem. Soc. Rev*., 2011, **40**, 57-78; (c) E. M. Perez, D. T. F. Dryden, D. A. Leigh, G. Teobaldi, F. Zerbetto, *J. Am. Chem. Soc*., 2004, **126**, 12210-12211.

5. (a) V. Bhalla, S. Pramanik, M. Kumar, *Chem. Commun*., 2013, **49**, 895-897; (b) Y. Peng, A. J. Zhang, M. Dong,.; Y. -W. Wang, *Chem. Commun*., 2011, **47**, 4505-4507; (c) Y. Erande, S. Chemate, A. More, N. Sekar, *RSC Adv*., 2015, **5**, 89482-8948.

6. (a) W. M. Singh, N. Barooah, J. B. Baruah, *J. Mol. Struct*., 2008, **875**, 329-338; (b) N. Phukan, J. B. Baruah, *ChemistrySelect*., 2016, **1**, 440-443.

7. K. L. VanDenburgh, Y. Liu, T. Sadhukhan, C. R. Benson, N. M. Cox, S. E. -Cakmak, B. Qiao, X. Gao, M. Pink, K. Raghavachari, A. H. Flood, *Org. Biomol. Chem*., 2020, **18**, 431-440.

8. (a) Y. Qian, S. Li, G. Zhang, Q. Wang, S. Wang, H. Xu, C. Li, Y. Li, G. Yang, *J. Phys. Chem. B*., 2007, **111**, 5861-5868; (b) T. He, X. Tao, J. Yang, D. Guo, H. Xia, J. Jia, M. Jiang, *Chem. Commun*., 2011, **47**, 2907-2909; (c) M. Cai, Z. Gao, X. Zhou, X. Wang, S. Chen, Y. Zhao, Y. Qian, N. Shi, B. Mi, L. Xie, W. Huang, *Phys. Chem. Chem. Phys*., 2012, **14**, 5289-5296.

9. Z. -F. An, C. Zheng, R. -F. Chen, J. Yin, J. -J. Xiao, H. -F. Shi, Y. Tao, Y. Qian, W. Huang, *Chem.Eur. J*., 2012, **18**, 15655-15661.

10. (a) Y. Liu, X. Tao, F. Wang, J. Shi, J. Sun, W. Yu, Y. Ren, D. Zou, M. Jiang, *J. Phys. Chem. C*, 2007, **111**, 6544-6549; (b) H. Liu, D. Cong, B. Li, L. Ye, Y. Ge, X. Tang, Y. Shen, Y. Wen, J. Wang, C. Zhou, B. Yang, *Cryst. Growth Des*., 2017, **17**, 2945-2949; (c) H. Liu, L. Yao, B. Li, X. Chen, Y. Gao, S. Zhang, W. Li, P. Lu, B. Yang, Y. Mad, *Chem. Commun*., 2016, **52**, 7356-7359.

11. J. -F. Lameere, N. Saffon, I. D. Santos, S. Fery-Forgues, *Langmuir*., 2010, **26**, 10210-10217; (b) S. M. Mooi, S. N. Keller, B. Heyne, *Langmuir*., 2014, **30**, 9654-9662; (c) I. F. Pierola, Y. Agzenai, *J. Phys. Chem. B*., 2012, **116**, 3973-3981.

12. Z. Luo, B. Liu, S. Si, Y. Lin, C. S. Luo, C. Pan, C. Zhao, L. Wang, *Dyes Pig*., 2017, **143**, 463-469; (b) J. H. Fu, Y. W. Wang, Y. Peng, *Chem. Commun*., 2017, **53**, 10524-10527; (c) S. Chaudhary, H. Sharma, M. D. Milton, *ChemistrySelect*., 2018, **3**, 4598-4608; (d) J. Wang, D. Wang, E. K. Miller, D. Moses, G. C. Bazan, A. J. Heeger, *Macromolecules*., 2000, **33**, 5153-5158; (e) D. C. Santra, M. K. Bera, P. K. Sukul, S. Malik, *Chem. Eur J*., 2016, **22**, 2012-2019.

13. (a) H. Liu, L. Yao, B. Li, X. Chen, Y. Gao, S. Zhang, W. Li, P. Lu, B. Yang, Y. Mad, *Chem. Commun*., 2016, **52**, 7356-7359; (b) S. Hisamats, H. Masu, M. Takahashi, K. Kishikawa, S. Kohmoto, *Cryst. Growth Des*., 2015, **15**, 2291-2302; (c) M. Sugino, K. Hatanaka, Y. Araki, I. Hisaki, M. Miyata, N. Tohnai, *Chem. Eur. J*., 2014, **20**, 3069-3076.

14. M. Sugino, K. Hatanaka, T. Miyano, I. Hisaki, M. Miyata, A. Sakon, H. Uekusa, N. Tohnai, *Tetrahedron Lett*., 2014, **55**, 732-736.

15. (a) S. F. M. van Dongen, S. Cantekin, J. A. A. W. Elemans, A. E. Rowan, R. J. M. Nolte, *Chem. Soc. Rev*., 2014, **43**, 99-122; (b) A. V. -Vidal, J. -L. A. -Gomez, M. M. Cid, M. M. Luna, *Supramol. chem*., 2019, **32**, 39-48.

16. (a) Y. Tokoro, N. Ohtsuka, S. -I. Fukuzawab, T. Oyama, *RSC Adv*., 2018, **8**, 25177-25180; (b) K. Kobayashi, H. Masu, A. Shuto, K. Yamaguchi, *Chem. Mater*. 2005, **17**, 6666-6673.

17. A. Pandith, A. Kumar, H. -S. Kim, *RSC Adv*., 2015, **5**, 81808-81816.

18. (a) B. Lou, S. R. Perumalla, C. C. Sun, *Cryst. Growth Des*., 2015, **15**, 24-28; (b) J. B. Baruah, *J. Chem. Sci*., 2018, **130**, 56. (c) S. Mohamed, A. A. Alwan, T. Friscic, A. J. Morris, M. Arhangelskis, *Faraday Discuss*., 2018, **211**, 401-424.

19. M. C. Etter, J. C. MacDonald, J. Bernstein, *Acta Cryst*., 1990, **B46**, 256-262.

20. E. A. Chandross, F. Ferguson, E. G. Mcray, *J. Chem. Phys*., 1966, **45**, 3546.

21. A. J. Cruz-Cabeza, J. Bernstein, *Chem. Rev*., 2014, **114**, 2170-2191.

22. S. P. Anthony, S. Varughese, S. M. Draper, *Chem. Commun*., 2009, 7500-7502.

23.(a) X. Xu, B. Li, W. Li, J. Zhao, S. Sun, Y. Pang, *Chem. Commun*., 2013, **49**, 4764-4766; (b) R. Mitra, A. Saha, *ACS Sustainable Chem. Eng*., 2017, **5**, 604-615.

24. A. P. de Silva, T. S. Moody, G. D. Wright, *Analyst*., 2009, **134**, 2385-2393.

25. (a) M. Boiocchi, L. Fabbrizzi, S. L. Cognata, L. Legnani, E. L. Presti, C. Mangano, A. Miljkovic, *Org. Chem. Front*., 2018, **5**, 391-397; (b) S. Kohmoto, T. Chuko, S. Hisamatsu, Y. Okuda, H. Masu, M. Takahashi, K. Kishikawa, *Cryst. Growth Des*., 2015, **15**, 2723-2731.

26. (a) A. Pandith, A. Kumar, J. -Y. Lee, H. -S. Kim, *Tetrahedron Letters*., 2015, **56** 7094-7099; (b) A. Tarai, J. B. Baruah, *New J. Chem*., 2017, **41**, 10750-10760; (c) A. Kumar, P. S. Chae, *Sensors and Actuators*., 2017, **240**, 1-9; (d) X. Cao, N. Zhao, H. Lv, Q. Ding, A. Gao, Q. Jing, T. Yi, *Langmuir*., 2017, **33**, 7788-7798.

27. T. Hinoue, Y. Shigenoi, M. Sugino, Y. Mizobe, I. Hisaki, M. Miyata, N. Tohnai, *Chem. Eur. J*., 2012, **18**, 4634-4643.

28. (a) X. Cao, L. Meng, Z. Li, Y. Mao, H. Lan, L. Chen, Y. Fan, T. Yi, *Langmuir*., 2014, **30**, 11753-11760; (b) Z. Zhang, Y. Zhang, D. Yao, H. Bi, I. Javed, Y. Fan, H. Zhang, Y. Wang, *Cryst. Growth Des*., 2009, **9**, 5069-5076; (c) X. -F. Fu, Y. -F. Yue, R. Guo, L. -L. Li, W. Sun, C. -J. Fang, C. -H. Xu, C. -H. Yan, *CrystEngComm*, 2009, **11**, 2268-2271; (d) D. Zhao, T. M. Swager, *Macromolecules*., 2005, **38**, 9377-9384.

29. P. G. Wu, L. Brand, *Anal. Biochem*., 1994, **218**, 1-13.

30. R. Wang, L. Yuan, D. H. Macartney, *Chem. Commun*., 2005, 5867-5869.

31. M. Sugino, Y. Araki, K. Hatanaka, I. Hisaki, M. Miyata, N. Tohnai, *Cryst. Growth Des*., 2013, **13**, 4986-4992.

Chapter 4

Detection of Hydroxyaromatics by (N,N'-bis(3-imidazolium-1-yl propyl)naphthalenediimide)di[bis-2,6-pyridinedicarboxylate ferrate] in Water

4.1: Introduction

Due to polluting[1] and hazardous nature of phenolic compounds,[2] detection and removal of traces of phenolic compounds present in water is an attractive topic. This is commonly done with the aid of fluorescent molecules as sensors. Large numbers of fluorescent sensors are developed in recent years.[3] Among them water soluble metal-organic frameworks[4] have emerged as receptors for detection of nitro-phenolic compounds. But there are limited examples on the use of low-nuclearity metal complexes in the detection of nitroaromatics.[5] A water soluble fluorescent metal complex would be easily decomposed and disposed after use. Generally, water has dissolved iron (3+) ions, which causes bad odour of water. The iron (3+) ion being paramagnetic, their presence in water influences fluorescence sensing by an analyte as paramagnetic ions are known to cause fluorescence quenching. This is, in general, is a set-back to use conventional fluorescence detection method to ascertain an organic pollutant in the presence of iron (3+) ions. This is also true for other paramagnetic ions such as copper ions present in water. In order to detect an organic pollutant thus it becomes necessary to remove or transform the metal ion to some other form that do not interfere the detection process. Chelation of paramagnetic sites has been used extensively to prevent direct contact of paramagnetic ions with fluorophores during fluorescence detection.[6] Due to easy synthesis, stability in solution, higher solubility and selectivity use of lower nuclearity fluorescent metal-complexes would have advantages in detection of phenolic compounds.[7] Diamagnetic zinc-2,6-pyridinedicarboxylate complex having fluorescent cation is used to detect nitrophenols.[8] On the other hand, anions of zinc-2,6-pyridinecarboxylate complex which have stacking abilities showed cation dependent selectivity in recognition of phenolic compounds.[7b] This provides a scope for the detection of phenolic compounds by the emission properties of a cationic part of 2,6-pyridinedicarboxylate or related dicarboxylate metal-complex, where the complex anionic part would guide the selectivity in chemical binding.[9] In such a complex, the paramagnetic metal-ion will not have direct contact with the cationic fluorescent species; hence will get rid of fluorescence quenching effect of the paramagnetic

ion. Thus, we decided to explore such a possibility by using N,N'-*bis*(3-imidazol-1-yl propyl)naphthalenediimide (**L**) whose protonated state has higher fluorescence[10] and interacts with nitrophenols showing emission changes.[11]

An iron (3+) complex of 2,6-pyridinedicarboxylic acid having H_2L^{2+} cation is chosen as a success on this complex would establish the necessary clues whether fluorescence detection of nitrophenolic compounds by **L** in the presence of iron (3+) would be possible directly. Moreover, from our laboratory we have demonstrated cocrystal formation of nitrophenols with **L**.[11] Hence, if an easily isolable, stable iron complex forms cocrystals with nitrophenols that would be removed from aqueous solution, thereby providing an integral process of detection and separation of the pollutants.

Accordingly, (N,N'-bis(3-imidazolium-1-yl-propyl) naphthalenediimide)di[bis-2,6-pyridinedicarboxylate ferrate]octahydrate (complex **4.1** of Figure 4.1) was synthesized and characterized to study the detection of phenolic compounds through emission spectroscopy. The complex was further used to prepare different cocrystals with different hydroxy-aromatic compounds in water that are listed in Figure 4.1.

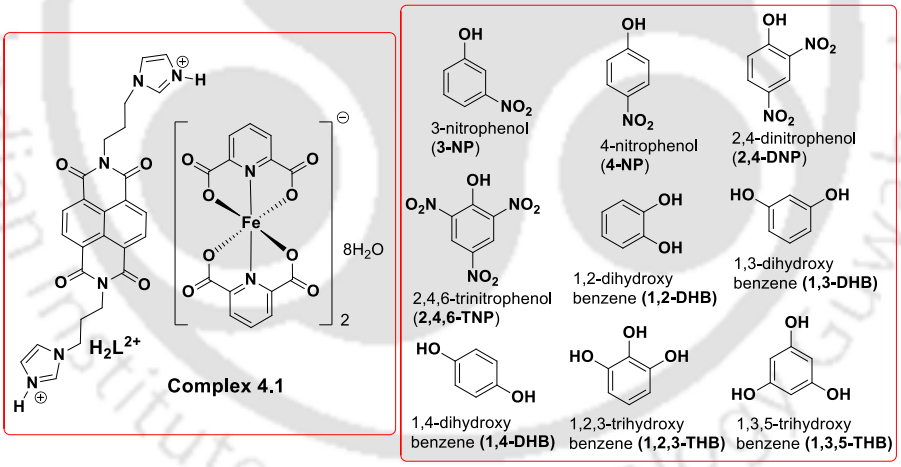

Figure 4.1: The iron (III) pyridinedicarboxylate complex (**4.1**) and various organic phenolic compounds used in this study.

4.2: Synthesis and Crystal Structure of the Iron (+3) bis-2,6-pyridinedicarboxylate (complex 4.1)

The iron complex (N,N'-bis(3-imidazolium-1-yl-propyl)naphthalenediimide)di[bis-2,6-pyridine dicarboxylate ferrate] (**4.1**) was prepared by reaction of 2,6-pyridinedicarboxylic acid with anhydrous ferric chloride and N,N'-*bis*(3-imidazol-1-yl-propyl)naphthalenediimide (**L**) in methanol. The complex **4.1** has eight water molecules of crystallization and is highly

soluble in water. The compound has a magnetic moment of 5.72 BM at 28° C. It corresponds to the spin-only magnetic moment for five unpaired electrons of the iron ion at +3 oxidation state. Our attempts to synthesize the analogous iron (+2) complex were not successful; only the iron (+3) complex was obtained starting from iron (+2) salts under aerobic conditions. The structure of complex **4.1** (Figure 4.2a) showed that the water molecules act as bridges between the cation and anion involving N1-H···O13 and N1-H···O14 charge-assisted hydrogen bonds ($d_{D\cdots A}$ = 2.794 Å and 2.823 Å), and moderate O14-H···O4 and O13-H···O4 hydrogen bonds ($d_{D\cdots A}$ = 2.831 Å and 2.755 Å). Out of the eight water molecules, six water molecules collectively interact to form water clusters within the lattice and utilise the available hydrogen bonding sites of the anions and cations to provide a tight packed structure. These water molecules mutually interact to form a robust hydrogen-bonded cyclic structure which has $R_6^4(12)$ notation (Figure 4.2b).[12] The water clusters have earlier been observed in 2,6-pyridinedicarboxylate complexes.[13] Water clusters were also suggested to make an impact on the emission patterns.[10] In general, the stacking interactions among anions and hydrogen bonding involving water molecules and organocations are crucial to decide the packing patterns of metal 2,6-pyridinedicarboxylate complexes.[14] The portion of the crystal lattice of complex **4.1** is shown in Figure 4.2a depicts a centroid-centroid distance of 3.801 Å between the naphthalenediimide ring and the pyridinedicarboxylate rings stacking over each other. This distance is away from a distance of 3.5 Å for an effective π-π interaction.[15] We also find in the crystal lattice that a set of rings of the two 2,6-pyridinedicarboxylate ligands of the complex anion are not stacked among themselves; but another set is located parallel to each other. The parallel stacks sandwich the naphthalenediimide rings of the protonated N,N'-*bis*-(3-imidazol-1-yl-propyl) naphthalenediimide($\mathbf{H_2L^{2+}}$). More precisely, the complex anions are arranged in linear arrays along the *c*-crystallographic axis without stacking interactions. This arrangement holds the imidazolium part of the cations between the intervening spaces between the anions so that the two ends of the cations are embedded in a layer-like arrangement. The anions form layer-like arrangements, where the 2,6-pyridinedicarboxylate rings in between the layers are parallel to each other (Figure 4.2c). Such arrangements are repeated along the *a*-crystallographic axis to form grid-like spaces in between the layers propagated along the c-axis. The grid-like spaces accommodate the naphthalenediimide part of the cations. The naphthalenediimide rings are sandwiched between two 2,6-pyridinedicarboxylate rings of two independent molecules from different layers. Such arrangements align the cations vertically between the layers.

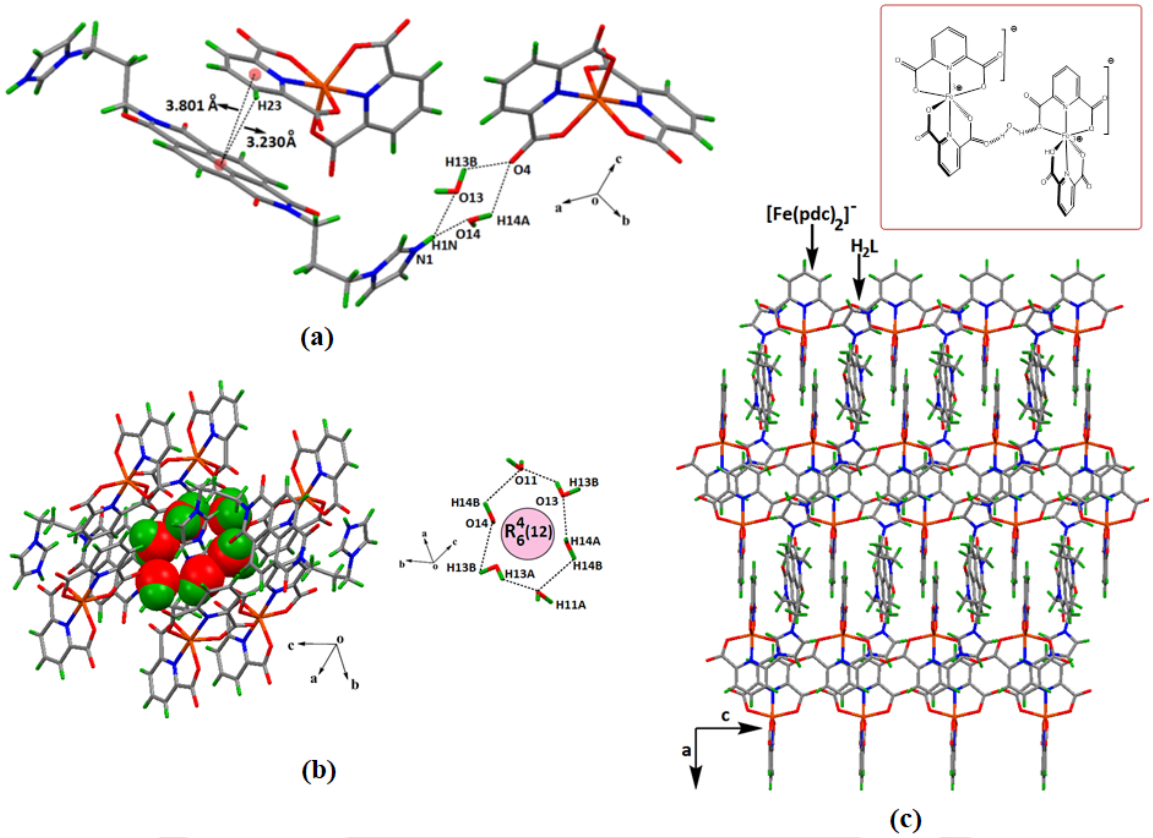

Figure 4.2: (a) π-Stacking in the lattice of complex **4.1** (interaction with one anion is shown for clarity), (b) Water cluster in the complex **4.1** (inset is the hydrogen bonds among the water molecules of a water cluster) and (c) Packing diagram of the complex **4.1** showing layer-like structure.

The complex **4.1** is fluorescent in the solid state, it has weak fluorescence emission maxima at 415 nm, 436 nm and 466 nm upon excitation at 350 nm (Figure 4.15). These emissions are characteristic of the cationic part.[10] The weakening in emission of the complex with respect to the protonated ligand found in other salts[10] is attributed to Dexter type of quenching[16] due to the sandwiching of naphthalenediimide part between the rings of pyridinedicarboxylates.

4.3. Interaction of the Complex 4.1 with Hydroxyaromatics

In aqueous solution the complex **4.1** has cation based absorptions at 362 nm, 383 nm, 480 nm and a very weak absorption at 675 nm (Figure 4.13 and 4.14). The complex is a high-spin d^5-system with A_{1g} ground-state; hence, the weak absorption at 675 nm is due to spin d-d transition relaxed by vibronic coupling. The complex is fluorescent in water; upon excitation at 340 nm it emits at 393 nm, 413 nm, and 440 nm with quantum yield of 0.38. The peaks are due to v_0- v_0, v_1-v_0, v_2-v_0 transitions of a π*-π transition. Our earlier study has shown that the

L is not soluble in water, but in polar organic solvents it shows weak emissions at 408 nm.[11] The imidazole's of **L** are protonated in the iron-complex **4.1**, hence an ON-state of **L** is observed as photo-electron transfer is not possible. As mentioned earlier, the paramagnetic ions in general are quenchers of fluorescence. Such quenching can be reduced or quenched by concealing the paramagnetic site by chelation.[17] It is found that complex **4.1** has such features and in solution the effect of the iron (3+) on quenching fluorescence of the cationic part is not seen. We also find that the fluorescence emission of a solution at 407 nm of **L** is quenched by adding a solution of ferric chloride and the quenched emission is recovered to original intensity upon a titration with a solution of 2,6-pyridine dicarboxylic acid (Figure 4.3). Thus, it is clear that the chelation by pyridinedicarboxylic acid can stop the effect of quenching caused by iron (III) ions on the emission of the **L**.

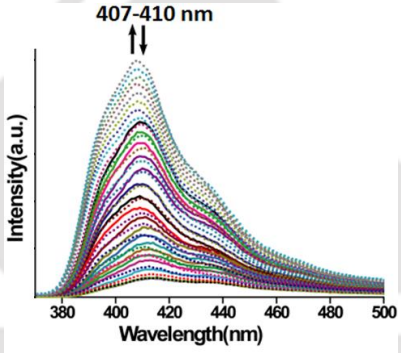

Figure 4.3: Fluorescence spectroscopic titration (λ_{ex} = 340 nm) of (3-imidazol-1-yl-propyl)naphthalenediimide (**L**) (10^{-4} M in ethanol) by adding $FeCl_3$ showing quenching of emission and upon addition of 2,6-pyridinedicarboxylic acid (10^{-4} M in 10 μL aliquots) showing enhancement of emission (dashed line).

Solubility and fluorescent nature of the complex **4.1** in water has enabled us to study the fluorescence emission changes of aqueous solution of complex **4.1** caused by a series of phenolic compounds listed in the Figure 4.1. Since the imidazole portions are protonated, there is a least scope for phenolic compounds to influence photo-induced electron transfer unless deprotonation of the imidazolium cation is caused in solution. It did not happen, hence the cationic species showed Dexter quenching due to interaction of the naphthalenediimide unit with aromatic rings of the phenolic compounds. We find that the phenolic compounds quench the fluorescence emission of complex **4.1**. Accordingly, the intensities of the emissions at 393 nm, 413 nm and 440 nm decrease proportionately upon addition of different phenolic compounds to an aqueous solution of complex **4.1**. The emission change in each

case is similar but the relative quenching differs (Figure 4.17 and 4.18). Hence, one representative titration is shown in Figure 4.4a. Among the four nitrophenols studied the relative quenching abilities are in the order of 2,4,6-TNP > 2,4-DNP > 4-NP > 3-NP. The invariance in the change in the emission pattern of complex **4.1** with respect to the skeletally similar phenols is a clear indication that a common emission quenching mechanism takes place. The plots of intensity against the concentration of hydroxyaromatics are found to provide non-linear plots. (Figure 4.4b-d). These plots are suggestive of quenching without change of the ground state of the fluorophore. As per earlier reports on the trend for emission through exciplex formation, these non-linear plots are also suggestive of the formation of exciplex[18] by the fluorophore with the non-emissive hydoxy-aromatics. The relative effectiveness of the fluorescence quenching is reflected in the quenching efficiency which is known to be determined by quenching constant (K_{sv} expressed as mol^{-1}). The quenching constant is defined as $(I_0/I) = K_{sv}[A] + 1$, where I_0 is the fluorescence intensity of the solution without hydroxyaromatic and I is the fluorescence intensity in the presence of hydroxyaromatic, and [A] is the molar concentration of the hydroxyaromatic.

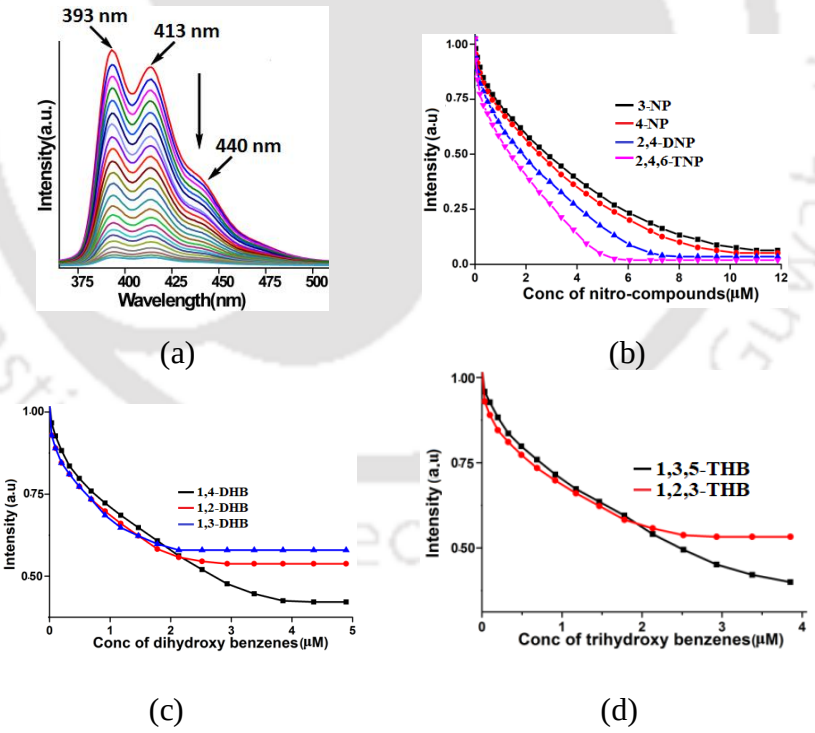

Figure 4.4: (a) Fluorescence spectroscopic titration (λ_{ex} = 340 nm) of the complex **4.1** (10^{-5} M in water) with 4-NP, (10^{-5} M in water, 10 μL in each aliquot) and (b)-(d) changes in the fluorescence intensity at 393 nm of the complex **4.1** at different concentrations of different hydroxyaromatics.

Table 4.1: Detection limits and quenching constants for different hydroxyaromatic compounds by complex **4.1**.

Compound	Detection limit ($3\sigma/k$) (μM)	quenching constant (K_{sv})(mol^{-1}).	Compound	Detection limit ($3\sigma/k$) (μM)	Quenching constant (K_{sv})(mol^{-1}).
3-nitrophenol	0.45	0.64×10^6	1,2-dihydoxybenzene	0.64	0.38×10^6
4-nitrophenol	0.44	0.97×10^6	1,3-dihydroxybenzene	0.66	0.34×10^6
2,4-dinitrophenol	0.41	1.75×10^6	1,4-dihydroxybenzene	0.61	0.39×10^6
2,4,6-trinitrophenol	0.39	3.98×10^6	1,2,3-trihydroxybenzene	0.58	0.42×10^6
			1,3,5-trihydroxybenzene	0.55	0.43×10^6

The efficiencies of quenching by different phenolic compounds are listed in Table 4.1. The values are similar for the hydroxyaromatics without a nitro group. On the other hand, the nitrophenols have a higher values of quenching constant due to their higher charge-transfer ability. Among the nitrophenols the quenching abilities varied; for example, 2,4,6-TNP has an approximately four times higher quenching constant than 4-nitrophenol. The quenching constant for 2,4,6-TNP is 3.98×10^6 mol^{-1}, comparable to other macromolecular receptors.[19] Based on the changes in emission intensities with concentrations, the detection limit for the phenolic compounds are determined and listed in Table 4.1. It is found that the detection ability of complex **4.1** to detect nitrophenols is higher than the other hydroxyphenols without a nitro-group on the ring. The detection limits of the three positional isomeric dihydroxybenzenes are comparable. The two trihydroxybenzenes can be detected at slightly lower concentrations than the dihydroxybenzenes. If the quenching primarily would have been due to deprotonation of the hyrdroxyaromatics, the positional isomers should have shown different detection limits from each other, but this is not the case. Thus, the stacking effect of the aromatics are predominantly contributing to the quenching. The similar effects caused by the positional isomers suggest that the anionic part has an insignificant role to dictate the interactions between the $\mathbf{(H_2L)^{2+}}$ in solution. The electron withdrawing ability of nitro-group/s causes favourable electron transfer in a nitrophenol interacting with complex **4.1**.

4.4. Synthesis of inclusion complexes of 4.1

The reaction of complex **4.1** with 1,4-dihydroxybenzene led to 1:1 inclusion complex whereas in the cases of 3-nitrophenol, 4-nitrophenol and 1,3,5-trihydroxybenzene, the 1:2 inclusion complexes are formed. The reactions are shown in the Scheme 4.1. Representing (N,N'-bis(3-imidazolium-1-yl-propyl)naphthalenediimide)di[bis-2,6-pyridine dicarboxylate ferrate] as $(H_2L)[Fe(pdc)_2]_2$. $8(H_2O)$ (**4.1**), the inclusion complexes are $(H_2L)[Fe(pdc)_2]_2.2$(3-

NP).4(H_2O) (**4.2**), (H_2L) [$Fe(pdc)_2]_2$.2(4-NP).2(H_2O) (**4.3**), (H_2L)[$Fe(pdc)_2]_2$.(1,4-DHB).10(H_2O) (**4.4**), and (H_2L) [$Fe(pdc)_2]_2$.2(1,3,5-THB).4(H_2O) (**4.5**) respectively. The complexes are characterized by recording the IR-spectra, UV–vis spectra, powder-XRD patterns (Figure 4.11), by thermogravimetry (Figure 4.19) and from their X-ray crystal-structures. The prominent visible peaks, the room temperature magnetic moments and emission maxima of the complexes **4.1**-**4.5** are listed in Table 4.2. The magnetic moments of the complexes are in the ranges of 5.72-5.97 BM at 25℃, which are supportive of high-spin d^5-electronic configuration.

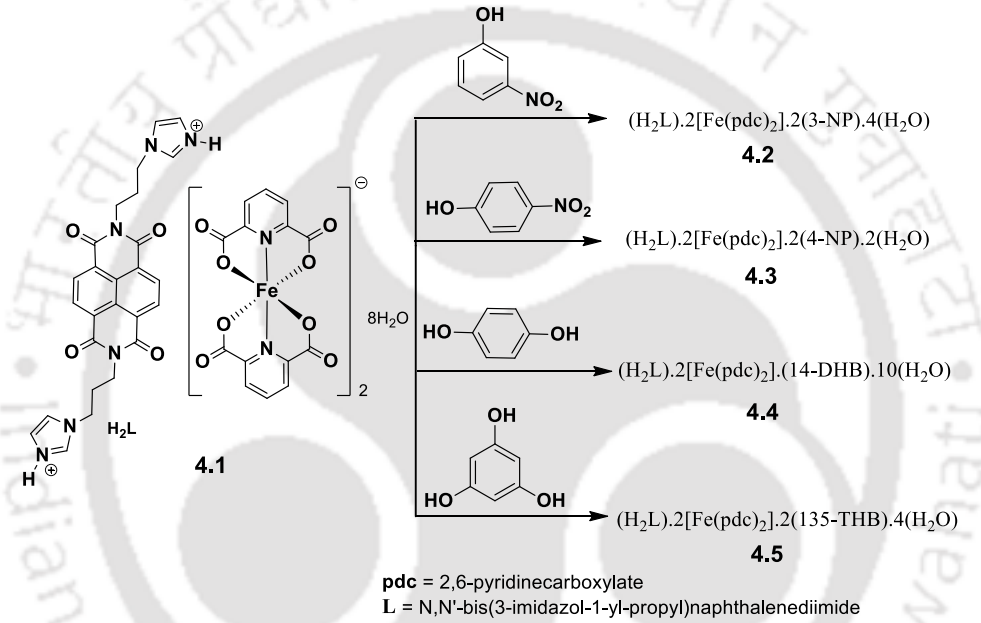

Scheme 4.1: Synthesis of various guest included complexes of **4.1**.

Table 4.2: The characteristic features of the complexes.

Complex	Magnetic moment (BM, 25˚C)	UV-absorptions [Extinction coefficient (Є= $dm^3\ mol^{-1}\ cm^{-1}$]	Emission (excitation 340 nm)@	Quantum yield
Complex **4.1**	5.72	480 [5.4×10^3] 675 [0.8×10^3]	393, 413, 440	0.38
Complex **4.2**	5.47	475 [1.4×10^3]	396, 413, 440	0.12
Complex **4.3**	5.38	475 [2.0×10^3]	396, 413, 440	0.10
Complex **4.4**	5.88	465 [2.7×10^3]	400, 413, 440	0.19
Complex **4.5**	5.97	430 [4.7×10^3]	398, 413, 440	0.21

@ =10^{-5} M in water

4.5. Self-assemblies of the inclusion complexes

In the crystal structure of complex **4.2**, the cations and anions are held by N1-H···O10 ($d_{D\cdots A}$ =2.764 Å) interactions and C2-H···O3 ($d_{D\cdots A}$ = 3.471 Å) interactions as illustrated in Figure

4.5a. The 3-nitrophenol is linked to $[Fe(pdc)_2]^-$ anion by an O11-H···O9 ($d_{D\cdots A}$ =2.652 Å) hydrogen bond and is anchored to the naphthalenediimide ring by a C10-H···O11 ($d_{D\cdots A}$ = 3.149 Å) interaction. A pyridinedicarboxylate ring of each anion is stacked parallel to the naphthalenediimide ring with centroid to centroid distance of 3.501 Å. Such interactions provide directional arrangements to expand as 2-D layer-like structure as illustrated in Figure 4.5b. The 3-nitrophenol molecules are held between such layer-like arrangements. The 3-nitrophenol molecules occur as pair of molecules where the nitro-group containing ends face each other in the pairs. The 3-nitrophenol molecules are located in close vicinity of the imidazolium rings. The imidazolium part of each cation remains at the interior of the layer-like arrangements formed by the naphthalenediimide rings sandwiched between the anionic layers. Hence, in this case the central portion of each cation is involved in layer-like arrangements of anions, whereas the projected cationic parts are held to the 3-nitrophenol.

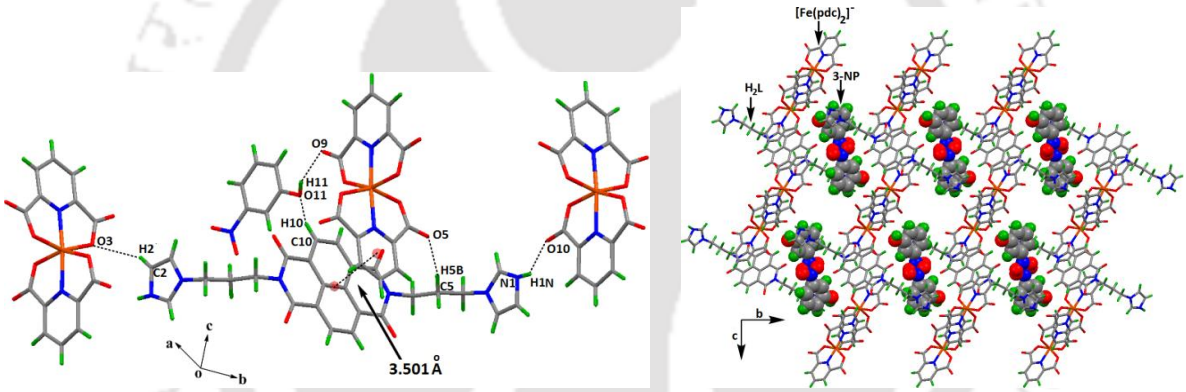

(a) (b)

Figure 4.5: (a) The π-stacks and hydrogen bonds in complex **4.2** and (b) the packing diagram showing the participation of cations and anions in the layer-like arrangements.

The self-assembly of the complex **4.3** shows large differences from the analogous inclusion complex with 3-nitrophenol (Figure 4.6). In this case there is π-stacking between the iron-pyridinedicarboxylate units in a pair-wise manner (Figure 4.6a). The centroid to centroid distance between these stacked rings is 3.556 Å. These pairs of anions propagate as a chain along the crystallographic *a*-axis. The cations are horizontally positioned in between the chains of anions and are linked to the 4-nitrophenol molecules. The 4-nitrophenol molecules are sandwiched between the rings of pyridine dicarboxylate and the naphthalenediimide ring with a centroid to centroid distance of 3.501 Å and 3.507 Å, respectively. Thus, 4-nitrophenols have strong π-interactions with the rings of anion and cation. These molecules

are also held by pyridinedicarboxylate by O11-H···O9 ($d_{D\cdots A}$ = 2.664 Å) hydrogen bonds. There are hydrogen bonds to connect the paired anions through intervening water molecules (Figure 4.6b). The water molecules provide bridges between the anions and also hold the cations through charge-assisted hydrogen bonds $^{(+)}$N1-H···O14 ($d_{D\cdots A}$ = 2.774 Å).

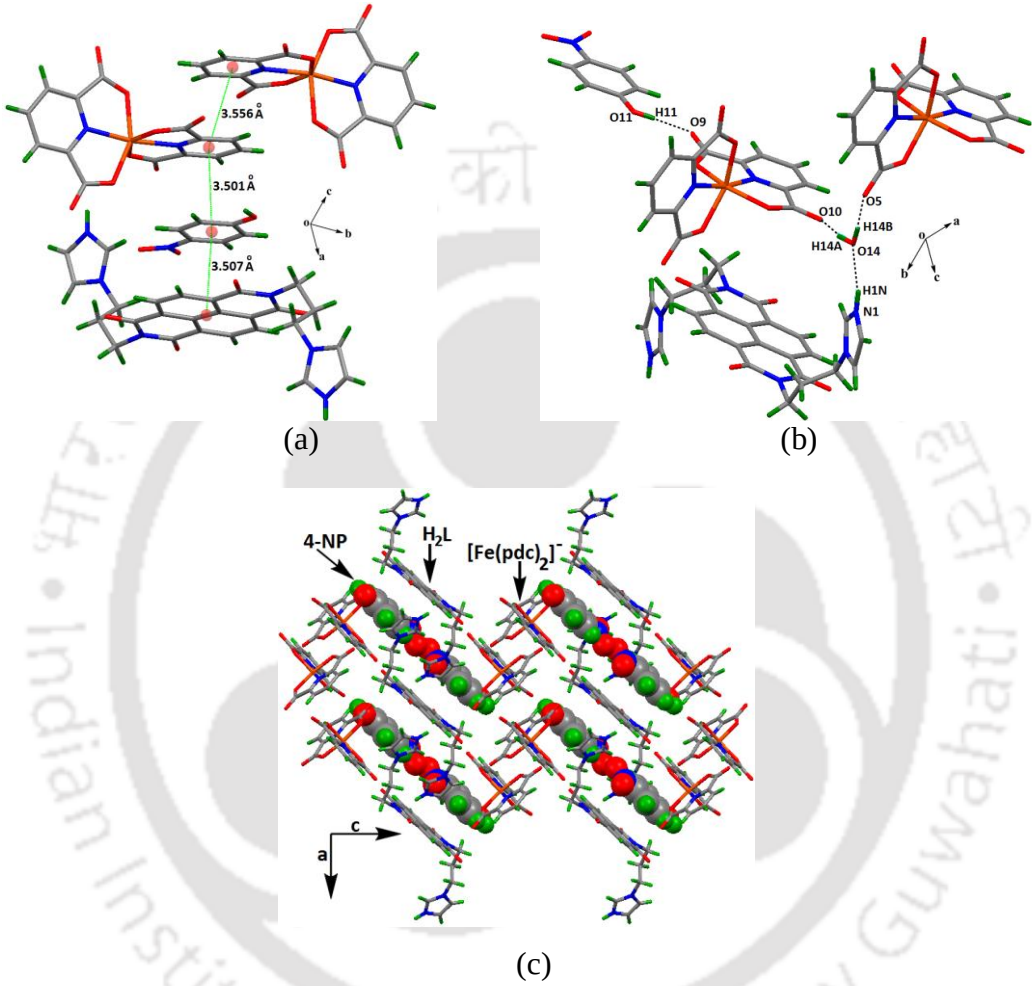

Figure 4.6: Self-assembly of the complex **4.3** showing (a) π-stacking, (b) other weak hydrogen bonds and (c) packing diagram of the structure.

The assembly of the complex **4.4** has several unique features making it distinguishable from the other inclusion complexes (Figure 4.7). It is a 1:1 inclusion complex. The cations and anions are linked through intervening water molecules involving O13-H···O5 ($d_{D\cdots A}$ = 2.827 Å) and N1-H···O13 ($d_{D\cdots A}$ = 2.863 Å) hydrogen bonds (Figure 4.7a). The cations are also held to neighboring anions by charge-assisted N1-H···O4 bonds ($d_{D\cdots A}$ = 2.945 Å). One set of 2,6-pyridinedicarboxylate rings of anions are parallel but the anions are located at a distance so they do not eclipse each other to have effective π-stacking interactions. This is

due to occupancies of water molecules that maximize the number of available hydrogen bond sites. The water molecules provide hydrogen bonds between the anion, cation and 1,4-dihydroxybenzene as illustrated in Figure 4.7b. The anions are systematically arranged in one direction and the 1,4-dihydroxybenzene molecules are located in between cations. Each 1,4-dihydroxybenzene molecule acts as an intervening molecule between the horizontally organized dications. This example shows a horizontal arrangement of the cations making room to hold the guest in an alternative manner and providing a layer-like structure.

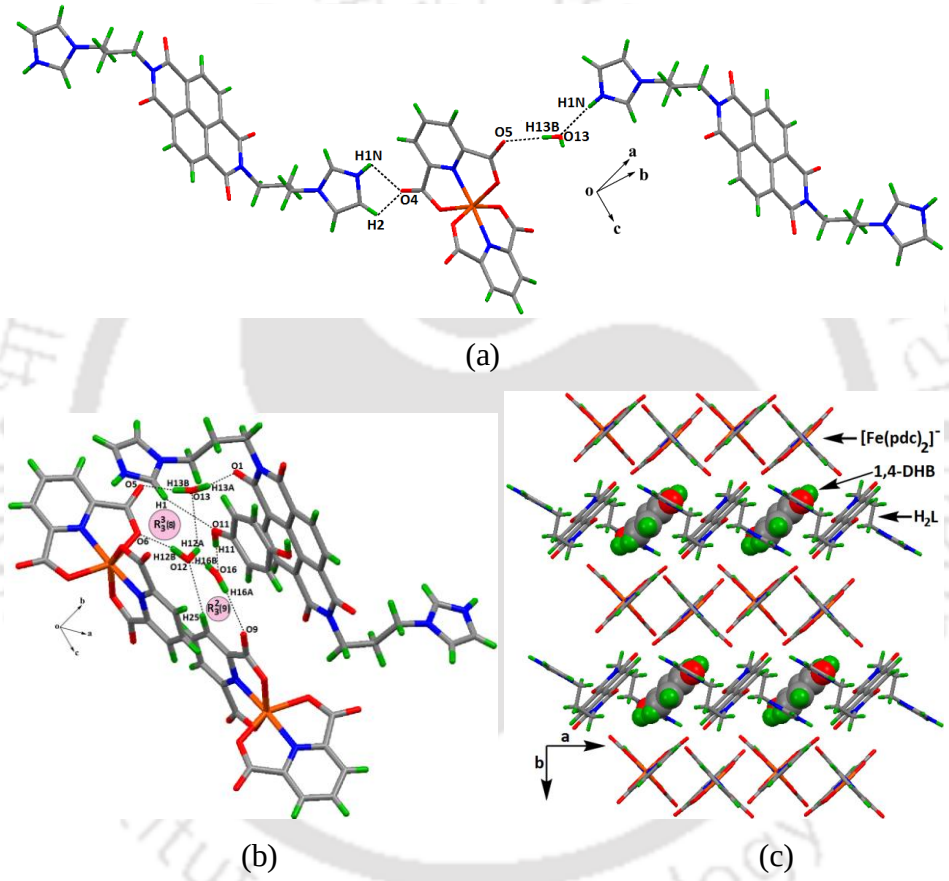

Figure 4.7: The structure of complex **4.4** (a) showing interaction between cation and anion, (b) Hydrogen bonded self-assembly and (c) Crystal packing diagram.

The complex **4.5** has extensive aromatic stacking interactions among the rings of anions, cations and 1,3,5-trihydroxybenzene molecules (Figure 4.8a). The distance between the parallel rings of neighboring anions is 3.457 Å. Due to this π-stacking, a chain-like arrangement is observed among the iron-2,6-pyridinedicarboxylate anions. The 1,3,5-trihydroxybenzene molecules are sandwiched between the naphthalenediimide and opposite faces of pyridinedicarboxylates of the complex. The distance between the centroids of rings of 1,3,5-trihydroxybenzene to the naphthalenediimide ring and pyridinedicarboxylate ring are

3.430 Å and 3.511 Å, respectively. The water molecules form hydrogen bonds with the anions, cations and 1,3,5-trihydroxybenzene molecules (Figure 4.8b). Two hydroxyl groups of the 1,3,5-trihydroxybenzene are hydrogen bonded to two independent iron (+3) pyridinedicarboxylate anions whereas the other hydroxyl group is hydrogen bonded to the oxygen atom of the naphthalenediimide ring. The tight packed structure shown in Figure 4.8c has the guest molecules held between the anionic and cationic layer-like structures.

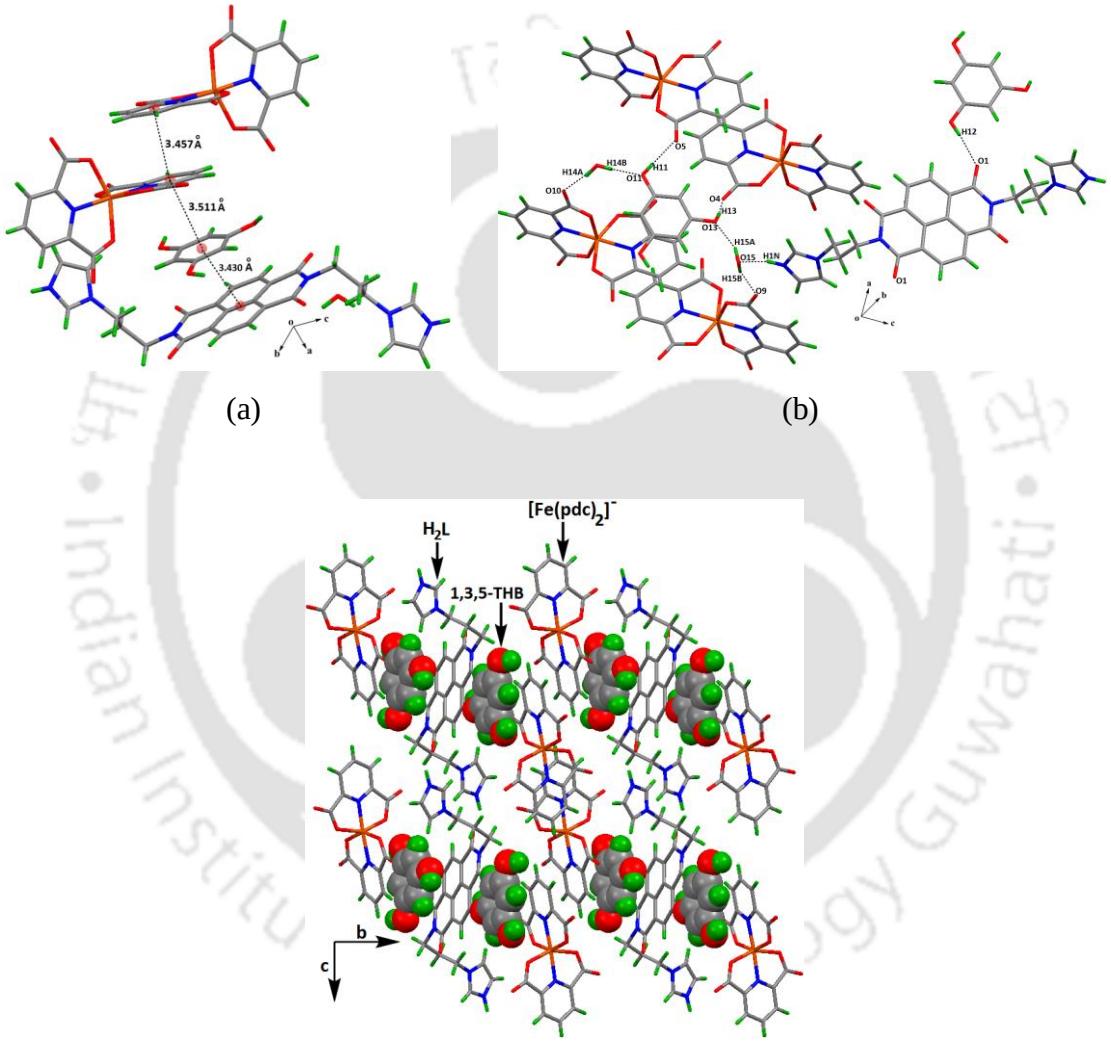

Figure 4.8: Self-assemblies of complex **4.5** (a) showing π-stacking, (b) The prominent weak interactions of 1,3,5-THB with $[Fe(pdc)_2]^-$, cation and water; and (c) The packing diagram of complex.

The structural analyses have revealed that the hydroxyaromatics cause large difference in the arrangement of cations and anions to provide variety of structures. From the cationic point of

view, two types of arrangements are apparent, in one case the cations are horizontally placed in between orderly arrangements of layer-like arrangements of the anions. This is observed in the three examples of the inclusion complexes, among the four. The only exception was the 3-nitrophenol included complex, in which the cations are vertically placed along the sheet-like arrangement of the anions of which the naphthalenediimide ring is also a part. This allows projection of two ends towards intervening spaces between the layers where the 3-nitrophenol molecules are located. In pyridinedicarboxylate complexes the interlayer spacing is generally guided by organocations.[20] The present example is a new example of such a kind in which a naphthalenediimide unit of the cation gets included into the layers of anions (Figure 4.9c), and the cationic portions projecting at two different sides anchor the guest counterpart. On the other hand, the arrangements of anions are broadly classified as discrete (without having stacking interactions among them) and with π- stacking (Figure 4.9a-b). A third category of arrangements has the cations sandwiched in between two pairs of iron-pyridinedicarboxylate units as in the case of the 3-nitrophenol inclusion complex.

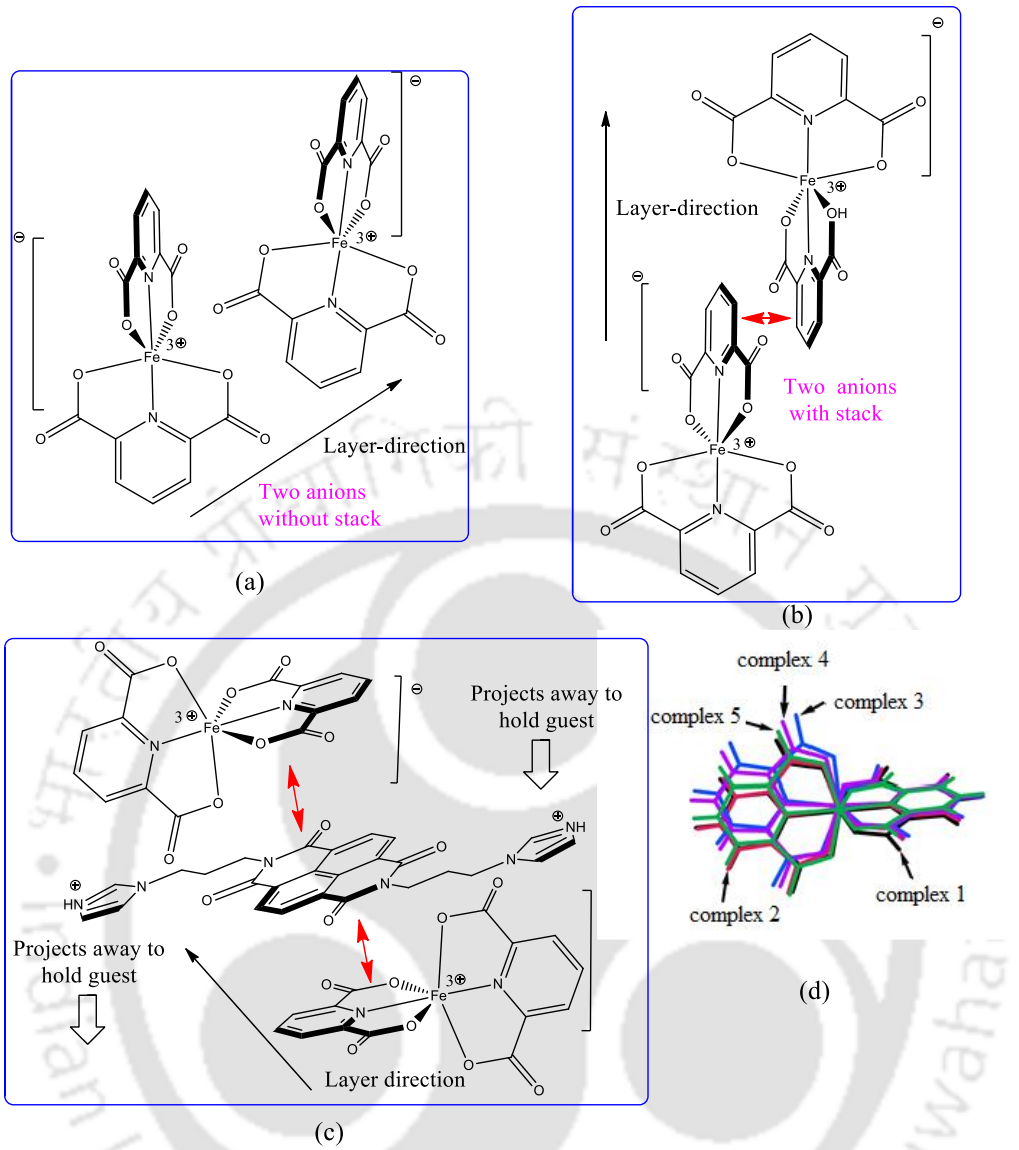

Figure 4.9: Arrangements among the $[Fe(pdc)_2]^-$ in the self-assemblies of the inclusion complexes (a) No stacking, (b) partial stacking, (c) cation eclipsed and (d) overlaid anions of different anionic parts of the complexes.

Since all the inclusion complexes are based on $[Fe(pdc)_2]^-$, three aspects mainly contributed to the architecture of the self-assemblies. These are (a) orientations of the flexible arms of cation, (b) the direction and way of participation of the hydroxyaromatics as hydrogen bond donors-acceptors and (c) the participation of water molecules in hydrogen bonds. The common feature in the complex is that each has structurally similar anions. However, the geometries around the iron ion slightly vary among the inclusion complexes. This is reflected in the overlaid geometries of the anionic part of the complexes shown in Figure 4.9d. The stacking among different components is found to be highly dependent on the

hydroxyaromatic under consideration. The naphthalenediimide rings are laterally or vertically placed between the anionic layer-like structures. The solid samples of the inclusion complexes are very weakly emitting (Figure 4.15); their quenched states are the consequence of the stacking of the fluorescent cation with the aromatic rings of the phenolic compounds as well as with the anions.

4.6: Thermal and life-time study of the complexes 4.1-4.5

The thermogravimetric analysis of the complexes were done and the thermogram of all the complexes are shown in Figure 4.19. The thermogravimetry study shows that complex **4.1** loses water molecules at 80˚-95°C. All the complexes show a weight loss due to water in the temperature range 75˚-105˚. The complexes finally transform to ferric oxide in each case in the temperature range 600˚-670 ˚C. The weight loss observed at different temperature ranges and calculated and observed weight loss are listed in Table 4.3.

Table 4.3: Thermogravimetry of complexes **4.1-4.5**.

Complex	Temperature range (°C)	Experimental weight loss from parent composition (%)	Interpretation of weight loss	Theoretically calculated weight loss (%)
Complex **4.1**	80-95	10.18	Loss of eight water	10.28
	230-275	43.51	Loss of one L	44.70
	340-630	89.81	Formation of Fe_2O_3	88.59
Complex **4.2**	90-105	4.54	Loss of four water	4.48
	145-180	22.58	Loss of two 3-np	21.78
	230-300	54.83	Loss of one L	51.79
	370-650	89.51	Formation of Fe_2O_3	90.06
Complex **4.3**	75-90	2.40	Loss of two water	2.29
	150-170	21.29	Loss of two 4-np	19.99
	220-300	51.85	Loss of one L	50.68
	395-610	89.72	Formation of Fe_2O_3	89.83
Complex **4.4**	80-100	11.21	Loss of ten water	11.63
	125-175	19.51	Loss of one 1,4-dhb	18.74
	190-255	51.21	Loss of one L	49.91
	340-600	90.24	Formation of Fe_2O_3	89.67
Complex **4.5**	85-95	4.86	Loss of four water	4.55
	200-240	20.29	Loss of two 1,3,5,-thb	20.49
	250-305	51.37	Loss of one L	50.99
	400-670	90.48	Formation of Fe_2O_3	89.89

The emission decay profiles of the complexes were determined (Figure 4.22–4.31). In solid state, the complex **4.1** shows a bi-exponential decay profile with life-times of 0.928 ns (95.98%) and 9.656 ns (4.02%), showing a predominance of the shorter life-time. The inclusion complexes show bi-exponential paths having a short and a relatively longer life-

time similar to the parent complex but the percentage of the species with the longer-life time increases drastically (35%–45%). The emission life-time decay profiles in water of complex **4.1** in the presence of phenolic compounds are substrate dependent, suggesting that the mechanistic paths of emissions in solution and solid are different.

4.7: Conformation of the cation

The cation derived from N,N'-bis(3-imidazol-1-yl-propyl)naphthalenediimide has two flexible arms comprised of $(-CH_2-)_3$ units. These flexible arms are organized in different manner to adopt different orientations which are shown in Figure 4.10a. The differences in the orientations of the imidazole-containing tethers are shown by keeping the naphthalenediimide ring in the same plane. A quantitative differentiation through identified torsion angles is listed in Table 4.4, showing that both the flexible arms of the cation are oriented identically across the naphthalenediimide ring.

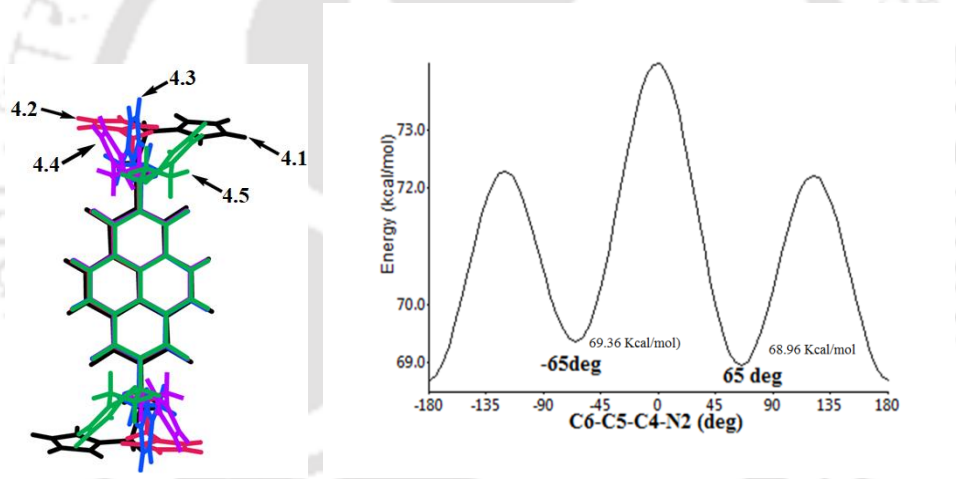

(a) (b)

Figure 4.10: (a) Overlaid diagram of cations in each complex showing the orientation of the cation in complexes **4.1-4.5** and (b) Karplus plot for the torsion angle C6-C5-C4-N2.

Table 4.4: Torsion angles of the cation in complexes **4.1**-**4.5**.

H_2L^+	Torsion angle (°)	**4.1**	**4.2**	**4.3**	**4.4**	**4.5**
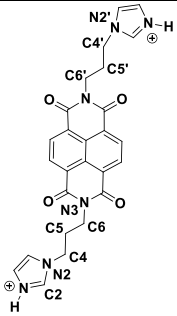	C6-C5-C4-N2	66.5(4)	174.8(3)	177.8(3)	177.3(2)	178.6(4)
	C6'-C5'-C4'-N2'	-66.5(4)	-174.8(3)	-177.8(3)	-177.3(2)	-178.6(4)
	C2-N2-C4-C5	-72.2(5)	-82.2(5)	72.3(5)	-90.6(3)	-81.0(7)
	N3-C6-C5-C4	-160.9(3)	-176.3(3)	-72.8(4)	59.9(3)	55.7(6)

In general, there can be infinite numbers of arrangements through C-C bond rotation but the conformation is defined as the one in which the energy maxima and minima are observed from a particular torsional angle in the domain of +180˚ to -180˚ rotation. Each torsion angle listed in Table 4.4 has its own characteristic Karplus plot to show maxima and minima. The energy profiles for these torsion angles have been evaluated by MM2 calculations and one representative case is shown in Figure 4.10b. The figure also suggests that the minima are at ± 65 ˚and ± 180˚ for the torsion angle C6-C5-C4-N2 whereas the maxima are at 0˚ and ± 135˚. The observed C6-C5-C4-N2 torsion of complex **4.1** is close to the second lowest minima in the Karplus plot; whereas in the other inclusion complexes these are close to the lowest energy. The Karplus plot of C2-N2-C4-C5 (Figure 4.20) has minima at 90˚. The complexes **4.2**, **4.4** and **4.5** have this torsion angles at -82.2˚, -90.6˚ and -81.0˚ respectively, which are close to the lowest energy. The torsion angle C2-N2-C4-C5 is of similar magnitude in complexes **4.1** and **4.3** (approximately ±72˚). In the event that such differences from the lower energy conformers are observed they are referred to as conformational adjustment.[19] similarly, the two minimum energies of the N3-C6-C5-C4 torsion (Figure 4.21) are at ± 65˚ and ± 180˚. However, the observed torsional angles show deviations from the one with minimum. Complexes **4.1** and **4.2** have the respective value away from energy minimum found in the Karplus plots. The complex **4.3** has this angle at -72.8˚ which differs by -7.8 ˚ from the -65˚ which is the second lowest energy conformer whereas in the case of complexes **4.4** and **4.5** conformational adjustments[21] away from the second lowest minimum by 5.1˚ and 9.3˚ took place. These analyses have suggested that there are changes in the orientations of the imidazole rings with respect to the naphthalenediimide unit in the inclusion complexes correspond to complex **4.1**. The obvious reasons for the differences are that different hydroxyaromatics are participating in the self-assemblies. It is also an established fact that

long flexible chains help in efficient quenching of emission in conjugate polymers.[22] Though it is not possible to decide the direct effects of the torsion on the overall fluorescence quenching process, the flexible arms direct the orientations of the imidazolium parts in each case (Figure 4.10a), these differences guiding the overall packing of molecules in solid state, hence are reflected in observed fluorescence emission of solid samples discussed earlier part of this chapter.

4.8: Conclusions

The complex **4.1** is a water soluble and fluorescent complex. It provides a means to detect and remove phenolic compounds from aqueous solution. Though the cationic part of the complex alone plays the major role in detection and formation of the inclusion complexes; the advantage of the use of this complex is the possibility of it being used as a model complex that has concealed a paramagnetic iron (+3) due to chelation by 2,6-pyridinedicarboxylate to avoid the quenching caused by the paramagnetic iron (+3) ions. The complex is formed under ambient condition from a reaction of ferric salt with 2,6 pyridinedicarboxylic acid. The large size of the cation in the complex also reduces the stacking among the cations and anions to decrease the effects from Dexter quenching, thereby giving a better sensitivity of the probe. It also stabilizes the cationic form of the receptor, influencing the photo-induced electron transfer to generate a fluorescence ON state suitable to detect phenolic compounds through emission quenching. In water, the cationic part of the complex interacts with phenolic compounds to show Dexter quenching, hence the quenching effect is useful in the detection of various hydroxyaromatics through emission quenching in a superlative manner. The detection shown in aqueous solution by complex **4.1** is better than that of commonly reported inorganic complexes and receptors of small molecules.[23] The method of preparation of complex **4.1** provides a logical means to have iron ions trapped from a solution. In the solid-state, the inclusion complexes of **4.1** with hydroxy-aromatics are non-emissive. They have the naphthalenediimide bearing dications either placed horizontally or laterally in between layer-like arrangements of the anions depending on the included hydroxyaromatic guest. A new example of inclusion complex having anion and a portion of cation forming layer-like arrangements to hold 3-nitrophenol guest molecules is demonstrated. The crystallization of iron and phenolic compounds together from solution in the form of inclusion complexes forecast to develop an appropriate means for an integrated process for the removal and detection of hydroxyaromatics from iron (+3) ion containing water.

4.9: Experimental section

The compound N,N'-bis(3-imidazol-1-ylpropyl)naphthalenediimide **(L)** was prepared by a reported procedure.[10]

$(H_2L)[Fe(pdc)_2]_2.8(H_2O)$ (**4.1)**: To a solution of 2,6-pyridinedicarboxylic acid (0.167 g, 1.0 mmol) in methanol (10 ml), a solution of anhydrous ferric chloride (0.053 g, 0.33 mmol) in methanol (10 ml) was added. A brown precipitate was obtained after stirring for half an hour. The precipitate was dissolved by adding 10 ml water. To this solution, N,N'-bis(3-imidazol-1-yl-propyl)naphthalenediimide (0.241g, 0.5 mmol) was added. The reaction mixture was stirred for 2 hrs at room temperature to obtain homogenous solution. The solution, on standing at room temperature for 5 days, resulted in the formation of crystals of complex **4.1**.

Synthesis of inclusion complexes:

Complexes **4.2, 4.3** and **4.5** were prepared by independently adding respective methanol solution (2 mmol in each case, 5 mL) of the hydroxyaromatic namely 3-nitrophenol, 4-nitrophenol, or 1,3,5-trihydroxybenzene to an aqueous solution of the complex **4.1** (1 mmol, 5 mL). The corresponding solution was allowed to stand in air, resulting in crystallization of the respective inclusion complex in 5-6 days. The complexe **4.4** was obtained by similar procedure using 1 mmol of 1,4-dihydroxybenzene and complex **4.1**.

Spectroscopic data of the complexes:

Complex **4.1:** Isolated yield 73 %. Elemental anal. calcd. For, $C_{54}H_{52}Fe_2N_{10}O_{28}$: C 46.30, H 3.74, N 10.00; found C 46.33, H 3.73, N 9.83. IR (KBr, cm^{-1}): 3412 (br), 3086 (s), 3048 (m), 1661 (s), 1585 (w), 1429 (m), 1330 (s), 1246 (s), 1168 (s), 1081 (s), 1026 (w), 970 (w), 912 (s), 861 (w), 823 (w), 774 (s), 745 (s), 690 (s), 635 (m), 439 (m), 415 (m). Magnetic moment (28 °C): 5.72 BM.

Complex **4.2:** Isolated yield 64%. Elemental anal. calcd. for $C_{66}H_{54}Fe_2N_{12}O_{30}$ (1606.91): C, 49.28; H, 3.36; N, 10.45; found C, 49.12, H 3.46, N, 10.66. IR (KBr, cm^{-1}): 3403 (br), 3141 (m), 1703 (m), 1650 (s), 1580 (m), 1526 (s), 1458 (m), 1428 (w), 1348 (s), 1304 (w), 1246 (s), 1172 (s), 1078 (s), 917 (m), 917 (m), 880 (s), 813 (s), 741 (s), 675 (s), 625 (m), 586 (m), 440 (s). Magnetic moment (28 °C): 5.47 BM.

Complex **4.3:** Isolated yield 60%. Elemental anal. calcd. for $C_{66}H_{50}Fe_2N_{12}O_{28}$ (1570.88): C 50.41, H, 3.18, N 10.69; found C, 50.78; H, 3.19; N 10.91. IR (KBr, cm^{-1}): 3414 (br), 3147 (m), 3086 (m), 1665 (s), 1585 (s), 1513 (w), 1493 (w), 1455 (m), 1330 (s), 1292 (s), 1248 (s),

1169 (s), 1111 (s), 1074 (s), 1031 (w), 915 (s), 856 (s), 811 (w), 768 (s), 741 (s), 681 (s), 632 (m), 591 (m), 539 (w), 500 (w), 437 (s), 418 (w). Magnetic moment (28 °C): 5.38 BM.

Complex **4.4:** Isolated yield 61%. Elemental anal. calcd.for $C_{60}H_{62}Fe_2N_{10}O_{32}$ (1546.89): C, 46.54; H, 4.00; N, 9.05; found C 46.93; H 4.07; N 9.32. IR (KBr, cm^{-1}): 3418 (br), 3087 (s), 3049 (m), 1658 (s), 1582 (w), 1547 (w), 1511 (m), 1472 (w), 1457 (w), 1428 (m), 1333 (s), 1246 (s), 1169 (s), 1082 (s), 1057 (w), 1029 (w), 971 (w), 913 (s), 861 (w), 826 (w), 767 (s), 745 (s), 680 (s), 590 (w), 440 (s), 416 (w). Magnetic moment (28 °C): 5.88 BM.

Complex **4.5:** Isolated yield 68%. Elemental anal. $C_{66}H_{56}Fe_2N_{10}O_{30}$ (1580.90): calcd. C 50.09, H 3.54, N 8.85; found C, 50.32; H, 3.42; N, 8.50. IR (KBr, cm^{-1}): 3426 (br), 3146 (m), 1702 (w), 1649 (s), 1534 (w), 1492 (s), 1456 (w), 1427 (m), 1336 (s), 1254 (w), 1154 (s), 1074 (s), 1032 (w), 1006 (w), 918 (s), 830 (s), 742 (s), 682 (s), 630 (m), 594 (m), 540 (w), 437 (w). Magnetic moment (28 °C): 5.97 BM.

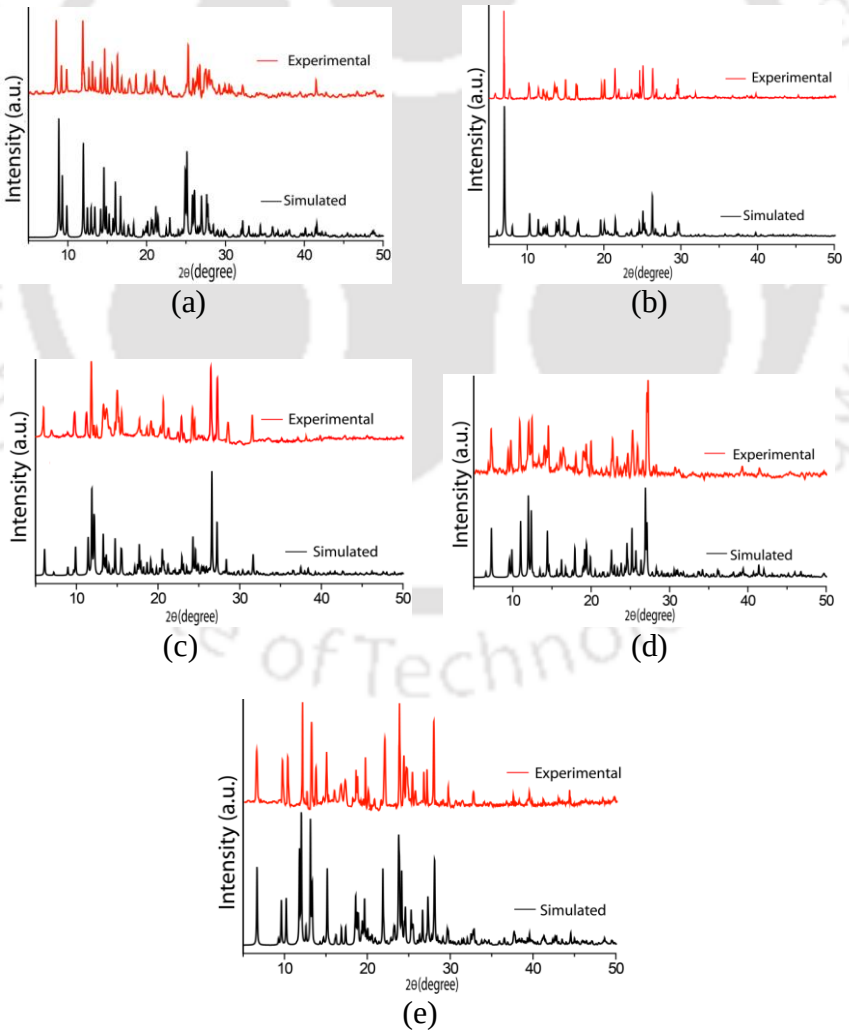

Figure 4.11: PXRD pattern of complexes (a) **4.1**, (b) **4.2**, (c) **4.3**, (d) **4.4** and (e) **4.5** (Red = Experimental, Black = Simulated). Simulated pattern generated from CIF file.

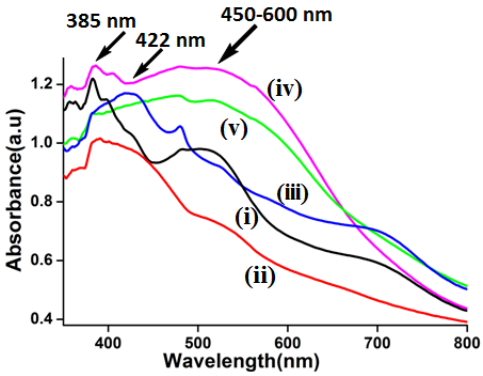

Figure 4.12: Solid state UV-Visible spectra of complexes (i) **4.1**, (ii) **4.2**, (iii) **4.3**, (iv) **4.4** and (v) **4.5**.

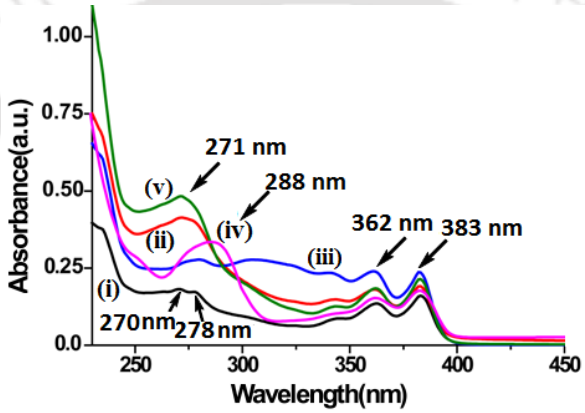

Figure 4.13: (a) UV-spectra of the solution of complex (i) **4.1**, (ii) **4.2**, (iii) **4.3**, (iv) **4.4** and (v) **4.5** (10^{-5} M in water).

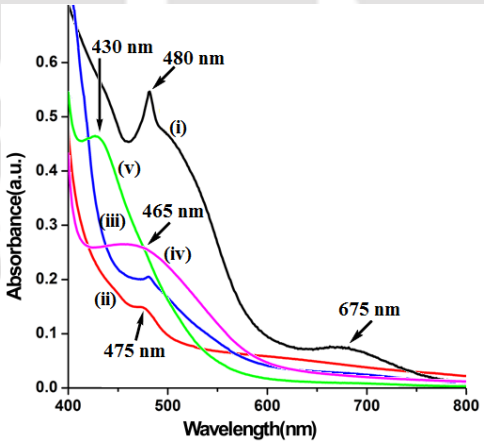

Figure 4.14: Visible spectra of the solution of complexes (i) **4.1**, (ii) **4.2**, (iii) **4.3**, (iv) **4.4** and (v) **4.5** (10^{-4} M in water).

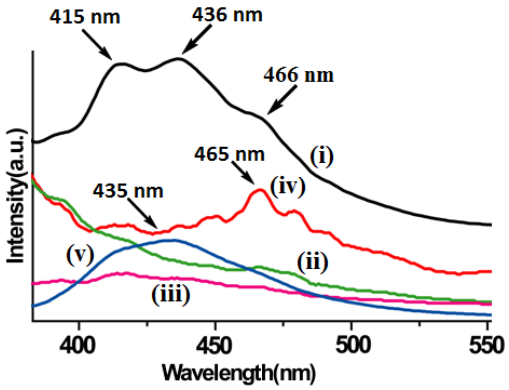

Figure 4.15: Fluorescence emission spectra of solid sample of complexes (i) **4.1**, (ii) **4.2**, (iii) **4.3**, (iv) **4.4** and (v) **4.5** (λ_{ex} = 350 nm).

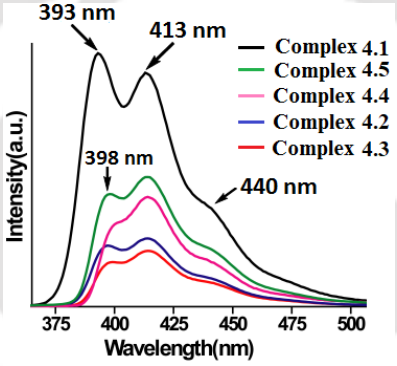

Figure 4.16: Fluorescence emission spectra of complexes **4.1-4.5** (λ_{ex} = 340 nm; 10^{-5} M in water).

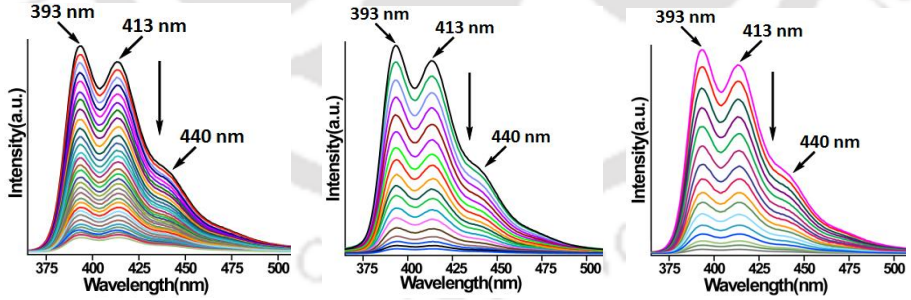

(a) (b) (c)

Figure 4.17: Fluorescence spectroscopic titration (λ_{ex} =340 nm) of complex **4.1** (10^{-5} M in water) with (a) 3-NP, (b) 2,4-DNP and (c) 2,4,6-TNP (10^{-5} M in water, 10 µL in each aliquot).

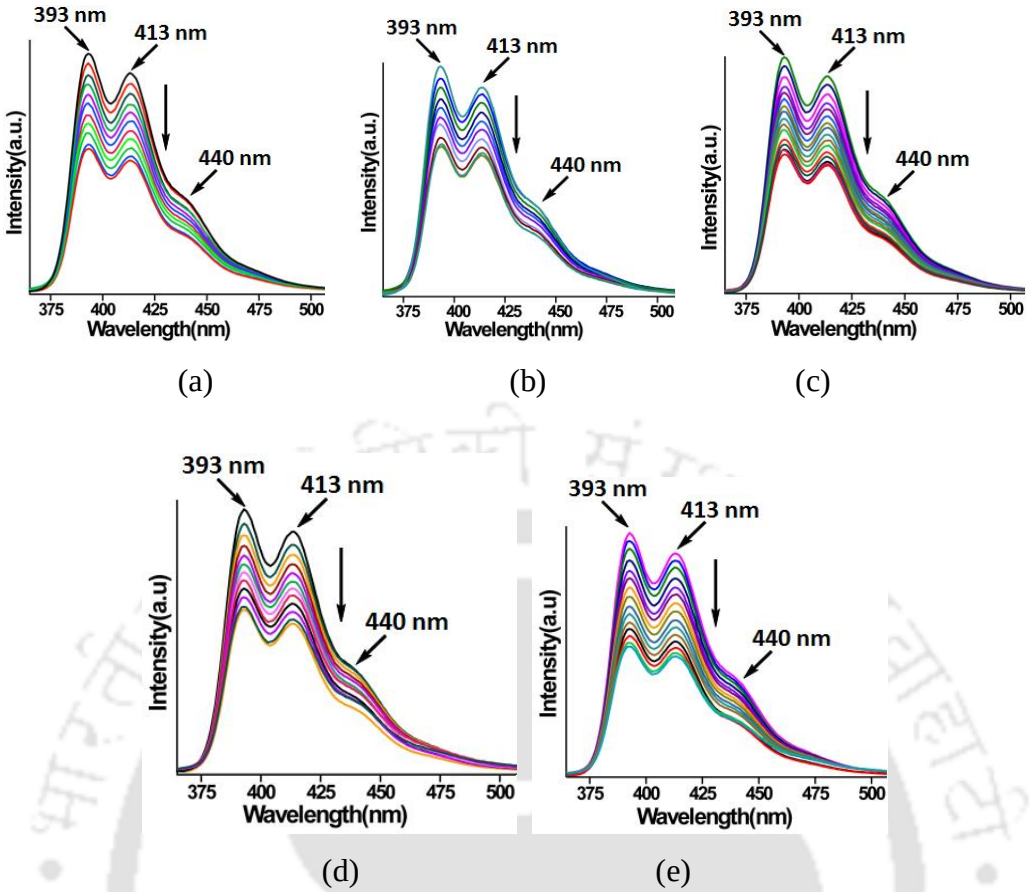

Figure 4.18: Fluorescence spectroscopic titration (λ_{ex} =340 nm) of complex **4.1** (10^{-5} M in water) with (a) 1,2-DHB, (b) 1,3-DHB, (c) 1,4-DHB, (d) 1,2,3-THB and (e) 1,3,5-THB (10^{-5} M in water, 10 µL in each aliquot).

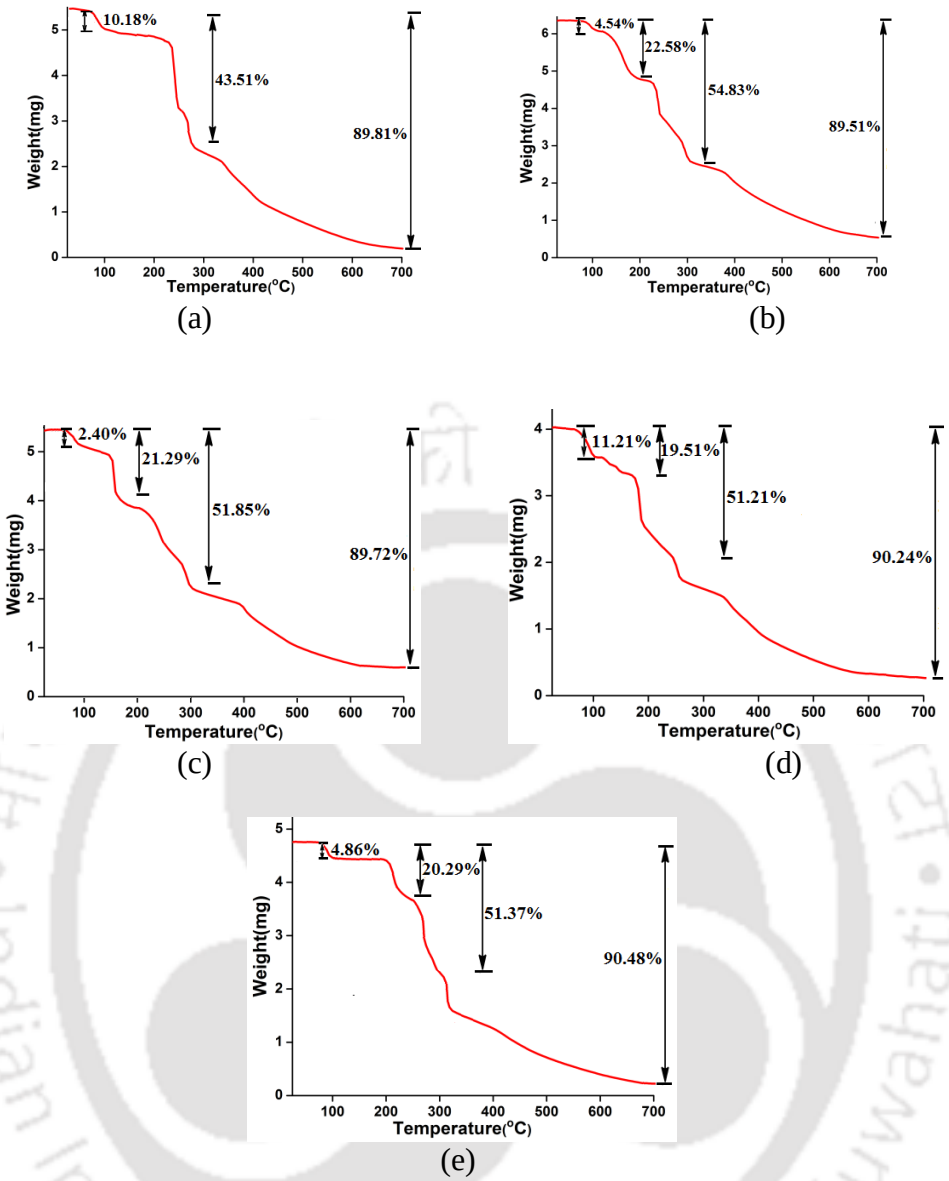

Figure 4.19: Thermogram of the complexes (a) **4.1**, (b) **4.2**, (c) **4.3**, (d) **4.4** and (e) **4.5** (heating rate 5 °C/min).

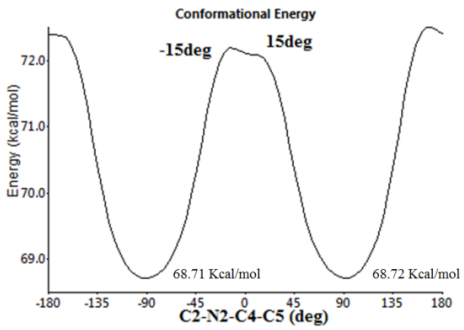

Figure 4.20: Karplus plot of torsion C2-N2-C4-C5 of **L**.

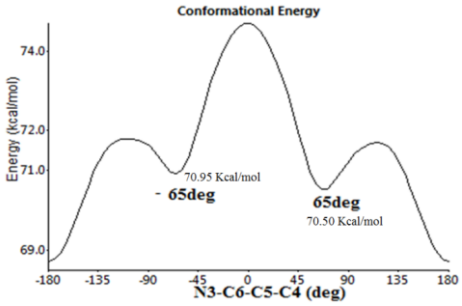

Figure 4.21: Karplus plot of torsion N3-C6-C5-C4 of **L**.

Table 4.5: Hydrogen bond parameters of the complexes.

Complex	D-H···A	d_{D-H} (Å)	$d_{H\cdots A}$ (Å)	$d_{D\cdots A}$ (Å)	∠D-H···A (º)
Complex 4.1	N(1)-H(1N)···O(14) [1-x,1/2+y,1/2-z]	0.86(4)	2.03 (2)	2.823(12)	153(2)
	N(1)-H(1N)···O(13) [1-x,1-y,-z]	0.86(3)	2.07(5)	2.794(9)	142(2)
	O(11)-H(11A)···O(7)) [x, y, z]	0.85(3)	2.45 (3)	2.837(7)	109(4)
	O(12)-H(12A)···O(13) [1-x,1/2+y,1/2-z]	0.91(2)	2.45(3)	3.119(12)	131(3)
	O(13)-H(13A)···O(12) [1-x,-1/2+y,1/2-z]	0.85(6)	2.35(3)	3.119(12)	150(4)
	O(13)-H(13A)···N(1) [1-x,1-y,-z]	0.85(5)	2.52(3)	2.794(9)	100(3)
	O(13)-H(13B)···O(4) [x, y, z]	0.85(2)	2.25(4)	2.755(11)	118(3)
	O(14)-H(14A)···O(4) [x, y, z]	0.85(5)	2.26(2)	2.831(9)	124(5)
	O(14)-H(14A)···N(1) [x, y, z]	0.85(5)	2.50(2)	3.207(10)	142(5)
	O(14)-H(14B)··· O(7) [x, y, z]	0.85(5)	2.55(4)	3.338(11)	154(2)
	O(14)-H(14B)··· O(11) [x, y, z]	0.85(3)	2.32(3)	2.732(9)	110(4)
	C(2)-H(2)···O(5) [1-x,1-y,1-z]	0.93(5)	2.46(2)	3.259(7)	144(5)
	C(3)-H(3)···O(8) [x, y, z]	0.93(5)	2.54(4)	3.345(5)	145(3)
	C(4)-H(4B)···O(10) [x,1/2-y,-1/2+z]	0.97(4)	2.55(3)	3.449(5)	154(5)
	C(6)-H(6A)···N(2) [x, y, z]	0.97(5)	2.58(2)	3.008(5)	107(4)
	C(6)-H(6B)···O(1) [x, y, z]	0.97(3)	2.37(4)	2.722(6)	101(2)
	C(17)-H(17)···O(2) [1-x,-1/2+y,1/2-z]	0.93(5)	2.52(4)	3.279(6)	139(4)
	C(23)-H(23)···O(10) [-x,1/2+y,1/2-z]	0.93(5)	2.49(4)	3.297(5)	145(5)
	C(24)-H(24)···O(12) [-x,-1/2+y,1/2-z]	0.93(2)	2.46(2)	3.350(10)	160(5)
	C(25)-H(25)···O(9) [-x,-1/2+y,1/2-z]	0.93(5)	2.46(4)	3.227(5)	140(2)
Complex 4.2	N(1)-H(1N)···O(10) [2-x,1-y,1-z]	0.84(4)	2.09(4)	2.764(5)	136(4)
	O(11)-H(11)···O(9) [1+x,1+y,z]	0.82(5)	1.95(4)	2.652(5)	143(4)
	O(14)-H(14B)···O(7)[1+x,y,z]	0.85(4)	2.08(4)	2.785(11)	140(5)
	O(15)-H(15A)···O(14)[x, y, z]	0.85(4)	2.25(4)	2.806(17)	123(4)
	C(3)-H(3)···O(2)[1-x,1-y,-z]	0.93(5)	2.40(5)	3.070(5)	129(5)
	C(4)-H(4A)···O(14)[x, y, z]	0.97(5)	2.46(2)	3.380(12)	158(2)
	C(5)-H(5B)···O(5) [x, y, z]	0.97(4)	2.46(3)	3.416(6)	169(4)
	C(6)-H(6B)···O(1) [x, y, z]	0.97(5)	2.32(2)	2.714(5)	103(2)
	C(10)-H(10)···O(11)[-1+x,-1+y,z]	0.93(3)	2.54(5)	3.149(6)	123(5)
	C(16)-H(16)···O(4)[2-x,-y,-z]	0.93(5)	2.45(2)	3.216(5)	139(5)
	C(23)-H(23)···O(3)[2-x,-y,1-z]	0.93(3)	2.52(2)	3.186(5)	129(4)
	C(24)-H(24)···O(1)[1-x,-y,1-z]	0.93(3)	2.38(4)	3.280(6)	162(5)
	C(25)-H(25)···O(6)[1-x,-y,1-z]	0.93(4)	2.59(2)	3.397(6)	146(4)
Complex 4.3	N(1)-H(1N)···O(14) [2-x,1-y,-z]	0.86(4)	2.04 (4)	2.774(5)	142(3)
	O(11)-H(11)···O(9)[1-x,1-y,1-z]	0.82(4)	1.85(3)	2.664(4)	173(4)
	O(14)-H(14A)···O(10)[1+x,y,z]	0.85(3)	2.05(3)	2.858(4)	159(5)
	O(14)-H(14B)···O(5) [x, y, z]	0.85(4)	1.92(5)	2.771(4)	176(3)
	C(1)-H(1)···O(12)[1-x,1-y,-z]	0.93(3)	2.59(4)	3.404(6)	146(3)
	C(4)-H(4A)···O(4)[1-x,1-y,1-z]	0.97(3)	2.47(4)	3.170(5)	129(4)
	C(6)-H(6A)···O(1) [x, y, z]	0.97(3)	2.34(3)	2.717(5)	102(4)
	C(6)-H(6B)···O(5)[x,1+y,z]	0.97(3)	2.47(3)	3.377(5)	156(4)
	C(9)-H(9)···O(10)[1+x,y,z]	0.93(4)	2.58(4)	3.446(5)	154(3)
	C(10-H(10)···O(14) [x, y, z]	0.93(3)	2.43(5)	3.287(5)	154(4)
	C(23)-H(23)···O(1)[-1+x,y,z]	0.93(3)	2.38(3)	3.263(5)	159(3)
	C(29)-H(29)···O(9)[1-x,1-y,1-z]	0.93(5)	2.51(3)	3.182(4)	130(3)

	C(32)-H(32)···O(12)[-x,1-y,-z]	0.93(3)	2.48(5)	3.375(5)	162(5)
Complex 4.4	N(1)-H(1N)···O(13)[1+x,y,z]	0.86(4)	2.08(3)	2.863(4)	150(3)
	N(1)-H(1N)···O(4)[2-x,1-y,1-z]	0.86(4)	2.52(4)	2.945(4)	111(3)
	O(11)-H(11)···O(16) [x, y, z]	0.82(4)	1.90(3)	2.718(5)	173(5)
	O(12)-H(12A)···O(10)[-1+x,y,z]	0.85(3)	2.44(4)	3.189(4)	148(3)
	O(12)-H(12B)···O(6) [x, y, z]	0.85(3)	2.10(4)	2.909(3)	159(3)
	O(13)-H(13A)···O(1) [x, y, z]	0.85(3)	1.99(4)	2.824(3)	169(3)
	O(13)-H(13B)···O(5) [x, y, z]	0.85(4)	1.98(4)	2.827(3)	171(4)
	O(14)-H(14A)···O(15) [x, y, z]	0.85(6)	1.94(4)	2.779(4)	168(4)
	O(14)-H(14B)···O(9) [x, y, z]	0.85(4)	2.02(5)	2.858(4)	171(4)
	O(15)-H(15A)···O(3)[-1+x,y,z]	0.85(5)	2.14(4)	2.921(4)	153(4)
	O(15)-H(15A)···O(4)[-1+x,y,z]	0.85(4)	2.46(5)	3.157(4)	140(4)
	O(15)-H(15B)···O(2)[-1+x,1+y,z]	0.85(5)	2.06(5)	2.856(3)	156(5)
	O(16)-H(16A)···O(9)[1-x,1-y,-z]	0.79(4)	2.19(4)	2.944(4)	161(4)
	O(16)-H(16B)···O(12) [x, y, z]	0.85(5)	1.97(5)	2.800(4)	166(4)
	C(2)-H(2)···O(4)[2-x,1-y,1-z]	0.93(5)	2.56(5)	2.972(4)	107(5)
	C(3)-H(3)···O(1)[1-x,-y,1-z]	0.93(5)	2.41(4)	3.336(3)	177(4)
	C(6)-H(6A)···O(1) [x, y, z]	0.97(4)	2.37(4)	2.707(3)	100(4)
	C(9)-H(9)···O(10)[-1+x,y,z]	0.93(4)	2.48(5)	3.085(4)	123(5)
	C(10)-H(10)···O(10)[-1+x,y,z]	0.93(5)	2.51(4)	3.097(4)	121(4)
	C(25)-H(25)···O(12)[1-x,1-y,-z]	0.93(5)	2.51(5)	3.378(4)	155(5)
Complex 4.5	N(1)-H(1N)···O(15)[x,1+y,z]	0.95(5)	1.81(5)	2.727(5)	161(4)
	O(11)-H(11)···O(5)[-1+x,y,z]	0.82(4)	1.89(5)	2.707(4)	174(5)
	O(12)-H(12)···O(1)[1-x,1-y,-z]	0.82(4)	2.04(4)	2.859(4)	173(5)
	O(13)-H(13)···O(4)[-x,1-y,-z]	0.82(7)	1.85(5)	2.658(4)	167(4)
	O(14)-H(14A)···O(10)[1+x,y,z]	0.85(4)	2.00(4)	2.812(7)	160(5)
	O(14)-H(14B)···O(11) [1+x,y,z]	0.85(5)	2.08(4)	2.906(5)	164(4)
	O(15)-H(15A)···O(13)[x,y,1+z]	0.85(5)	2.03(4)	2.839(4)	158(4)
	O(15)-H(15B)···O(9)[1-x,1-y,1-z]	0.74(4)	1.99(4)	2.695(5)	159(4)
	C(1)-H(1)···O(2)[-x,2-y,1-z]	0.93(7)	2.47(7)	2.992(5)	115(5)
	C(1)-H(1)···O(14)[1-x,1-y,1-z]	0.93(7)	2.31(7)	3.148(7)	150(7)
	C(6)-H(6A)···O(2) [x, y, z]	0.97(5)	2.35(5)	2.697(5)	100(5)
	C(9)-H(9)···O(12)[1-x,1-y,-z]	0.93(5)	2.60(3)	3.481(4)	159(5)
	C(18)-H(18)···O(1)[1-x,1-y,-z]	0.93(7)	2.57(5)	3.270(4)	132(7)
	C(33)-H(33)···O(5)[-1+x,y,z]	0.93(5)	2.56(4)	3.214(4)	128(5)

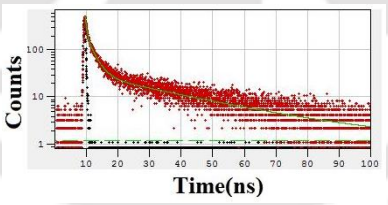

Fitting range : [375; 4096] channels

χ^2 : 1.173

	B_i	ΔB_i	f_i (%)	Δf_i (%)	τ_i (ns)	$\Delta\tau_i$ (ns)
1	0.0676	0.0027	17.733	10.000	0.346	0.181
2	0.0171	0.0005	31.381	1.015	2.423	0.010
3	0.0023	4.2e-5	50.886	0.929	8.902	0.001

Shift : -0.178 ns (± 1.293 ns)

Decay Background : 1.114 (± 0.197)

IRF background : 0

Figure 4.22: Time resolved fluorescence emission decay profile of complex **4.1** (10^{-5} M in water) (λ_{ex} = 336 nm).

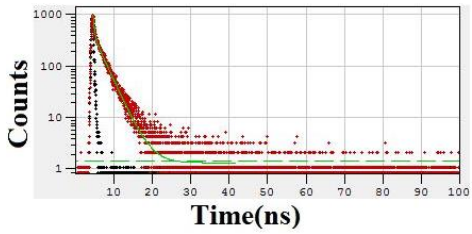

Fitting range : [168; 1700] channels

χ^2 : 1.054

	B_i	ΔB_i	f_i (%)	Δf_i (%)	τ_i (ns)	$\Delta\tau_i$ (ns)
1	676.2199	11.6268	16.063	4.299	0.317	0.079
2	422.9228	3.9702	83.937	0.862	2.650	0.002

Shift : 0 ns (± 0 ns)

Decay Background : 1.342 (± 0.070)

Figure 4.23: Time resolved fluorescence emission decay profile of complex **4.2** (10^{-5} M in water) (λ_{ex} = 336 nm).

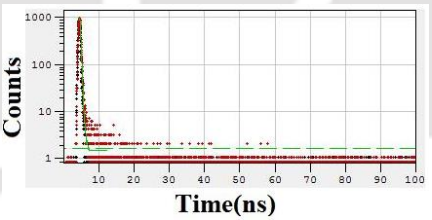

Fitting range : [167; 500] channels

χ^2 : 1.024

	B_i	ΔB_i	f_i (%)	Δf_i (%)	τ_i (ns)	$\Delta\tau_i$ (ns)
1	0.1805	0.0026	100.000	56.612	0.173	0.096

Shift : -0.068 ns (± 0.246 ns)

Decay Background : 1.525 (± 0.109)

IRF background : 0

Figure 4.24: Time resolved fluorescence emission decay profile of complex **4.3** (10^{-5} M in water) (λ_{ex} = 336 nm).

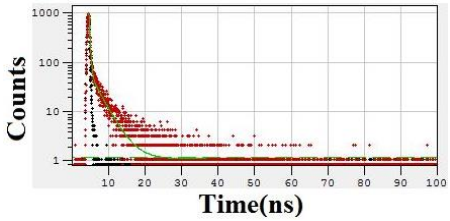

Fitting range : [170; 1500] channels

χ^2 : 1.018

	B_i	ΔB_i	f_i (%)	Δf_i (%)	τ_i (ns)	$\Delta\tau_i$ (ns)
1	1104.9050	10.4951	60.096	9.022	0.267	0.038
2	63.8561	1.4741	39.904	1.004	3.065	0.006

Shift : 0 ns (± 0 ns)

Decay Background : 1.121 (± 0.071)

Figure 4.25: Time resolved fluorescence emission decay profile of complex **4.4** (10^{-5} M in water) (λ_{ex} = 336 nm).

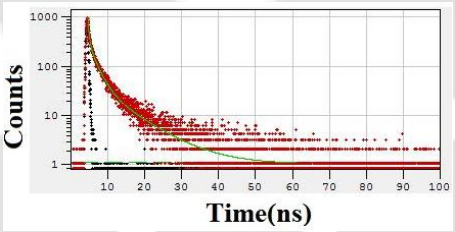

Fitting range : [170; 2500] channels

χ^2 : 1.009

	B_i	ΔB_i	f_i (%)	Δf_i (%)	τ_i (ns)	$\Delta\tau_i$ (ns)
1	780.2767	11.0217	19.639	5.421	0.300	0.079
2	284.5071	5.4440	47.713	1.227	1.999	0.013
3	46.5541	3.0052	32.648	2.125	8.359	0.005

Shift : 0 ns (± 0 ns)

Decay Background : 1.065 (± 0.081)

Figure 4.26: Time resolved fluorescence emission decay profile of complex **4.5** (10^{-5} M in water) (λ_{ex} = 336 nm).

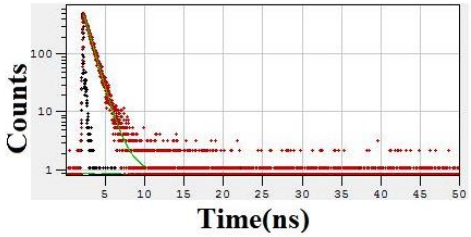

Fitting range : [164; 800] channels

χ^2 : 1.067

	B i	ΔB i	f i (%)	Δf i (%)	τ i (ns)	Δτ i (ns)
1	0.1142	0.0051	95.984	7.350	0.928	0.030
2	0.0005	0.0019	4.016	17.420	9.656	1.870

Shift : -0.337 ns (± 3.868 ns)

Decay Background : -0.193 (± 22.061)

Figure 4.27: Time resolved fluorescence emission decay profile of solid sample of complex **4.1** (λ_{ex} = 336 nm).

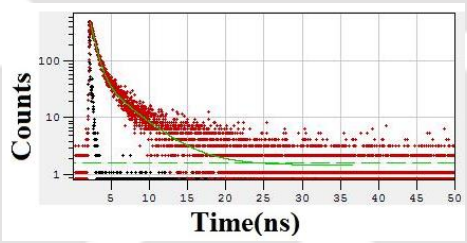

Fitting range : [166; 3000] channels

χ^2 : 1.069

	B_i	ΔB_i	f_i (%)	Δf_i (%)	τ_i (ns)	$\Delta\tau_i$ (ns)
1	434.2183	3.2015	57.116	1.910	0.658	0.017
2	58.4391	1.7277	42.884	1.331	3.674	0.005

Shift : 0 ns (± 0 ns)

Decay Background : 1.481 (± 0.052)

Figure 4.28: Time resolved fluorescence emission decay profile of solid sample of complex **4.2** (λ_{ex} = 336 nm).

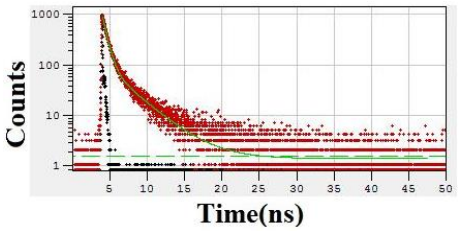

Fitting range : [311; 3900] channels

χ^2 : 1.001

	B_i	ΔB_i	f_i (%)	Δf_i (%)	τ_i (ns)	$\Delta\tau_i$ (ns)
1	852.6022	4.3487	59.880	1.555	0.591	0.012
2	99.1604	1.9144	40.120	0.817	3.405	0.004

Shift : 0 ns (± 0 ns)

Decay Background : 1.429 (± 0.040)

Figure 4.29: Time resolved fluorescence emission decay profile of solid sample of complex **4.3** (λ_{ex} = 336 nm).

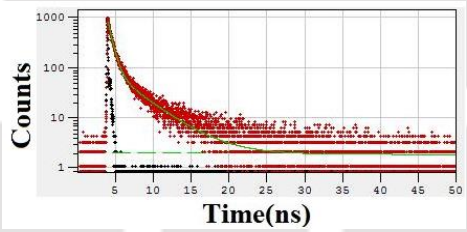

Fitting range : [310; 4096] channels

χ^2 : 1.210

	B_i	ΔB_i	f_i (%)	Δf_i (%)	τ_i (ns)	$\Delta\tau_i$ (ns)
1	770.2178	4.6228	57.531	1.712	0.589	0.014
2	88.0027	1.7267	42.469	0.872	3.806	0.003

Shift : 0 ns (± 0 ns)

Decay Background : 1.881 (± 0.045)

Figure 4.30: Time resolved fluorescence emission decay profile of solid sample of complex **4.4** (λ_{ex} = 336 nm).

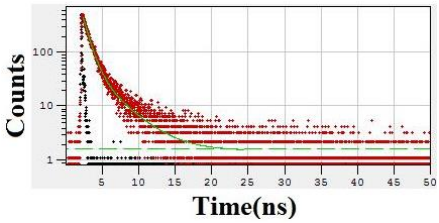

Fitting range : [177; 2000] channels

χ^2 : 1.082

	B_i	ΔB_i	f_i (%)	Δf_i (%)	τ_i (ns)	$\Delta\tau_i$ (ns)
1	387.1915	3.7578	64.871	2.081	0.838	0.019
2	53.9503	3.7047	35.129	2.545	3.258	0.012

Shift : 0 ns (± 0 ns)

Decay Background : 1.510 (± 0.098)

Figure 4.31: Time resolved fluorescence emission decay profile of solid sample of complex **4.5** (λ_{ex} = 336 nm).

4.10: References

1. (a) S. Singh, *J. Hazard. Mater.*, 2007 **144** 15-28; (b) C. Vorbeck, H. Lenke, P. Fischer, H. J. Knackmuss, *J. Bacteriol*, 1994 , **176**, 932-934.

2. S. J. Kulkarni, J. P. Kaware, *Int. J. Sci. Res. Publ*, 2013, **3**, 1-4.

3. (a) N. Venkatramaiah, S. Kumar, S. Patil, *Chem. Commun.*, 2012, **48**, 5007-5009; (b) S. Shanmugaraju, P. S. Mukherjee, *Chem. Commun.*, 2015, **51**, 16014-16032; (c) S. Shanmugaraju, S. A. Joshi, P. S. Mukherjee, *J. Mater. Chem.*, 2011, **21**, 9130-9138; (d) X. Sun, Y. Wang, Y. Lei, *Chem. Soc. Rev.*, 2015, **44**, 8019-8061.

4. (a) S. S. Nagarkar, B. Joarder, A. K. Chaudhari, S. Mukherjee, S. K. Ghosh, *Angew. Chem. Int. Ed.*, 2013, **52**, 2881-2885; (b) X. -G. Liu, C. -L. Tao, H. -Q. Yu, B. Chen, Z. Liu, G. -P Zhu, Z. Zhao, L. Shen, B. Z. Tang, *J. Mater. Chem. C.*, 2018, **6**, 2983-2988; (c) S. S. Nagarkar, A. V. Desai, P. Samanta, S. K. Ghosh, *Dalton Trans.*, 2015, **44**, 15175-15180; (d) T. Xia, F. Zhu, Y. Cui, Y. Yang, Z. Wang, G. Qian, *Journal of Solid State Chemistry.*, 2017, **245**, 127-131128; (e) H. -H. Yu, J. -Q. Chi, Z. -M. Su, X. Li, J. Sun, C. Zhou, X. -L. Hu, Q, Liu, *CrystEngComm*, 2020, **22**, 3638-3643; (f) S. Senthilkumar, R. Goswami, N. L. Obasi, S. Neogi, *ACS Sustainable Chem. Eng.*, 2017, **5**, 11307-11315.

5. (a) A. Kumar, A. Kumar, D. S. Pandey, *Dalton Trans.*, 2016, **45**, 8475-8484; (b) A. Das, S. Jana, A. Ghosh, *Cryst. Growth Des.*, 2018, **18**, 2335-2348.

6. (a) K. Shankar, J. B. Baruah, *ChemistrySelect*., 2016, **1**, 5152-5158; (b) K. Shankar, M. P. Singh, J. B. Baruah, *Inorg. Chim. Acta*., 2018, **469**, 440-446; (c) K. Shankar, J. B. Baruah, *Polyhedron*., **126**, 2017, 262-267.

7. (a) K. Shankar, J. B. Baruah, *Inorg. Chim. Acta*., 2016, **453**, 135-141; (b) K. Shankar, A. Kirillov, J. B. Baruah, *Dalton Trans*., 2015, **44**, 14411-14423; (c) Y. Deng, N. Chen, Q. Li, X. Wu, X. Huang, Z. Lin, Y. Zhao, *Cryst. Growth Des*., 2017, **17**, 3170-3177.

8. M. P. Singh, K. Shankar, J. B. Baruah, *Inorg. Chim. Acta*., 2019, **489**, 204-210.

9. (a) K. Shankar, B. Das, J. B. Baruah, *RSC Adv.*, 2013,**3**, 26220-26229; (b) K. Shankar, B. Das, J. B. Baruah, *Eur. J. Inorg. Chem*., 2013, 6147-6155.

10. J. K. Nath, J. B. Baruah, *New J. Chem*., 2013, **37**, 1509-1519.

11. A. Tarai, J. B. Baruah, *New J. Chem*., 2017, **41**, 10750-10760.

12. O. Zafer, Y. Incillker, S. R. Refat, H. Ishida, *Polyhedron*., 2010, **29**, 2345-2351.

13. B. Das, J. B. Baruah, *J. Mol. Struct*., 2013, **1034**, 144-151.

14. J. C. MacDonald, P. C. Dorrestein, M. M. Pilley, M. M. Foote, J. L. Lundburg, R. W. Henning, A. J. Schutlz, J. L. Manson, *J. Am. Chem. Soc*., 2000, **122**, 11692-11702.

15. C. A. Hunter, J. K. M. Sanders, *J. Am. Chem. Soc*., 1990, **112**, 5525-5534.

16. (a) D. L. Dexter, *J Chem Phys*., 1953, **21**, 836-850; (b) C. B. Murphy, Y. Zhang, T. Troxler, V. Ferry, J. J. Martin, W. E. Jones, *J. Phys. Chem. B*., 2004, **108**, 1537-1543.

17. K. Shankar, J. B. Baruah, *ChemistrySelect*., 2016, **1**, 3038-3044.

18. L. B. Picraux, B. T. Weldon, J. K. McCusker, *Inorg. Chem*., 2003, **42**, 273-282; (b) D. Kim, M. Jung, H. Kim, W. -j. Chung, H. Lee, *Photochem. Photobiol. Sci*., 2019, **18**, 2688-2695; (c) A. Bhattacharyya, N, Guchhait, *New J. Chem*., 2020, **44**, 10671-10680.

19. (a) A. Saxena, M. Fujiki, R. Rai, G. Kwak, *Chem. Mater*., 2005, **17**, 2181-2185; (b) J. C. Sanchez, A. G. DiPasquale, A. L. Rheingold, W. C. Trogler, *Chem. Mater*., 2007, **19**, 6459-6470.

20. (a) K. Shankar, B. Das, J. B. Baruah, *RSC Adv*., 2013, **3**, 26220-26229; (b) M. P. Singh, K. Shankar, J. B. Baruah, *Inorg. Chim. Acta*., 2019, **489**, 204-210.

21. A. J. Cruz-Cabeza, J. Bernstein, *Chem. Rev*., 2014, **114**, 2170-2191.

22. J. Wang, D. Wang, E. K. Miller, M. Moses, G. M. Bazan, A. J. Heeger, *Macromolecules*., 2000, **33**, 5153-5158.

23. P. Ghosh, S. K. Saha, A. Roychowdhury, P. Banerjee, *Eur. J. Inorg. Chem*., 2015, 2851-2857; (b) S. S. Nagarkar, A. V. Desai, S. K. Ghosh, *Chem. Commun*., 2014, **50**, 8915-8918; (c) Y. -X. Shi, F. -L Hu, W. -H. Zhang, J. -P. Lang, *CrystEngComm*, 2015, **17**, 9404-9412;

(d) H. Ma, C. He, X. Li, O. Ablikim, S. Zhang, M. Zhang, *Sensors and Actuators B.*, 2016, **230**, 746-752.

Chapter 5

Photo-physical Properties of Ag, Zn, Cd Complexes Having N-(4-Pyridylmethyl)-1, 8-naphthalimide

5.1: Introduction

Photo-luminescent metal complexes have generated interest in various spheres of life.[1] Metal complexes, in the form of metal-organic frameworks[2] or assemblies,[3] show interesting material properties. Metal ion, ligand and counter ion of a metal complex influences its photo-luminescence properties.[4] There is interest in understanding the nano-dimensional domains of solids, which can be changed by external stimuli to affect photoluminescence properties.[5] Guest inclusion,[6] hydration[7] and packing pattern,[8] of a complex also influence photo-emission properties. The interplay of weak interactions controls the orientations of a structurally flexible ligand. Such changes in orientations modulate emission properties.[9] On the other hand, presence of water in a solution of a fluorophoric compound dissolved in non-aqueous solvent affects fluorescence emission of the compound and such a change generally occurs through a process named as aggregation-induced emission.[10] Several articles describe aggregation-induced emissions of small metal complexes.[11] Conventionally, metal-to-ligand charge transfer in diamagnetic d^{10}-metal complexes influence the emissions of a fluorescent ligand.[12] Furthermore as discussed in earlier chapters of the thesis the emission properties of a compound measured in solution may differ from those of the same compound measured from a solid sample.[13] Hence, it is a challenge to systematically crystallize complexes of similar origin to ascertain the influence of packing on emission properties.[14] Reger and coworkers carried out extensive structural studies on naphthalimide derivatives and complexes having napthalimide as a part of their ligands. They have illuminated various packing patterns of metal naphthalimide-containing complexes by determining crystal structures, indicating the need for a crystal enginneering[15] in such studies. Naphthalimide derivatives are also studied as diads by varying flexible tethers to modulate their exciplex emissions.[16] Effects of the environment on emission properties were observed in different gels of naphthalimide derivatives.[17] The geometrical features associated with a tether connecting a functional group to naphthalimide ring control stacking arrangements among the fluorophores. Hence, the changes administered by spatial changes cause the relay of electronic effects to influence fluorescence emissions.[18] Cofacial orientations between two

naphthalimide rings may result in assemblies having head-to-head, head-to-tail, or translated orientation of naphthalimides. There are also other weak interactions such as C-H···π or C-H···O [19b] also contribute to self-assembly of a naphthalimide derivative (Figure 5.1A-E). Non-covalent assemblies and coordination polymers having an ease to protonate species, are of central points to study pyridine containing ligands. For example, pyridylmethyl naphthalimide is such a ligand that shows interesting fluorescence emission properties.[18,19] In this chapter, three d^{10}-metal formylbenzoate complexes possessing N-(4-pyridylmethyl)-1,8-naphthalimide **5.2-5.4** (Scheme 5.1) are presented in which a study to understand the role of weak interactions in their photoluminescence properties is presented. Formylbenzoate ligands on these complexes are expected to modulate the electron density of the metal ion and participate in hydrogen bonding in the self-assemblies.[20] Furthermore, presence of a free aldehyde group on a complex would provide scope to understand the fundamental reactivity and obtain information to link it to a functional group like amine group, which is a common functionalizable group found in biological systems. One may also anticipate the reactivity of the aldehyde group of 4-formylbenzoate to transform to another functional group and influence photoluminescence properties.

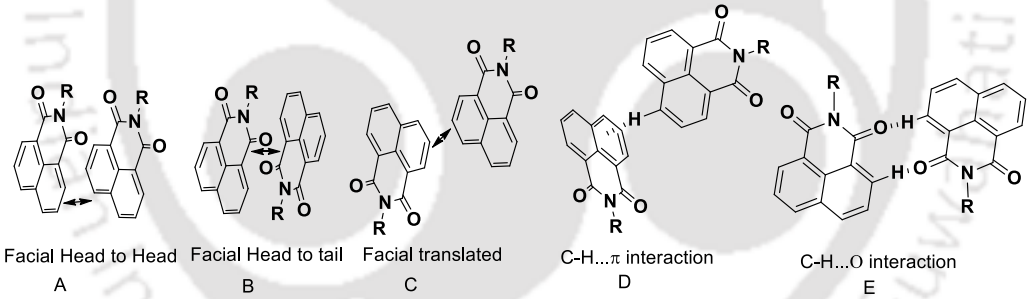

Figure 5.1: Different stacking interactions among naphthalimide rings.

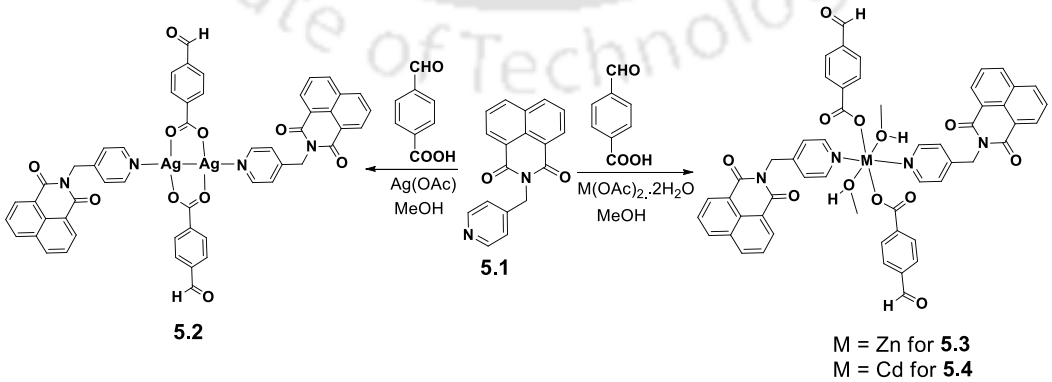

Scheme 5.1: Synthesis of the complexes **5.2**-**5.4**.

5.2: Synthesis and Characterisation of the Complexes

A dinuclear silver complex namely di-μ-η^2-4-formylbenzoato-bis[N-(4-pyridylmethyl)-1,8 naphthalimide)silver(I)] (Complex **5.2)**, two mononuclear complexes namely di-methanol-di[N-(4-pyridylmethyl)-1,8-naphthalimide-di(4-formylbenzoato)zinc(II) (Complex **5.3)** and di-methanol-di[N-(4-pyridylmethyl)-1,8-naphthalimide-di(4-formylbenzoato) cadmium(II) **(**Complex **5.4)** were prepared by reacting 4-formylbenzoic acid and N-(4-pyridylmethyl)-1,8-naphthalimide with corresponding metal acetate. The complexes were characterized by IR, ^{1}H-NMR, ^{13}C-NMR spectroscopy, elemental analyses and also by determining crystal structures. Powder X-ray diffraction patterns of each complexes were recorded, and phase purity of individual complex was confirmed by matching the experimental powder diffraction pattern with the simulated diffraction pattern (Figure 5.20). All these complexes are diamagnetic complexes, have metal ions in d^{10}-electronic configuration. They show ^{1}H-NMR signals of the respective ligands with expected integrations of protons. Complexes have the characteristic sharp IR signal for the aldehyde group at 1699-1701 cm^{-1}, suggesting free aldehyde groups in each complex. Thermogravimetric study suggested that these complexes lose ligand **5.1** at around 235°C-312°C and finally transform to the corresponding metal oxide in the range of 310°C-390°C (Table 5.4 and Figure 5.23). The methanol molecules of the zinc complex present as ligand are lost at 75°C -97°C, whereas the cadmium complexes lose them at 60°C-75°C.

5.3: Crystal Structure of the Complexes

The crystal structure of the silver-complex has proved it as a binuclear complex; it has two formylbenzoate ligands bridging two silver ions (Figure 5.2a). The complex has one coordinated N-(4-pyridylmethyl)-1,8-naphthalimide ligand per silver ion coordinated through the pyridine nitrogen atom. The Ag···Ag distance in the complex is 2.79 Å, which is shorter than the 2.89 Å observed in metallic silver, which suggests that the complex has strong interactions between the silver ions.[21] The dinuclear silver complex is highly symmetric; each molecule possesses a centre of inversion. Each silver ion possess a distorted T-shaped coordination geometry with respect to ligating oxygen and nitrogen atoms, having dissimilar <O-Ag-N and <O-Ag-O angles. The silver-oxygen bond distances are 2.19 Å to 2.20 Å and silver-nitrogen bond distance is 2.35 Å; these distances agree well with conventional Ag-O and Ag-N bond distances found in silver(I) complexes. The naphthalimide rings belonging to neighbouring molecules of the silver complexes in lattice form dimeric synthons (E of Figure 5.1). Such synthons are formed by interactions of a C=O with C-H on a neighbouring ring

through C4-H4···O1 hydrogen bonds ($d_{D\cdots A}$ = 3.308 Å, <DHA = 140°) (Figure 5.2b). These dimerichydrogen bonded synthons have $R_2^2(10)$ graph-set notations. One naphthalimide ring of such a dimeric synthon also aromatic-stacking with another neighbouring naphthalimide ring present at parallel position over it. Such superpositions are in a head to tail manner (B of Figure 5.1). The centroids of the planes of the aromatic-stacks have 3.507 Å distance from centroid of two interacting rings. This distance is suitable for π-π interactions between these rings.[22] The oxygen atom of the C13=O bond of naphthalimide unit is involved in C-H···O interaction with C15-H bond of the pyridine ring of another counterpart. There are also other C-H···O interactions present in the self-assembly; notable among them are the one involving C=O of the aldehyde group, contributing to stability of the self-assembly.

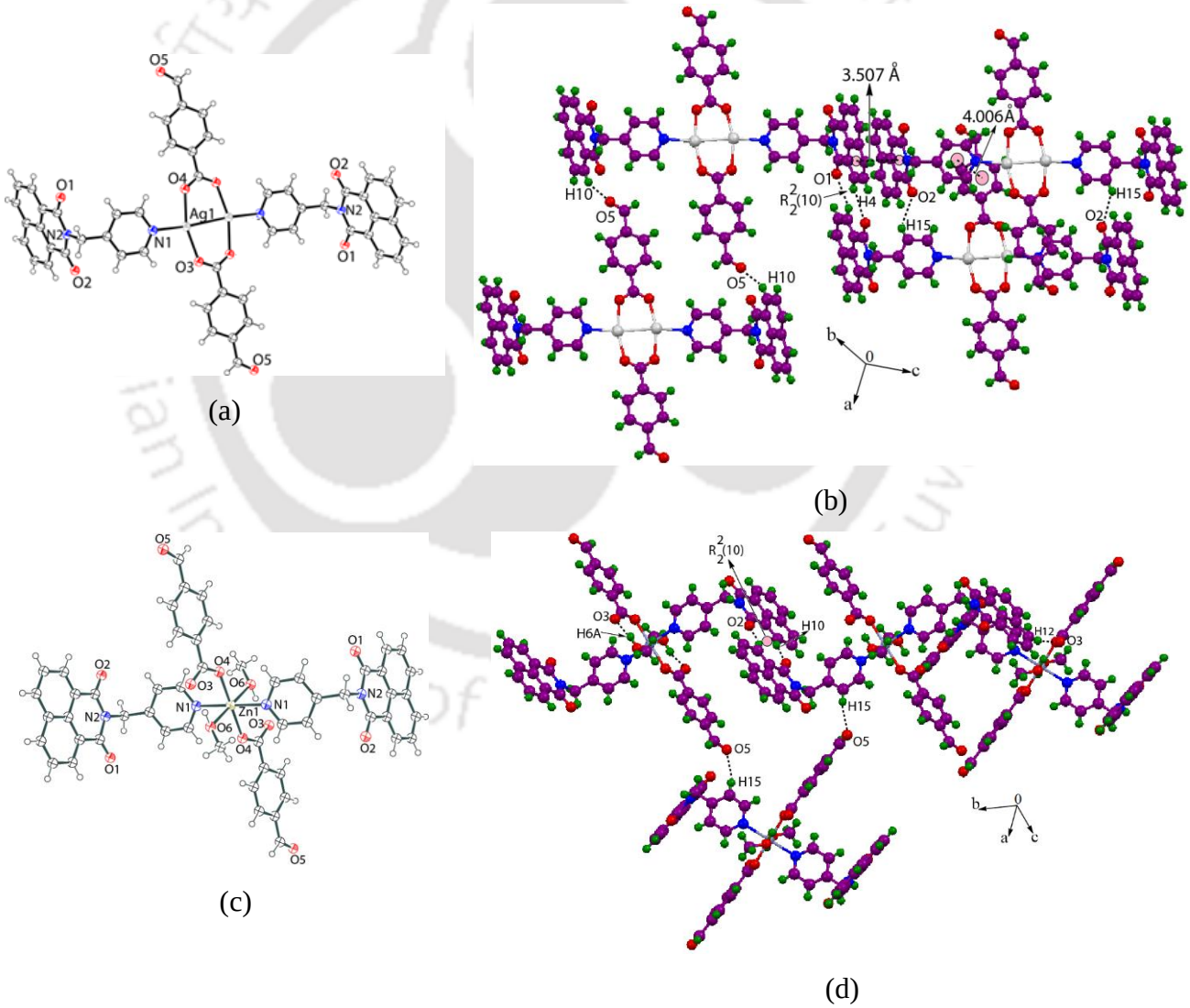

Figure 5.2: (a) ORTEP and (b) packing diagram of the complex **5.2**; (c) ORTEP and (d) packing diagram of the complex **5.3**. (ORTEPs are with 50 % thermal ellipsoids).

The two zinc and cadmium complexes are isostructural; each has two each of the three coordinating ligands to the respective metal ion, namely, **5.1**, formylbenzoate and methanol. Geometric features and packing patterns of these two complexes are also similar. The formylbenzoate ligands of these complexes are monodentate, located at trans positions across the metal ion of these two distorted octahedral metal complexes. The methanol molecules coordinate to each metal ion, whereas the ligand **5.1** occupies two coordination sites of the metal loctated at opposite direction to each other by coordinating through the nitrogen atom of the pyridine unit on the ligand. The prominent metal-ligand bond parameters of the two complexes are listed in the Table 5.1. In the respective zinc and cadmium complexes, the Zn-O in zinc complex and Cd-O bonds in cadmium complex are comparable (Table 5.1), suggesting that the methanol molecules are as tightly held as those of formylbenzoate.

Table 5.1: Metal-ligand bond parameters of complexes.

Complex	M-L	Distance (Å)	< L-M-L	Angle (°)
5.2	Ag1-O3	2.198(4)	O3-Ag1-O4	161.45(19)
	Ag1-O4	2.204(4)	O3-Ag1-N1	101.25(16)
	Ag1-N1	2.352(5)	O4-Ag1-N1	92.33(17)
	Ag1-Ag1	2.7885(9)		
5.3	Zn1-O4	2.0754(2)	O4-Zn1-O4	180.0
	Zn1-O6	2.118(2)	O4-Zn1-O6	90.83(8)
	Zn1-N1	2.195(2)	O4 -Zn1-N1	89.07(7)
			O6 Zn1 N1	85.42(8)
5.4	Cd1-O4	2.260(3)	O4-Cd1-O4	180.0
	Cd1-O6	2.308(3)	O4-Cd1-O6	90.35(11)
	Cd1-N1	2.348(3)	O4-Cd1-N1	91.05(10)
			O4-Cd1-N1	88.95(10)

It may be mentioned that the O-H groups on the methanol molecules are intra-molecularly hydrogen bonded to C=O of formylbenzoate ligands by O(6)-H(6A)···O(3) interactions (in complex **5.3**, $d_{D\cdots A}$ = 2.641 Å, <DHA = 163°; in complex **5.4**, $d_{D\cdots A}$ = 2.646 Å, <DHA = 130°). The obvious difference of the longer M-L bond distances in the cadmium complex over the similar distances of the zinc complex is due to the relative size of the metal ions. Structures of zinc and cadmium complexes exhibit similar $R_2^2(10)$ graph-set motifs in their respective packing (Figure 5.2d). The C=O groups of aldehyde units are involved in intermolecular C-H···O interactions (in zinc complex C15-H···O5, $d_{D\cdots A}$ = 3.361 Å and in cadmium complex C18-H···O5, $d_{D\cdots A}$ = 3.468 Å) to connect different molecules in the lattice.

The ^{13}CNMR of the ligand **5.1** shows carbonyl signals at 163.55 ppm, whereas the signals for this carbon in complexes **5.2** to **5.4** are at 163.56 ppm, 163.59 ppm and 163.56 ppm, respectively. ^{13}CNMR signals are generally sensitive to the local environment, but hardly any

change from original positions of the chemical shifts of the naphthalimide carbonyl groups of the complexes with respect to the chemical shifts for the same in the ligand were observed.

The ^{13}C-signal for the aldehydic carbon appeared in chemical shifts ranging between 193.09 ppm to 193.15 ppm, showing similar chemical shift of aldehydic C=O for complexes. This is expected, as the aldehyde group remains uncoordinated. However, the carboxylate carbon of complexes **5.2** to **5.4** appear at 169.14 ppm, 170.44 ppm and 171.02 ppm, respectively, suggesting that relative deshielding takes place according to sequence Cd > Zn > Ag. The Metal-$O_{formylbenzoate}$ bond distances in the complexes follow the order Cd > Ag > Zn. Hence, the difference in the ^{13}CNMR chemical shifts of these three metal complexes are due to metal-to-ligand charge transfer in individual complex. The characteristic carbon NMR signals for the carboxylates in each complex suggest ligands are not dislodged from the complex in solution. Unfortunately, our attempts to understand any possible dissociation of the complexes in solution are limited by lack of adequate sensitive reproducible ESI-mass signal in the mass spectrometry from the complexes.

5.4: Aggregation-Induced Emission (AIE), NMR and Dynamic Light Scattering Study of the Ligand 5.1 and Complexes 5.2-5.4

The aggregation-induced emission properties of the ligand and the complexes in solution were examined by measuring the emission of their solution in DMSO followed by adding water. The emission wavelength, quantum yield, lifetime in solution of the parent compound and complexes are listed in Table 5.2. The ligand has flexible sp3-hybrid cabon containing tether and can organise the fluorophoric naphthalimide unit differently as the solute-solvent interactions are comparable to energy required for C-C bond rotation. The emission intensities of the ligand and complexes are responsive, showing increase in intensity in each case upon the addition of water, satisfying the prerequisites of AIEgens.[11] The changes in emission upon addition of different fraction of water to the solutions of the ligand **5.1** and complexes are shown in Figure 5.3 and 5.24. Two notable observations from the experiments in solution are (a) the emissions of ligand and complex in solutions are similar in wavelength and quantum yield; (b) all of them showed similar trends in the enhancement of emission upon the addition of water.

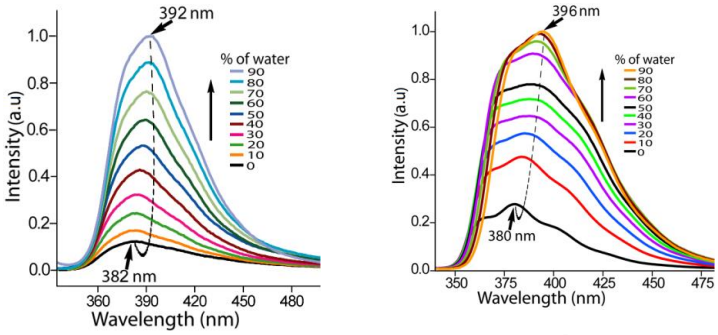

(a) (b)

Figure 5.3: Fluorescence emission (λ_{ex} = 320 nm) enhancement of (a) **5.1** and (b) complex **5.2** with different proportions of water in DMSO.

Table 5.2: Emission, quantum yield, fluorescence lifetime of the complexes in solution.

Compound	Emission wavelength) λ_{em}(nm) *	(PLQY) Φ_F	Lifetime in ns (% contribution)	Goodness to fit (χ^2)
5.1	382	0.31	0.237(66.19), 1.214 (33.81)	0.969
5.2	380	0.35	0.707 (100.00)	1.012
5.3	380	0.38	0.478 (100.00)	1.009
5.4	380	0.36	0.438 (96.84), 1.439 (3.16)	0.967

To see whether there is solute-solvent interaction at ground state, ^{1}H-NMR titrations were carried out by externally adding deuterated water to the ligand **5.1** (Figure 5.26), complex **5.2** (Figure 5.4) and complex **5.4** (Figure 5.27). The ^{1}HNMR recorded in DMSO-d_6 solution showed broadening of the aromatic signals with the increase in concentration of D_2O. The signal of the aldehydic proton of each metal complex is affected significantly. For example, complex **5.2** in DMSO shows an aldehydic proton signal at 10.04 ppm (Figure 5.4). As the concentration of water increases, the signal shifts upfield and appear at 9.89 ppm. The observed shifts upon the addition of water could be either due to the participation of the carbonyl oxygen in hydrogen bonds to form self-assembly, or due to the dissociated ligand forming a new self-assembly. Dynamic light scattering (DLS) of a solution of **5.1** in DMSO shows an unimodal pattern with average particle size 316.3 nm. Similar experiments carried out in DMSO-water mixed solvent shows average particle size 759.3 nm, suggesting a doubling of the average particle size due to aggregation (Figure 5.5). On the other hand, the addition of water to a solution of the complex **5.2** also nearly doubles the average particle size of complex **5.2** in DMSO solution, increasing the average size from 117.9 nm to 233.4 nm (Figure 5.6). Hence, the average particle size of the ligand or complex **5.1** are

approximately doubled on addition of water. The enhancement of intensity by water is apparently from aggregation. In an earlier study, a similar phenomenon in solution was observed from the 2-coordinated silver complex of a naphthalimide-based ligand, but data from zinc and cadmium complexes (Figure 5.29 and 5.30) suggested that in solution, similar ligand-based emissions[7b] are observed. This suggests that metal ions have very insignificant effect to change the emission spectra in solution.

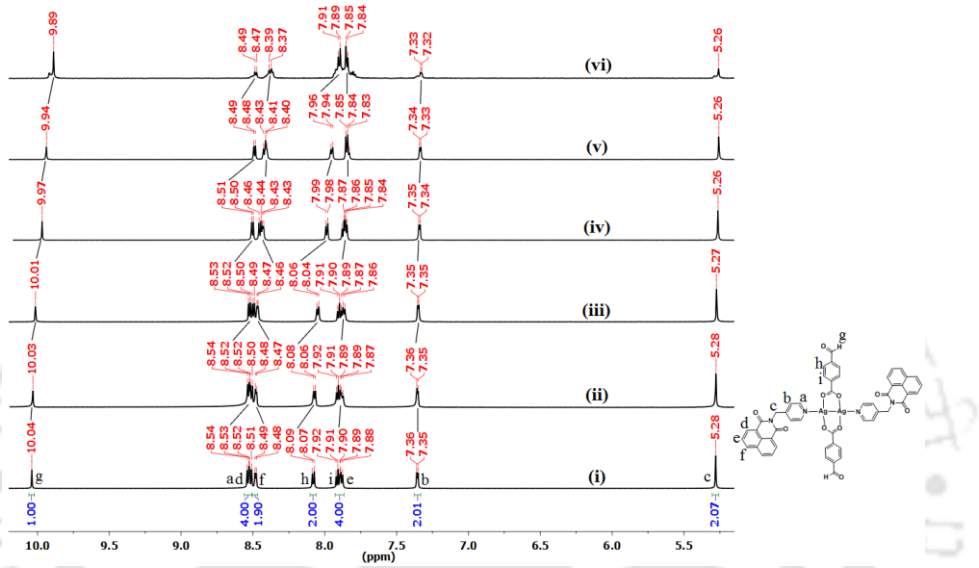

Figure 5.4: ^{1}HNMR (600 MHz) spectra of complex **5.2** in (i) DMSO-d_6 and with different amounts of D_2O (ii) 10 %, (iii) 20 %, (iv) 30%, (v) 40 % and (vi) 50 %.

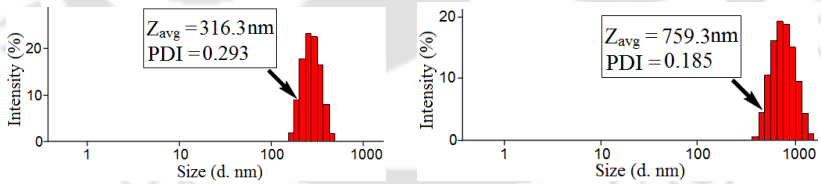

Figure 5.5: Particle size distribution of **L** in (a) DMSO and (b) 1:9 DMSO–H_2O solvent mixture from DLS.

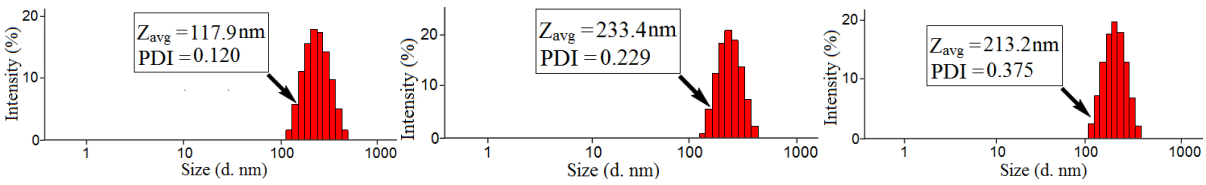

Figure 5.6: Particle size distribution of Complex **1** in (a) DMSO, (b) 1:9 DMSO–H_2O solvent mixtures and (c) 1:1 DMSO–hydrazine hydrate from DLS.

The effects of aggregation are reflected in the FESEM images showing the morphology of the solid samples obtained from evaporation of solvent from samples dissolved in DMSO and DMSO-water mixed solvents. For example, the crystalline samples of **5.1**, upon addition of water, turn to a fibre-like structure (Figure 5.7).

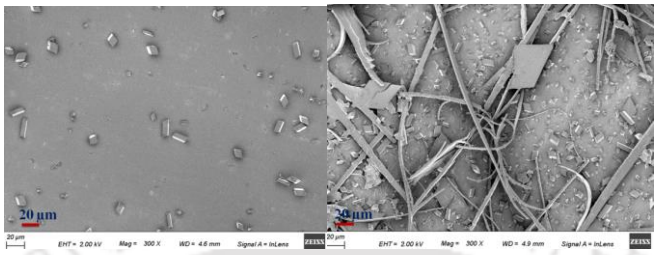

(a) (b)

Figure 5.7: FESEM image of (a) **5.1** (b) after addition of water.

Similarly, due to aggregation, the morphology of the samples obtained from the individual complexes from respective solutions in DMSO changes to provide different threadlike or fibrous structures supporting the aggregations (Figure 5.8).

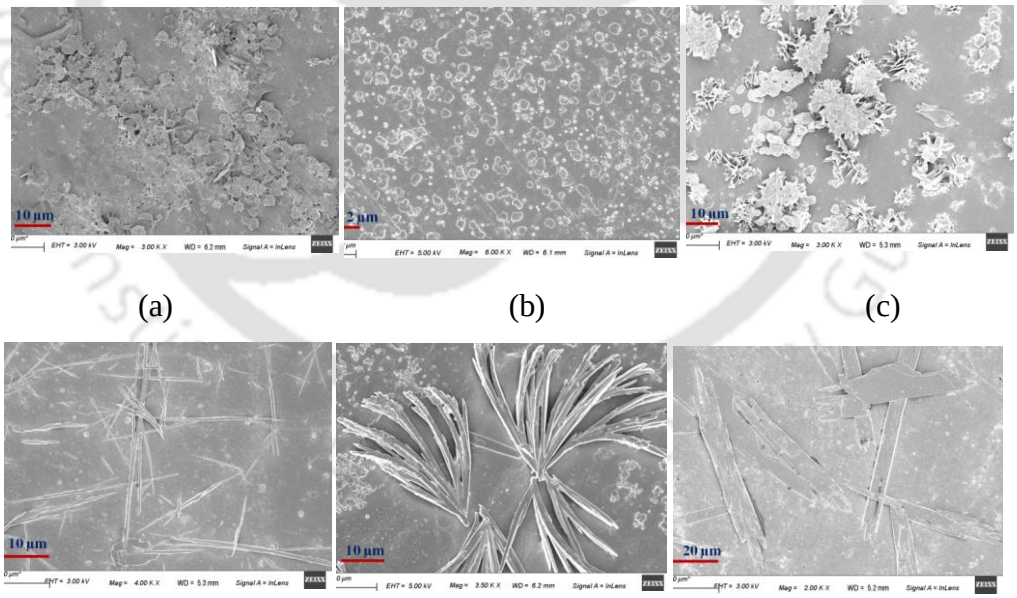

(a) (b) (c)

(d) (e) (f)

Figure 5.8: FESEM image of complexes (a) **5.2**, (b) **5.3**, (c) **5.4** and after addition of water (d) **5.2**, (e) **5.3**, (f) **5.4**.

The morphologies of aggregates of naphthalimide based compounds in gels are substrate dependent, as the morphologies of the solids or gels are related to internal packing arrangements among the molecules, hence, the differences in morphologies also influences the emission properties in confined medium as well as in solids.[23] Furthermore, in solution the naphthalimide derivatives interact with solvent, depending on the nature of solvents, the self-assemblies changes, thus the changes are reflected in the fluorescence emission. There are examples in literature on naphthalimide derivatives, suggesting that the weak interactions such as C-H···π or C-H···O interactions cause changes in fluorescence emission properties.[24,25]

5.5: Effect of C=O to C=N Formation on Emission of the Complexes

Water molecules generally are responsible for changing emission of a solid from the form having water as solvent of crystallization. Whereas in solution, presence of water with another solvent not only changes dielectric and also changes the solute-solvent interactions. Hence, the observed emission changes of a solution of the complexes dissolved in dimethylsulfoxide upon addition of water is due to changes in internal structures of the self-assemblies. But the effect is different when a reactive component which have apparently having ability to form hydrogen bonding is used. For example, hydrazine added to a solution of the complex **5.2** in DMSO, shows quenching with increasing amounts of hydrazine. But the addition of hydrazine hydrate under a similar condition to a solution of ligand did not change the emission spectra of the ligand. So the quenching caused by hydrazine followed a trend opposite that of water, which made us curious whether there is some other inherent factor that is responsible for this opposite trend, other than aggregation in this particular case. Noble metal complexes are easily reduced to metallic species by reducing agents like hydrazine.[26] However, we have not observed deposition of metallic species nor Plasmon transition[27] other than the ligand-based transition upon the addition of hydrazine to the solution of ligand or complexes.

Hence, ^{1}HNMR titration of complex **5.2** and **5.4** by adding hydrazine (Figure 5.9 and 5.28) was carried out. Aldehyde group is transformed to hydrazone, and as a result, a new signal appears at 7.71 ppm in the solution of complex **5.2**; in complex **5.4**, this peak develops at 7.70 ppm upon addition of hydrazine.

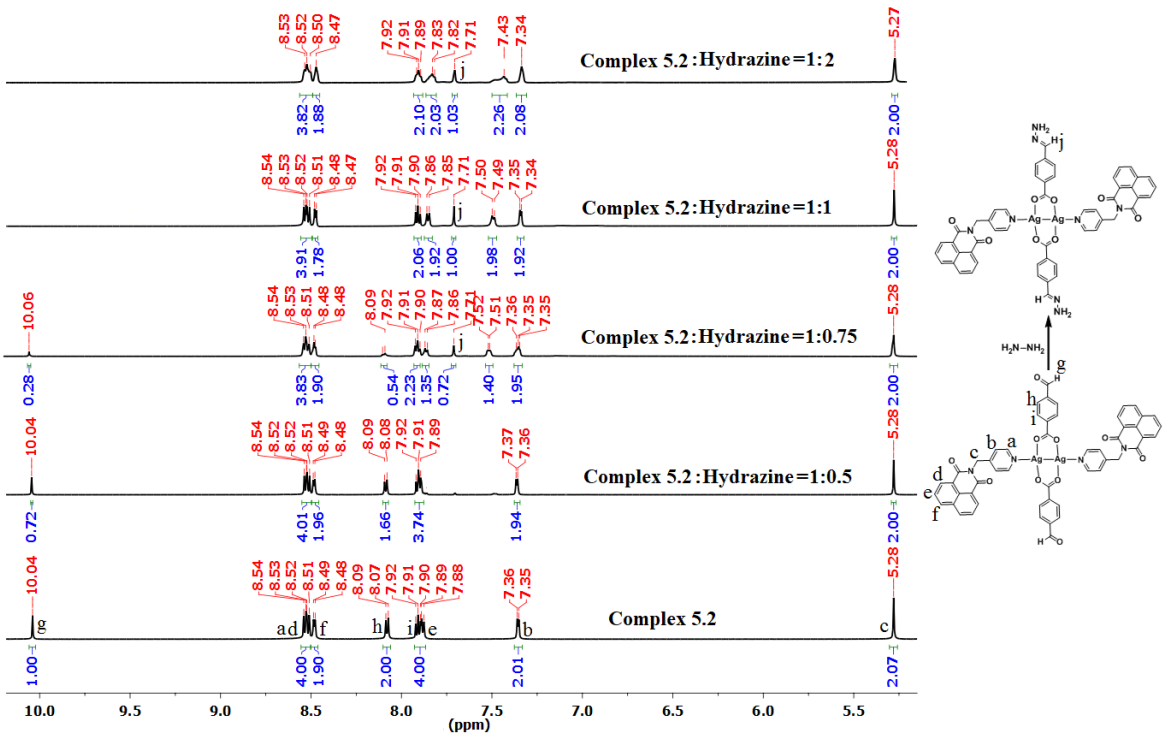

Figure 5.9: ^{1}HNMR (600 MHz) spectra of complex **5.2** in DMSO-d_6 and with different concentrations of hydrazine.

Addition of hydrazine to the solution of complex **5.2** shows an average particle size of 213.2 nm (Figure 5.6c) in the dynamic light scattering study, which is comparable to the average size of the complex in DMSO-water. Having similar average particle sizes from the addition of hydrazine to the one observed upon addition of water, but reverse trends in emission changes, suggests that the changes in the environment of the fluorophores are important. Hence, both water and hydrazine addition change the aggregation of complexes; in the latter case, a corresponding hydrazone is formed. These processes affect the photo-induced electron transfer emission path of naphthalimide in an opposite way.

5.6: Solid-state photoluminescence and DFT calculations

The power sample of ligand **5.1** shows a broad absorption at 360 nm (Figure 5.21); so, we have excited at 330 nm to study the florescence emission of the ligand. The excitation was done at a wavelength slightly away from the absorption maximum to avoid saturation upon excitation at the excited level, while recording the emission spectra. The solid powdered samples of the ligand and complexes showed large differences in position and intensity of emission (λ_{ex} = 330 nm) compared to that observed in solution (Figure 5.10). The ligand **5.1**

shows emission at 500 nm, with photoluminescence quantum yield (PLQY) value of 0.46. The silver complex has emission at 515 nm with PLQY value of 0.19. There is a shift of emission wavelength towards the visible side, whereas the efficiency of emission is reduced by more than twice the efficiency of parent ligand. Silver-based compounds with silver–silver interaction are known to enhance emission.[28]

In our earlier study, we observed dual emission from a mononuclear 2-coordinated silver complex of a pyridine-based ligand with naphthalimide, which arose from twisted intramolecular charge transfer emission.[7b] In the present case, we do not observe emission at a shorter wavelength. The difference of the present complex from the earlier example of silver complex is not only the difference of tether holding the naphthalimide, but in the present case, the complex is an anhydrous dinuclear complex. The earlier one, was a mononuclear hydrated silver complex. We also find that the emission shown by the zinc and the cadmium complexes are observed at lower wavelengths than the emission of the ligand **5.1**. Emission wavelengths for the zinc and cadmium complexes are at 435 nm (ϕ = 0.24) and 470 nm (ϕ = 0.22), respectively. The photoluminescence properties of the complexes obtained from solid samples and HOMO-LUMO energy gaps are listed in Table 5.3.

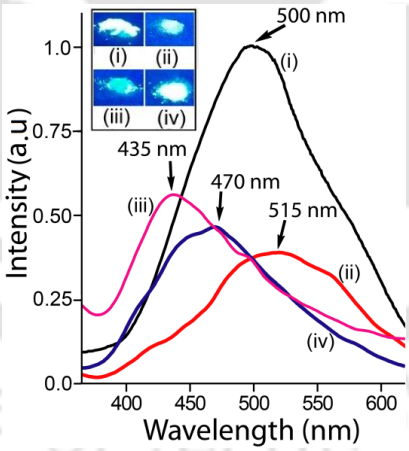

Figure 5.10: Fluorescence emission spectra (excitation at 330 nm) of the solid samples of (i) **5.1**, and complexes (ii) **5.2**, (iii) **5.3**, and (iv) **5.4**. The inset figure is showing fluorescence images of **5.1** and complexes on exposure to 365 nm UV-light.

Table 5.3: Photoluminescence characteristics of the solid samples and energy gaps of the ligand and complexes.

Compound	Emission wavelength) λ_{em}(nm) *	(PLQY) Φ_F	Lifetime in ns (% contribution)	Goodness to fit (χ^2)	DFT calculated HOMO-LUMO gap (eV)
5.1	500	0.46	0.30 (6.51), 10.955 (93.49)	1.043	3.6085
5.2	515	0.19	0.386 (65.06), 4.185 (34.94)	1.086	2.6961
5.3	435	0.24	0.683 (16.40), 4.023 (24.78), 12.306 (58.82)	1.025	3.7957
5.4	470	0.22	0.391 (30.28), 2.088 (27.37), 9.696 (42.35)	1.099	3.7021

Density functional theory (DFT)-based methods are popular in the calculation of the HOMO-LUMO gap of metal complexes. Among the various functionals used in DFT calculations, the most accurate results, tallying with experimental results in the calculated energies of noble metal complexes, were obtained when the LANL2DZ basis set was used.[29] So, we carried out DFT calculations with B3LYP as functional and Lanl2dz as basis. These calculations showed that the HOMO-LUMO gap of complex **5.2** is much less than that of the parent naphthalimide, but such gaps in complex **5.3** and complex **5.4** are comparable to that of the naphthalimide ligand (Table 5.3). There is a bathochromic shift of 15 nm for the silver complex, whereas there is a hypsochromic shift of 35 nm and 70 nm, respectively, in complex **5.3** and complex **5.4** from the ligand **5.1**. The self-assembly of complex **5.2** is primarily guided by C–H···O and π–π interactions. The interesting feature in each case is that the π-π interactions of naphthalimides are among the rings organized with the same dipoles opposite each other. The π–π interaction is a very common factor influencing the intensity and position of emissions of aromatic fluorophores.[24] Parent ligand **5.1** has cofacial π–π interactions involving head-to-tail arrangements.[19a] As a matter of practice, C-H···O interactions influence fluorescence emissions,[25] zinc and cadmium complexes have such interactions. The π-stacks in the packing of **5.1** and silver complex contribute to a shift in the intensity of emissions to longer wavelengths. zinc and cadmium complexes showed monomer-like emission at shorter wavelength. In the case of the ligand, π-stacking among the naphthalimides is prominent[19a] and favors excimer emission, whereas the silver complex has dimers of C-H···O interactions, which stack with naphthalimide, once again favoring excimer emissions.

The HOMO-LUMO energy gaps of a π-stacked head-to-tail dimer of **5.1** and a planar dimer of **5.1** formed by C-H···O interactions (Figure 5.11 and 5.12) are comparable; these are -

3.8483 eV and -3.7135 eV, respectively (Table 5.6). This fact supports the participation of a modified state involving excited state in shifting the emission wavelength of **5.1** and the silver complex to a longer side. But the major difference arises in two forms from the localisation of the orbitals. HOMO and LUMO, in the case of π-stacked head-to-tail dimer, are localised in the naphthalimide ring, but in the case of planar C-H···O interaction-guided dimer, HOMO is localised in pyridine and LUMO is in the naphthalimide ring.

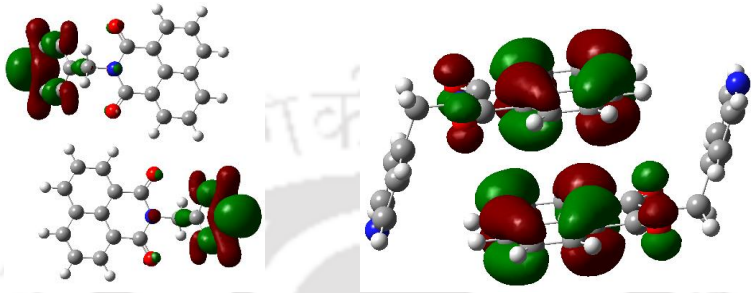

(a) (b)

Figure 5.11: HOMO of dimer of **5.1** (a) form **I (**C-H…O guided**)**, (b) form **II** (with π-stacking).

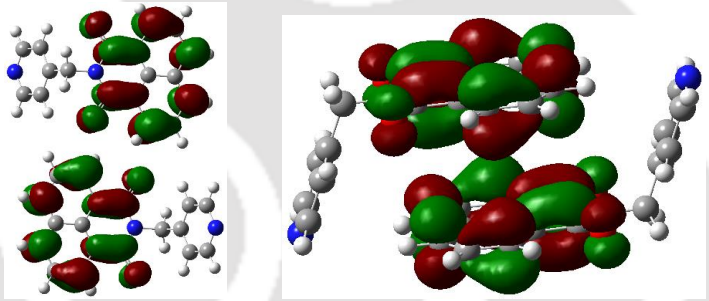

(a) (b)

Figure 5.12: LUMO of dimer of **5.1** (a) form **I (**C-H…O guided**)**, (b) form **II** (with π stacking).

The emission lifetime measurement of the solid sample of **5.1** (Figure 5.33) by excitation at 336 nm (a suitable wavelength available to us with the equipment used) has revealed that the decay of a major portion of the excited species has a relatively long lifetime of ∼11 ns, whereas a minor portion is short-lived, with a lifetime of 0.30 ns. This result suggests prominence of excimer emission. Excimer emission of naphthalimide derivatives occurs at a relatively longer wavelength.[16] The silver complex followed a bi-exponential decay profile, with lifetimes of 0.39 ns and 4.19 ns in 6.5:3.5 proportion (Figure 5.34). In this case, shorter-lived species predominate, and the decay path is also relatively shorter lived than the excited state of the free ligand. Thus, S_1 to S_0 transitions of monomers and excimer to S_0 transitions

occur in the silver complex, which are observed as a broad emission peak. In the cases of zinc and cadmium complexes, (Figure 5.35 and 5.36) decay profiles are tri-exponential and are probably from a combinatorial path involving S_1 to S_0, charge-transfer and excimer emissions. The metal–ligand charge transfer is apparent in these complexes. The combinatory paths of emissions are reflected in an emission plot, with tailing of the intensity at longer wavelengths, which otherwise would have been a normal Gaussian shape. Generally, the emission of the zinc and cadmium complexes is related to the metal-to-ligand charge transfer.[30] Lifetime decay profiles in DMSO solution of the compound **5.1** and complexes (Figure 5.37-5.40) do not show longer lifetime paths, suggesting the absence of excimer, but the appearance of emission at a shorter wavelength is possibly due to an intramolecular charge transfer mechanism operating in solution.

5.7: Conclusions

Photoluminescence properties of powdered samples of **5.1** and its silver, zinc and cadmium complexes differ significantly from that observed in solution. The solid samples of the ligand **5.1** and complex **5.2** show emission at longer wavelengths due to cofacial π-stacks facilitating excimer formation. Solid samples of zinc and cadmium complexes show emission peaks at shorter wavelengths, as C–H···O interactions between pairs of coplanar naphthalimide rings and they have HOMO and LUMO in the rings of pyridine and naphthalimide, respectively. ^{1}H-NMR experiments show the interaction of water with the compound to influence the ground state; hence, a combination of dynamic and static mechanisms are operative to produce broad emission in solution. The fluorescence emission of each solid sample of the complexes differs, whereas they closely resemble each other in solution, suggesting a difference in emission mechanisms of the solution and solid samples. In solution, fluorescence ON or OFF process upon the addition of water or hydrazine, respectively, occurred due to a change of the hydrogen bond donor sites through chemical transformation, which in turn modulates photoinduced electron transfer (PET) process in each case. This study clearly establishes that the excimer emission of solid powder samples of the ligand can be modulated by coordination to metal ions to show monomer- or excimer-like emissions.

5.8: Experimental Procedure

N-(4-pyridylmethyl)-1,8-naphthalimide (**5.1**) was prepared by reported procedure.[19b]

Di-μ-η^2-4-formylbenzoato-bis[N-(4-pyridylmethyl)-1,8-naphthalimide)silver(I)] (Complex **5.1)** : A solution of **5.1** (0.29g, 1 mmol) in methanol (10 mL) was prepared by warming. To this solution silver(I) acetate (0.166g, 1 mmol) was added and stirred for half an hour. A homogeneous mixture was obtained, to which 4-formylbenzoic acid (0.15g, 1 mmol) was added and refluxed for about 2 hours. The solution on cooling resulted an off-white precipitate. The precipitate was dissolved by adding about 10 ml of water. The solution was then kept undisturbed for 7 days, which resulted in crystals of complex **5.2**. Isolated yield = 69 %. ^{1}HNMR (600 MHz, DMSO-d_6): 10.04 (s, 1H), 8.54-8.51 (m, 4H), 8.49 (d, J = 6 Hz, 2H), 8.08(d, J = 12 Hz, 2H), 7.92 (d, J = 6 Hz, 2H), 7.89 (t, J = 6 Hz, 2H), 7.36 (d, J = 6 Hz, 2H), 5.28 (s, 2H). ^{13}CNMR (125 MHz, DMSO-d_6) : 193.09, 169.14, 163.56, 150.18, 147.14, 142.75, 136.97, 134.70, 131.39, 131.07, 129.92, 129.08, 127.62, 127.31, 122.41, 121.90, 42.29. IR (KBr, cm^{-1}): 3060 (w), 1699 (s), 1655 (s), 1584 (s), 1543 (s), 1423 (s), 1375 (s), 1333 (m), 1307 (m), 1231 (s), 1197 (s), 1137 (m), 1081 (m), 1009 (s), 949 (s), 857 (m), 805 (s), 778 (s), 765 (s), 688 (m), 654 (s), 603 (s), 529 (s), 505 (s). Elemental anal. calcd. for $C_{52}H_{34}N_4O_{10}Ag_2$: C, 57.21; H, 3.11; N, 5.13; found C, 57.31, H 3.16, N, 5.15.

Di-methanol-di[N-(4-pyridylmethyl)-1,8-naphthalimide-di(4-formylbenzoato)zinc(II) (Complex **5.2)** and Di-methanol-di[N-(4-pyridylmethyl)-1,8-naphthalimide-di(4-formylbenzoato) cadmium(II) (Complex **5.3)** : To prepare complex **5.3**, zinc(II) acetate dihydrate (0.219g, 1 mmol) was added to a warm solution of **5.1** (0.29g, 1 mmol) in methanol (10 mL) and stirred. 4-Formylbenzoic acid (0.15g, 1 mmol) was added to the reaction mixture and refluxed for about 2 hours to obtain a white precipitate. Work up procedure for both the complexes was identical as that of complex **5.2**. To prepare complex **5.4**, an identical procedure to complex **5.3** was used but cadmium(II) acetate dihydrate (0.266g, 1 mmol) was used instead of zinc acetate. Complex **5.3**: Isolated yield: 64 %. ^{1}H NMR (600 MHz, DMSO-d_6): 10.07 (s, 1H), 8.53-8.51 (m, 6H), 8.13(d, J = 12 Hz, 2H), 7.95 (d, J = 12 Hz, 2H), 7.90 (t, J = 12 Hz, 2H), 7.41 (d, J = 6 Hz, 2H), 5.29 (s, 2H). ^{13}CNMR (600 MHz, DMSO-d_6) : 193.15, 170.44, 163.59, 149.44, 148.02, 140.07, 137.71, 134.74, 131.41, 131.11, 130.11, 129.26, 127.65, 127.33, 122.62, 121.92, 42.37. IR (KBr, cm^{-1}): 3063 (br), 2845 (m), 1699 (s), 1657 (s), 1589(s), 1560 (m), 1502 (m), 1379 (m), 1349 (m), 1233 (s), 1199 (s), 1132 (w), 1032 (w), 953 (s), 860 (m), 813 (s), 771 (s), 688 (s), 653 (s), 615 (s), 532 (w), 488 (m).

Elemental anal. calcd. for $C_{54}H_{42}N_4O_{12}Zn$: C, 64.52; H, 4.18; N, 5.57; found C, 64.39, H,4.21, N, 5.51.

Complex **5.4**: Isolated Yield: 66 %. ^{1}H NMR (600 MHz, DMSO-d_6): 10.07 (s, 1H), 8.53-8.49 (m, 6H), 8.14(d, J = 12 Hz, 2H), 7.95 (d, J = 12 Hz, 2H), 7.91 (t, J = 6 Hz, 2H), 7.35 (d, J = 4.8 Hz, 2H), 5.27 (s, 2H). ^{13}CNMR (600 MHz, DMSO-d_6): 193.14, 171.02, 163.56, 149.65, 146.57, 140.55, 137.51, 134.70, 131.42, 131.10, 130.18, 129.21, 127.64, 127.31, 122.21, 121.89, 42.30. IR (KBr, cm^{-1}): 3056 (w), 1701 (s), 1658 (s), 1587(s), 1545 (m), 1498 (m), 1426 (s), 1380 (s), 1337 (m), 1313 (s), 1231 (s), 1203 (s), 1177 (s), 1145 (m), 1089 (s), 1013 (s), 951 (s), 867 (w), 848 (s), 828 (s), 775 (s), 692 (s), 655 (s), 609 (s), 530 (w), 508 (s). Elemental anal. calcd. for $C_{54}H_{42}N_4O_{12}Cd$: C, 61.63; H, 3.99; N, 5.32; found C, 61.56, H,4.03, N, 5.35.

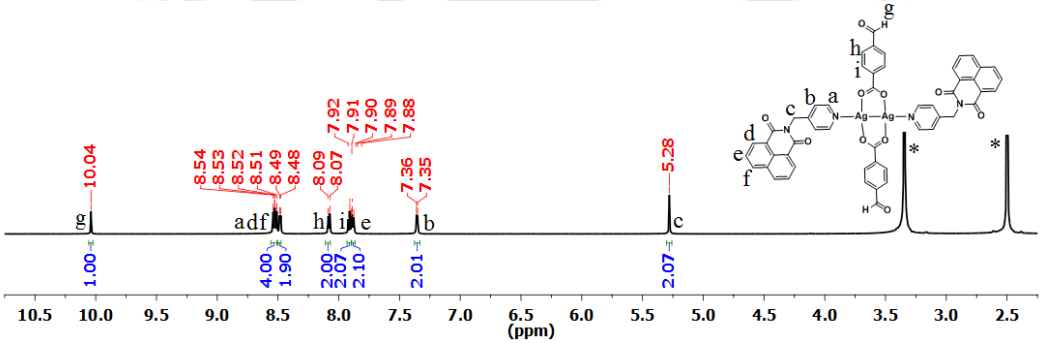

Figure 5.13: ^{1}H-NMR (600 MHz, DMSO-d_6) spectra of Complex **5.2**.

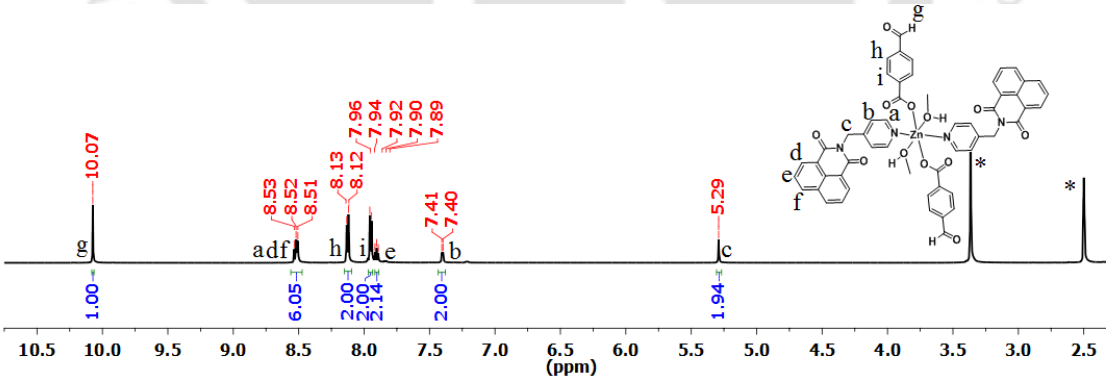

Figure 5.14: ^{1}H-NMR (600 MHz, DMSO-d_6) spectra of Complex **5.3**.

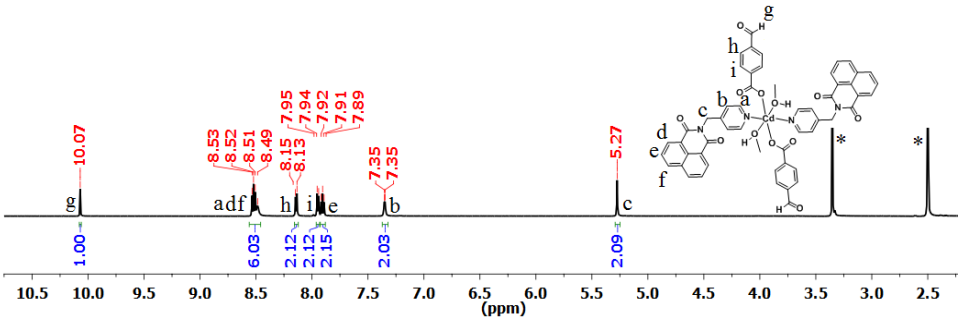

Figure 5.15: ^{1}H-NMR (600 MHz, DMSO-d_6) spectra of Complex **5.4**. (* peaks from solvent in all cases).

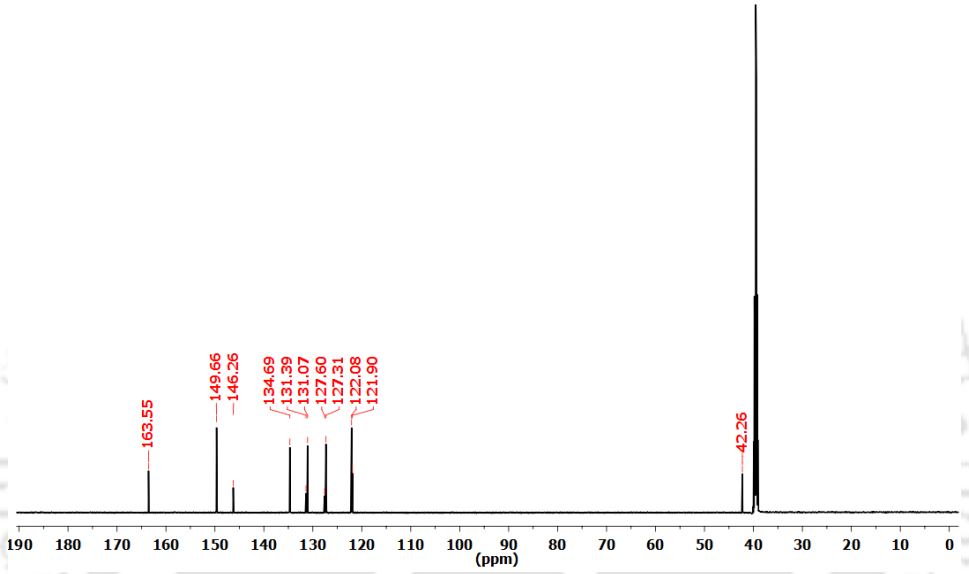

Figure 5.16: ^{13}CNMR (150 MHz) spectra of **5.1** in DMSO-d_6.

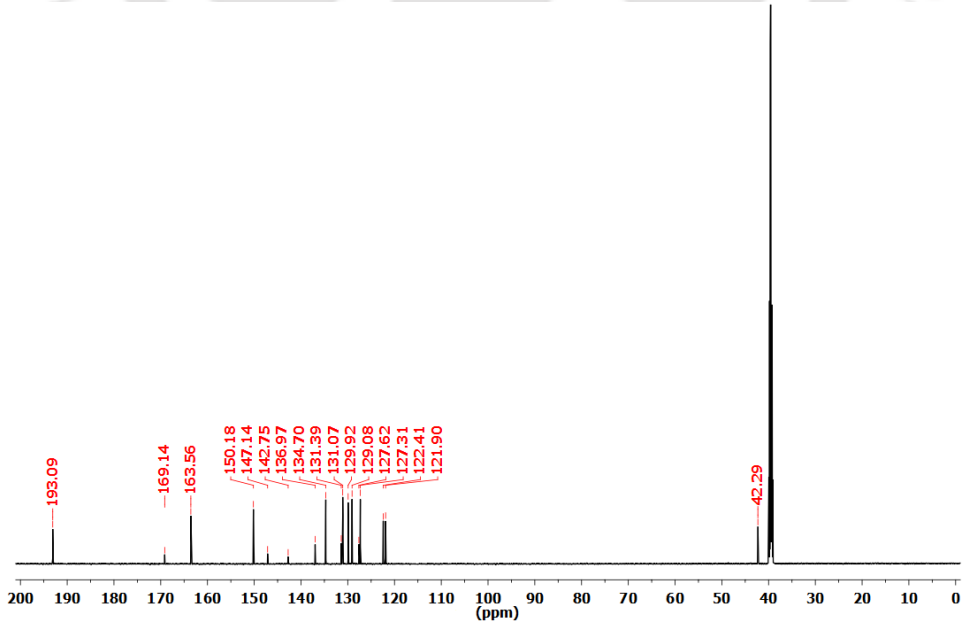

Figure 5.17: ^{13}CNMR (150 MHz) spectra of Complex **5.2** in DMSO-d_6.

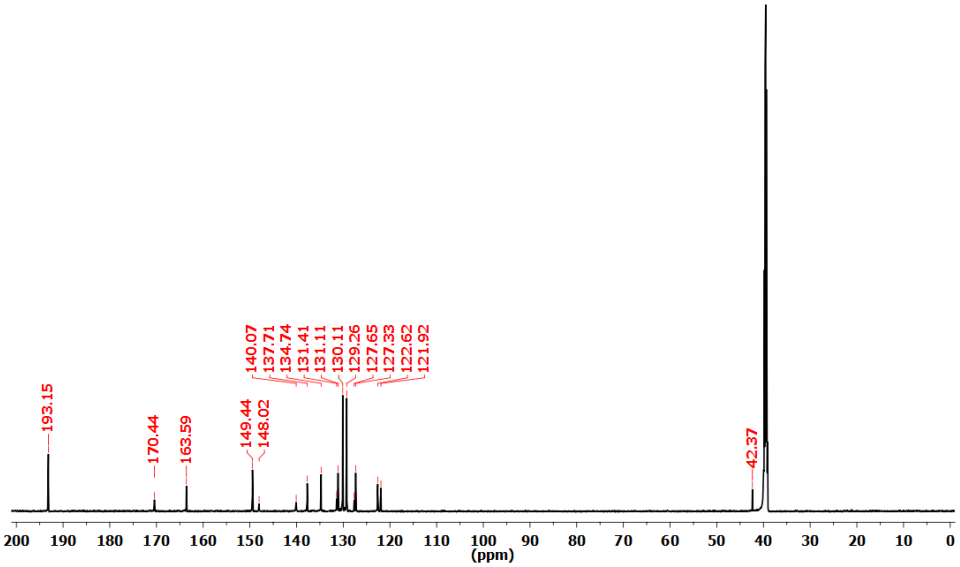

Figure 5.18: ^{13}CNMR (150MHz) spectra of Complex **5.3** in DMSO-d_6.

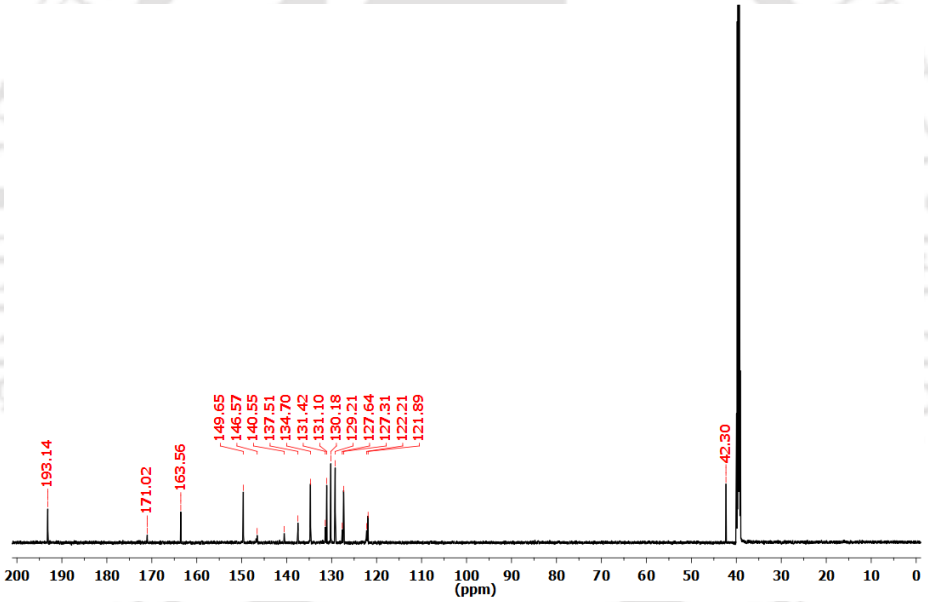

Figure 5.19: ^{13}CNMR (150 MHz) spectra of Complex **5.4** in DMSO-d_6.

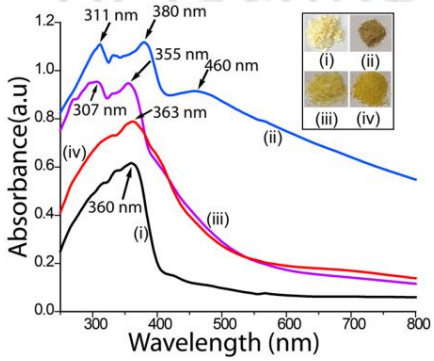

Figure 5.21: UV-visible spectra of the solid samples of (i) **5.1**, and complexes (ii) **5.2**, (iii) **5.3**, and (iv) **5.4**. Colour of **5.1**, and complexes are shown in inset.

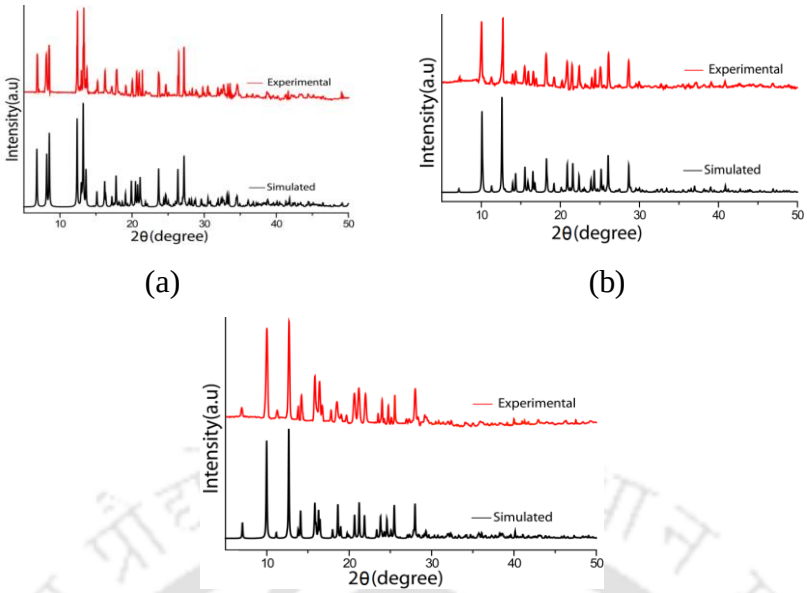

Figure 5.20: PXRD patterns of complexes (a) **5.2**, (b) **5.3**, and (c) **5.4**. Simulated patterns generated from crystallographic information files (Red = Experimental, Black = Simulated).

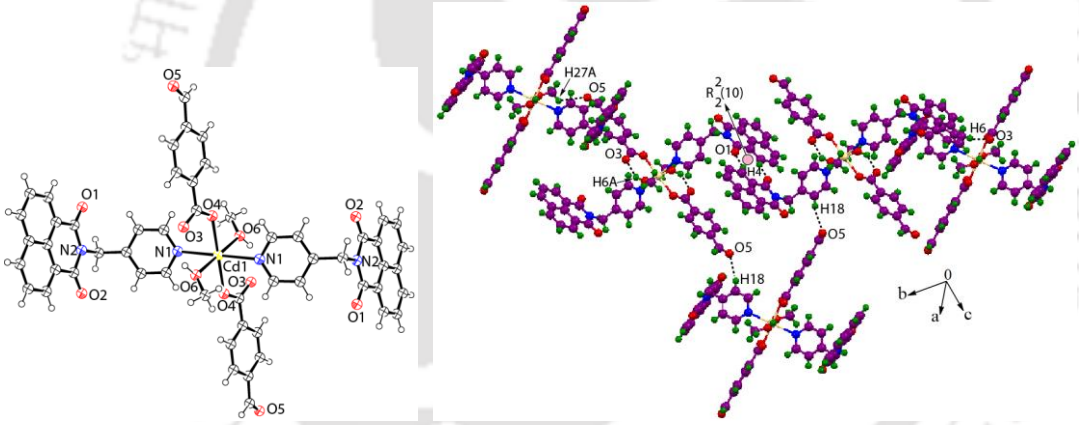

Figure 5.22: (a) ORTEP diagram of the structure of complex **5.4**, ellipsoids are drawn with 50% probability level; (b) Packing diagram of the complex **5.4**.

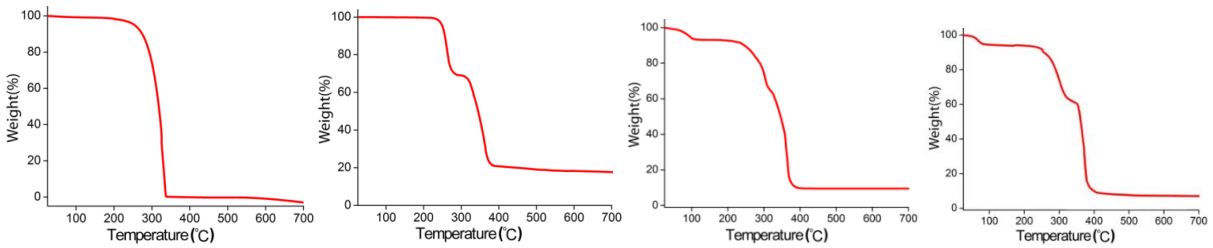

Figure 5.23: Thermogram of the (a) **5.1**, and complexes (b) **5.2**, (c) **5.3**, (d) **5.4** (heating rate 5 ºC/min).

Table 5.4: Thermogravimetry of **5.1** and complexes.

Compounds	Temperature range (°C)	Experimental weight loss from parent composition (%)	Interpretation of weight loss	Theoretically calculated weight loss (%)
5.1	264-339	100	Loss of 5.1	100
5.2	235-275	27.23	Loss of one 5.1	26.41
	Above 380	78.97	Formation of Ag_2O	78.75
5.3	75-97	6.57	Loss of two methanol	6.38
	235-305	35.67	Loss of one 5.1	35.06
	Above 380	92.15	Formation of ZnO	91.89
5.4	60-75	6.81	Loss of two methanol	6.09
	251-312	34.17	Loss of one 5.1	33.49
	Above 380	88.81	Formation of CdO	87.78

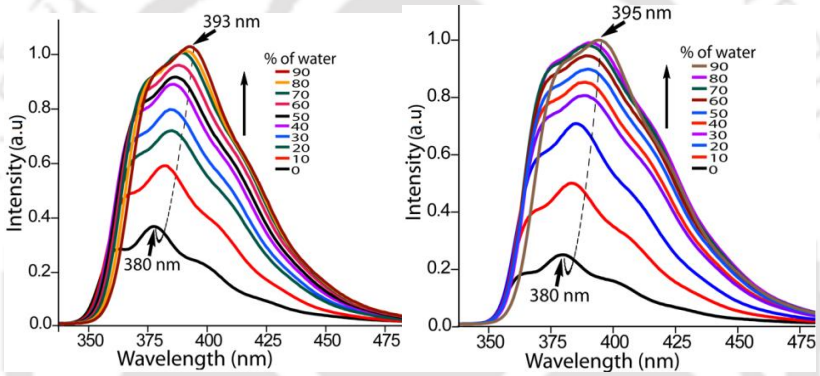

(a) (b)

Figure 5.24: Fluorescence emission (λ_{ex} = 320 nm) enhancement of complexes (a) **5.3** and (b) **5.4** with different proportions of water in DMSO.

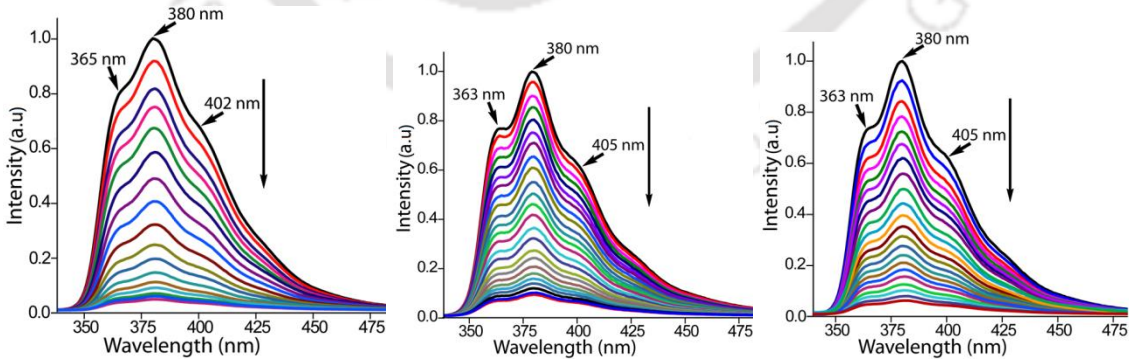

(a) (b) (c)

Figure 5.25: Fluorescence titration (λ_{ex} =320 nm) of complexes (10^{-5} M in DMSO) with hydrazine hydrate (a) **5.2**, (b) **5.3** and (c) **5.4**. (10^{-5} M in DMSO, 10 µL in each aliquot).

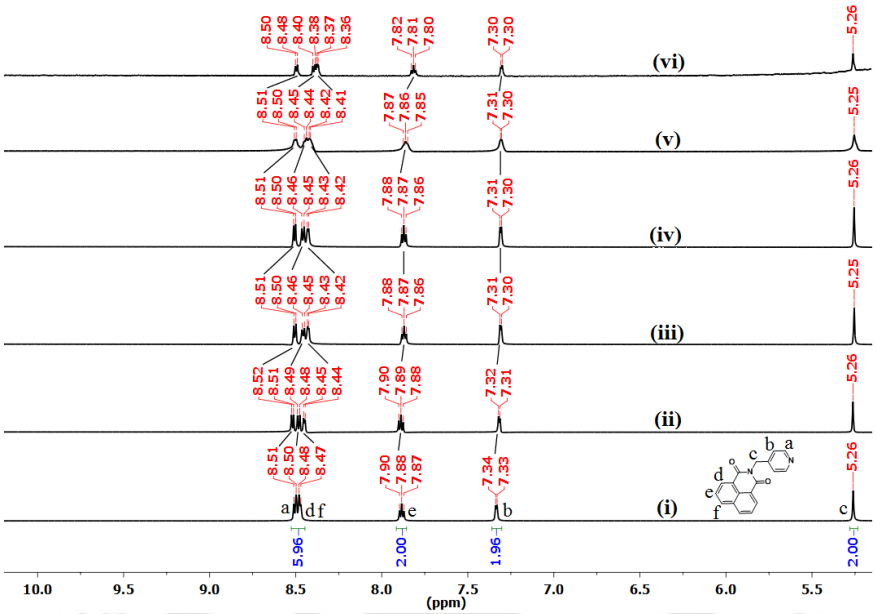

Figure 5.26: ^{1}HNMR (600 MHz) spectra of **5.1** in (i) DMSO-d_6 and with different fractions of D_2O (ii) 10%, (iii) 20%, (iv) 30%, (v) 40% and (vi) 50%.

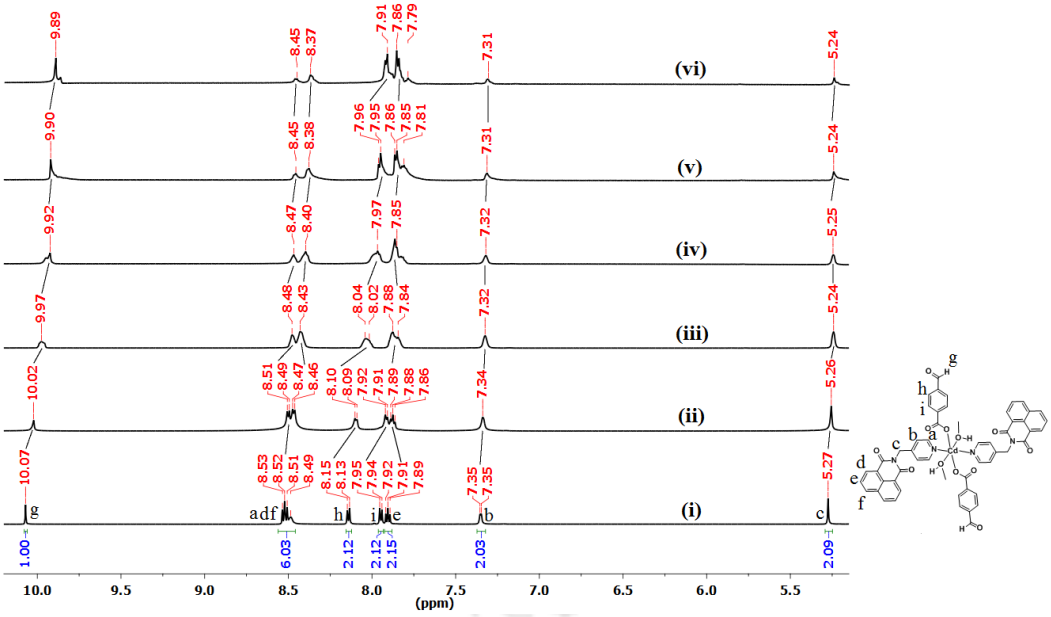

Figure 5.27: ^{1}HNMR (600 MHz) spectra of complex **5.4** in (i) DMSO-d_6 and with different fractions of D_2O (ii) 10%, (iii) 20%, (iv) 30%, (v) 40% and (vi) 50%.

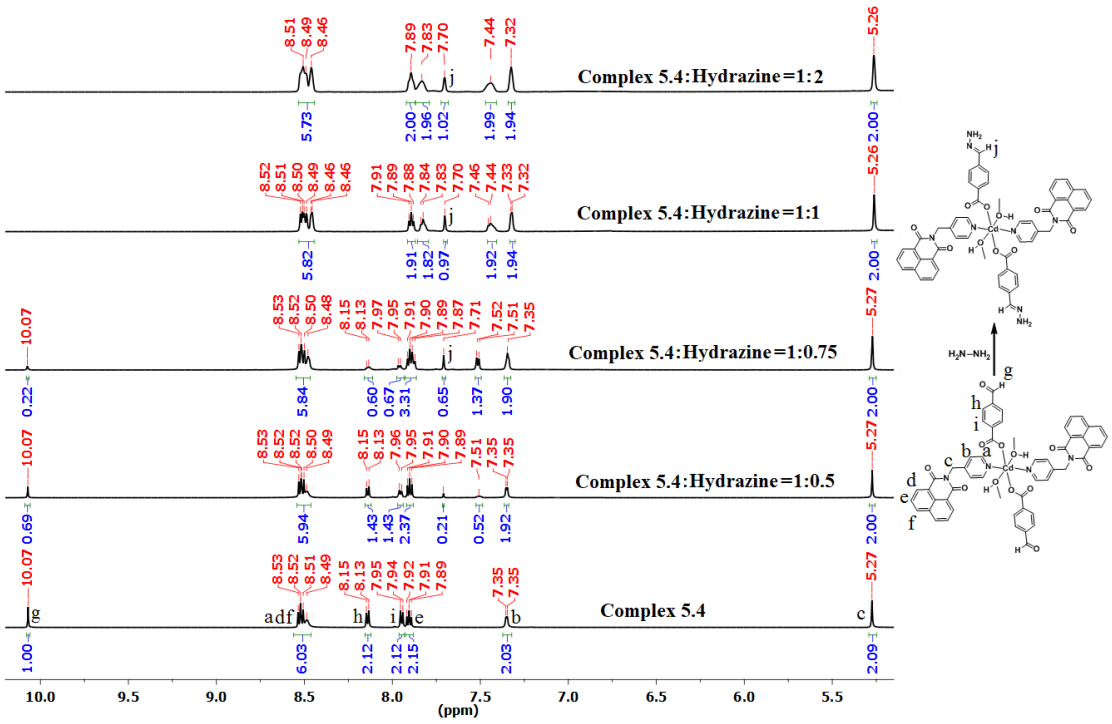

Figure 5.28: ^{1}HNMR (600 MHz) spectra of complex **5.4** in DMSO-d_6 and with different concentrations of hydrazine.

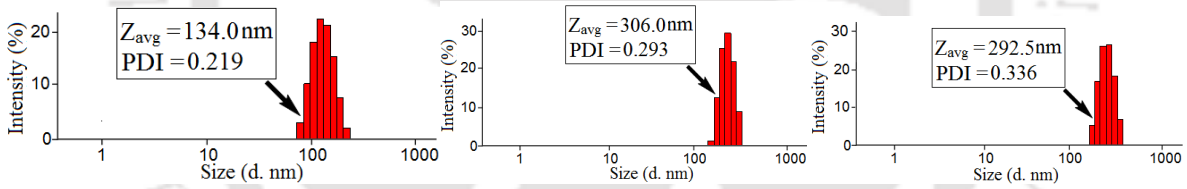

(a) (b) (c)

Figure 5.29: DLS-based particle size analysis of Complex **5.3** from (a) DMSO, (b) 1:9 DMSO−H_2O solvent mixture and (c) 1:1 DMSO−Hydrazine mixture.

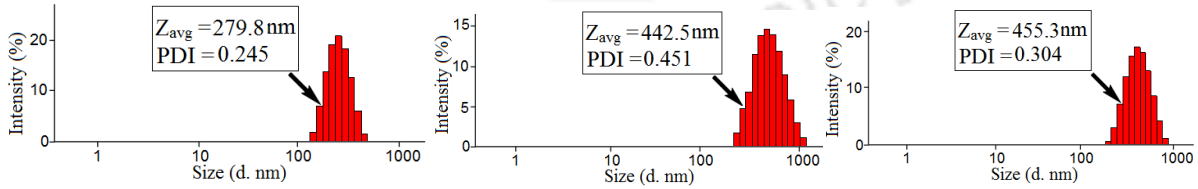

(a) (b) (c)

Figure 5.30: DLS-based particle size analysis of Complex **5.4** from (a) DMSO, (b) 1:9 DMSO−H_2O solvent mixture and (c) 1:1 DMSO−Hydrazine mixture.

Table 5.5: Energy details from DFT calculation using B3LYP functional using Lanl2dz as basis set.

Compounds	HOMO (eV)	LUMO (eV)	Energy difference = HOMO-LUMO (eV)	Optimized energy ($KJmol^{-1}$)
5.1	-6.6183	-3.0098	-3.6085	-2502080.258379
5.2	-5.8041	-3.1080	-2.6961	-8571275.7155049
5.3	-6.8493	-3.0536	-3.7957	-8585825.8962982
5.4	-6.7810	-3.0789	-3.7021	-8539742.4790538

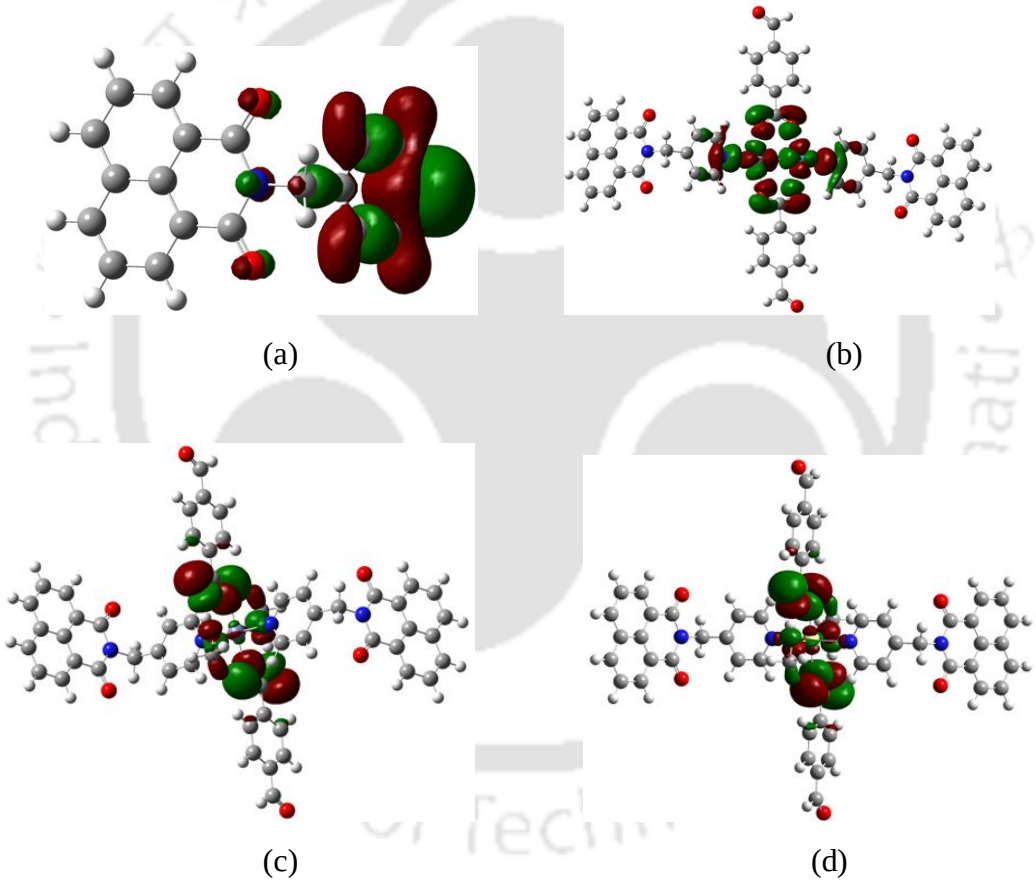

Figure 5.31: HOMO of (a) **5.1**, and complexes (b) **5.2**, (c) **5.3**, (d) **5.4**.

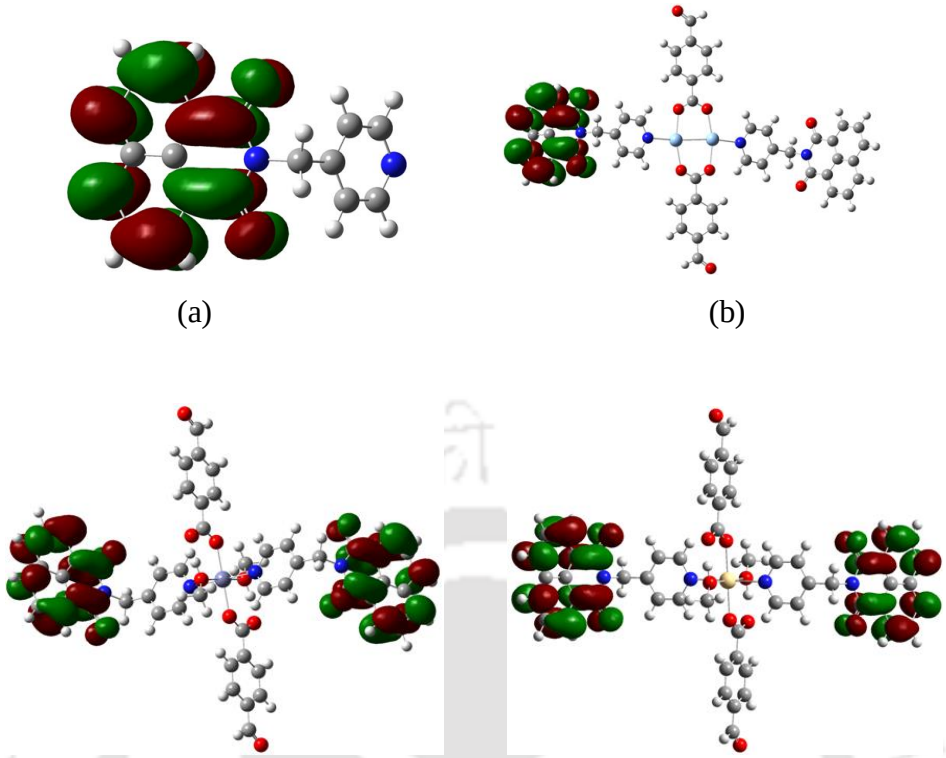

(a) (b)

(c) (d)

Figure 5.32: LUMO of (a) **5.1**, and complexes (b) **5.2**, (c) **5.3**, (d) **5.4**.

Table 5.6: Energy details of dimers of **5.1** from DFT calculation using B3LYP functional using Lanl2dz as basis set.

Compounds	HOMO (eV)	LUMO (eV)	Energy difference = HOMO-LUMO (eV)	Optimized energy ($KJmol^{-1}$)
Dimer form **I** (planar)	-6.7263	-3.0128	-3.7135	-5004184.3867563
Dimer form **II** (stacked)	-6.8608	-3.0125	-3.8483	-5004173.0188655

Table 5.7: Prominent Hydrogen bond parameters of the complexes

Complexes	D-H···A	d_{D-H} (Å)	$d_{H\cdots A}$ (Å)	$d_{D\cdots A}$ (Å)	∠D-H···A (º)
5.2	C(1)-H(1A)···O(1) [x,y,z]	0.97	2.33	2.708(8)	102
	C(4)-H(4)···O(1) [1-x,2-y,-z]	0.93	2.54	3.308(9)	140
	C(10)-H(10)···O(5) [3-x,1-y,1-z]	0.93	2.51	3.086(10)	121
5.3	O(6)-H(6A)···O(3) [x, y, z]	0.95(5)	1.72(4)	2.641(3)	163(4)
	C(10)-H(10)···O(2) [-x,1-y,-z]	0.93	2.42	3.295(4)	158
	C(12)-H(12)···O(3) [1/2+x,1/2-y,-1/2+z]	0.93	2.51	3.406(4)	163
	C(16)-H(16)···O(4) [x, y, z]	0.93	2.45	3.063(3)	124
	C(18)-H(18)···O(2) [x, y, z]	0.93	2.51	3.147(3)	126
5.4	O(6)-H(6A)···O(3) [x, y, z]	0.88(4)	1.99(5)	2.646(5)	130(4)
	C(4)-H(4)···O(1) [-x,1-y,1-z]	0.93	2.41	3.279(5)	155
	C(6)-H(6)···O(3 [1/2-x,1/2+y,1/2-z]	0.93	2.48	3.392(6)	167
	C(15)-H(15)···O(1) [x, y, z]	0.93	2.51	3.169(5)	128

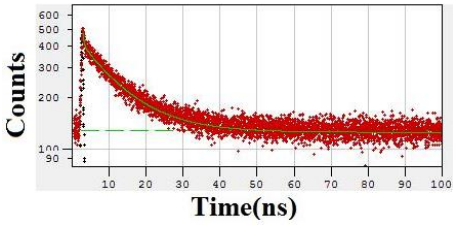

Fitting range : [102; 4096] channels

χ^2 : 1.043

	B_i	ΔB_i	f_i (%)	Δf_i (%)	τ_i (ns)	$\Delta\tau_i$ (ns)
1	0.0541	0.0279	6.511	3.357	0.300	0
2	0.0213	0.0005	93.489	1.985	10.955	0.0008

Shift : -0.610 ns (± 9.121 ns)

Decay Background : 125.690 (± 0.253)

IRF background : 0

Figure 5.33: Time resolved fluorescence emission of solid sample of **5.1** (λ_{ex} = 336 nm, λ_{em} = 500 nm).

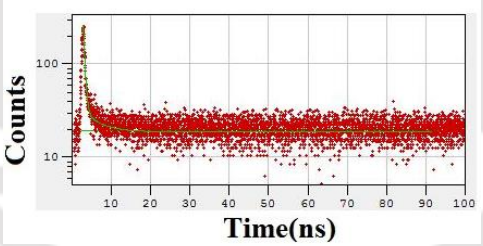

Fitting range : [99; 3750] channels

χ^2 : 1.086

	B_i	ΔB_i	f_i (%)	Δf_i (%)	τ_i (ns)	$\Delta\tau_i$ (ns)
1	254.0846	6.3964	65.060	16.079	0.386	0.086
2	12.5704	1.7264	34.940	5.059	4.185	0.031

Shift : 0 ns (± 0 ns)

Decay Background : 18.669 (± 0.083

Figure 5.34: Time resolved fluorescence emission of solid sample of complex **5.2** (λ_{ex} =336 nm, λ_{em} = 515 nm).

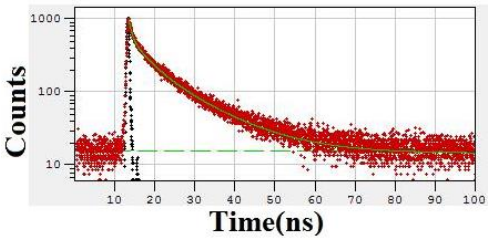

Fitting range : [537; 4096] channels

χ^2 : 1.025

	B_i	ΔB_i	f_i (%)	Δf_i (%)	τ_i (ns)	$\Delta\tau_i$ (ns)
1	0.0542	0.0118	16.403	5.664	0.683	0.087
2	0.0139	0.0007	24.779	1.366	4.023	0.016
3	0.0108	0.0005	58.818	2.944	12.306	0.002

Shift : -0.690 ns (± 7.060 ns)

Decay Background : 14.547 (± 0.159)

IRF background : 0

Figure 5.35: Time resolved fluorescence emission of solid sample of complex **5.3** (λ_{ex} = 336 nm, λ_{em} = 435 nm).

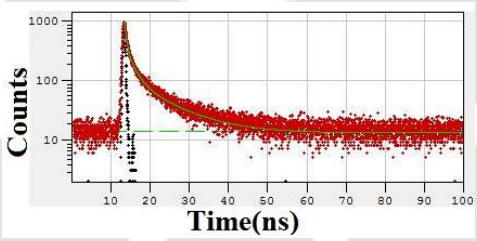

Fitting range : [531; 4096] channels

χ^2 : 1.099

	B_i	ΔB_i	f_i (%)	Δf_i (%)	τ_i (ns)	$\Delta\tau_i$ (ns)
1	0.0685	0.0017	30.275	11.774	0.391	0.142
2	0.0116	0.0007	27.371	1.986	2.088	0.028
3	0.0039	0.0002	42.354	1.960	9.696	0.003

Shift : -0.235 ns (± 0.893 ns)

Decay Background : 13.673 (± 0.104)

IRF background : 0

Figure 5.36: Time resolved fluorescence emission of solid sample of complex **5.4** (λ_{ex} =336 nm, λ_{em} = 470 nm).

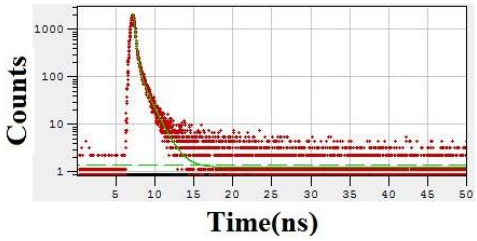

Fitting range : [575; 4096] channels

χ^2 : 0.969

	B_i	ΔB_i	f_i (%)	Δf_i (%)	τ_i (ns)	$\Delta\tau_i$ (ns)
1	2104.6074	10.1398	66.194	8.216	0.237	0.028
2	209.8424	4.5839	33.806	1.008	1.214	0.010

Shift : 0 ns (± 0 ns)

Decay Background : 1.235 (± 0.035)

Figure 5.37: Time resolved fluorescence emission of **5.1** (10^{-5} M in DMSO) (λ_{ex} = 336 nm, λ_{em} = 382 nm).

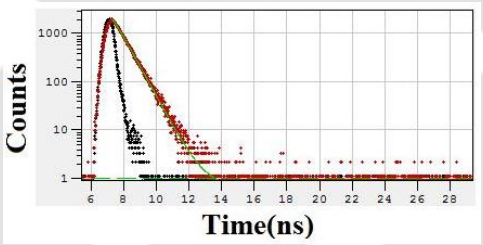

Fitting range : [583; 1150] channels

χ^2 : 1.012

	B_i	ΔB_i	f_i (%)	Δf_i (%)	τ_i (ns)	$\Delta\tau_i$ (ns)
1	0.0343	0.0002	100.000	1.353	0.707	0.005

Shift : -0.134 ns (± 0.599 ns)

Decay Background : 0.702 (± 0.175)

IRF background : 0.100

Figure 5.38: Time resolved fluorescence emission of complex**5.2** (10^{-5} M in DMSO) (λ_{ex} =336 nm, λ_{em} = 380 nm).

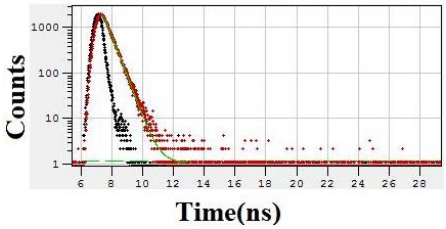

Fitting range : [587; 1050] channels

χ^2 : 1.009

	B_i	ΔB_i	f_i (%)	Δf_i (%)	τ_i (ns)	$\Delta\tau_i$ (ns)
1	0.0424	0.0003	100.000	2.524	0.478	0.008

Shift : -0.049 ns (± 0.505 ns)

Decay Background : 1.071 (± 0.173)

IRF background : 0.100

Figure 5.39: Time resolved fluorescence emission of complex **5.3** (10^{-5} M in DMSO) (λ_{ex} = 336 nm, λ_{em} = 380 nm).

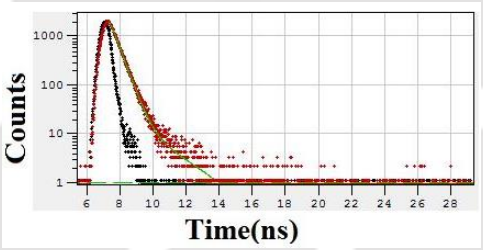

Fitting range : [588; 1110] channels

χ^2 : 0.967

	B_i	ΔB_i	f_i (%)	Δf_i (%)	τ_i (ns)	$\Delta\tau_i$ (ns)
1	0.0442	0.0004	96.838	6.199	0.438	0.024
2	0.0003	0.0001	3.162	1.439	2.379	0.174

Shift : -0.073 ns (± 0.653 ns)

Decay Background : -0.482 (± 1.576)

IRF background : 0.100

Figure 5.40: Time resolved fluorescence emission of complex **5.4** (10^{-5} M in DMSO) (λ_{ex} =336 nm, λ_{em} = 380 nm).

5.9: References

1. (a) A. D. Phillips, L. Gonsalvi, A. Romeros, F. Vizza, M. Peruzzini, *Coord. Chem. Rev*., 2004, **248**, 955-993; (b) K. K. W. Lo, S. P. -Y. Li, *RSC Adv*., 2014, **4**, 10560-10585.

2. (a) M. D. Allendorf, C. A. Bauer, R. K. Bhakta, R. J. T. Houk, *Chem. Soc. Rev*., 2009, **38**, 1330-1352; (b) Y. Cui, Y. Yue, G. Qian, B. Chen, *Chem. Rev*., 2012, **112**, 1126-1162; (c) L. E. Kreno, K. Leong, O. K. Farha, M. Allendorf, R. P. V. Duyne, J. T. Hupps, *Chem. Rev*., 2012, **112**, 1105-1125.

3. J. B. Pollock, G. L. Schneider, T. R. Cook, A. S. Davies, P. J. Stang, *J. Am. Chem. Soc*., 2013, **135**, 13676-13679.

4. (a) J. Li, X. Wang, R. Li, W. Zhang, H. Bai, Y. Liu, Z. Liu, T. Yu, Z. Liu, Y. Yang, Y. Zhu, *Cryst. Growth Des*., 2019, **19**, 3785-3806; (b) H. H. Wang, H. Y. Yang, C. H. Shu, Z. Y. Chen, L. Hou, Y. Y. Wang, *Cryst. Growth Des*., 2016, **16**, 5394-5402; (c) S. Mukherjee, D. Samanta, P. S. Mukherjee, *Cryst. Growth Des*., 2013, **13**, 5335-5343; (d) S. Sanda, S. Parshamoni, A. Adhikary, S. Konar, *Cryst. Growth Des*., 2013, **13**, 5442-5449; (e) X. L. Sun, Z. J. Wang, S. Q. Zang, W. C. Song, C. X. Du, *Cryst. Growth Des*., 2012, **12**, 4431-4440; (f) H. Y. Liu, H. Wu, J. F. Ma, Y. Y. Liu, B. Liu, J. Yang, *Cryst. Growth Des*., 2010, **10**, 4795-4805; (g) X. Chen, B. Zhang, F. Yu, M. Su, W. Qin, B. Li, G. L. Zhuang, T. Zhang, *CrystEngComm*, 2016, **18**, 6396-6402; (h) A. Castineiras, N. F. Hermida, I. G. Santos, J. L. P. Lustres, I. R. Gonzále, *Dalton Trans*., 2012, **41**, 3787-3796.

5. (a) Y. Sun, C. Chen, P. J. Stang, *Acc. Chem. Res*., 2019, **52**, 802-817; (b) K. Acharyya, P. S. Mukherjee, A fluorescent organic cage for picric acid detection, *Chem. Commun*., 2014, **50**, 15788-15791.

6. S. Nigam, G. Durocher, *J. Phys. Chem*., 1996, **100**, 7135-7142.

7. (a) X. Yu, X. Ge, L. Geng, H. Lan, J. Ren, Y. Li, T. Yi, *Langmuir*., 2017, **33**, 1090-1096; (b) A. Tarai, J. B. Baruah, *Cryst. Growth Des*., 2018, **18**, 456-465; (c) S. Parshamoni, H. S. Jena, S. Sanda, S. Konar, *Inorg. Chem. Front*., 2014, **1**, 611-620.

8. (a) X. Cao, L. Meng, Z. Li, Y. Mao, H. Lan, L. Chen, Y. Fan, T. Yi, *Langmuir*., 2014, **30**, 11753-11760; (b) A. K. Srivastava, A. Singh, L. Mishra, *J. Phys. Chem. A*., 2016, **120**, 4490-4504; (c) F. Cheng, R. Fu, Y. Wen, Y. Y. Yang, C. Zeng, Y. Zhang, S. Hu, X. Wu, *J. Mater. Chem. C*., 2018, **6**, 12341-12346; (d) X. Cao, Q. Ding, A. Gao, Y. Li, X. Chang, Y. Wu, *New J. Chem*., 2018, **42**, 6305-6314; (e) D. P. Harding, A. N. Bootsma, S. E. Wheeler, *J. Phys. Chem. B*., 2019, **123**, 487-495.

9. C. Wang, Z. Li, *Mater. Chem. Front*., 2017, **1**, 2174-2194.

10. (a) J. Mei, Y. Hong, J. W. Y. Lam, A. Qin, Y. Tang, B. Z. Tang, *Adv. Mater*., 2014, **26**, 5429-5479; (b) J. Mei, N. L. C. Leung, R. T. K. Kwok, J. W. Y. Lam, B. Z. Tang, *Chem. Rev*., 2015, **115**, 11718-11940; (c) S. Gan, J. Zhou, T. A. Smith, H. Su, W. Luo, Y. Hong, Z. Zhao, B. Z. Tang, *Mater. Chem. Front*., 2017, **1**, 2554-2558; (d) J. Wang, J. Mei, R. Hu, J. Z. Sun, A. Qin, B. Z. Tang, *J. Am. Chem. Soc*., 2012, **134**, 9956-9966.

11. (a) Y. Tian, Z. Y. Wang, S. Q. Zang, D. Li, T. C. W. Mak, *Dalton Trans*., 2019, **48**, 2275-2279; (b) R. U. Melero, J. Y. Mevellec, N. Gautier, N. Stephant, F. Massuyeau, S. Perruchas, *Chem. - Asian J*., 2019, **14**, 3166-3172.

12. (a) V. W. W. Yam, V. K. Man, A. Sammual, Y. L. Leung, *Chem. Rev*., 2015, **115**, 7589-7728; (b) S. L. Zheng, J. H. Yang, X. L. Yu, X. M. Chen, W. T. Wong, Syntheses, *Inorg. Chem*., 2004, **43**, 830-838; (c) L. Zhu, Z. Yuan, J. T. Simmons, K. Sreenath, *RSC Adv*., 2014, **4**, 20398-20440; (d) M. Bardaji, A. B. M. Coello, P. Espinet, *Inorg. Chim. Acta*., 2012, **386**, 93-101.

13. (a) A. Tarai, J. B. Baruah, *Cryst. Growth Des*., 2016, **16**, 126-135; (b) M. P. Singh, A. Tarai, J. B. Baruah, *CrystEngComm*, 2019, **21**, 4898-4909.

14. (a) B. Panunzi, S. Concilio, R. Diana, R. Shikler, S. Nabha, S. Piotto, L. Sessa, A. Tuzi, U. Caruso, *Eur. J. Inorg. Chem*., 2018, 2709-2716; (b) B. Panunzi, F. Borbone, A. Capobianco, S. Concilio, R. Diana, A. Peluso, S. Piotto, A. Tuzi, A. Velardo, U. Caruso, *Inorg. Chem. Commun*., 2017, **84**, 103-108.

15. (a) D. L. Reger, R. F. Semeniuc, J. D. Elgin, V. Rassolov, M. D. Smith, *Cryst. Growth Des*., 2006, **6**, 2758-2768; (b) D. L. Reger, E. Sirianni, J. J. Horger, M. D. Smith, R. F. Semeniuc, *Cryst. Growth Des*., 2010, **10**, 386-393; (c) D. L. Reger, A. P. Leitner, M. D. Smith, *Cryst. Growth Des*., 2016, **16**, 527-536.

16. R. Ferreira, C. Baleizao, J. M. Munoz-Molina, M. N. Berberan-Santos, U. Pischel, *J. Phys. Chem. A*, 2011, **115**, 1092-1099.

17. C. F. -Leon, F. Galindo, J. F. Miravel, *Nanoscale*., 2018, **10**, 17060-17069.

18. J. K. Nath, A. Mondal, A. K. Powell, J. B. Baruah, *Cryst. Growth Des*., 2014, **14**, 4735-4748.

19. (a) R. J. Sarma, C. Tamuly, N. Barooah, J. B. Baruah, *J. Mol. Struct*., 2007, **829**, 29-36; (b) J. K. Nath, J. B. Baruah, *CrystEngComm*, 2015, **17**, 8575-8595.

20. J. Nath, A. Tarai, J. B. Baruah, *ACS Omega*., 2019, **4**, 18444-18455.

21. J. Hu, Y. Zhao, F. Yang, C. Liao, J. Zhao, *J. Coord. Chem*., 2018, **71**, 1368-1379.

22. C. A. Hunter, J. K. M. Sanders, *J. Am. Chem. Soc*., 1990, **112**, 5525-5534.

23. M. A. Kobaisi, S. V. Bhosale, K. Latham, A. M. Raynor, S. V. Bhosale, *Chem. Rev*., 2016, **116**, 11685-11796.

24. (a) H. Zhang, Z. Zhang, K. Ye, J. Zhang, Y. Wang, *Adv. Mater*., 2006, **18**, 2369-2372; (b) M. Brinkmann, G. Gadret, M. Muccini, C. Taliani, N. Masciocchi, A. Sironi, *J. Am. Chem. Soc*., 2000, **122**, 5147-5157; (c) E. A. Meyer, R. K. Castellano, F. Diederich, *Angew. Chem., Int. Ed*., 2003, **42**, 1210-1250.

25. A. Tarai, J. B. Baruah, *ChemistrySelect*., 2018, **3**, 11406-11413.

26. J. P. Chen, L. L. Lim, *Chemosphere*, **49**, 2002, 363-370.

27. J. Tashkhourian, M. R. Hormozi-Nezhad, M. Fotovat, *Spectroscopy letters*., **46**, 2013, 73-76.

28. K. K. Bisht, A. C. Kathalikkattil, E. Suresh, *RSC Adv*., 2012, **2**, 8421-8428.

29. F. S. Legge, G. L. Nyberg, J. B. Peel, *J. Phys. Chem. A*., 2001, **105**, 7905-7916.

30. (a) Y. Hasegawa, T. Nakagawa, T. Kawai, *Coord. Chem. Rev*., 2010, **254**, 2643-2651; (b) X. Liang, J. Jiang, X. Xue, L. Huang, X. Ding, D. Nong, H. Chen, L. Pan, Z. Ma, *Dalton Trans*., 2019, **48**, 10488-10504.

Thesis Conclusion

The fluorescence emission property of a compound is dependent on intra or inter-molecular weak interactions, which warrants understanding of structural aspects of supramolecular features of a fluorescent compound individually or as various adducts with partner molecules or ions. Accordingly, a comprehensive study on solid-state self-assemblies of three cyclic imides and an anthracene derivative, and their salts, cocrystals and multicomponent systems were studied through a crystal engineering approach. The compounds chosen are such that the fluorophores are tethered through linkers to imidazole and pyridine moieties which allowed them to form salts, cocrystals and metal complexes. The cyclic imides and anthracene were functionalized to anchor imidazole through intervening propylene units to provide flexible geometry to the host component. Such systems have the ability to hold the guest molecules and served as a model to understand different anion assisted assemblies of protonated cyclic imides or anthracene derivatives.

The photo-physical properties of all the adducts in solid state are compared with the properties observed in solution. The solid state optical properties of the compounds have differences due to the tight packed structure in solid, whereas in solution solute-solvent interactions are possible. The non-covalent self-assemblies of cyclic imides and related compounds are different due to formation of different homo or hetero supramolecular synthons in the assembly. The phenolic compounds can form strong intermolecular hydrogen bonds with π decorated small fluorophoric compounds. The differences in self-assemblies of nitrophenolate salts of cyclic imide and anthracene compounds in solid state and solution were reflected in absorption and emission spectroscopies. Protonation and π-interactions also influence photo-luminescence properties of such systems. Photo-luminescence of those systems in cocrystal, salt and metal complexes changes from the original compound. These results have helped in modulating fluorescence emission spectra as well as absorption spectra enabling to distinguish nitrophenols. Majority of the nitrophenol assisted assemblies of imidazole tethered anthracene or cyclic imides have imidazole-phenol, phenol-imide and different stacking interactions. Phenol-imidazole interactions control the photo-luminescence activities. There is also competition between the intramolecular hydrogen bonds and the intermolecular imide-phenol interactions in the self-assemblies of cyclic imide derivatives. Compounds with conformational flexibility are suitable for showing aggregation induced emission. Upon addition of water to a solution of these compounds changes the orientation of

the flexible arm resulting in conformation adjustments which influenced the emission spectra of the compounds. Water of crystallization in the self-assemblies also makes a large difference in the packing pattern and influence the photoluminescence properties of such compounds. Different geometrical arrangement of flexible propylene unit of the tethered provided different orientation of imidazole ring with respect to imide ring, consequence of which were reflected in the emission properties. Fluorescence quenching of these derivatives are caused by nitrophenols due to the charge transfer at the remote site linked to the fluorophore. The magnitude of fluorescence quenching by nitro-phenols differs due to the intrinsic acidity associated with them. π-stacking plays the decisive role to increase or decrease fluorescence intensity of cyclic imides and anthracene compounds in the solid state. In case of cyclic imide imidazole tethered compounds quenching of fluorescence take place whereas anthracene based imidazole compounds **3.1** the protonation of secondary amine NH of **3.1** affect the PET and generate fluorescence ON-state at low concentrations and at high concentration of nitrophenols charge-transfer is predominant over the PET phenomenon resulting fluorescence OFF-state.

A water soluble iron (3+) complex of 2,6-pyridinedicarboxylic acid having naphthalenediimide di cation tethered to imidazole through propylene units was prepared. This complex has the ability to hold the guest phenolic compounds. The iron ion remains chelated in the complex and the paramagnetic quenching of iron ion could be avoided in this complex. Hence the fluorescence emission of the cationic part of the complex was utilized to detect the phenolic compounds in presence of water and it operates in similar capacity as the conventional metallo-organic frameworks used in hydroxy-aromatic compounds detection by fluorescence technique. By virtue of properties in solution and solid state, different phenolic compounds were distinguished by the fluorescence technique.

To understand the modulation of emission properties of 1,8-naphthalimide at a remote site from a metal ion, 1,8-naphthalimide was tethered to pyridine and a series of mononuclear and dinuclear d^{10}-metal complexes were prepared. We found that the emission property of all the complexes were different in solid state, whereas they closely resemble each other in solution, suggesting a difference in emission mechanisms of the solution and solid samples. Aggregation induced emission of N-(4-pyridylmethyl)-1,8-naphthalimide (**5.1**) and its metal complexes were observed on adding water to the solution of the compounds in organic solvents.

Since the inter or intra molecular packing arrangement plays a significant role in the formation of supramolecular assemblies and photophysical properties of the cyclic imides and anthracene compounds, This may be of great benefit for evaluating the biomedical applications of different supramolecular assemblies i.e. generated from similar molecular species. In conclusion, the differences in fluorescence emission of powdered solid samples from that observed in solution are established. Further to this the relative fluorescence emission quenching caused by phenolic compounds and role of aromatic stacking interactions are established.

In summary, this thesis has delineated weak interactions of cyclic imide and anthracene compounds tethered with imidazole and pyridine through a flexible arm, which generated new supramolecular assemblies with interesting optical properties in solid or solution state that are useful for molecular and ion recognitions.

Details of the analytical equipment

X-Ray Crystallography

The X-ray crystallographic data were collected at 296 K with Mo Kα radiation (λ = 0.71073 Å) using a Bruker Nonius SMART CCD diffractometer or Oxford SuperNova diffractometer. CrysAlis Pro[1] software was used for analysis of data obtained by Oxford SuperNova diffractometer; whereas SAINT and XPREP softwares[2] were used for Bruker Nonius SMART APEX CCD diffractometer. The structures were solved by direct methods and refined by full-matrix least-square calculations using SHELXTL-14 and SHELXTL-97 software.[3] All the non-H atoms were refined in the anisotropic approximation against F^2 of all reflections. All the H atoms were refined in isotropic approximation and treated as 'riding' in calculated positions. The locations of the H atoms of the protonated organic molecules were justified by difference Fourier synthesis map. The H-atoms attached to water molecules were located in the difference Fourier synthesis maps, and refined with isotropic displacement coefficients. It was also necessary to apply restrains to optimize the distances of some hydrogen atoms of water molecules. The CIF of all the compounds characterized by single crystal X-ray structure are included in the soft copy.

Powder X-ray diffraction pattern were collected on a Bruker D2 Phaser diffractometer in Bragg-Brentano Θ-Θ geometry with Cu Kα radiation (λ = 1.5406 Å) equipped on a glass surface of air dried sample using a secondary curved graphite monochromator. Diffraction patterns were collected over a 2θ range of 5-45º at a step scan rate of 0.02º. ORTEP-3 for windows[4] version 2.0 was used for drawing the supramolecular assemblies of cocrystals, salts and metal complexes in the thesis. For molecular packing diagram we used mercury-3.7 software.[5]

FT-IR, UV-visible, Fluorescence, NMR, Mass spectroscopy, Quantum yields and Lifetime measurements

The FT-IR spectra were recorded with a Perkin Elmer Spectrum One spectrophotometer in the spectral region 4000-400 cm^{-1} using KBr pellets. UV-visible absorption spectra were recorded using Perkin-Elmer Lambda 750 spectrophotometer equipped with double cell compartment. Fluorescence emissions were measured using Horiba Jobin Yvon Fluoromax-4 spectrofluorometer by taking definite amount of solutions and powder samples by exciting at required wavelengths. ^{1}H-NMR was recorded on a Varian 400 MH_Z and BRUKER Ascend 600 MH_z NMR spectrometer using TMS as internal standard. Mass spectra were recorded on

a micro mass Q-TOF (waters) mass spectrometer by using acetonitrile / formic acid matrix. Quantum yields were measured by of powdered solids and solution were done by exciting at the stipulated wavelength in a Horiba Jobin Yvon Fluoromax-4 spectrofuorometer. PQLY of powdered solids were determined by Petite integrating sphere method. The fluorescence emission (E_c) and the scatter (L_c) for the sample and blank (L_a and E_a) were recorded. From these spectral measurements (sample and blank), the quantum yields were calculated by using the equation $\varphi = [(E_c\text{-}E_a)/(L_a\text{-}L_c)]$. Lifetime decay profiles were measured on an Eddinburg

Instrument, Model: FSP920 (by using excitation source 336 nm).

All the chemicals and solvents used were as obtained from the standard suppliers such as Sigma Aldrich, E. Merck, Ranbaxy etc. The solvents for spectroscopic were of HPLC grade (Aldrich or Merck) and used as such.

Thermal analyses (TGA and DSC), elemental analyses, magnetic moment DLS, ITC, FESEM and Hirshfeld analyses

Thermogravimetric analysis (**TGA**) and Differential scanning calorimetry (**DSC**) were performed using thermal analyzer SDTQ600 simultaneous DTA/TGA systems, under nitrogen with a heating rate of 10°C/min. Elemental analyses were performed with a Perkin-Elmer PE 2400 II CHNS micro analytical analyzer. Magnetic moments were measured using a Sherwood scientific magnetic susceptibility balance. Dynamic light scattering (**DLS**) experiments was carried out on a Malvern Zetasizer Nano ZS instrument equipped with a 4.0 mW He-Ne laser operating at a wavelength of 633 nm. The samples and the background were measured at room temperature (25 °C) at a scattering angle of 173°. Isothermal titration calorimetry (**ITC**) analysis was performed at 27 ºC with 25 injections at 90s time interval. After subtractions of control, the final fitting was obtained in single binding site model. **FESEM** imaging studies were performed by a drop (2 μL) cast method on glass plates covered with aluminium foil using a Gemini 300 FESEM instrument (Carl Zeiss). **Hirshfeld** analyses are done by using Crystal Explorer 3.1 software[6].

References:

1. Oxford Diffraction (2008), CrysAlis Pro and RED (version 171.32), Oxford Diffraction Ltd., Abingdon, England.
2. 5.1 ed.; Siemens Industrial Automation Inc.: Madison, WI 1995. G. M. Sheldrick.

3. (a) G. M. Sheldrick, *Acta Cryst*., 2008, **A64**, 112-122; (b) G. M. Sheldrick, *Acta Cryst*., 2015, A**71**, 3-8.
4. L. J. Farrugia, *J. Appl. Cryst*., 1997, **30**, 565.
5. C. F. Macrae, P. R. Edgington, P. McCabe, E. Pidcock, G. P. Shields, R. Taylor, M. Towler, J. van de Streek, *J. Appl. Cryst*., 2006, **39**, 453-457.
6. M. A. Spackman, D. Jayatilaka, *CrystEngComm*, 2009,**11**, 19-32.

Crystallographic data and refinement parameters for compounds

Compound No.	**2.1.3**	**2.1.4**	**2.1.5**	**2.2.2**
Formulae	$C_{20}H_{16}N_6O_9$	$C_{34}H_{26}N_{12}O_{18}$	$C_{34}H_{32}N_{10}O_{16}$	$C_{18}H_{16}N_3O_2Br$
CCDC No.	**1827136**	**1588774**	**1588773**	**1818414**
Mol. wt.	484.39	890.67	836.69	386.25
Space group	P -1	P -1	P -1	P -1
a /Å	8.1727(6)	7.1363(6)	7.3971(12)	11.0554(11)
b /Å	11.9810(8)	11.6686(15)	10.9168(18)	13.1131(15)
c /Å	12.3922(8)	12.5640(12)	12.430(2)	13.7176(15)
α/°	64.393(4)	113.665(11)	66.862(11)	86.042(7)
β/°	79.892(5)	96.408(7)	81.718(12)	68.760(7)
γ/°	84.021(5)	95.450(8)	87.804(11)	68.865(6)
V/ Å^3	1076.70(13)	940.95(19)	913.2(3)	1724.5(3)
Density/g.cm^{-3}	1.494	1.572	1.521	1.488
Abs. Coeff. /mm^{-1}	0.121	0.130	0.123	2.399
F(000)	500	458	434	784
Total No. of reflections	3717	3332	3165	5908
Reflections, $I > 2\sigma(I)$	2501	1965	2200	3442
Max. θ/°	25.049	25.040	25.048	25.050
Ranges (h, k, l)	−9 ≤ h ≤ 9 −13 ≤ k ≤ 14 −14 ≤ l ≤ 14	−8 ≤ h ≤ 8 −13 ≤ k ≤ 12 −14 ≤ l ≤ 14	−8 ≤ h ≤ 8 −9 ≤ k ≤ 12 −13 ≤ l ≤ 14	−13 ≤ h ≤ 13 −15 ≤ k ≤ 15 −16 ≤ l ≤ 16
Complete to 2θ (%)	97.50	99.90	98.00	96.60
Data/				

Restraints/Parameters	3717/1/320	3332/1/293	3165/3/283	5908/0/388
Goof (F^2)	1.053	1.034	1.067	1.032
R indices [$I > 2\sigma(I)$]	0.0749	0.0570	0.0501	0.0683
wR_2 [$I > 2\sigma(I)$]	0.1663	0.1240	0.1422	0.1521
R indices (all data)	0.1036	0.1021	0.0726	0.1240
wR_2 (all data)	0.1663	0.1570	0.1625	0.1746

Compound No.	**2.2.3**	**2.2.4**	**2.2.5**	**3.2**
Formulae	$C_{18}H_{16}N_4O_5$	$C_{48}H_{38}N_{10}O_{14}$	$C_{24}H_{18}N_6O_9$	$C_{33}H_{31}N_5O_6$
CCDC No.	**1818415**	**1588771**	**1588772**	**1867450**
Mol. wt.	368.35	978.88	534.44	593.63
Space group	I 2/c	P -1	P -1	P -1
a /Å	17.4523(11)	11.2891(7)	7.3732(8)	10.674(3)
b /Å	11.0437(7)	11.3644(8)	9.5675(13)	11.727(3)
c /Å	18.4000(11)	17.8952(13)	17.998(2)	12.647(3)
α/°	90	83.461(6)	79.916(8)	94.364(5)
β/°	95.491(6)	80.963(6)	82.514(9)	108.528(4)
γ/°	90	78.968(6)	68.621(8)	97.669(5)
V/ Å^3	3530.1(4)	2217.1(3)	1160.9(3	1475.7(6)
Density/g.cm^{-3}	1.386	1.466	1.529	1.336
Abs. Coeff. /mm^{-1}	0.104	0.111	0.120	0.094
F(000)	1536	1016	552	624
Total No. of reflections	3116	7851	4048	5348
Reflections, $I > 2\sigma(I)$	2094	4628	2778	3533
Max. θ/°	25.037	25.046	25.049	25.25
Ranges (h, k, l)	$-10 \le h \le 20$ $-13 \le k \le 11$ $-21 \le l \le 21$	$-11 \le h \le 13$ $-13 \le k \le 13$ $-16 \le l \le 21$	$-8 \le h \le 8$ $-11 \le k \le 9$ $-21 \le l \le 20$	$-12 \le h \le 12$ $-14 \le k \le 14$ $-15 \le l \le 15$

Complete to 2θ (%)	99.80	99.80	98.10	100.00
Data/ Restraints/Parameters	3116/0/248	7851/3/657	4048/0/360	5348/0/398
Goof (F^2)	1.074	1.020	1.027	1.027
R indices [$I > 2\sigma(I)$]	0.0641	0.0747	0.0493	0.0547
wR_2 [$I > 2\sigma(I)$]	0.1255	0.1513	0.1230	0.0993
R indices (all data)	0.0941	0.1230	0.0759	0.0815
wR_2 (all data)	0.1255	0.1754	0.1360	0.1127

Compound No.	**3.3**	**3.4**	**3.5**	**3.6**
Formulae	$C_{27}H_{25}N_5O_5$	$C_{27}H_{24}N_6O_7$	$C_{28}H_{26}N_4O_4$	$C_{28}H_{27}N_3O_4$
CCDC No.	**1867318**	**1867320**	**1867319**	**1867317**
Mol. wt.	499.52	544.52	482.53	469.52
Space group	P -1	P -1	P -1	P -1
a /Å	10.4383(8)	8.800(2)	8.985(2)	9.0814(5)
b /Å	11.4715(10)	13.141(3)	11.283(3)	10.8169(7)
c /Å	11.7976(9)	13.204(3)	13.060(4)	13.2198(10)
α/°	63.382(8)	113.694(7)	67.661(3)	71.227(6)
β/°	73.600(7)	99.703(7)	81.101(3)	77.368(6)
γ/°	86.147(7)	107.153(7)	77.003(3)	76.688(5)
V/ $Å^3$	1208.67(19)	1262.1(5)	1189.7(6)	1181.67(14)
Density/g.cm^{-3}	1.373	1.433	1.347	1.320
Abs. Coeff. /mm^{-1}	0.097	0.106	0.092	0.089
F(000)	524	568	508	496
Total No. of reflections	4263	4479	4316	4174
Reflections, $I > 2\sigma(I)$	2563	1955	2977	3137

Max. θ/°	25.05	25.05	25.25	25.05
Ranges (h, k, l)	−12≤ h ≤ 12 −12 ≤ k ≤ 13 −14 ≤ l ≤ 14	−6≤ h ≤ 8 −9 ≤ k ≤ 5 −43≤ l ≤ 45	−10≤ h ≤ 10 −13 ≤ k ≤ 13 −15≤ l ≤ 15	−10≤ h ≤ 10 −12 ≤ k ≤ 12 −15≤ l ≤ 15
Complete to 2θ (%)	99.60	100.00	99.90	99.80
Data/ Restraints/Parameters	4263/1/342	4479/0/361	4316/0/325	4174/0/318
Goof (F^2)	1.078	0.948	1.046	1.069
R indices [$I > 2\sigma(I)$]	0.0587	0.0564	0.0432	0.0439
wR_2 [$I > 2\sigma(I)$]	0.0893	0.1049	0.0831	0.0913
R indices (all data)	0.1028	0.1229	0.0686	0.0619
wR_2 (all data)	0.1110	0.1187	0.0938	0.1017

Compound No.	**4.1**	**4.2**	**4.3**	**4.4**
Formulae	$C_{54}H_{52}N_{10}O_{28}Fe_2$	$C_{66}H_{54}N_{12}O_{30}Fe_2$	$C_{66}H_{50}N_{12}O_{28}Fe_2$	$C_{60}H_{62}N_{10}O_{30}Fe_2$
CCDC No.	**1888496**	**1888492**	**1888493**	**1888494**
Mol. wt.	1400.75	1606.91	1570.88	1546.89
Space group	P $2_1/c$	P -1	P -1	P -1
a /Å	15.9412(5)	9.1151(4)	9.2055(3)	9.5665(6)
b /Å	13.2154(5)	13.7030(12)	12.3939(11)	12.5265(11)
c /Å	14.3335(6)	15.2454(8)	14.7103(11)	13.8746(10)
α/°	90	103.581(6)	95.836(7)	87.510(6)
β/°	107.641(4)	90.573(4)	90.136(4)	84.392(6)
γ/°	90	106.205(6)	91.583(5)	82.603(6)

V/ Å^3	2877.6(2)	1771.6(2)	1669.0(2)	1640.1(2)
Density/g.cm^{-3}	1.617	1.506	1.563	1.566
Abs. Coeff. /mm^{-1}	0.607	0.507	0.534	0.545
F(000)	1444	826	806	800
Total No. of reflections	5005	6234	5845	5802
Reflections, $I > 2\sigma(I)$	3704	4949	4362	4521
Max. θ/°	25.050	25.049	25.049	25.050
Ranges (h, k, l)	−18≤ h ≤ 17 −15 ≤ k ≤ 11 −17 ≤ l ≤ 17	−10≤ h ≤ 10 −13 ≤ k ≤ 16 −18 ≤ l ≤ 18	−10≤ h ≤ 9 −12 ≤ k ≤ 14 −17 ≤ l ≤ 17	−10≤ h ≤ 11 −14 ≤ k ≤ 14 −16 ≤ l ≤ 16
Complete to 2θ (%)	98.30	99.50	98.90	99.80
Data/ Restraints/Parameters	5005/5/433	6234/4/501	5845/1/491	5802/0/489
Goof (F^2)	1.004	1.015	1.038	1.041
R indices [$I > 2\sigma(I)$]	0.0587	0.0595	0.0535	0.0463
wR_2 [$I > 2\sigma(I)$]	0.1663	0.1784	0.1361	0.1044
R indices (all data)	0.0845	0.0740	0.0731	0.0635
wR_2 (all data)	0.1663	0.2018	0.1566	0.1149

Compound No.	**4.5**	**5.2**	**5.3**	**5.4**
Formulae	$C_{66}H_{56}N_{10}O_{30}Fe_2$	$C_{52}H_{34}N_4O_{10}Ag_2$	$C_{54}H_{42}N_4O_{12}Zn$	$C_{54}H_{42}N_4O_{12}Cd$
CCDC No.	**1888495**	**1974678**	**1974679**	**1974680**

Mol. wt.	1580.90	1090.57	1004.28	1051.31
Space group	P -1	P-1	P $2_1/n$	P $2_1/n$
a /Å	9.5174(5)	7.2353(5)	7.6965(5)	7.5973(5)
b /Å	13.3262(8)	11.8726(10)	17.3729(11)	17.7923(12)
c /Å	13.7708(8)	14.1900(10)	17.6113(11)	17.7217(12)
α/°	87.033(5)	108.038(7)	90.0	90.0
β/°	74.570(5)	100.678(6)	95.011(4)	92.451(4)
γ/°	86.487(5)	101.982(7)	90.0	90.0
V/ $Å^3$	1679.30(17)	1092.21(15)	2345.8(3)	2393.3(3)
Density/g.cm^{-3}	1.563	1.658	1.422	1.459
Abs. Coeff. /mm^{-1}	0.533	0.965	0.595	0.526
F(000)	814	548	1040	1076
Total No. of reflections	5946	3813	4046	4020
Reflections, $I > 2\sigma(I)$	4431	2794	2966	2905
Max. θ/°	25.050	25.037	25.05	25.05
Ranges (h, k, l)	$-11 \le h \le 11$ $-13 \le k \le 15$ $-16 \le l \le 16$	$-8 \le h \le 8$ $-12 \le k \le 14$ $-16 \le l \le 16$	$-9 \le h \le 9$ $-20 \le k \le 20$ $-20 \le l \le 20$	$-9 \le h \le 7$ $-19 \le k \le 20$ $-19 \le l \le 21$
Complete to 2θ (%)	99.80	98.7	97.40	95.20
Data/ Restraints/Parameters	5946/0/504	3813/0/307	4046/0/327	4020/4/315
Goof (F^2)	1.003	1.033	1.053	1.044
R indices [$I > 2\sigma(I)$]		0.0498	0.0404	0.0439

	0.0553			
wR_2 [$I > 2\sigma$ (I)]	0.1431	0.1313	0.1183	0.1166
R indices (all data)	0.0760	0.0768	0.0641	0.0658
wR_2 (all data)	0.1656	0.1313	0.1297	0.1257

1. **M. P. Singh**, J. B. Baruah, Detection of hydroxyaromatics in a superior manner by a water soluble fluorescent iron-complex, *Inorg.Chim.Acta*., 2020, **504**, 119467.
2. **M. P. Singh**, J. B. Baruah, Photophysical properties of Ag, Zn and Cd - *N*-(4-pyridylmethyl)-1,8-naphthalimide complexes: influences of π-stacking and C–H···O interactions, *CrystEngComm*, 2020, **22**, 4374-4385.
3. **M. P. Singh**, A. Tarai, J. B. Baruah, Photo-physical properties of salts of a di-topic imidazole-tethered anthracene derivative in solid and solution, *CrystEngComm*, 2019, **21**, 4898-4909.
4. **M. P. Singh**, J. B. Baruah, Photophysical Properties of Phthalimide and Pyromellitic Diimide Tethered Imidazolium Nitrophenolate Salts, *ChemistrySelect*., 2019, **4**, 10-16.
5. **M. P. Singh**, A. Tarai, J.B. Baruah, Changes in Emission Properties by π-Stacking and Conformation Adjustment of an Imidazole-Tethered Naphthalimide Derivative, *ChemistrySelect*., 2018, **3**, 6364-6373.
6. R. Brahma, **M. P Singh**, J. B. Baruah, Stacking among the clips of the poly-aromatic rings of phenazine with hydroxy-aromatics and photophysical properties, *RSC Adv.*, 2019, 9, 33403-33412.
7. **M. P. Singh,** J. B. Baruah, Combinations of Tautomeric Forms and Neutral-Cationic Forms in the Cocrystals of Sulfamethazine with Carboxylic Acids, *ACS Omega*., 2019, 4, 11609-11620.
8. **M. P. Singh**, K, Shankar, J. B. Baruah, Study on the interactions of nitrophenols with *bis*-8-hydroxyquinolinium zinc-2,6-pyridinedicarboxylate, *Inorg .Chim. Acta*., 2019, 489, 204-210.
9. **M. P. Singh**, A. Tarai, J. B. Baruah, Neutral, Zwitterion, Ionic Forms of 5-Aminoisophthalic Acid in Cocrystals, Salts and Their Optical Properties, *ChemistrySelect*., 2019, 4, 5427-5436.
10. **M. P. Singh,** N. Phukan, J. B. Baruah, Emission of Pyrene Connected to Benzothiazole Unit via Resonance and Intramolecular Charge Transfer, *ChemistrySelect*., 2018, 3, 963-967.
11. K. Shankar, **M. P. Singh**, J. B. Baruah, Extent of protonation of 4,4′-bipyridinium cations and nature of host influences the amount of guest intake by cobalt(II) 2,6-pyridinedicarboxylate, *Inorg. Chim. Acta*., 2018, 469, 440-446.

12. P. Khakhlary, **M. P. Singh**, A. Bhuyan, J. B. Baruah, Cocrystals of Naphthalenediols with Aliphatic Amines and Their Photoluminescence Properties, *ChemistrySelect*., 2018, 3, 7983-7990.
13. **M. P. Singh**, J. B. Baruah, Modulation of dual fluorescence modes and emissions of 2-(1,4-dioxo-1,4-dihydro-naphthalen-2-yl-amino)benzoic acid, *Journal of Molecular Structure*., 2017, 1149, 315-322.
14. **M. P. Singh,** J. B. Baruah, Dual Modes and Dual Emissions of an Amino-Naphthoquinone Derivative, *J Fluoresc*., 2017, 27,1923-1928.
15. **M. P. Singh**, J. B. Baruah, Stable host–guest complexes of bis-2,6-pyridinedicarboxylate iron(III) with dihydroxybenzenes, *Polyhedron*., 2017, **138**, 103-108.